



**HAL**  
open science

# Eco-conversion de résidus lignocellulosiques de l'agriculture en matériaux composites durables à matrice biopolyester.

David Grégoire

► **To cite this version:**

David Grégoire. Eco-conversion de résidus lignocellulosiques de l'agriculture en matériaux composites durables à matrice biopolyester.. Autre. Université Montpellier, 2019. Français. NNT : 2019MONTG030 . tel-02481223

**HAL Id: tel-02481223**

**<https://theses.hal.science/tel-02481223>**

Submitted on 17 Feb 2020

**HAL** is a multi-disciplinary open access archive for the deposit and dissemination of scientific research documents, whether they are published or not. The documents may come from teaching and research institutions in France or abroad, or from public or private research centers.

L'archive ouverte pluridisciplinaire **HAL**, est destinée au dépôt et à la diffusion de documents scientifiques de niveau recherche, publiés ou non, émanant des établissements d'enseignement et de recherche français ou étrangers, des laboratoires publics ou privés.

# THÈSE POUR OBTENIR LE GRADE DE DOCTEUR DE L'UNIVERSITÉ DE MONTPELLIER

En Biomatériaux

École doctorale GAIA :  
Agroressources, Procédés, Aliments, Produits

Unité de recherche :  
Ingénierie des Agropolymères et des Technologies Émergentes

**Éco-conversion de résidus lignocellulosiques de  
l'agriculture en matériaux composites durables à  
matrice biopolyester.**

Présentée par Grégoire DAVID  
Le 9 octobre 2019

Sous la direction de Hélène ANGELLIER-COUSSY  
et de Nathalie GONTARD

Devant le jury composé de

Véronique MICHAUD, professeur, École Polytechnique Fédérale de Lausanne

Caroline SABLAYROLLES, maître de conférences, ENSIACET-INP Toulouse

Laurent HEUX, directeur de recherche, CERMAV-CNRS Grenoble

Bernard CUQ, professeur, SupAgro Montpellier

Hélène ANGELLIER-COUSSY, maître de conférences, Université de Montpellier

Nathalie GONTARD, directrice de recherche, INRA Montpellier

Rapporteure

Rapporteure

Examineur

Examineur / Président du jury

Directrice de thèse

Co-directrice de thèse



UNIVERSITÉ  
DE MONTPELLIER



*« Nous n'héritons pas de la terre de nos parents,  
nous l'empruntons à nos enfants »*

*Antoine de Saint-Exupéry*



# Remerciements

Je souhaite tout d'abord remercier ma directrice de thèse Hélène Angellier-Coussy, maître de conférences à l'Université de Montpellier qui m'a laissé l'opportunité de réaliser ma thèse au sein de son équipe. Je lui suis très reconnaissant pour son soutien, sa patience et le temps qu'elle m'a accordé au cours de ces trois dernières années. J'ai beaucoup appris à ses côtés grâce à ses qualités pédagogiques et ses compétences scientifiques. Je remercie également Nathalie Gontard, directrice de recherche INRA, qui m'a intégré dans le projet NoAW.

J'exprime tous mes remerciements à l'ensemble des membres d'avoir accepté de participer à mon jury de thèse : Madame Véronique Michaud, Madame Caroline Sablayrolles, Monsieur Laurent Heux et Monsieur Bernard Cuq.

Je souhaite également dire merci à toutes les personnes qui ont accepté de faire des collaborations durant ma thèse :

- Anna Ekman Nilsson (RISE, Suède), Giovanna Croxatto Vega, Joshua Sohn (DTU, Danemark) et Arnaud Helias (ELSA).
- Guillaume Billerach et Hélène Fulcrand (SPO)
- David Guérin (CTP), Laurent Heux et Emilie Ressouche (CERMAV)
- Emmanuelle Gastaldi (UMR-IATE)
- Micaela Vannini (UNIBO, Italie)
- Jean-Michel Salmon (INRA)
- Jérôme Lecomte (CIRAD)
- Didier Cot (IEM), Philippe Dieudonné (CNRS) et Vincent Darcos (IBMM).

Je souhaite remercier les 2 stagiaires que j'ai eu la chance d'encadrer : Gaël Broussard et Julie Michel.

Un grand merci également aux « Young researchers » et plus largement aux partenaires du projet NoAW.

Je remercie aussi l'IUT Génie Biologique de Montpellier-Sète où j'ai pu découvrir l'enseignement durant 2 de mes 3 années de thèse.

Enfin, je remercie chaleureusement tous les membres de l'UMR IATE et particulièrement les doctorants et post-docs pour les très bons moments passés ensemble. Mention spéciale à Sébastien Gaucel pour le dépannage d'ordinateur de dernière minute.

Merci à ma famille et mes proches.

# Valorisation des travaux de recherche

## Published articles

G. David, N. Gontard, D. Guérin, L. Heux, J. Lecomte, S. Molina-Boisseau, H. Angellier-Coussy, (2019). Exploring the potential of gas-phase esterification to hydrophobize the surface of micrometric cellulose particles. *European Polymer Journal* 115, 138-146.

G. David, N. Gontard, H. Angellier-Coussy, (2019). Mitigating the impact of cellulose particles on the performance of biopolyester-based composites by gas-phase esterification. *Polymers* 11, 200.

## Articles waiting for submission

G. David, N. Gontard, H. Angellier-Coussy. A quick view of vine shoots variability as regards biocomposite application: inter-varieties and inter-seasonality.

G. David, L. Heux, S. Pradeau, N. Gontard, H. Angellier-Coussy. Upcycling vine shoots for biocomposites applications: About the interest of filler surface esterification to improve their performance.

G. David, M. Vannini, L. Sisti, A-M. Celli, N. Gontard, H. Angellier-Coussy. Eco-conversion of two winery lignocellulosic wastes into fillers for biocomposites: Vine Shoots and Wine Pomace

G. David, G. Croxatto, J. Sohn, A. Ekman Nilsson, A. Helias, N. Gontard, H. Angellier-Coussy. Life Cycle Assessment of biocomposite packaging materials introducing vine shoots as fillers

G. David, J. Michel, E. Gastaldi, N. Gontard, H. Angellier-Coussy. How vine shoots as fillers impact the biodegradation of PHBV-based composites.

## Posters in international congress

G. David, N. Gontard, C. Mayer, H. Angellier-Coussy, *Eco-conversion of lignocellulosic materials in PHBV-biocomposites*, European Advanced Energy Materials and Technology Congress (EAMC) annual meeting, Stockholm (Sweden), August 22-24, 2017.

## Oral presentation in national congresses

G. David, J. Lecomte, E. Ressouche, L. Heux, D. Guérin, N. Gontard, H. Angellier-Coussy, *Gas-phase esterification of lignocellulosic particles for the production of PHBV based biocomposite*, 3<sup>ème</sup> Séminaire du GDR SYMBIOSE, La Grande Motte (France), May 29- June 1, 2017.

G. David, N. Gontard, H. Angellier-Coussy, *Sarments de vigne: évaluation de leur potentiel pour des applications biocomposites*, 4ème Journées Jeunes Chercheurs Eco-composites et Composites Bio-sourcés, Alès (France), March 28-29, 2019.

Oral presentation in international congresses

G. David, N. Gontard, J. Lecomte, L. Heux, H. Angellier-Coussy, *Gas-esterification of cellulose particles for the production of PHBV based biocomposites*, 3<sup>rd</sup> International EPNOE Junior Scientists Meeting, Maribor (Slovenia), May 14-15, 2018.

G. David, N. Gontard, L. Heux, H. Angellier-Coussy, *Surface gas-phase esterification of lignocellulosic particles for biocomposites applications*, 4<sup>th</sup> International Conference on Bio-based Polymers and Composites (BiPoCo), Balatonfüred (Hungary), September 2-6, 2018

G. David, N. Gontard, H. Angellier-Coussy, *Assessing the potential of vine shoots particles as fillers in biopolyester based biocomposites*, Eurofiller Polymer Blends Conference 2019, Palermo (Italy), April 23-26, 2019



# Sommaire

<b>INTRODUCTION</b>	<b>2</b>
<b>CHAPTER I. STATE OF THE ART</b>	<b>14</b>
<b>I. LIGNOCELLULOSIC FILLERS</b>	<b>15</b>
I-1 SOURCES OF LIGNOCELLULOSIC BIOMASS	15
I-1.1 Dedicated cultures	15
I-1.2 Forest, agricultural and food industries residues	16
I-2 BIOCHEMICAL COMPOSITION OF LIGNOCELLULOSE BIOMASS	17
I-2.1 Cellulose	18
I-2.2 Hemicellulose	18
I-2.3 Lignin	19
I-2.4 Pectins	19
I-2.5 Proteins	20
I-2.6 Extractives	20
I-2.7 Methods to assess the biochemical composition of lignocellulosic biomass	21
I-3 FOCUS ON VINE SHOOTS	21
I-3.1 Vineyard cultivation practices	22
I-3.2 Other wine residues	23
I-3.3 Chemical composition	24
I-3.4 Current and potential uses of vine shoots	25
I-4 KEY PROPERTIES OF FIBERS FOR COMPOSITE	28
I-4.1 Chemical composition	28
I-4.2 Morphology	28
I-4.3 Surface condition: surface chemistry	29
<b>II. LIGNOCELLULOSE FILLER MODIFICATION</b>	<b>31</b>
II-1 MOTIVATION FOR FILLER MODIFICATION	31
II-2 PHYSICAL SURFACE TREATMENTS	33
II-2.1 Plasma treatment	33
II-2.2 Gamma or e-beam irradiation	34
II-3 CHEMICAL SURFACE TREATMENTS	34
II-3.1 Treatment with isocyanates	35
II-3.2 Treatment with organosilanes	35
II-3.3 Esterification	36
II-3.4 Other chemical treatments	40
II-4 CHARACTERIZATION OF THE GRAFTING EXTENT	41

II-4.1	Characterization of the degree of substitution (DS)	41
II-4.2	Parameters impacting the efficiency of the grafting (DS)	42
II-5	CHARACTERISATION OF THE FILLER	42
II-5.1	Surface free energy	42
II-5.2	Surface topography and morphology	43
II-5.3	Crystallinity	43
II-5.4	Thermal stability	43
II-5.5	Water vapor sorption	44
II-5.6	Biodegradability	44
II-6	CHARACTERISATION OF THE FILLER/MATRIX INTERPHASE.	45
II-6.1	Microscopic analysis	45
II-6.2	Mechanical analysis	46
II-6.3	Thermal analysis	46
II-6.4	Mass transfer properties	47
II-7	IMPACT OF SURFACE TREATMENT ON THE REINFORCING PROPERTIES OF LIGNOCELLULOSIC FILLERS	47
<b>III.</b>	<b>ECO-DESIGN OF BIOCOMPOSITES</b>	<b>50</b>
III-1	BIOSOURCED AND BIODEGRADABLE POLYMER MATRICES	50
III-1.1	Categories of bioplastics	50
III-1.2	Polyhydroxyacanoates (PHAs)	52
III-2	PHA/SHORT FIBER-BASED BIOCOMPOSITES	53
III-2.1	Processing	53
III-2.2	Properties of PHA-based biocomposites	54
III-2.3	Thermal stability of PHAs upon processing	55
III-3	BIODEGRADABILITY OF BIOCOMPOSITES	55
III-3.1	Assessing the biodegradability of materials	55
III-3.2	Biodegradability of lignocellulosic-based biocomposites	56
III-4	LIFE CYCLE ASSESSMENT	57
III-4.1	General principle	57
III-4.2	LCA of biocomposites	61
III-4.3	Consideration of the end of life of materials	62
III-5	TOWARDS EARLY DESIGN	63
<b>CHAPTER II. MATERIALS AND METHODS</b>		<b>68</b>
<b>I.</b>	<b>MATERIALS</b>	<b>68</b>
I-1	POLYMER MATRIX	68
I-2	FILLERS	69
<b>II.</b>	<b>METHODS</b>	<b>72</b>
II-1	FILLER MODIFICATIONS	72
II-2	PRODUCTION OF COMPOSITE MATERIALS	75
II-3	CHARACTERIZATION OF FILLERS AND BIOCOMPOSITES	78

<b>I. EXPLORING THE POTENTIAL OF GAS-PHASE ESTERIFICATION TO HYDROPHOBIZE THE SURFACE OF MICROMETRIC CELLULOSE PARTICLES (ARTICLE 1)</b>	<b>99</b>
I-1 INTRODUCTION	100
I-2 MATERIALS AND METHODS.	102
I-2.1 Materials	102
I-2.2 Methods	102
I-3 RESULTS AND DISCUSSION	105
I-3.1 Quantification of the gas-phase esterification efficiency	105
I-3.2 Impact of gas-phase esterification on cellulose particles intrinsic characteristics	108
I-4 CONCLUSION	114
<b>II. MITIGATING THE IMPACT OF CELLULOSE PARTICLES ON THE PERFORMANCE OF BIOPOLYESTER-BASED COMPOSITES BY GAS-PHASE ESTERIFICATION (ARTICLE 2)</b>	<b>116</b>
II-1 INTRODUCTION	117
II-2 MATERIALS AND METHODS	118
II-2.1 Grafting of Cellulose	119
II-2.2 Preparation of Composite Materials	120
II-2.3 Characterization of Films	120
II-3 RESULTS AND DISCUSSION	124
II-3.1 Impact of Gas-Phase Esterification on Some Macromolecular Parameters of PHBV	124
II-3.2 Impact of Gas-Phase Esterification on Interfacial Adhesion: Qualitative Evaluation	127
II-3.3 Impact on Water Transfer Properties in Resulting Composites	127
II-3.4 Impact on Gas-Phase Esterification on Mechanical Properties of the Resulting Composites	132
II-4 CONCLUSIONS	134
<b>III. COMPLEMENTARY RESULTS</b>	<b>136</b>
III-1 XPS: X-RAY PHOTOELECTRON SPECTROSCOPY	136
III-3 HOMOGENEITY AND REPEATABILITY OF THE GAS-PHASE ESTERIFICATION OF CELLULOSE.	138
III-5 COLOR OF THE SAMPLES	140

---

**CHAPTER IV. EXPLORING THE UPCYCLING OF VINE SHOOTS FOR THE DEVELOPMENT OF NEW BIOCOMPOSITES**

---

**144**

<b>I. A QUICK VIEW OF VINE SHOOTS VARIABILITY AS REGARDS BIOCOMPOSITE APPLICATION: INTER-VARIETIES AND INTER-SEASONALITY (ARTICLE 3)</b>	<b>145</b>
I-1 INTRODUCTION	145
I-2 MATERIALS AND METHODS	147
I-2.1 Raw materials	147
I-3 RESULTS AND DISCUSSION	150
I-3.1 Biochemical composition	150

I-3.2	Thermal stability	153
I-3.3	Color	154
I-3.4	Particles size	155
I-4	CONCLUSION	156
<b>II.</b>	<b>UPCYCLING VINE SHOOTS FOR BIOCOMPOSITES APPLICATIONS: ABOUT THE INTEREST OF FILLER SURFACE ESTERIFICATION TO IMPROVE THEIR PERFORMANCE (ARTICLE 4)</b>	<b>157</b>
II-1	INTRODUCTION	157
II-2	EXPERIMENTAL	160
II-2.1	Raw materials	160
II-2.2	Gas-phase esterification of ViSh particles	160
II-2.3	Preparation of composite materials	161
II-3	RESULTS AND DISCUSSION	164
II-3.1	Impact of gas-phase esterification on ViSh particles intrinsic characteristics	164
II-3.2	Functional properties of PHBV/ViSh composites	169
II-4	CONCLUSION	174
<b>III.</b>	<b>ECO-CONVERSION OF TWO WINERY LIGNOCELLULOSIC WASTES INTO FILLERS FOR BIOCOMPOSITES (ARTICLE 5)</b>	<b>175</b>
III-1	INTRODUCTION	175
III-2	MATERIALS AND METHOD	177
III-2.1	Materials	177
III-2.2	Methods	178
III-2.2.1	Extraction of polyphenols	178
III-3	RESULTS AND DISCUSSION	181
III-3.1	Intrinsic properties of wine pomace and vine shoots particles	181
III-3.2	Impact of biomass origin and exhaustion on the properties of biocomposites	186
III-4	CONCLUSION	192
<b>IV.</b>	<b>COMPLEMENTARY RESULTS</b>	<b>193</b>
IV-1	XPS: X-RAY PHOTOELECTRON SPECTROSCOPY	193
IV-2	REPEATABILITY OF THE GAS-PHASE ESTERIFICATION OF VINE SHOOTS PARTICLES	194
IV-4	COLOR OF THE SAMPLES	195
IV-5	PUKÁNSZKY'S MODEL	196
<b>CHAPTER V. SUSTAINABILITY OF BIOCOMPOSITES</b>		<b>200</b>
<hr/>		
<b>I.</b>	<b>LIFE CYCLE ASSESSMENT OF BIOCOMPOSITE PACKAGING MATERIALS INTRODUCING VINE SHOOTS AS FILLERS (ARTICLE 6)</b>	<b>201</b>
I-1	INTRODUCTION	201
I-2	METHODOLOGY	203
I-2.1	Goal and scope	203
I-2.2	Functional unit and system boundary	204

I-2.3	System description and inventory	206
I-2.4	Raw materials	206
I-2.5	Production of biocomposite trays	206
I-2.6	End of life	207
I-3	RESULTS AND DISCUSSION	208
I-3.1	Environmental impact of 100% virgin plastic trays: Comparison of PHBV, PLA and PP	208
I-3.2	Effect of the incorporation of ViSh fillers on the environmental performance of trays	211
I-3.3	Identification of the hot spots	215
I-3.4	Economic vs environmental balance analysis	217
I-4	CONCLUSION	218
<b>II.</b>	<b>HOW VINE SHOOTS AS FILLERS IMPACT THE BIODEGRADATION OF PHBV-BASED COMPOSITES (ARTICLE 7)</b>	<b>220</b>
II-1	INTRODUCTION	220
II-1.1	Materials and Methods	222
II-1.2	Materials	222
II-1.3	Biodegradation tests	223
II-2	RESULTS AND DISCUSSION	225
II-2.1	Biodegradability of ViSh fillers	225
II-2.2	Biodegradability of PHBV-based composites	228
II-3	CONCLUSION	232
<b>III.</b>	<b>COMPLEMENTARY RESULTS</b>	<b>233</b>
III-1.1	Supplementary results	233
III-1.2	Supplementary inventory	240
<b>GENERAL CONCLUSION</b>		<b>ERREUR ! SIGNET NON DEFINI.</b>
<b>REFERENCES</b>		<b>254</b>

# Abbreviations

AGU: anhydroglucose unit

DSC: differential scanning calorimetry

DS: degree of substitution

DVS: dynamic vapor sorption

LCA: life cycle assessment

PHA: poly(hydroxyalkanoate)

PHBV: poly(hydroxybutyrate-co-hydroxyvalerate)

PLA: polylactic acid

PP: polypropylene

RH: relative humidity

SEM: scanning electron microscopy

TGA: thermogravimetric analysis

ViSh: vine shoots

WiPo: wine pomace

WVP: water vapor permeability

XRD: X-ray diffraction



# General Introduction



# Introduction

L'agriculture génère chaque année des milliards de tonnes de résidus organiques liquides, solides et gazeux. Un résidu peut être défini comme une matière qui résulte d'un processus de production et qui n'est pas le produit final que ce processus vise à produire (article L. 541-1-1 du Code de l'Environnement). Il est considéré que ce terme inclut les déchets, les sous-produits et les coproduits. Un déchet consiste en une substance ou tout objet dont le producteur cherche ou a l'obligation de se débarrasser. Les sous-produits représentent toute matière n'étant pas le produit final visé, mais dont l'utilisation ultérieure et directe est certaine. Leur valorisation est partielle, spécifique ou locale. Au contraire, la valorisation économique des coproduits est totale. Les résidus agricoles peuvent être considérés comme l'une des ressources les plus abondantes, peu chères et renouvelables [1]. En Europe, les résidus de l'agriculture représentent 50% de la masse des récoltes et une énergie potentielle de 89 millions de tonnes d'équivalent pétrole [2]. Or actuellement une part non négligeable de ces résidus est incinérée ou enfouie sans contrôle, ce qui cause des problèmes environnementaux dans tous les compartiments : air, sol et eau. Le potentiel de pollution des résidus agricoles est élevé à long terme. Valoriser ces résidus permet de ne pas consommer des ressources primaires tout en produisant des produits durables. Il existe une grande diversité de résidus agricoles, issus de cultures annuelles (pailles, canes, fanes) ou pérennes (sarments, bois de taille), d'effluents d'élevage (fumier, lisiers), de déchets de bocage ou encore de cultures de plantes à parfum (paille de lavandin), qui peuvent être utilisés dans de nombreux secteurs. Ces effluents solides sont valorisables comme engrais mais peuvent également être convertis pour la production de bioénergies, biomatériaux ou biomolécules. Ils constituent donc une ressource importante dont il faut tirer profit. Leur utilisation ne requiert pas de culture dédiées et n'entre donc pas en compétition avec des usages alimentaires et ne présente pas d'effets néfastes sur la biodiversité. Au-delà de la réduction et du recyclage des résidus agricoles, de nouveaux procédés émergent pour utiliser cette matière première. Ceci répond aux ensembles de règles et de réglementations concernant l'environnement (Directive Européenne 2008/98) mais également à la production de nouveaux produits à plus haute valeur ajoutée. La Commission Européenne finance ainsi de nombreux projets relatifs aux technologies de traitement des résidus de l'agriculture visant à valoriser les sous-produits et à récupérer de l'énergie tout en minimisant les impacts sur l'environnement.

Dans ce contexte, le projet sino-européen H2020 “No Agricultural-Waste” (NoAW, 2016-2020, <http://noaw2020.eu>) vise à contribuer à la mise en place d’une “économie sans déchets”. Le projet NoAW regroupe 32 partenaires publics et privés d’une douzaine de pays (Figure 1).

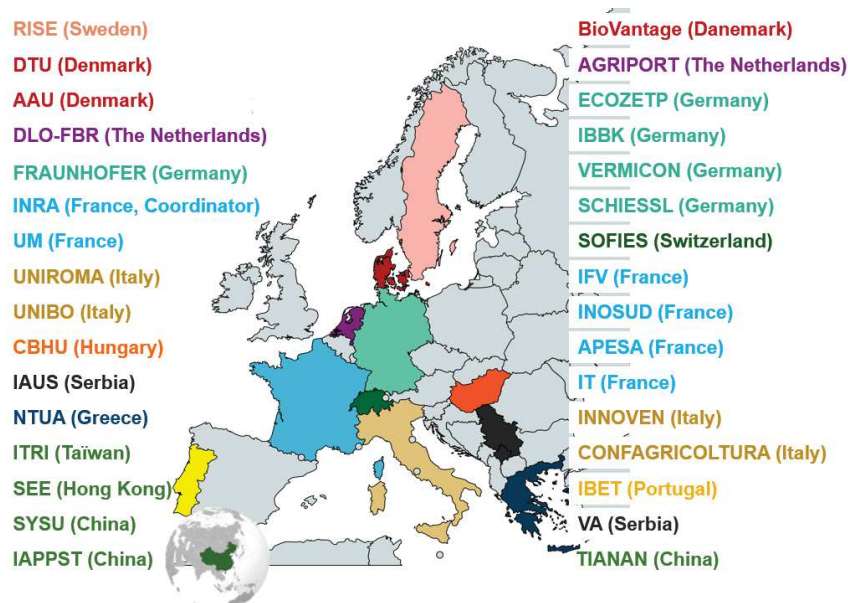


Figure 1. Partenaires impliqués dans le projet NoAW

L'équipe internationale de NoAW entend mettre en pratique les principes de l'économie circulaire en valorisant des résidus agricoles, et plus particulièrement les résidus de productions viti-vinicoles (e.g. sarments et marcs de vin), de blé (e.g. paille) et animales (e.g. fumier). NoAW vise à étudier le potentiel des agro-résidus afin de les transformer en un éventail de produits éco-efficaces, et ce en utilisant moins de ressources et en polluant moins. L'accent est mis sur la production de bioénergies, biofertilisants, biomatériaux et biomolécules. La conversion de ces résidus en bioproduits permet de remplacer une gamme importante de produits équivalents d'origine non-renouvelable, tout en apportant de la valeur ajoutée à des résidus pas ou peu valorisés. Ce travail est réalisé en se focalisant sur les contraintes et les opportunités territoriales et saisonnières ainsi que sur le développement d'outils de prédiction précoces des bénéfices environnementaux. Trois régions sont à l'étude : le Languedoc-Roussillon en France, la Vénétie en Italie et la Bavière en Allemagne. Un processus en cascade de valorisation des résidus agricoles est appliqué afin de maximiser leur potentiel (Figure 2). Un concept de bioraffinerie durable est élaboré autour de la digestion anaérobie. Les effets attendus sont la diminution de l'utilisation des ressources fossiles et la réduction des impacts négatifs d'une gestion inappropriée de la biomasse. Le projet NoAW cherche à apporter des solutions aux décideurs politiques et aux entreprises via :

- ✓ La création de concepts durables de bioraffinerie des résidus agricoles,

- ✓ Le développement et l'utilisation d'approches intégratives, en accordant une attention particulière aux impacts environnementaux du produit et de son processus, notamment en phase de conception,
- ✓ L'apport d'outils innovants et robustes pour le développement de stratégies de récupération des ressources résiduelles et minimiser les impacts négatifs sur l'eau, l'air et le sol.

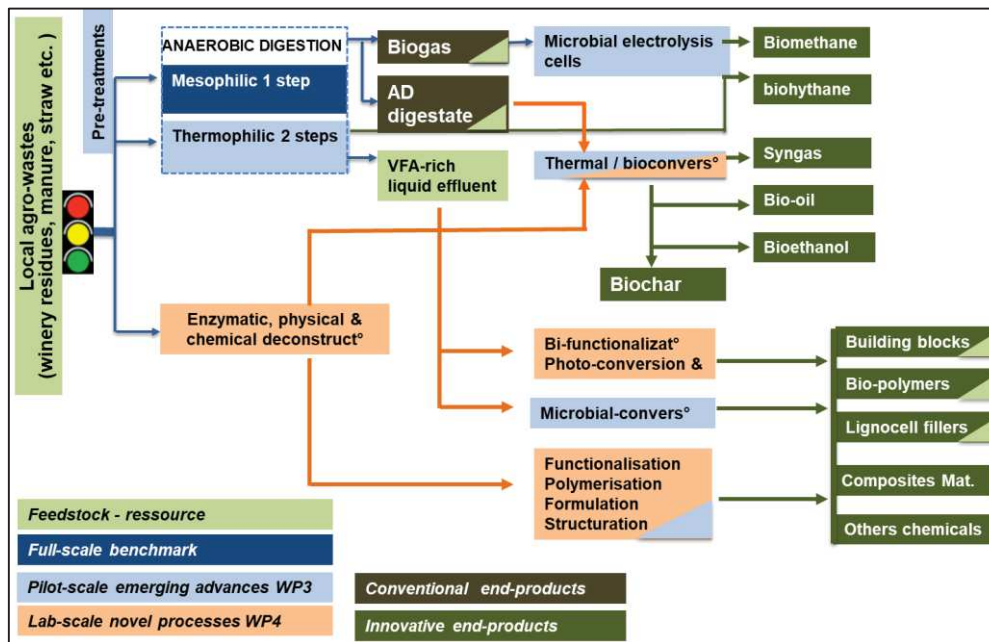


Figure 2. Approche générale du projet NoAW concernant la gestion des résidus agricoles

Le projet s'appuie sur 8 tâches (work packages ou WP) étroitement connectées (Figure 3). Des stratégies optimales de valorisation des résidus agricoles à une échelle régionale sont proposées (WP1), leur impact sur l'environnement est pris en compte (WP2) et de nouveaux modèles économiques sont élaborés (WP5). Des technologies sont développées notamment pour améliorer la digestion anaérobie (méthanisation) et la production d'un biopolyester bactérien, le polyhydroxybutyrate-co-valérate (PHBV) (WP3). Dans le WP4, des schémas de bioraffinerie sont proposés via l'exploration de nouvelles voies de valorisation en amont et en aval de la méthanisation afin de donner le maximum de valeur ajoutée aux résidus agricoles. En amont d'une valorisation par digestion anaérobie, l'extraction de molécules d'intérêts tels que les polyphénols et la production de charges de renfort pour des applications composites sont à l'étude. La digestion anaérobie conduisant à la production d'acides gras volatiles (VFAs) conjointement à la production de biogaz est explorée ainsi que leur valorisation de ces derniers pour la synthèse de PHBV en aval de cette technologie. Finalement, les technologies les plus prometteuses et les plus matures sont transposées à plus grande échelle dans le cadre du WP6.

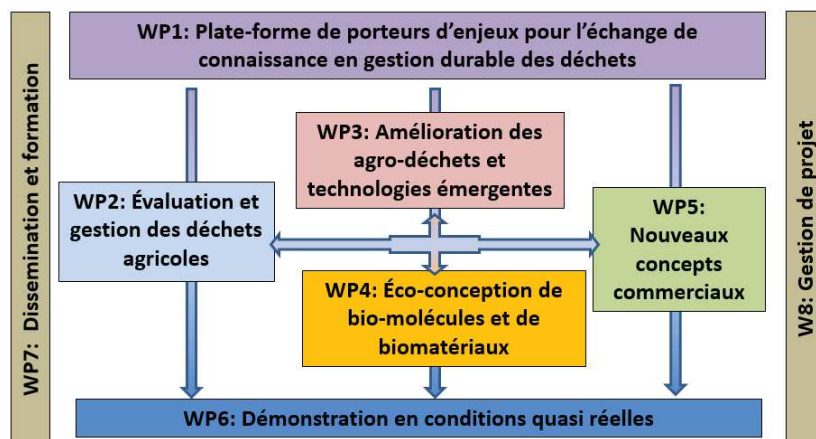


Figure 3. Articulation des principales tâches du projet NoAW

Dans le WP4, une attention particulière est accordée à la valorisation des résidus viti-vinicoles (sarments de vigne, marcs de vin), des déchets des industries de transformation des fruits et légumes en particulier de la pomme de terre pour des applications dans le domaine des matériaux. Dans un premier temps, des composés « plate-forme » sont produits ou extraits à partir de ces résidus agricoles (polyphénols, fibres lignocellulosiques...). Un même résidu peut donner lieu à la production de différents composés d'intérêt. Inversement, une classe de composés, par exemple les polyphénols, peut être obtenue à partir de différents agro-résidus, en utilisant également différents procédés. Puis, ces composés « plate-forme » sont combinés et transformés afin de développer des produits à valeur ajoutée. Cette thèse s'inscrit dans le WP4 et vise à valoriser les sarments de vigne pour une application dans le domaine des matériaux composites, en utilisant comme matrice polymère le PHBV développé dans le cadre du WP3 (Figure 4).

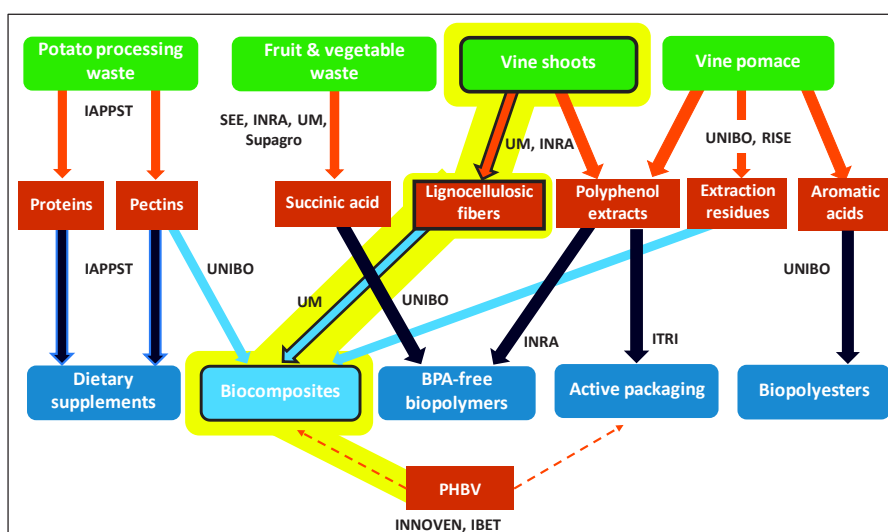


Figure 4. Positionnement de la thèse au sein du WP4 du projet NoAW

La plupart des résidus agricoles solides correspondent à de la biomasse lignocellulosique, mélange complexe de cellulose, d'hémicellulose, de lignine, de minéraux et d'une petite quantité d'extractibles. Ils correspondent aux résidus de cultures, c'est-à-dire aux parties de la plante qui ne présentent pas de valeur nutritive pour l'Homme. Les principales sources sont les pailles de céréales et d'oléagineux (culture annuelle) et les sarments de vigne (culture pérenne). En France, environ 55 millions de tonnes de résidus de culture sont produits chaque année [3]. Ces résidus lignocellulosiques peuvent être utilisés comme matières premières pour l'élaboration de charges de renfort pour la fabrication de matériaux biocomposites, pour des applications dans les domaines de l'emballage, de la construction, de l'horticulture ou de l'automobile. Comparativement aux fibres de verre, les fibres lignocellulosiques présentent également l'intérêt d'être moins denses, et moins abrasives vis-à-vis des équipements de transformation et de mise en forme [4]. Elles ont également un impact sur l'environnement réduit et sont biodégradables en conditions naturelles [5]. Les charges de renforts issues de résidus lignocellulosiques (agriculture, forêts, ville, industrie alimentaire) ont l'avantage de ne pas être issues de cultures dédiées contrairement aux fibres naturelles techniques telles que les fibres de coton, de lin ou de chanvre. Leur incorporation dans des matrices polymères réduit donc le coût environnemental et économique des produits. Les premières utilisations de biocomposites remontent aux années 1 500 av. JC quand un mélange de boue et de paille fût utilisé pour créer des bâtiments solides et durables. La paille a continué à renforcer les anciens objets composites, notamment la poterie et les bateaux. Parmi les résidus agricoles solides, on trouve les sarments de vigne. Les sarments de vigne correspondent au bois de taille de la vigne et sont récoltés en hiver, entre décembre et février selon les régions. Ils constituent un sous-produit viticole qui n'est actuellement pas bien valorisé. Les sarments sont le plus souvent broyés et laissés à même le sol ou retirés des rangs pour être brûlés malgré les interdictions car certains vigneronns souhaitent s'en débarrasser. On trouve également quelques applications dans le domaine des granulés pour chaudière, de la fabrication de panneaux de particules ou encore comme combustible pour barbecues mais cela reste marginal. Les sarments secs peuvent être collectés gratuitement ou négociés aux alentours de 60€/t [6]. Ils sont l'un des principaux résidus étudiés dans le projet NoAW car il s'agit d'une ressource locale abondante et peu valorisée en région Languedoc-Roussillon, l'une des régions viticoles les plus importantes d'Europe.

D'autre part, une problématique liée à l'usage de plastique a fait son apparition ces dernières années. Le plastique possède de nombreux avantages : léger, peu cher et facile à transformer. Mais d'importants inconvénients poussent à repenser sa production, son usage et sa fin de vie. Les plastiques sont pour la plupart pétro-sourcés et représenteront 20% de la consommation en pétrole et 15% des émissions de gaz à effet de serre d'ici 2050 si le rythme de production continue [7]. En effet, la production mondiale de plastique augmente chaque année et a atteint les 350 millions de tonnes en 2018 [7]. Cette augmentation va de pair avec une accumulation exponentielle des déchets plastiques non biodégradables dans l'environnement. En 2016, en

Europe, seulement 27 millions de tonnes de plastiques ont été collectés et traités (recyclage, incinération, ou enfouissement) sur les 60 millions de tonnes produites. La différence va en partie dans le stock actuellement utilisé (in-use stock) mais entre en grande partie dans la pollution globale plastique. Geyer et al. [8] ont estimé que 60% de tout le plastique déjà produit a été rejeté et s'accumule dans des centres d'enfouissement ou dans l'environnement naturel (Figure 5). Les déchets plastiques sont si répandus dans l'environnement qu'ils peuvent être utilisés comme un indicateur géologique de l'Anthropocène [9]. Ainsi une part significative de plastiques finit dans les sols et les océans et le terme de « septième continent » a fait son apparition. Les plastiques dans les milieux marins sont en train de devenir un sérieux problème du fait de leur persistance et de leurs effets sur la vie sauvage et les humains. Les débris plastiques se désagrègent progressivement, se fragmentent en microparticules qui deviennent extrêmement difficiles à collecter et sont malheureusement faciles à ingérer. Les organismes ne sont pas adaptés à cette pollution aux particules fines, de plus, les plastiques peuvent facilement devenir des vecteurs de pénétration d'éléments toxiques. Les effets des plastiques sur la santé sont encore peu connus.

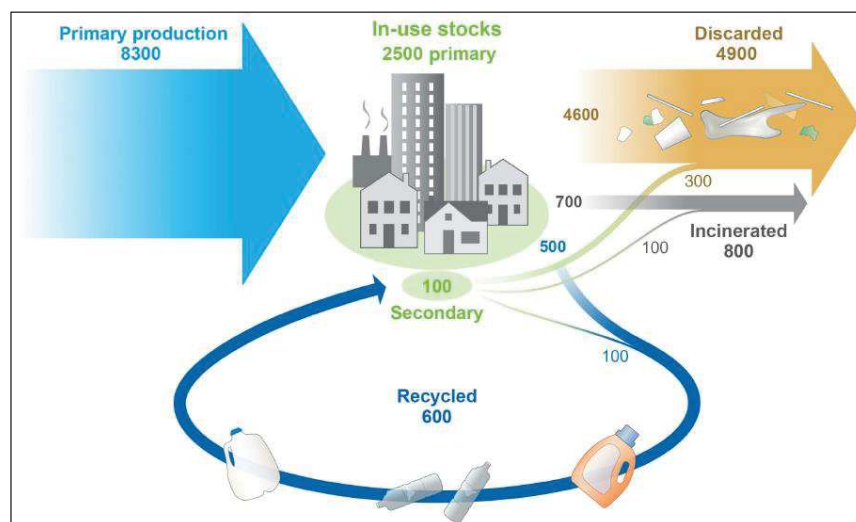


Figure 5. Production mondiale, usage et fin de vie des plastiques (de 1950 à 2015; en millions de tonnes) [8].

Le développement de matériaux biocomposites biodégradables en conditions naturelles avec incorporation de fibres issues de la conversion de résidus agricoles constitue une des réponses à ces problèmes. Dans le secteur de l'emballage alimentaire (65% des emballages), le secteur le plus consommateur de plastique, l'enjeu est particulièrement important en raison d'une très courte durée de vie par rapport aux autres secteurs. Actuellement, le polyéthylène (PE) et le polypropylène (PP) sont les plastiques les plus utilisés dans ce secteur. Ils sont dérivés de ressources fossiles et ne sont pas biodégradables. L'emballage alimentaire a été identifié comme un secteur émergent pour les matériaux biocomposites [10].

Il y a un problème de suremballage, utilisant plus de plastique que le produit n'en a réellement besoin, mais l'absence complète d'emballage n'est pas une solution. En effet, il assure la protection du contenu contre les dommages physiques, la contamination chimique et microbienne et, dans une moindre mesure, il constitue un support d'informations sur le produit. Or, près du tiers de la nourriture comestible produite pour la consommation humaine est perdue ou gaspillée dans le monde, ce qui représente environ 1,3 milliard de tonnes par an [11]. La substitution des ressources fossiles par des ressources renouvelables n'implique pas nécessairement une réduction de l'impact environnemental associé. Dans le secteur des matériaux, le recyclage est considéré comme le meilleur scénario. Cependant, la majorité des plastiques ne peut pas être recyclée et contient des additifs toxiques. De plus, il existe toujours des fuites dans le système de collecte et dans le cas d'emballage alimentaire le recyclage n'est pas toujours viable. Des matériaux biodégradables peuvent être un atout contre l'accumulation des déchets plastiques.

Le développement de matériaux durables, notamment pour des applications dans le domaine de l'emballage, est ainsi devenu une nécessité. Le matériau doit être fonctionnel, avoir l'impact environnemental le plus faible possible tout en restant économiquement viable. Les réglementations à l'échelle européenne cherchent à limiter l'usage du plastique à usage unique. Par exemple, la loi EGalim, promulguée en novembre 2018, interdit 8 produits plastiques dont les cotons tiges ou les bâtonnets mélangeurs pour boissons. La Commission Européenne vise à encourager le développement de matériaux biodégradables en conditions naturelles pour substituer les plastiques d'origine fossile et non biodégradables, et finance ainsi de nombreux projets sur cette thématique. Par exemple, les projets GLOPACK, Res Urbis, ou encore USABLE sont en cours. Parmi les polymères biosourcés et biodégradables en conditions naturelles, on trouve les polyhydroxyalcanoates (PHAs) qui constituent toute une famille de copolymères. Ces polyesters sont produits par des bactéries à partir de sucres et de lipides qui peuvent notamment venir de résidus des industries agro-alimentaires (lactosérum, margines d'olive, résidus de fruits et légumes, etc.), de résidus agricoles (fumiers, rafles de maïs, etc...) ou de résidus urbains. Il existe une grande variété de monomères possible pouvant entrer dans la composition des PHAs, leurs donnant des propriétés différentes. Le poly(3-hydroxybutyrate-co-valérate) (PHBV) est un polymère thermoplastique qui présente des propriétés qui se rapproche de celles du PP. Ces biopolymères sont cependant encore très coûteux, peu disponibles à échelle industrielle et ne possèdent pas toutes les propriétés fonctionnelles souhaitées par rapport aux plastiques conventionnels.

L'utilisation de résidus agricoles lignocellulosiques pour l'application composite soulève un certain nombre de défis scientifiques. Le principal verrou de ces fibres naturelles est leur caractère hydrophile, conduisant à une faible compatibilité avec de nombreuses matrices polymères apolaires et une grande sensibilité à l'eau (une variation de l'humidité relative peut

conduire à un gonflement ou une rétractation des fibres générant une décohésion de l'interface et une modification des propriétés fonctionnelles du matériau). Une augmentation de l'affinité entre les deux constituants est donc souvent recherchée pour améliorer l'adhésion interfaciale fibre/matrice et limiter la formation d'agrégats de fibres dans le matériau composite. A titre d'exemple, lors d'un précédent projet européen coordonné par l'équipe (FP7 EcobioCap 2011-2015), des matériaux biocomposites PHBV/fibres de paille de blé ont été mis au point et il a été conclu qu'un taux de charge élevé permettrait de réduire le coût et l'impact environnemental du matériau [12]. Il avait été également mis en évidence la difficulté à discriminer les phénomènes impactant les relations structure/propriétés du fait des changements de la structure et donc des propriétés de la matrice polymère lors de l'introduction des charges lignocellulosiques, de la réactivité intrinsèque des constituants et de la complexité de structure et de composition des fibres lignocellulosiques (Berthet et al., 2015). Les propriétés à l'interface charge/matrice ont tout de même été identifiées comme un facteur clé influençant les propriétés finales du composite. Un pré-traitement des fibres de paille par torréfaction avait ainsi été investigué pour augmenter l'hydrophobicité des fibres de paille [13]. L'inconvénient d'un tel traitement est qu'il conduit à une modification de l'ensemble des propriétés intrinsèques de la charge (i.e. composition, cristallinité, morphologie), rendant encore plus difficile la compréhension de l'effet de renfort. L'usage d'un pré-traitement de surface des fibres sans solvant permettrait de mieux comprendre l'effet de la modification des propriétés interfaciales.

Un deuxième verrou est lié à la variabilité, la saisonnalité, la complexité et l'hétérogénéité de la ressource. Dans le cas des sarments de vigne, les propriétés intrinsèques de la biomasse varient selon le cépage, la date de la taille, la localisation des vignes et les conditions climatiques [14]. Il existe une grande variété de cépages (plus de 50), de mode de taille et donc de sarments de vigne. Un des cépages le plus représenté est la Syrah, il est le plus répandu en Languedoc-Roussillon (16.4% des surfaces en vigne) [15]. Cette variabilité de la ressource peut être un obstacle à l'usage des résidus agricoles par les industriels. Les fibres naturelles ont des structures plus complexes et hétérogènes que les fibres synthétiques ce qui leur donne leurs propriétés intéressantes mais également rajoute une difficulté à leur utilisation. De nouvelles voies impliquant différents procédés doivent être mises en place pour la gestion de ces résidus et leur transformation en charges de renfort. Le défi à relever est donc la production de charges lignocellulosiques à partir de sarments de vigne présentant des caractéristiques contrôlées (Figure 6). Une des expertises de l'UMR IATE est le fractionnement par voie sèche. Dans le cadre du projet EcoBioCAP et du projet MALICE, les charges de renfort ont été produites par fractionnement par voie sèche de la biomasse native [16,17]. La combinaison de procédés de broyage et éventuellement de tri permet d'obtenir des particules avec une morphologie et un diamètre médian apparent contrôlés, paramètres clés impactant



les propriétés finales des matériaux composites. A ce jour, les sarments de vigne n'ont été étudiés que très rarement pour la production de charges de renfort [18,19].

Dans ce contexte général, cette thèse vise à développer et étudier de nouveaux matériaux composites biosourcés et biodégradables dont les constituants sont tous dérivés de résidus agricoles : le PHBV (produits à partir de résidus agricoles) comme matrice et les sarments de vigne comme charges de renfort (Figure 6 et Figure 7). Cela doit permettre de répondre à deux enjeux majeurs : la valorisation des résidus agricoles et la substitution des plastiques non biodégradables et d'origine fossile. L'application souhaitée est une barquette alimentaire rigide. L'objectif est de produire un matériau respectant la contrainte fonctionnelle tout en minimisant l'impact environnemental. De nouvelles connaissances sur les relations entre le procédé de mise en œuvre des biocomposites, leur structure et leurs propriétés fonctionnelles sont attendues. Les propriétés mécaniques mais aussi les propriétés de transferts de matière liées à l'application emballage sont examinées. De plus, les biocomposites sont développés en considérant une balance performance/coût environnemental.

Cette thèse se focalise ainsi sur deux questions scientifiques majeures :

- (i) étude de l'impact de l'interface charge/matrice sur les propriétés fonctionnelles des matériaux biocomposites via un pré-traitement de surface des particules lignocellulosiques
- (ii) étude de la durabilité de tels matériaux par évaluation dès la conception des impacts environnementaux, de leur biodégradabilité et de l'impact de la variabilité de la biomasse.

Une approche globale et transversale autour des matériaux biocomposites développés est recherchée. Ainsi différentes disciplines sont abordées : chimie organique, génie des procédés, sciences des matériaux et sciences de l'environnement.

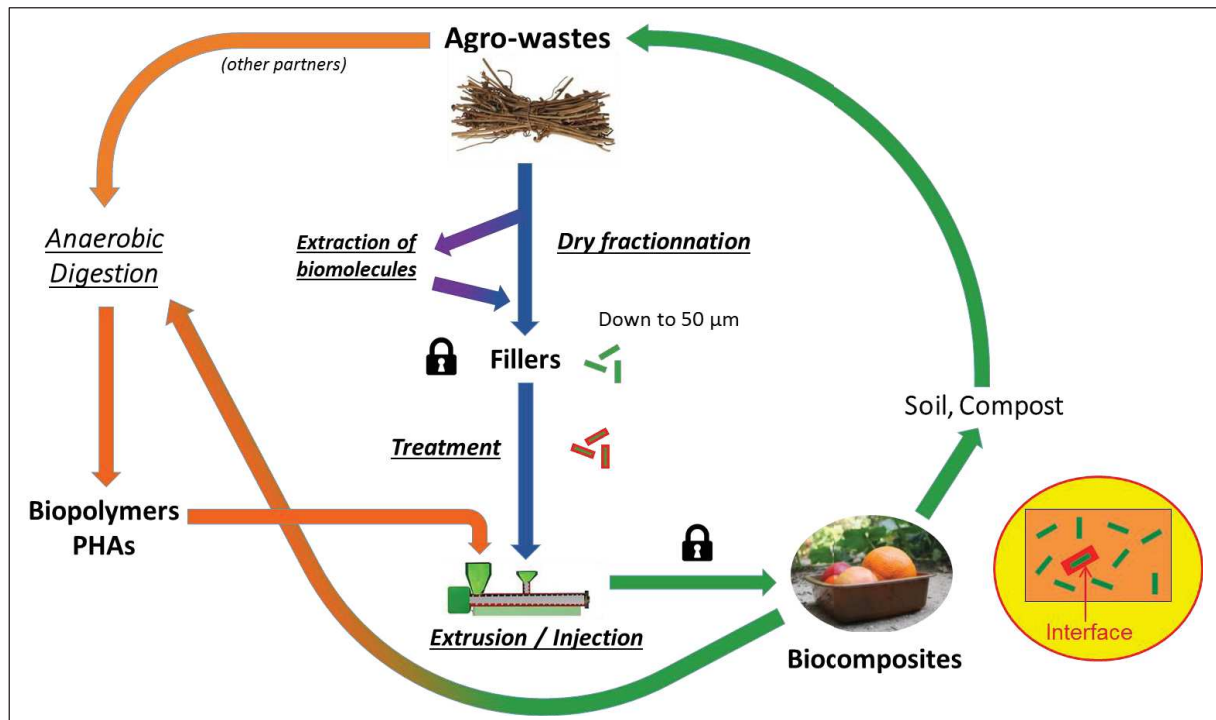


Figure 6: Etapes de la thèse avec les verrous

Une présentation de l'état de l'art dans le chapitre 1 aidera à positionner cette thèse au regard des travaux antérieurs. Puis, le chapitre 2 recensera l'ensemble des méthodes utilisées afin de pouvoir mener les recherches des 3 chapitres suivants.

La modulation des interactions charge/matrice est explorée dans le chapitre 3. Il s'agit de parvenir à l'optimisation des propriétés des composites en explorant un pré-traitement des fibres, en modulant l'interphase. L'estérification en phase gaz est d'abord examinée sur des particules micrométriques modèle de cellulose. Les conditions de ce pré-traitement et son effet sur la cellulose sont étudiés. Une fois les conditions expérimentales fixées, les particules de cellulose greffées sont incorporées dans du PHBV et leurs propriétés fonctionnelles déterminées et discutées en lien avec la structure des matériaux.

Dans le chapitre 4, la possibilité d'utiliser les sarments de vigne comme matière première pour la production de charges de renfort est explorée. L'impact de la variabilité des sarments sur les propriétés intrinsèques des sarments est évaluée via la collecte d'échantillons issus de 4 cépages durant 3 années consécutives. Les sarments récupérés sont préalablement séchés puis broyés finement par voie sèche. Les particules obtenues sont caractérisées avant d'être incorporées dans une matrice PHBV. Le traitement étudié dans le chapitre 3 est également appliqué aux particules de sarments de vigne. Son effet sur les fibres puis dans le composite est examiné et discuté. Dans une logique de valorisation en cascade, l'effet de renfort de sarments épuisés

(après extraction de polyphénols) est comparé à celui des sarments bruts. De plus, la performance de composites à base de marcs de raisin, un autre résidu de la filière viti-vinicole, sera confrontée à celle des matériaux à base de sarments de vigne.

Finalement, la durabilité des matériaux est évaluée dans le chapitre 5. L'impact environnemental de l'usage des sarments de vigne pour l'application composite est déterminé via une analyse de cycle de vie. Les données permettant cette étude proviennent des acteurs de la filière à la fois viticoles mais aussi de la plasturgie. Des barquettes alimentaires rigides de différentes compositions sont comparées d'un point de vue environnemental mais aussi économique. L'impact de la formulation et du procédé de production des charges de renfort sur la biodégradabilité des matériaux composites est également évaluée.

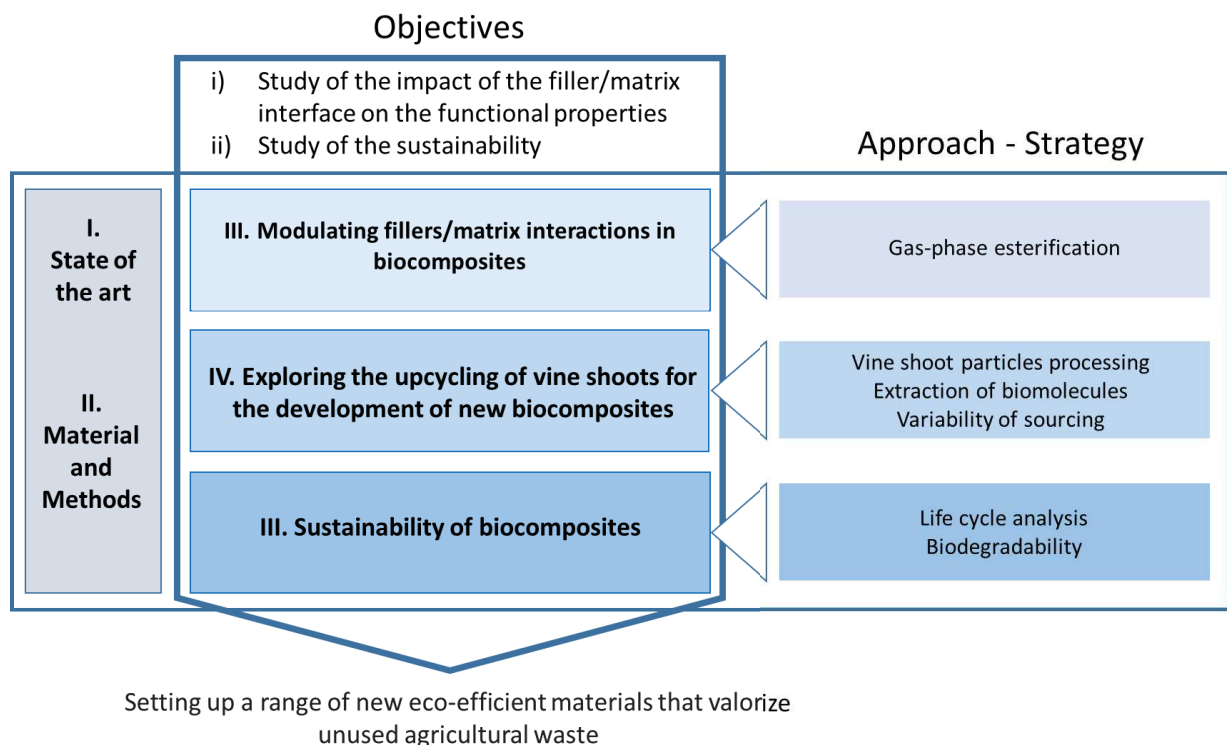


Figure 7. Relations stratégie-objectifs de la thèse

# Chapter I. State of the art

## Chapter I. State of the art

Cet état de l'art vise à donner aux lecteurs une vue d'ensemble du contexte dans lequel s'inscrit la thèse et à identifier les verrous à lever afin de valoriser les sarments de vigne par la production de biocomposites. Il se compose de trois grandes parties.

La première partie se focalisera sur les caractéristiques de la biomasse lignocellulosique et son utilisation pour la production de charges de renfort. Une attention particulière sera accordée aux sarments de vigne en détaillant leurs usages actuels et les voies de valorisation potentielles de ce résidu viticole. Les principales propriétés des charges de renforts jouant sur la qualité des composites finaux seront abordées.

Dans une deuxième partie, les techniques de modification des fibres naturelles afin d'améliorer leur compatibilité avec les matrices polymères seront présentées. L'accent sera porté sur les traitements de surface par estérification, leurs effets sur les propriétés des fibres lignocellulosiques et des composites.

Finalement, les caractéristiques des bioplastiques existants et particulièrement des PHAs seront rappelées. La biodégradabilité et les analyses du cycle de vie des biocomposites seront examinées afin de définir les enjeux environnementaux actuels liés aux biocomposites.

## I. Lignocellulosic fillers

To better understand the behavior of composite materials filled with lignocellulosic fillers and thus to apprehend the fiber/matrix interface, we will present in a first part the different possible sources of natural fillers and their variability will be exposed. Then, the main constituents of the lignocellulosic biomass will be exposed. Then, a special attention will be given to vine shoots, the lignocellulosic residue that has been selected in this thesis. Finally, main intrinsic properties of natural fillers known to impact final functional properties of composites will be described.

### I-1 Sources of lignocellulosic biomass

Natural fibers include those produced by animals (silk, wool), plant and geological processes (asbestos). The focus will be on vegetal fibers, i.e. lignocellulosic fibers, which are widely available all around the world at a quite low cost. They are generally annually produced, except for wood, which needs several years before being exploited. Such materials are inherently fully biodegradable, due to their enzymatic generated structure, which can be depolymerized by other suitable enzymes. As listed by Satyanarayana et al. [20], lignocellulosic fibers have many significant advantages such as renewability, sustainability, lower impact on global warming, biodegradability, low cost and non-dangerous emissions during processing, storage and disposal. They display also a low density (around  $1.5 \text{ g.cm}^{-3}$ ) as compared for example to glass fibers ( $2.5$  to  $2.6 \text{ g.cm}^{-3}$ ), giving the possibility to obtain lighter composite materials. They are non-abrasive for machinery and display high stiffness and less impact on the health of composite manufacturers. However, they are thermally sensitive and have a hydrophilic character [21]. They also display a lack of consistency of fiber qualities, high levels of variability in fiber properties related to the location and time of harvest, processing conditions [22]. The lignocellulosic biomass that can be used as fillers in composites is here classify from their source: dedicated culture, forest residues, agricultural residues and food industries residues.

#### I-1.1 Dedicated cultures

For centuries, vegetal fibers have been exploited for craft products such as textile, rope production, furniture, and much more applications. The most famous natural technical fibers include flax, hemp, cotton lint, and sisal fibers. Today, these fibers are globally produced up to million tons. Depending on the final uses these fibers were chosen according to their mechanical properties. Indeed, textile and rope are submitted to deformations and tensions to which they have to withstand. Therefore, most of craft fibers exhibit high tensile strength, typically  $200\text{-}800 \text{ MPa}$  [22]. They also are quite rigid, as reflected by their generally high tensile modulus. In the field of biocomposites research, craft fibers have been widely studied precisely

for these high performances. In these cases, the plant or selected cultivars are produced in dedicated fields.

## I-1.2 Forest, agricultural and food industries residues

On the opposite, residues-based composites were studied in order to valorize large amounts of biomass residues from agriculture, forestry and food industries, regardless of their intrinsic properties. Production of the main product accounts for more than billions of tons and usually generate 50% of residues. Their mechanical properties are less documented than craft fibers, i.e. their tensile strength and tensile modulus are lower [23]. The extraction of biomass from forests to produce paper, furniture and energy generates large amounts of forest residues (branches, tops, bark, etc) [24]. In agriculture, the annual crops residues are mainly cereals' straws (wheat, barley, maize), oleaginous (rapeseed, sunflower, soy, linseed) or protein crops (beans, peas, lupine). In case of straws, they are ground and landfilled or pressed into bales to be exported. It is considered that one third of cereal straw are used as litter for breeding. Straws can be used directly as fuel or be transformed into pellets for furnace. The use of straw as materials (insulation, pulp ...) is still very marginal. Usually, most the agricultural residues are not well valorized. Table 1 presents some lignocellulosic residues studied as fillers in composites materials.

Table 1. Works about the use of residues in composites

Fiber reinforcement	Matrix polymer	Source
Animal manure	PE, PP	[25]
Bagasse	PE, PP	[26,27]
Corn stalk	PP, PE	[27,28]
Grape pomace	PBS	[29]
Olive pomace	PHBV	[30]
Rice straw	PE	[26]
Sunflower stalk	PP	[27]
Vine shoot	PE, PP	[18,19]
Wheat straw	PP, PE, PHBV	[31-33]
Wood flour	PE, PP	[34,35]

The reduction of waste in the food and agriculture processing has become a mandatory standard within the most developed countries. The European Union in Directive 2008/98/EC stated that “waste prevention should be the first priority of waste management, and that reuse and material recycling should be preferred to energy recovery from waste.” Thus, new alternatives to manage the large amounts of biomass residues become one of the biggest challenge.

## I-2 Biochemical composition of lignocellulose biomass

Lignocellulose is a complex hierarchical build-up of several biopolymers, which is found in different biomass: wood, stem, leaf, fruit or seed. Its chemical composition varies within the parts of the plant but also from a plant to another according to the climate or the maturity of plant cells. The predominant components are carbohydrates that includes cellulose, hemicelluloses and pectins. These sugar-based biopolymers are associated with a complex polymer named lignin. In lower amounts, there are also proteins, extractives (fatty acids, waxes...) and inorganic compounds (ashes). This part will give key elements on these constituents.

The chemical compositions of natural fibers vary extensively between the distinct fiber types. Biochemical compositions of some natural fillers from various origins are given in Table 2.

Table 2. Biochemical composition of some natural fillers (adapted from [23,36,37])

Natural filler	wt% cellulose	wt% hemicellulose	wt% lignin	wt% pectin	wt% fat/wax	wt% ash
Hardwood	38-51	17-31	21-31	0-1	0.4-0.5	0-0.5
Softwood	33-41	20-29	27-32	0-1	0.4-0.5	0-1
Bagasse	25-45	28-32	15-25	-	-	1-4
Coir	32-53	0.2-0.3	40-45	3-4	1-2	2-10
Corn stalks	35-40	17-35	7-18	-	-	6-11
Flax	60-81	11-21	0.9-5	0.9-3.8	1.3-1.7	1.5
Grasses	25-40	25-50	10-30	-	-	5-7
Hemp	57-92	6-22	2.8-13	0.8-2.5	0.7-0.8	0.7-3
Jute	51-84	12-24	5-14	0.2-4.5	0.4-0.8	0.5-2
Miscanthus	37-45	18-36	20-26	-	1-2	2-6
Rice straw	29-35	23-26	17-19	-	-	10-20
Wheat straw	29-55	15-27.2	12-28	-	9.5-11.2	3-9

Cell walls of natural fibers comprise microfibrils of cellulose that are embedded in a matrix of hemicellulose, pectins, proteins and a lignin network. It is forming a tri-dimensional bio-assembly complex (Figure 8).

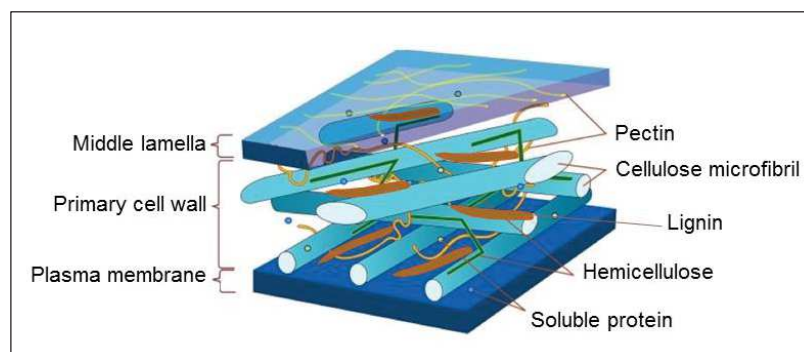


Figure 8. Structure of the wall of fiber cell



The elementary fibers are separated by the middle lamella rich in pectin and lignin. The amount of non-cellulosic components decreases gradually within the inner walls of fibers.

## I-2.1 Cellulose

Cellulose is the main resource from the biomass and the more abundant macromolecule on the planet. It represents more than half of the biomass in Earth [38]. It is one of the primary constituents of plant cell wall and it is associated with other polysaccharides and lignins. Cellulose is the succession of several homogeneous and linear chains of D-glucopyranose, or anhydroglucose unit (AGU), linked by glycosidic bonding  $\beta$ -(1-4). The base unit is cellobiose, a dimer of glucose (Figure 9). The degree of polymerization of cellulose varies between 1000 and 30000 with a large polydispersity [39].

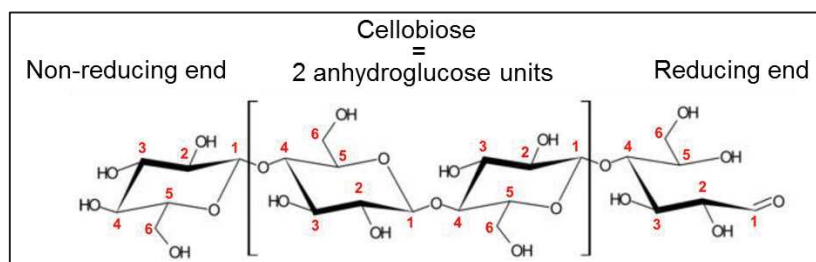


Figure 9. Molecular structure of the cellulose

Individual cellulose chains are linked together by intra and inter-molecular bonding (hydrogen bonds, Van der Waals). Crystalline cellulose is obtained when the cellulose chains are aligned and aggregated in larger entities. The main lattice form is type I for native cellulose. Thanks to this crystallized structure, cellulose provides stiffness, strength and structural stability to natural fibers.

The cellulose is widely used in different applications: energy, building (wood); paper, packaging (pulp), textile (viscose), or even plastics after modification (acetates, nitrates).

## I-2.2 Hemicellulose

Hemicelluloses are branched polysaccharides with low DP ( $<200$ ) and they form amorphous structures in the cell wall. Main classes of hemicellulose are xylans, glucomannans, and xyloglucans. They are mainly composed of 5 and 6 carbon sugars: D-glucose, D-xylose, D-galactose, L-fucose, D-glucuronic acid, L-arabinose and D-mannose. These sugars are linked by  $\beta$ -(1-4) bonds and branching points such as (1-2), (1-3) or (1-6). Hemicellulose polymers are

non-crystallizable but contribute to the structural organization of cell wall as matrix component. Hemicelluloses are associated with cellulose fibrils by hydrogen bonds. They are easily hydrolysable molecules, which are easy to separate from cellulose during paper treatments.

### I-2.3 Lignin

It is a non-linear phenolic polymer composed of phenylpropene units. This amorphous macromolecule is the second most abundant natural polymeric materials in plants (about 20 to 30% of the carbon in plants). Its complex structure, with a lot of and highly cross-linking, is still not deeply understood. Usually, lignin is composed of three basic buildings blocks: p-hydroxyphenyl, guaiacyl, syringyl units (Figure 10). Other aromatic compounds can be also present such as coumaric and ferulic acids. Lignin is responsible for strength, rigidity, impermeability and protection against microbial pathogens of cell walls. Lignins are intimately associated with hemicellulose and cellulose within plant cell walls through covalent and non-covalent interactions [40].

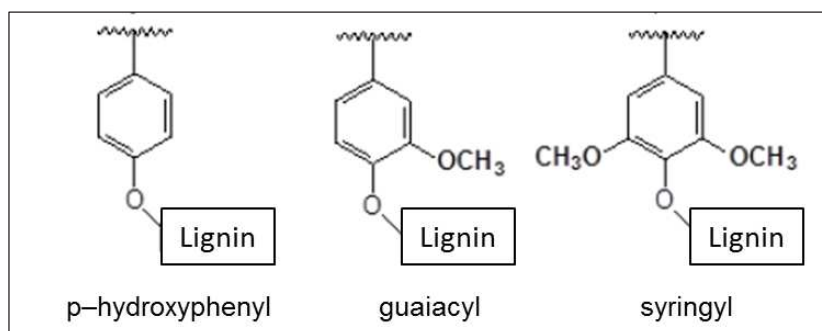


Figure 10. Chemical structure of p-hydroxyphenyl, guaiacyl and syringyl units that compose lignin.

### I-2.4 Pectins

Pectins are also polysaccharides. They are composed of a main chain of galacturonic acids linked by  $\alpha$ -(1,4) bonds. Rhamnose molecules are intercalated by 1,2 and 1,4 bonds forming a characteristic zigzag chain. Branchings with galactan and arabinan are also present on this main chain. Pectins are matrix components in the cell walls and act as adhesives in the middle lamellae between plant cells. Pectins are mainly present in non-wood fibers.

## I-2.5 Proteins

The proteins are polymers of amino acids mainly proline, glycine, hydroxylamine in plants. They play a key role in the building of the cell walls interacting with other cell walls components during cell growth. They are present in a small amounts and enzymes or toxins are part of them.

## I-2.6 Extractives

Extractives are small molecular organic compounds that can be extracted with organic solvents or water. The composition varies greatly between and within species. They include fatty acids, fatty alcohols, free sterols, ferulic acid, esters, waxes, sterols, and other aromatic compounds.

Among the extractives, polyphenols represent the main organic extractives from grapevine. Polyphenols are characterized by the presence of phenolic groups, associated in structures of various complexity. They are part of secondary metabolites of plants and are usually produced by the plant during stresses and as defences against UV or different pathogens (fungi, insects, bacteria) [41]. Polyphenols are divided into several categories that are represented in Figure 11.

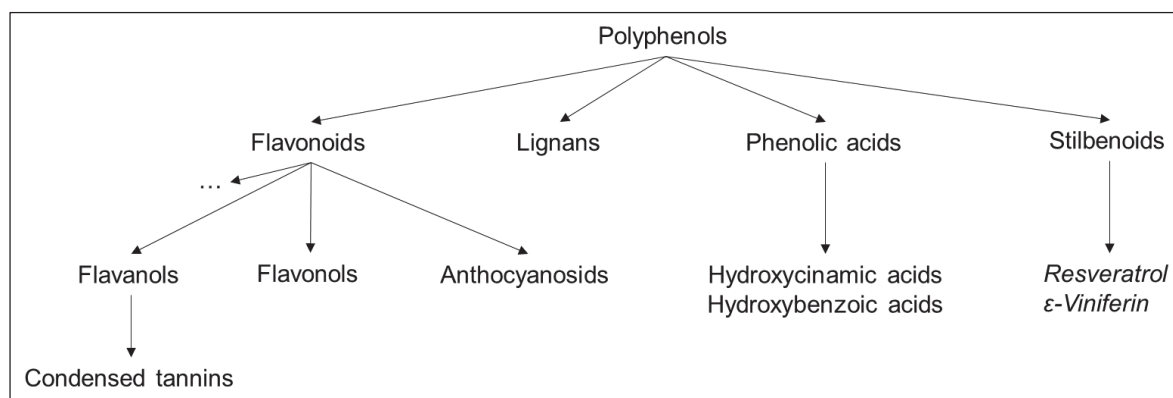


Figure 11. Categories of polyphenols

Polyphenols are frequently found in fruits and vegetables; their quantity varies according to environmental factors of growth and storage. Polyphenols play a fundamental role in the sensory analysis of compounds (color and organoleptic character). The pigments that indicate that fruits and vegetables are ripe are also part of the polyphenol family. In addition, the polyphenols have antioxidant properties and are therefore of interest to the pharmaceutical and cosmetic sector. In grapes, the most famous stilbene example is resveratrol (Figure 12) that can be also extracted from vine shoots (see I-3.4).

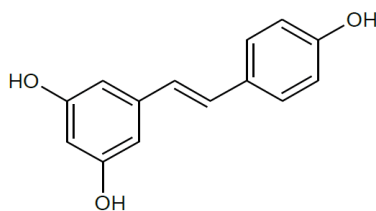


Figure 12. Chemical structure of trans-resveratrol.

## I-2.7 Methods to assess the biochemical composition of lignocellulosic biomass

There are different techniques to determine the composition of natural particles, the main methods are summarized in Table 3.

Table 3. Methods to determine the composition of lignocellulosic biomass

Methods	Description	Source
Van Soest	The substrate is attacked using a neutral and then acidic detergent solution, followed by a treatment with sulfuric acid 72%. Three residues are obtained: <ul style="list-style-type: none"> <li>• neutral detergent fiber (NDF): insoluble total fiber (cellulose + hemicellulose + lignin)</li> <li>• acid detergent fiber (ADF): lignin-cellulose complex</li> <li>• sulfuric lignin (ADL): lignin</li> </ul>	[42]
Double hydrolysis	Double hydrolysis with sulfuric acid, first concentrated, then diluted. The cellulose and hemicellulose are hydrolyzed and solubilized. They are, then, quantified by HPLC, through their constitutive sugars. The lignin is determined according to Klason method.	[43]
Gravimetric	A Soxhlet extraction to remove extractives, is followed by a treatment with a sodium hydroxide solution (solubilization of hemicellulose). The lignin is determined according to Klason method. The cellulose content is calculated by difference.	[44]

## I-3 Focus on vine shoots

Vine is one of the most spread cultures in the world. It is one of the main agricultural activities in European Mediterranean countries. According to the International Organisation of Vine and Wine, the world total area dedicated to vineyard was around 7.6 million hectares in 2016. Europe represents a little less than the half with 3.3 million hectares and 785 thousand hectares are in France.

Vine is an Angiosperm, belonging to *Vitaceae* family, *Vitis* genus, that gives in natural state climber shrub like liana species. The vine from *Vitis vinifera* is the most cultivated because of the quality of the fruits. The vine is perennial plant that is harvested once a year, being a

seasonal crop and after that, it is pruned. Vine shoots are agricultural residues from this annual pruning.

Vine shoots are the canes that comes from the vine cordon (Figure 13). Their main function is to bring the sap to the various organs of the vine to promote their development.

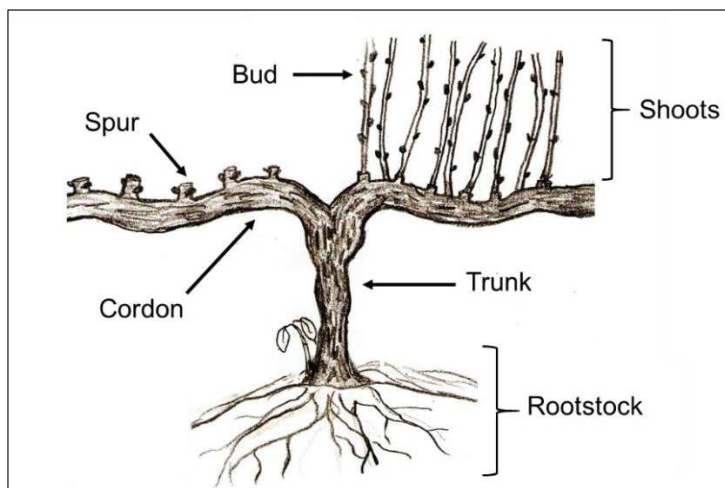


Figure 13. General scheme of a vine

There are different words employed for vine shoots: vine pruning wood, vine canes, vine trimming wood, vine stems, etc...

### I-3.1 Vineyard cultivation practices

During the spring, young green shoots are growing then, before winter, shoots undergo physiological changes and turn woody. This phenomenon, called “hardening”, is a lignification process. Usually, grapes are produced on shoots that have grown from the buds of the previous year. Thus, winegrowers need to properly prune during winter. Moreover, in order to get a good harvest with mature grapes, it is necessary to regulate the number and the volume of bunches of grapes. Vine pruning allows to reach the balance between vegetative and fruit growth to get the higher quality and quantity of grapes. Pruning also affects vine form, shape, and size. Every year, it generates an important quantity of agricultural residues: the vine shoots. These residues correspond to 93% of the wastes obtained in the viticulture [45]. The annual average production is estimated around 2 tons per hectare and per year. In France, it represents 1.3 million of tons of vine shoots (dry matter) that need to be processed.

The research of Velázquez-Martí et al. showed that the shape of the plantation structure has a strong influence on the productivity of vine shoots [3]. It was found that in the vineyards cultivated for fresh grape production, the horizontal trellis produced 4.2 t/ha, with a yield of dry matter per vine tree more than double respect to the high trellis system, and more than

triple compared to the standard trellis. In the vineyards cultivated for wine production, the difference between standard trellis and vase shape was less pronounced.

Depending on the density of plantation, climate and vigor of species, the pruning can generally generate between 1 and 2.5 tons per hectare and per year (dry matter). In France, according to the region, the productivity of vine shoots change Table 4.

Table 4. Productivity of vine shoots according the main wine regions in France adapted from [6].

Region	Vine Surface (ha)	Productivity of vine shoots (t/ha/year dry matter)
Aquitaine	148 900	1.80
Bourgogne	30 600	1.20
Champagne-Ardenne	30 100	1.20
Languedoc-Roussillon	262 900	2.13
Midi-Pyrénées	38 900	1.20
Pays de la Loire	37 400	1.02
Poitou-Charentes	86 200	1.13
PACA	94 100	2.13

### I-3.2 Other wine residues

Vine shoots are not the only residue from wine production (Table 5). Grape pomaces are composed of the skin and the seeds that are removed after juice and wine production. Grape stalks are the skeleton of the bunch of grapes that are obtained during the grape stripping operation. Wine lees are the residues formed at the bottom of recipients containing wine, after fermentation. Filter cake is the result of the filtration step.

Table 5. Residues from grape processing and their conventional uses.

Residue	Conventional uses	Quantity	Sources
Vine shoots	Spreading or burning in the field	1 - 3 t/ha (d.b.)	[6][46]
Vine stock and ceps (replacement/uprooting)	Spreading or burning in the field	0.5 t/ha	[6]
Stalks	Land-spreading; burning; landfill; animal feed; compost	3%–5% of the processed grape	[46]
Pomace/skin	Distillation; coloring agents; land- spreading; incineration	20%–25% of the received grape	[46]
Pomace/seeds	Oil recovery; burning		
Lees	Distillation; tartaric acid; coloring agents; nutritional supplements; incineration; landfill; land-spreading	2%–6% of the total volume of wine produced	[46]

Filter cakes	Tartaric acid; landfill; land-spreading; incineration	n.d.	[46]
--------------	---	------	------

### I-3.3 Chemical composition

The average composition of dry vine-shoots is 38% of cellulose, 23% of hemicellulose, 24% of lignin, 3% of ashes (Table 6) and the rest includes a group of large molecules of different chemical families [47,48]. The minor components of vine-shoots are intermingled between polysaccharides and lignin. They include small amounts of lipids and water soluble organic low molecular weight compounds such as stilbenes, flavonoids, phenolic acids and alcohols, terpenes and aldehydes [49,50]. Phenolic compounds are well known for their antioxidant properties. As a matter of fact, most of the recent research on vine shoots are focused on their phenolic content, in order to obtain products with high added value such as resveratrol, one of the stilbenes [49,51,52]. Vine shoots contain in average 4.7 g/kg of stilbenoids, with 2.2 g/kg of  $\epsilon$ -viniferin, and 0.8 g/kg of resveratrol [53]. Flavonoids are other polyphenols presents in vine shoots. Monomeric flavanols are exemplified by catechin and epicatechin at levels between 0.5 and 0.8 g/kg of shoot and 0.2 and 0.4 g/kg of shoot, respectively [54]. In the ashes, mineral and metallic compounds extracted from the soil by the plant can be found. Their concentration depends on the type of soil and on the vine variety, among other factors [49,55]. The presence of minerals is associated with the so-called “terroir effect” of the vines. The vine shoots composition is related to the variety, time of pruning, location, etc... but also to the techniques of characterization used. Especially for the extractive it depends largely on the extraction procedures.

Table 6. Chemical composition of vine shoots

Cellulose (%)	Hemicellulose (%)	Lignin (%)	Ash (%)	Other (%)	Method	Source
34.1	19	27.1	n.d.	19.8	Double hydrolysis, Klason lignin	[56]
33.2	27	26.7	2.6	10.5	Double hydrolysis, Klason lignin	[47]
35.4	28.3	29.4	n.d.	6.9	Chinese Textile Industry standard method	[19]
65.4 (holocellulose)		28.1	3.9	2.6	Wise et al. Method, Klason lignin	[57]
33.5	21.7	14.8	1.85	28.15	Portuguese Standards NP2029 and ME-414	[58]
46.2	20.5	16.2	n.d.	17.1	Van Soest et al.	[59]
41.1	26	20.27	3.49	9.14	Wise et al. Method, TAPPI 203, 222, 211	[60]
34	19	27	n.d.	20	Double hydrolysis, Klason lignin	[61]
42.1	24	20.9	3.19	9.81	Wise et al. Method, TAPPI 203, 222, 211	[48]

### *Extraction*

Conventional solid–liquid extraction (CSLE) system was the most applied technique to extract bioactive compounds. It was used for the extraction of phenolic compounds from vine shoots. It generally implies high temperatures (up to 200°C), long extraction times (up to 1 h), and methanol/water mixtures (v/v) as solvents. Conventional methods for the extraction of phenolic compounds have traditionally been based on stirring of ground material. The interest of vine shoot and other wine by-products compounds has required the development of new extraction methods based on nontoxic solvents. First, methanol–water mixtures [51], which is a toxic solvent was replaced by acetone-water [62] or ethanol–water mixtures [50]. Besides, auxiliary energies such as microwave or ultrasounds were used for enhancing the extraction yields [63,64]. Superheated liquid extraction (SHLE), is an attractive industrial alternative. It allows to raise the temperature above the boiling point of the solvent while keeping it in liquid state, decreasing the extraction time and amount of solvent needed. Besides, the absence of light and air reduces the degradation and oxidation of target compounds. Delgado-Torre *et al.* showed that SHLE with a ethanol-water mixture had better extraction efficiencies as compared to microwave and ultrasound assisted extractions [50].

### I-3.4 Current and potential uses of vine shoots

Due to their low apparent density, vine shoots need to be packed before transportation. Vine shoots are usually ground directly in the field and left on the ground, or burned. Studies for other purposes are quite recent and restricted at the laboratory scale. The availability of vine shoots highly depends on the winegrowers and their practices. Currently, as vine shoots have little or no value, it is quite easy to find them but this would probably change in the future. Drawbacks from their transport cost due to their low density needs to be solved [65].

### *Combustion/burning*

Since a long time, the common practice has been to dispose of vine shoots by burning after pruning in the field [46]. The results are production of carbon dioxide and toxic compounds derived from the lignin or carbohydrates combustion such as benzopyrene, catechol, hydroquinone, phenanthrene, and naphthalene. These compounds cause environmental and human health problems [45]. Besides, exogenous components from the phytosanitary treatments which are usually carried out in the vineyards can be also released. Vine shoots have been used as a heating source as domestic fuel but the emission of organic contaminants must be thus controlled.

In recent years wood pellets are being produced by coarse dry grinding and used for its energy efficiency use. Vine shoots could be an interesting option [55]. Vine shoots were converted into energy by generating heat and electricity on a small scale, to supply the needs of vineyards themselves or nearby locations. A higher heating value (HHV) of 16.9 MJ/kg, which



corresponds to amount of heat released, was determined. It is worth noting that this application may be replaced by other energy sources, more sustainable. The potential energy generated by their gasification was also studied [66]. The shoots combustion also leads to the loss of bioactive compounds with potential value.

#### *Agricultural purposes*

Soil amendment is the other main current application of vine shoots after burning. The shoots are ground and left in the field. It is worth noting that removing the vine shoots from fields induces a decrease of organic matter and is time consuming. Yet, the organic matter improves soil structure and its water retention capacity, biological activity and mineral nutrition of cultivation are favored. Viticultural soils generally have a low organic matter level of around 1% in the Mediterranean area. The Chamber of Agriculture of Languedoc-Roussillon emphasizes the need to compensate for the export of organic matter from the vines, the cost of adding compost is estimated at 44 €/ha spread [6]. However, this practice is not the most efficient as regard as the nitrogen cycle and organic fertilizing. Indeed, the mineralization of vine shoots, which have a high C/N ratio, consumes nitrogen once in the soil. Besides, this nitrogen consumption happens when the vine needs it for this growth. This nitrogen competition is detrimental to ensure an efficient fertilizing effect [67]. Moreover, They are still debates about the fact that the vine shoot can be vectors of diseases of the vine [68,69]. Globally, when the vine is disease-free, the shoots can be used as soil amendment, otherwise it is preferable to remove them.

Another study has described how use them as substrates for the mushroom cultivation [70]. Vine shoots have an interesting phenolic and mineral content which may be assimilated by plants or fungi. The potential of using their aqueous extracts as grape biostimulants or fertilizer was shown [49].

#### *Extraction of biomolecules*

Vine shoots can be exploited as a source of renewable sugars and be converted into products such as lactic acid [61,71], xylitol [72], and ethanol [73].

Phenolic compounds are the most studied compounds from vine shoots [49,50,52,61]. These compounds can be part of lignin or found as extractives in vine shoots. Thus, vine shoots can be seen as a renewable source of bioactive molecules. Stilbenoids are a class of polyphenols deeply studied. Among them, trans-resveratrol and its dimer,  $\epsilon$ -viniferin are considered as high added value compounds because of their antioxidant properties [51]. The chemopreventive activity of trans-resveratrol had been studied [74]. Extraction of biomolecules can contribute in obtaining high-added value products for the food, pharmaceutical, pharmacological, cosmetic, oenological, and nutraceutical industries [50].

Vine shoots are an attractive precursor for the preparation of activated carbons [58,65,75]. These activated carbons are, for example, use for the removal of dyes from water streams

[76] or in food industry. The competitive cost for biosurfactant production can be obtained by using carbon from vine shoots [77].

Being a polyphenols source, vine shoots are currently investigated in valorization studies. An extract of vine shoot has been thus developed and is currently marketed under the name Vineatrol® by the company Actichem (Montauban, France). This extract was evidenced to have antioxidant, anti-cancer or cardioprotective activity thanks in particular to its high content in resveratrol and  $\epsilon$ -viniferin [78]. In Europe, the commercialization of a vine shoot extract is not possible in health food because of the absence of this part of the vine in the list of authorized plants ([www.legifrance.gouv.fr](http://www.legifrance.gouv.fr)). However, since the legislation varies from one country to another, dietary supplements based on vine extract can be sold for example in Japan. Vineatrol® can be also used in oenology as an alternative to SO<sub>2</sub>, a wine preservative [79] or vine protecting agent [80]. Other extracts of vine shoots are marketed by the same company for applications in cosmetics.

#### *Food industry*

Food additives are produced by bacteria fed from shoots hydrolysis [81]. They are also raw materials for the preparation in activated carbon to develop a fining agent for white wine treatment [75]. Ferulic and gallic acid were extracted from vine shoots, these compounds are used in the food, pharmaceutical and cosmetic industries [61]. Ferulic acid can be used as feedstock for the production of flavorings and aroma including vanillin. Recently, the effect of toasting process on phenolic compounds from vine shoots was studied, suggesting their potential exploitation as oenological additives [82]. The thermal process increased the content in volatile compounds such as vanillin, and in the non-volatile compound trans-resveratrol. The last one is appreciated for its beneficial effects on human health and is not presented in other woods.

#### *Materials*

Their use as raw materials for particleboards with urea-formaldehyde (UF)-resin as binder was also investigated [83,84]. Results showed that partial substitution of wood by vine shoots negatively affects all board properties but exceed the minimum requirements of the relevant European Standards. Production of paper pulp was studied and vine shoots provided a pulp of lower quality than other agricultural residues wheat straw [48,60].

To the best of our knowledge, only two recent papers have dealt with the use of vine shoots as fillers for composite. The first paper assessed the reinforcing potential of eleven different plants, either technical fibers or industrial by-products [18]. PP and LDPE-based composites were prepared with a filler content of 30 wt% and they were mechanically tested. Composites with vine shoots displayed the lowest density. It was shown that in the composite, technical fibers had the higher mechanical properties, then stem fractions and finally by-products. This ranking is the same concerning the price. In the second study, vine shoot reinforced high density

polyethylene (HDPE) composite materials were characterized [19]. It was concluded that tensile and flexural strengths of HDPE increased up to vine shoot loading of 10%, beyond which it started to decrease. As a result, vine shoot powder was considered as an alternative reinforcement material for HDPE.

## I-4 Key properties of fibers for composite

### I-4.1 Chemical composition

The properties of the natural fibers are governed by their main chemical constituents; cellulose, hemicelluloses and lignin (Figure 14).

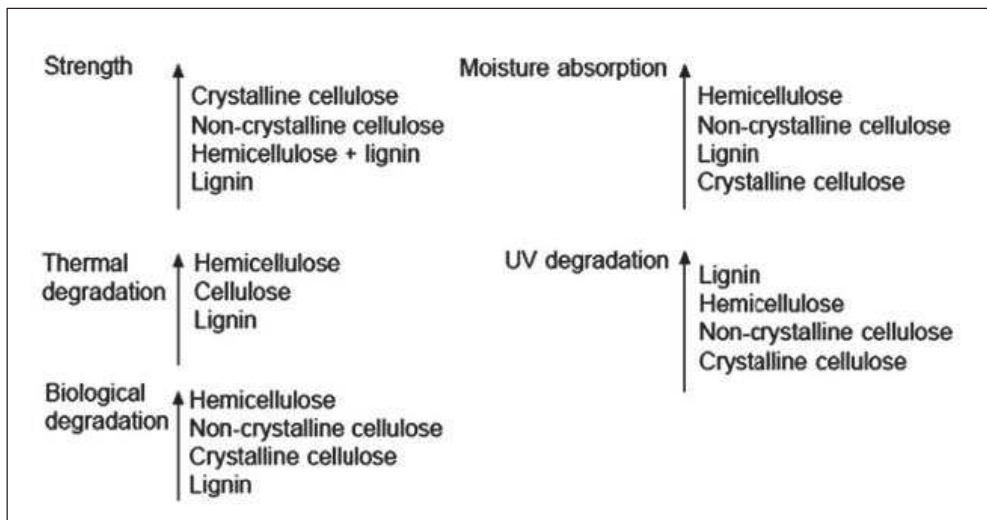


Figure 14. Properties of natural fibers according to their chemical components [85]

### I-4.2 Morphology

#### *Structure of fibers*

Even within the fibers, due to their hierarchical and complex structure, interfaces are present. Cellulose microfibrils are embedded in a biopolymer matrix composed of hemicellulose, lignin, pectins and proteins. At cell scale, several layers with various biochemical compositions and structures form the plant cell walls. Finally, elementary fibers, that are individualized and slender cells, are glued by non-cellulosic components and are clustered in fiber bundles. Thus, there are intra and inter-cellular interface within the natural fibers.

Pores present in natural fibers and their complex structures are parameters to be considered. It is difficult to give a complete and accurate description of the porous system in lignocellulosic particles. The pore size analysis is highly dependent of the technique chosen. It can be measured by small angle X-ray scattering (SAXS), mercury porosimetry [39] or nitrogen adsorption measurements [86]. The surface area of the particles is higher than the geometrical outer surface

due to the porosity. Natural particles display a wide variation in terms of porosity and surface area because of their different structure densities. Typically, in the literature it ranges from 0 to 20% for the porosity and from 0.2 to 5 m<sup>2</sup>/g for the specific surface area [39]. These two parameters need to be considered regarding the accessibility and reactivity of natural fibers. Possible coupling agents will migrate differently in the particles bulk according to their molecular weight and reactivity. Surface roughness induced by porous structures can also be determinant in the wettability and interfacial adhesion in composites. The wettability with the matrix decreases with micro-scaled texturation of the fillers [87] but it enhances the interfacial mechanical interlocking [88]. Once again, the porosity, surface area and roughness are highly dependent on pre-treatment of the fibers. For example, pore volumes decrease irreversibly with drying-wetting cycles of natural fibers. The smallest pores close, it is called hornification [89]. On the contrary, an increase of pore volume is observed with the removal of non-cellulosic components with solvents or alkaline or acidic solutions [90].

The Aspect ratio (length/diameter), has an influence on the mechanical properties of the composite.

### I-4.3 Surface condition: surface chemistry

#### *Surface Physico chemistry*

The surface physico-chemistry of natural fibers is characterized by the surface free energy and its dispersive and polar components. It can be determined by contact angles with different solvents or by inverse gas chromatography (IGC) measurements. The work of adhesion between the fillers and the matrix can be calculated. Because of the heterogeneous distribution of lignocellulosic components, some natural fiber can display low polarity and low surface energy. Indeed, the more polar components, cellulose, is generally in the bulk of fibers. The results highly depend on the techniques.

Table 7. Physico-chemistry of some natural fibers and their cell wall components by contact angles and Owens-Wendt calculation [37].

Substrate	$\gamma$ (mJ/m <sup>2</sup> )	$\gamma^d$ (mJ/m <sup>2</sup> )	$\gamma^p$ (mJ/m <sup>2</sup> )
Wood (various species)	40.0-87.8	0.4-45	11.5-86.14
Flax	43.5-23.5	23.5	20
Hemp	35.2	20	15.2
Wheat straw	44.5	21.1	23.4
Cellulose	50	30	20
Hemicellulose	35.3-39.5	-	-
Lignin	57-58.8	33.7-44.5	31.1-23.4

*Surface chemistry*

The reactivity of the cellulose is principally determined by the hydroxyl groups. In case of natural fibers, there are a wide variety of possible reactive functional groups at their surface. Hydroxyl groups are from cellulose, of course, but also from non-cellulosic components. Because bound to saturated carbons (cellulose, hemicellulose, pectins) or to unsaturated carbons (phenols of lignin), they have not the same reactivity. For example, it was reported that the phenolic hydroxyl groups have a higher reactivity due to their acidic character than hydroxyl groups of cellulose with organosilanes [91]. Natural fibers surface can also present carboxyl groups that are primary bear by hemicellulose (galacturonic and glucuronic acids), pectins and also by some proteins [92]. Lastly, low amount of aldehydes and esters can be found on lipophilic components such as fats and waxes. Thus, most of the common reactions at the fiber surface involve the hydroxyl groups of cellulose but, many side reactions happen with the other functional groups from other components (phenols, carboxyl acid, aldehydes and esters). It is worth to notice that some of the non-cellulosic components can be easily removed by chemical or mechanical treatments because they are weakly bonded to cell walls. Lipophilic components are extracted by ethanol or toluene, pectins by acidic treatments, alkaline treatments can be used to remove lignin, hemicellulose and pectins [93,94]. Some oligosaccharides and pectins can be extracted only by hot water. In addition, the mechanical frictions or shearing that happen during processing can also eliminate weakly-bonded components. Therefore, for composite application, the treatment overcome by fibers is critical to better understand the surface properties and the interfacial interactions with a coupling agents or a polymer matrix [93].

## II. Lignocellulose filler modification

### II-1 Motivation for filler modification

As many of polymeric matrices are hydrophobic, the inherent polar character of lignocellulosic matters may give rise to two major limitations when used as reinforcing fillers in composites. The first limitation is associated with their strong sensitivity to water and even moisture, which induces a loss of the mechanical properties of the composite during ageing. The second limitation, that is largely reported, is their poor compatibility with hydrophobic polymer matrices. This is known to cause weak interfacial adhesion and poor filler dispersion, thus resulting usually in a decreased performance of the composites.

In the field of composite materials, the interfacial zone between the filler and the matrix, is called *interphase*. It is a transition phase of variable thickness (from few hundreds of nanometers to several microns [95,96]) and including the contact zone between the fiber and the matrix, which is known to play a crucial role in the functional properties of composites. Indeed, the interphase contributes to the transmission of mechanical forces, and rupture at the interface is one of the most common modes of damage in composites that occurs in the case of weak filler/matrix adherence. Increasing the filler/matrix adherence would allow favoring the rupture of the material within the matrix, by keeping fibers bonded to the polymer matrix. Nevertheless, a strong interfacial interaction is not necessarily sought since, in one hand, it may induce an increase in material brittleness and, in the other hand, the energy upon impact is better absorbed by a flexible interphase of weak adherence [37]. The quality of the interphase also has an important role with regard to the ageing of composites. As an example, a poor interfacial adhesion would favor moisture diffusion, leading to the swelling of the filler and its decohesion during drying [97]. In the field of food packaging, a strong adhesion is not necessarily targeted because high water vapor and oxygen permeabilities can prove to be essential, especially for respiring food products such as fruits and vegetables. As a result, an appropriate compromise between these two competing aspects should be found according to the expected properties of composites.

To overcome this issue, the challenge concerning natural fillers is then to decrease their sensitivity to water without affecting their integrity, and to modulate surface free energy of lignocellulosic particles in such a way as to increase their similarity with the targeted polymer matrices. Many treatments have been proposed to improve the interfacial quality in composite materials and have been already largely reviewed [22,37,91,98,99]. Despite numerous studies, this field of research remains very dynamic driven by the need for developing greener (solvent-free, water-based...), more efficient and less aggressive processes of fiber modification.

Overall, three main strategies have been investigated so far: (i) filler modification, (ii) polymer matrix treatment or (iii) the addition of a compatibilizer (Figure 15). Due to the will of maintaining the intrinsic properties of the matrix and keeping a two component-based system, only the first strategy has been investigated in the present work. Another important criterion of choice was to select treatments enabling to preserve, as much as possible, the bulk properties of lignocellulosic fillers. The following state of the art will thus focus on the possible strategies reported in literature to modify the surface of lignocellulosic fillers.

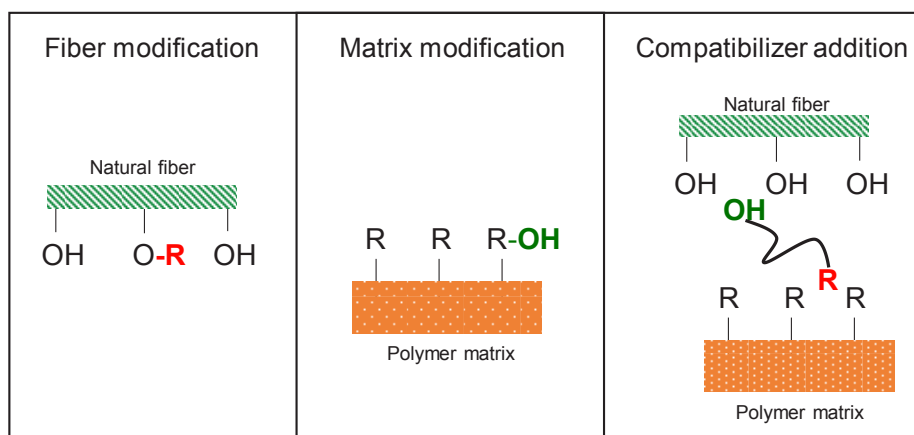


Figure 15. Strategies to modify the filler/matrix interface in biocomposites

Interfacial adhesion in composites is controlled by the nature and strength of interactions, as well as the extent of the surface involved. Two phenomena can be distinguished: the adhesion and the adherence [37]. The adhesion represents all the physico-chemical phenomena that occurs when two materials are in close contact, and the related theories are based on the formation of specific links or interactions. It characterizes the wettability of the natural fillers with the polymer matrix upon their first contact along the process. On the other hand, the adherence is the force or energy required to separate two materials joined by a common surface. As shown in Figure 16, several options can be chosen to control composite interfacial adhesion. The nature of bonding depends on the chemical composition of fillers and matrix, but also on the filler morphology and the diffusivity of each elements in the considered system [100]. In addition to covalent bonds, hydrogen bonds, Van der Waals forces and other low energy forces may also be involved. First, the quality of interfacial interactions can be improved through the creation of new physico-chemical interactions. The wetting and impregnation of fillers by the matrix can be favored by modifying their surface free energy, especially the polar and dispersive components, through chemical or physical treatments. The reactivity of fibers towards the matrix are enhanced by functionalization. The molecule grafted on the surface of fillers has an improved affinity with the matrix and can create covalent bonds, hydrogen bonds or favor physical entanglements within the matrix. Secondly, the quantity of interfacial interactions is also a key factor. Mechanical interlocking is enhanced by surface roughness of fiber. A good

dispersion of the fillers within the matrix increases the specific surface area of fillers and therefore the quantity of interfacial interactions.

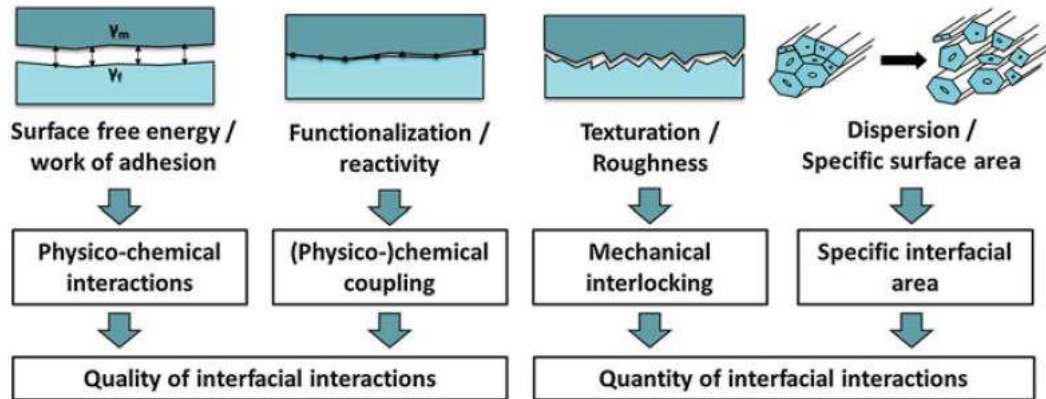


Figure 16. Possible strategies to improve interfacial adhesion in biocomposites [37].

Numerous studies on interfaces in composites are about the mechanical properties because the main applications are automotive, building, sports. Interfacial interactions between filler and matrix and fillers dispersion playing a vital role in the resulting mechanical properties of biocomposites, it is important to control it. Surface modifications of natural fillers can be typically divided into physical and chemical approaches.

## II-2 Physical surface treatments

Physical treatments change structural and surface properties of fibers and can even allow grafting molecules at their surfaces. The physical activation of reactive sites of fibers allows fast reactions. Another advantage is that these treatments do not need solvents and can therefore be considered in eco-friendly processes.

### II-2.1 Plasma treatment

Plasma source is an ionized medium obtained by the excitation of a gas under the action of an electrical discharge. This active medium is constituted of neutral atoms, ions and free electrons which modify the physiochemical nature of the surface of fibers without affecting bulk properties if it is well controlled [101]. It offers a wide range of possibilities for grafting or revealing functional groups depending on the nature of the gases used (argon, nitrogen, oxygen, fluorinated gas...) and the operating conditions (power, pressure, treatment time, gas flow rate). Surface energy can be varied to get specific properties to the material surface [102]. With fluorinated gases, the surface becomes more hydrophobic whereas it is more hydrophilic after



air plasma treatment. The surface reactivity of the fibers is increased due to the creation of free radicals resulting from the cleavage of chemical bonds (C-C and C-H) by plasma energy. Coupling with chemical treatment, it activates efficiently the functionalization. In this regards, cold plasma was used to graft fatty acids onto softwood kraft pulps and get hydrophobic fibers [103]. Corona treatment on flax and hemp fabrics increased fiber roughness thus enhancing mechanical interlocking with the matrix [104]. The treatment time was a critical parameter because more than 15 min of treatment led to a severe degradation of the fibers. The treatment of miscanthus fibers by corona discharge which results in a surface oxidation and an etching effect as shown by X-ray photoelectron spectroscopy and scanning electron microscopy, led to an improvement of the interfacial compatibility between matrix and fillers [105]. The mechanical properties measured by classical tensile tests were improved (Young's moduli increased around 10–20% for 20wt% of fibers) as well as the thermal stability. Plasma treatments can therefore improve interfacial adhesion with mechanical interlocking and physico-chemical interactions as long as the operating conditions are controlled.

## II-2.2 Gamma or e-beam irradiation

Irradiations have been widely used to treat various lignocellulosic biomass to improve their reactivity to reagents or enzymes and to increase enzymatic hydrolysis yield for the production of ethanol and 2<sup>nd</sup> generation biofuels [39,106]. One of the main difference between irradiation and plasma treatment is that irradiation is more penetrating and can act in the bulk of the fibers. High radiation energies can drastically degrade the natural fibers by chain scission and oxidation phenomena. Pre-irradiations at low irradiation doses (<30 kGy) on henequen fibers were studied as well as their effect on resulting PP and PBSA based composites [86,107]. It was shown that only a part of non-cellulosic components (waxes, impurities, pectins...) was removed and the surface roughness was increased. In the review of Le Moigne *et al.* [108], it was also mentioned that the irradiation could activate free radical reactions inducing the grafting and polymerization of carrying C=C bonds molecules onto natural fibers [109].

## II-3 Chemical surface treatments

Chemical approaches are more represented within the literature than physical ones, owing to better improvements obtained to date [14]. Briefly, a largely used method is alkali treatment, also called mercerization. It removes non-cellulosic fiber constituents including hemicellulose, lignin, pectin, fat and wax which exposes cellulose and increases surface roughness/area to improve interfacial interactions.

The other chemical treatments consist of reacting with functional groups (mainly hydroxyl groups) of natural fibers while bringing new functional groups able to interact with the matrix

and for example forming a bridge of chemical bonds between the fiber and the matrix. Figure 17 displays the main chemical treatments applied to natural fibers including carbamylation (isocyanates treatment), esterification and silanization. In the following sections, the main chemical treatments will be described with a focus on the esterification method.

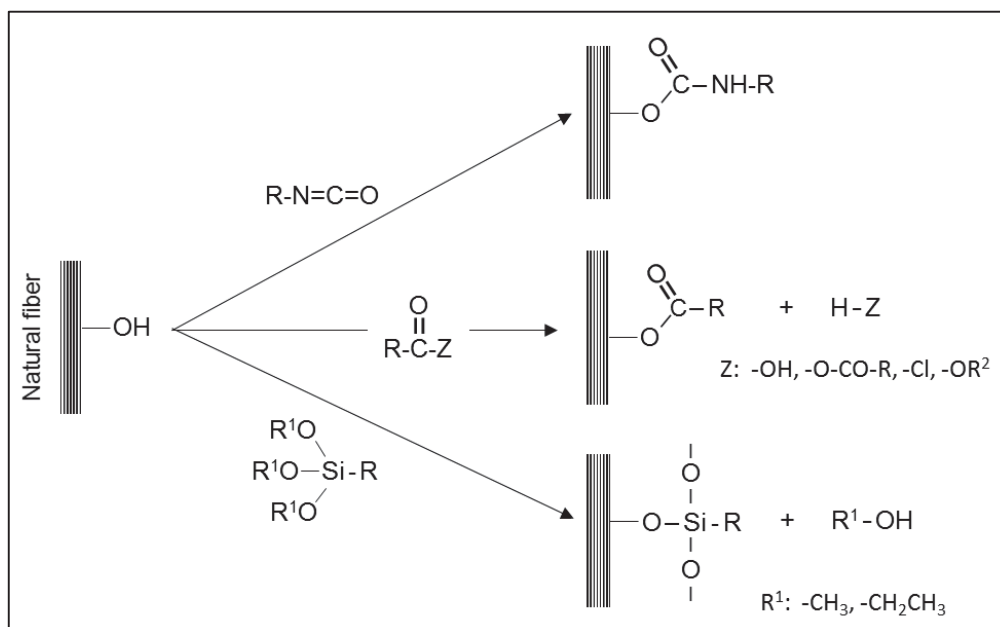


Figure 17. Most common chemical reactions targeting hydroxyl groups of natural fibers

### II-3.1 Treatment with isocyanates

Isocyanates are reagents with a functional group ( $-N=C=O$ ) very reactive towards hydroxyl groups of cellulose and phenols of lignin, forming stable urethane bonds. The main advantage of isocyanates is the absence of reaction by-products (Figure 17) such as water that can damage the composite. In case of diisocyanates, the remaining function can react with the matrix during processing [110]. Lee and Wang studied treatment with isocyanates on bamboo fibers used in PBS or PLA based composites [111]. Water resistance and a slight improvement of tensile properties were reported. However, some isocyanates can decompose in water and form heterocyclic diamines that are suspected to be carcinogenic. Thus, isocyanate reaction may not be a viable treatment for natural fibers, especially for food packaging applications, because of its toxicity.

### II-3.2 Treatment with organosilanes

Treatment with organosilanes is widely used for composites with glass fibers. It can be also used on lignocellulosic substrates [112]. The alkoxy groups of silanes (commonly methoxy or ethoxy) can be hydrolyzed in water to form silanols that can then condense with hydroxyl groups of the fibers upon thermal treatment (Figure 17). Silanes can also condense themselves

into siloxane linkages  $\text{-Si-O-Si-}$  forming a network on the fiber surface [91,112]. To improve the interfacial adhesion in biocomposites, numerous natural fibers were successfully treated with organosilanes : pure cellulose [113], ramie [114], sisal [115], flax [96] or oak wood flour [116]. The organosilane should be chosen according to the targeted polymer matrix as demonstrated by Li *et al.* with methacryloxypropyl trimethoxy silane (MPS) and aminopropyl triethoxy silane (APS) [115]. Only MPS-treated sisal can have Van der Waals interactions with the HDPE matrix, inducing an improvement of the interfacial shear strength. Generally, mechanical properties of the composites with silane-treated fibers are significantly improved.

### II-3.3 Esterification

In the last decades, a renewed interest on the chemical modification of natural fibers and cellulose was observed, in response to the increasing interest in non-toxic and renewable-source based materials. It includes esterification which is a potential way to produce biodegradable cellulose esters plastics [117,118] or to obtain reinforcing materials for composites [119–121]. Esterification is a classical approach to functionalized hydroxyl groups and it is one of the most common chemical transformations. The hydrophilic hydroxyls are transformed into ester bonds with aliphatic groups, which increase the hydrophobicity of the fibers and thereby the fiber-matrix compatibility.

Cellulose esters are one of the more important groups of cellulose derivatives. The esterification between an alcohol and a carboxylic acid is a reversible reaction with an equilibrium. It is possible to use carboxylic acid derivatives such as acyl chlorides, anhydrides or esters to promote the ester formation. The carboxylic acid can be also activated in reaction medium by different compounds such as tosyl chloride, carbonyldiimidazole, or an iminium chloride [122]. The most known cellulose ester is cellulose acetate. It is industrially produced by the heterogeneous pathway in anhydrous acetic acid with acetic anhydride and a small amount of catalyst (e.g. sulfuric acid). The cellulose is almost completely esterified with this method and it can be then hydrolyzed back to the desired intermediate degree of substitution (DS) [123]. DS corresponds to the molar ratio of the introduced functions per glucose unit. Cellulose acetate are used in various applications as film base in photography, as frame for eyeglass or as cigarette filters. Complete heterogeneous esterification of cellulose can be applied until butanoic anhydride, but for longer chains, the modification remains partial [124].

The fundamental challenge in chemical modification of natural fillers is that cellulose is weakly reactive and not soluble in common solvents. Its supramolecular structure makes it difficult to transform and the cellulose does not automatically obey the common rules of organic chemistry. For example, cellulose hydroxyl groups are alcohols but they do not form esters with carboxylic acids under normal conditions.

The esterification according to the different possible reagents are presented in the following section.

### II-3.3.1 Carboxylic acid

A one-step acid-catalyzed esterification (known as Fischer esterification) involving the heating of a mixture containing the protonated form of a carboxylic acid represents the most straightforward method for esterification [125]. During this approach, there are the simultaneous occurrence of cellulose hydrolysis and esterification of hydroxyl groups. Peydecastaing *et al.* [126] proposed a reaction with fatty acid salts that were used as non-acidic catalyst in order to limit cellulose degradation. Highly hydrophobic products were obtained with low degree of substitution (DS).

The reaction can be carried out in systems enabling cellulose solvation. Among solvents of cellulose, the solvent system N,N-dimethylacetamide (DMAc) and lithium chloride (LiCl) have been largely used for cellulose ester synthesis [127]. Carboxylic acids need to be activated *in situ* with a co-reagent to form a more reactive entity capable of grafting the fatty chain to cellulose. For example, the mixed anhydride formed with dicyclohexylcarbodiimide (DCC) reacts with 4-pyrrolidinopyridine (PP) to give a very reactive specie [128]. This method was efficient to get variable DS. Tosyl chloride (TsCl, also called p-toluenesulfonyl chloride) is another co-reagent largely used and generating a mixed anhydride and a carboxylic anhydride able to react with cellulose [129]. TsCl was first used in combination with acetic acid in N, N-dimethylformamide (DMF) [130].

In a heterogeneous method (no solubilization of the cellulose), sulfuric acid was used as catalyst in a mixture of fatty acids and acetic anhydride as co-reagent [131]. The products, mixed esterified celluloses, were highly hydrophobic with a maximum DS of 0.66 and this method avoids the use of LiCl/DMAc medium. To sum up, carboxylic acids can be used in esterification of fibers but they need specific conditions to be able to react.

### II-3.3.2 Anhydrides

The relative drastic conditions and activations required for esterification with carboxylic acids push to use anhydrides that are generally more reactive, forming esters at lower temperatures. They are typically produced by heating two molar units of carboxylic to drive off one molar unit of water. They have been widely employed for acetylation lignocellulosic substrates, where substitution of hydroxyl groups with acetyl moieties occurs primarily on lignin and hemicelluloses. The adhesion between flax fibers and PHBH was promoted by surface acetylation [132] but not so much with PLA [133]. Flax fiber intrinsic strength and tenacity could decrease according to acetylation conditions. Baiardo *et al.* [134] showed that a decrease in fiber tenacity would be detrimental to obtain strength improvement in the composite, highlighting that having similar surface tensions for matrix and fibers was not a sufficient

condition. Vapor-phase esterification of cellulose was achieved by exposing filter paper and tunicate cellulose film to mixed vapor of acetic and trifluoroacetic anhydrides [135].

LiCl/DMAc medium allows esterification of cellulose with anhydrides in homogeneous condition with a good control of the DS, so that no hydrolysis is required after reaction. Pyridine is usually used to activate the acyl group and then capture the acid to protect the cellulose from acid hydrolysis [136]. The advantage of acylation in homogeneous phase lies in the fact that it takes place at temperatures below 40 °C in the presence of pyridine or under the action of microwaves [137], and it allows excellent control of DS and an uniform distribution of functional groups along the polymer chain. The main disadvantage of this type of esterification remains the high cost of lithium salt recycling.

Esterification of nanofibrillated cellulose in ionic liquid (IL) was carried out using different anhydrides [138]. This heterogeneous reaction gave DS around 0.3 for acetic, butyric and hexanoic anhydrides. Sehaqui *et al.* [139] found similar results with DS from 0.4 to 0.1 with increasing chain length in the range of from 2 to 16. In addition to being easily recyclable, ILs have attractive properties such as high chemical and thermal stability. In homogeneous phase, cellulose had been dissolved assisted by microwave and DS higher than 2 were obtained for anhydrides from acetic to hexanoic [140].

Maleic anhydride is not only used to modify fiber surface but also to functionalize the matrix. The use of maleated polyolefins allows esterification reaction with lignocellulosic substrate. Maleic anhydride is one of the most popular types of coupling agents for composite applications [141,142]. Maleated polyolefins (mainly PP and PE) are directly incorporated during the composite reactive extrusion. Therefore, compatibilization by reactive extrusion does not require the use of solvents.

Alkenyl succinic anhydride (ASA) can also be used for acylating the surface of cellulose [143,144]. Alkylketene dimers (AKD) can be regarded as being similar to anhydrides and react with hydroxyl groups when suitably heated [145].

### II-3.3.3 Acid chlorides

In general, acid chlorides are more reactive towards hydroxyl groups than the corresponding anhydrides or carboxylic acids. A convenient way to produce them is the reaction of carboxylic acid with thionyl chloride [146]. However, the main downside of using acid chlorides for esterification is the formation of HCl as by-product. The resulting acidic conditions can damage the cellulosic materials in some cases. For example, a drop in degree of polymerization of microcrystalline cellulose was observed after treatment with dodecanoyl and octadecanoyl chloride in toluene [120]. Thus, adding pyridine (or trimethylamine) as a catalyst and HCl trapping agent, is usually found to overcome this drawback. A greater DS was obtained when using a solvent, such as dimethylformamide (DMF), with higher swelling ability for cellulose [146]. In the same study, it was shown that DS decreased significantly when the chain length

of fatty acids increased. A high DS promoted decrystallization of cellulose while it did not enhance hydrophobicity comparing to a lower DS. Extensive acylation reduced slightly the thermal stability of the fibers. Used in LDPE composite, acylated fibers enhanced mechanical properties and improved water resistance [121]. It was demonstrated that the DS should be controlled to get better composite performances. Benzoylation, through condensation of benzoyl chloride and hydroxyls, was also used in fibers treatment since it decreased surface hydrophilicity of fibers and notably improved their interactions with polystyrene matrix [147].

Previous homogeneous and heterogeneous systems described for anhydride were suitable for esterification with acid chlorides. Kwatra *et al.* [148] were the first to develop a solvent-free esterification technique (the reagent itself played the role of solvent). In the protocol described, the cellulose, previously activated with a solution of NaOH, and the reagent (palmitic acid chloride) were introduced into a round bottom flask that was kept under vacuum. The HCl formed was aspirated as it was formed. They showed that the degree of substitution depended on temperature and reaction kinetics. A few years later, Thiebaud and Borredon esterified sawdust using a similar technique, in which the HCl formed was removed by a stream of nitrogen bubbling and sweeping the reaction medium [149].

An efficient gas-phase esterification was developed for cellulosic substrate with high crystallinity involving palmitoyl chloride and demonstrating an evolving growth of esterification from the shell to the crystalline core [150]. Fumagalli *et al.* [151] used also acid chlorides for gas-phase esterification of nanocellulose aerogels. It was confirmed that the esterification with mono-functional fatty acid derivatives progressed from the surface of the substrates to their core. On the contrary, diacyl chlorides derivatization was limited to the nanocellulose surface.

#### II-3.3.4 Transesterification

Transesterification reactions were also applied to cellulose by using for example vegetable oil triglycerides [152]. The surface tension of scoured cotton cellulose was divided by two.

#### II-3.3.5 Purification

The products obtained after chemical treatment may still contain reagent residues. Therefore, a subsequent purification is required. Three main ways are found in the literature for the purification of the substrate after esterification. In case of homogeneous esterification, the ester is first precipitated in water and then washed with water [153] or extracted by an organic solvent as methanol or ethanol [154]. For heterogeneous esterification, a method consists of the dissolution in chloroform of the esterified cellulose then the precipitation in methanol or ethanol [137,155]. Finally, the Soxhlet extraction is the most used method. The extraction solvents can be methanol [124,156], ethanol [146] or acetone [157].

### II-3.3.6 Industrial treatment processes

Treatments of natural fibers for composites should take into account industrial feasibility. At industrial level there are new constraints to fulfill such as investments, running costs, compatibility with REACH policy and, of course, the scale-up of the process. Solvent-free processes that use minimal energy and water have become a major challenge. A promising technique consists of treatments in vapor phase. The functionalizing molecule is heated, vaporized and then condensed on the substrate to be treated. Thus, the reagent must be thermally stable in order to avoid any degradation during the vaporization. These techniques have been mostly developed in the pulp and paper industries to use less solvent. For the functionalization of cellulose, a vapor deposition process with a carrier gas has been developed [158]. Trichloromethylsilane (TCMS) carried by nitrogen reacts with cellulose and the produced hydrochloric acid is removed by the gas bubbling in a NaOH aqueous solution. The treatment of cellulose with this process was fast and efficient resulting notably in the drastic increase of contact angle with water. Another process in vapor phase was studied in the thesis of Stinga and Berlioz [159,160]. The process, called chromatogenic chemistry, is used for grafting long-chain fatty acid chloride reagents on the surface of cellulose. After having finely dispersed the reagent on the substrate, a hot inert gas stream is applied to reach the vapor pressure of the reagent. The liquid/vapor equilibrium and the gas stream allow the diffusion and the grafting of the molecules on cellulose by esterification. To avoid cellulose degradation, by-products, mainly hydrochloric acid, are evacuated by the gas flow. With this process, the authors obtained interesting hydrophobic properties of the modified cellulose that remained biodegradable. The chromatogenic chemistry has been implemented on paper by *Centre Technique du Papier* (CTP) in France and has been patented [161]. These vapor phase processes are of great interest (solvent-free, fast, effective) but their adaptation to natural fibers for composite application still need to be investigated.

### II-3.4 Other chemical treatments

Other chemical graftings are possible via the substitution of hydroxyl groups of lignocellulosic substrate. For example, poly(ethylene glycol) grafting on flax fibers improved the tensile strength of PLA composites [133]. Nevertheless, pre-treatments are necessary to create reactive alcoholates as suggested by the procedure followed to graft the flax surface [162].

## II-4 Characterization of the grafting extent

### II-4.1 Characterization of the degree of substitution (DS)

The degree of substitution (DS) of cellulose esters, and likewise of all cellulose derivatives, is a parameter used to know the average number of sites that have reacted per anhydroglucose unit (AGU). There are numerous techniques to characterize the DS of cellulose esters.

Saponification, followed by titration of alkali excess is the oldest technique [117,149]. This method can be difficult if the sample is highly substituted with a high hydrophobic character and steric hindrance preventing a complete hydrolysis [118]. Moreover, the result of the titration can be also disturbed by precipitation of the fatty acid salts at room temperature.

After alkaline hydrolysis, the free acids can be also quantified by GC-MS after derivatization [163,164]. Capillary electrophoresis [165] or reversed-phase liquid chromatography [166] are other possibilities after base hydrolysis.

The DS of cellulose ester can be calculated by gravimetry from the difference between initial and final substrate weight knowing the molar mass of AGU, reagent and the by-product [151]. The precision of the balance is the limitation for low DS.

Another method is the aminolysis of the ester groups with pyrrolidine followed by gas-chromatographic separation of the corresponding fatty acid derivatives [131,167], but appropriated standards (acylpyrrolidines) for GC calibration are not easily available nor easy to prepare.

The DS can be determined by elemental analysis [168], a simple and efficient method, that provides accurate DS-values ( $\pm 0.10$  in most cases) if H-content determinations are within  $\pm 0.1\%$ . Equations allow determination of DS of cellulose derivatives bearing not only one but also two different acyl substituents.

Spectroscopic techniques can be employed such as infra-red (FTIR) using the absorption ratio between  $1750$  and  $1060\text{ cm}^{-1}$  with a calibration curve [169]. It allows to differentiate only sorbed reagent from reagent linked with covalent bonds. Near-infrared spectral (NIR) analysis is efficient even when DS values is low which is difficult to do by using FTIR [170]. Nuclear magnetic resonance (NMR) of hydrogen or carbon is another possibility in case of sample soluble in deuterated solvents. This method is based on the ratio of the grafted chains signals integrations to those of cellulose [124,137,155,171]. In addition to the quantitative analysis, this technique gives structural information such as the distribution of functional groups. However, it is not applicable for low DS cellulose esters because a complete solubilization of the sample is required. To solve this issue, solid-state NMR can be used with CP/MAS methods [124,164].

It is worth noting that other techniques allow to evidence the chemical treatment. X-ray photoelectron spectroscopy (XPS) is a non-destructive method which allows the study of the chemical structure of solids surface (0-10 nm). From XPS data, a degree of surface substitution



(DSS) can be calculated [138]. Time-of-Flight Secondary Ion Mass Spectrometry (ToF-SIMS) is a technique that can be used to characterize the grafting at the extreme surface (2 nm). It was, for example, used to characterized esterification of flax fibers [172].

## II-4.2 Parameters impacting the efficiency of the grafting (DS)

Numerous parameters influence the final properties of modified fillers notably the method implemented. The degree of substitution (DS) depends on the parameters of the reaction: reaction time, temperature, amount of reagent, chain length of the reagent.

DS generally increases with temperature and reaction time until an optimum, then it decreases because of substrate degradation and also partial hydrolysis of ester bonds formed. DS decreases with the number of carbons attached to the carbonyl group because of the reagent reactivity is lower (higher inductive effect, polarity) and the steric hindrance is higher. Thus, the esterification with long chain reagent is more difficult than the cellulose acetate synthesis.

Hydroxyl groups in the amorphous region are more readily to react than in the crystalline region due to their close packing and extensive inter-chain hydrogen bonding. The reagent cannot diffuse into the crystalline region. An initial reaction occurs mainly on the surface and on chain ends of the crystallites. It results in the opening of some hydrogen-bonded chains which produces amorphous cellulose explaining the reduction in crystallinity for high DS.

## II-5 Characterization of the filler

Several properties can be studied with multiple techniques to assess the impact of the esterification on the natural fillers. The two main parameters of the esterification are the DS and the chain length of the grafted moiety.

### II-5.1 Surface free energy

In order to determine the surface free energy, contact angle measurements are the most established methods. These techniques, described in chapter II, consist of measuring the contact angle  $\vartheta$  formed between the filler and standard liquids. The liquid is considered as wetting ( $\vartheta < 90^\circ$ ) or non-wetting ( $\vartheta > 90^\circ$ ) depending on the  $\vartheta$  value. The surface free energy is deduced from these angles through the Owens-Wendt approach. Besides, the work of adhesion which is the strength of the physicochemical interactions can be calculated from the polar and dispersive components. Inverse gas chromatography (IGC) is another commonly used technique to characterize the physicochemical surface properties of either nano- or micro-particles.

It was observed a decrease in the surface energy of the cellulose fibers after esterification, essentially due to the reduction in the polar component, because of the replacement of the

surface hydroxyl groups by hydrophobic long aliphatic chains. The surface energy of the esterified fibers decreases only slightly with the DS [146]. Another study reported that the water contact angle increased with the alkyl chain length [138].

## II-5.2 Surface topography and morphology

Scanning electron microscopy (SEM) and Atomic force microscopy (AFM) are often used to characterize the effect of chemical treatments of natural fibers on their surface topography. SEM can only provide a qualitative analysis, whereas AFM provides detailed data on the surface roughness. Larger fibers were observed by SEM after esterification of cotton cellulose [173]. On the contrary, in another study fibers had an unchanged structure and morphology after esterification [172]. The initial cellulose generally displays a smooth surface, whereas the treatment leads to rough surface indicating that modification has affected the structure. The porosity of the fibers increases with the length of alkyl chain inducing a lower density [138].

## II-5.3 Crystallinity

X-ray diffraction (XRD) is a common technique used for the study of crystalline structures. XRD is frequently used to evaluate the crystalline index of natural fibers and its evolution after treatment. Solid state NMR can also be used to follow the evolution of filler crystallinity.

Depending on the experimental conditions and DS, the original cellulose structure shown in XRD can be maintained after treatment. However, the grafting is generally associated to a decrease of the crystallinity index which could be explained on the basis that grafting causes disruption in the crystalline regions of the fiber leading to the creation of amorphous regions. Thus, as the DS increases, the amorphous regions become more and more predominant [37].

## II-5.4 Thermal stability

Thermal analyses were often used to characterize the natural fillers before and after chemical modifications. Thermogravimetric analysis (TGA) is the most popular method to study their thermal stability.

Treated cellulose starts to decompose at temperature lower than unmodified cellulose. It is attributed to the decreased crystallinity associated with the substitution of hydroxyl groups with fatty acid chain. The thermal stability of the cellulose ester decreases with increasing alkyl chain length of the grafted fatty acids [173]. On the contrary, the thermal stability of wood was improved after chemical modification with palmitoyl chloride [174]. In another work, the thermal degradation of the cellulose esters was only marginally influenced by the DS and the fatty acids chain length [146]. In the same study it was shown that from a sufficient DS,

degradation temperature increases because of the formation of a new order region due to the crystallization of the long side chains. The thermal stability depends more on the experimental conditions of the treatment than in the DS or grafted chain length.

## II-5.5 Water vapor sorption

Dynamic Vapour Sorption (DVS) is a method used to measure the water sorption of a material according to the relative humidity. Cellulose esters with high DS values have a lower water adsorption because the hydroxyl groups were partially replaced by fatty acid chains [138]. The moisture sorption decreased with the length of the alkyl chain grafted.

## II-5.6 Biodegradability

Esterified cellulose can be considered as among the more biodegradable cellulose derivatives [175]. It was found that the DS is a very significant factor in the biodegradability of cellulose acetate. Samios *et al.* [176] showed that low DS eased the biodegradation. The crystallinity decreased with increasing DS, meaning that the DS was a predominant factor to hinder biodegradation compared to crystallinity [176]. In another paper, cellulose acetate only degraded for DS lower to 2.4 [177]. A work on enzymatic degradations evidenced significantly the role of the degree of substitution and substituent size on the biodegradability of ester with longer chains (up to C14) [154]. For low DS, the substrates were easily degraded whatever the length of the substitute chains. Then, the biodegradability collapsed for different DS threshold according to the grafted chain: 1.7 for propionate (C3), 0.3 for laurate (C12) and 0.2 for myristate (C14).

To sum up, the treatment of natural fibers by esterification allows to decrease the polarity and increase their resistance to water absorption (Table 8). However, the intrinsic fiber properties can be affected, for example the crystallinity can collapse.

Table 8. Summarize of DS and chain length on key properties of fillers

Parameters	Crystallinity	Thermal stability	Hydrophobicity (water contact angle)	Moisture absorption	Biodegradability
DS ↗	↘	↘ or ↗	↗ or →	↘	↘
Chain length ↗	↘ or ↗	↘ or →	↗	↘	↘ or →

For composite application, it is interesting to esterified only surface hydroxyl groups of natural fibers in order to avoid change in morphology and crystallinity. Cellulose esters with very low

DS ( $<0.3$ ) and that are synthesized in heterogeneous conditions retain the structure of cellulose while permitting to acquire interesting properties such as water repellency [126].

## II-6 Characterization of the filler/matrix interphase.

A proper characterization of composite interfaces remains tricky because most of them are located inside the composite material. The microscopic or nanoscopic nature of interfaces requires characterization and measurement techniques with ultrahigh magnification and resolution. Thus, there are many difficulties often encountered in the physico-chemical analyses of interfaces. A convenient way to characterize composite interfaces is to analyze the surfaces of the composite constituents before they are combined together. Techniques from the section II-5 can be used.

There are no standardized methods to assess the quality of the interface/interphase in natural fiber reinforced composites. However, there are different approaches that are widely used in scientific communities.

### II-6.1 Microscopic analysis

SEM analyses provide direct visualization of the morphology at the filler/matrix interface. The qualitative criteria are mainly the occurrence of failure surfaces, fiber pull-outs, interfacial gaps around the fibers and debonding, or wetting, of fibers by the polymer (Figure 18). SEM observations are generally performed on manually cryo-fractured surfaces. These surface layers represent only a small part of the total volume of the composite. SEM can be only used as a qualitative mean to compare the fiber/matrix interfacial adhesion in different formulations and to discriminate different failure surface morphologies.

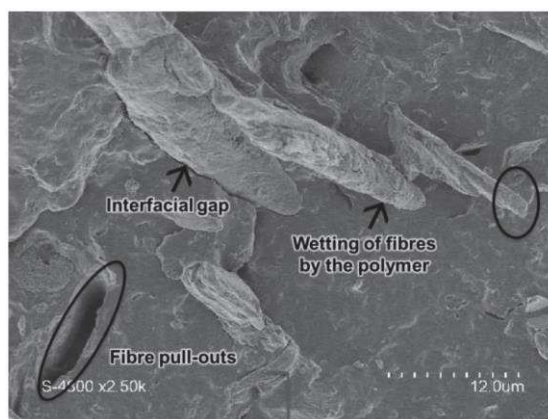


Figure 18. SEM picture of cryo-fractured surface of PHBV/wheat straw fibers (20 wt%) composites

Polarized Optical Microscopy (POM) is a technique used to evidenced transcrystallization. In the case of semi-crystalline polymers, POM observations of the crystallization phenomenon

from the melt materials can be used to highlight the occurrence (or not) of interfacial transcrystallization and/or particle nucleating effect, both indicators of filler/matrix interactions.

X-ray tomography is a technique that can provide a visual analysis of the 3D structure, including the 3D porosity and distributed voids. The main limit is the difference of density between the lignocellulosic fibers and the polymer matrix that may be too low to obtain exploitable images.

## II-6.2 Mechanical analysis

Micromechanical analyses rely on the study of the mechanical behavior of a model microcomposite composed of a single fiber embedded in a small volume of the matrix. Stress transfer between fiber and matrix can be quantified by interfacial shear strength (IFSS). This characteristic can be determined using micromechanical tests such as pull-out or fragmentation tests. Nevertheless, they are not possible in case of short fibers or particles.

Static mechanical testing at the macroscopic scale is the most common technique used for assessing the mechanical performances of composite materials. There are also in situ tensile test by SEM that is a micromechanical characterization technique of composite materials which consists in submitting a coupon to a tensile mechanical loading while observing it by SEM.

Dynamic mechanical analysis (DMA) is a technique dedicated to the assessment of the viscoelastic behavior of materials, mainly polymers and composites. A specimen is submitted to sinusoidal stress in tension, bending, shearing or torsion and the resulting strain is measured, allowing determining the stress/strain ratio as a complex modulus. A poorly bonded interface potentially leads to local sliding-friction mechanisms and thus to additional global dissipation which tends to increase the damping factor while a strong interface cohesion tends to decrease it.

## II-6.3 Thermal analysis

Thermogravimetric analysis (TGA) is commonly used to determine the thermal stability of natural fibers. The presence of grafted molecules onto natural fibers modifies their thermal stability but it is generally more due to side effect of the reaction such as extraction of non-cellulosic components or decrease of cellulose crystallinity than to the grafted moieties. Only few papers were focused on the understanding of thermal degradation mechanisms within biocomposites in relation to the filler/matrix interface. Fan and Naughton [178] suggested that an increase in temperature leads first to the interfacial separation due to filler shrinkage.

Differential Scanning Calorimetry (DSC) can be used to study the effect of fiber addition on thermal properties of the matrix. Concerning the polymer crystallization, two factors are influenced by the interface modifications: (i) the nucleating effect of fillers that impacts

crystallization kinetics, and (ii) the steric hindrance that alters the growth of crystals and could inhibit crystallization. A decrease of the nucleating effect of the treated fillers is explained by enhanced interactions between the matrix and the fillers [96]. Similarly, an increase of the glass transition temperature is explained by a decrease of polymers chains mobility due to enhance filler/matrix interactions [179].

## II-6.4 Mass transfer properties

Mass transfer properties can also give information of the filler/matrix interphase, especially water vapor permeability (WVP). In most cases, the WVP of biocomposite increases with the filler addition. In addition to aggregation and percolation phenomena, a poor filler/matrix adhesion would generate voids in the polymers which ease the transport of the water molecules throughout these regions [180].

## II-7 Impact of surface treatment on the reinforcing properties of lignocellulosic fillers

Table 9 sums up the effect of some fiber surface functionalization on the mechanical properties of biocomposites as compared to untreated fiber based composites.

Table 9. Examples of the effect of fiber surface functionalization on the mechanical properties of biocomposites (E: Young's modulus,  $\sigma$ : tensile strength,  $\epsilon$ : strain at break) as compared to untreated fiber based composites.

Chemical treatment	Reagent	Fiber type	Matrix	Fiber content	E	$\sigma$	$\epsilon$	Source
Esterification	Dodecanoyl chloride (C12)	Cellulose fibers	LDPE	15 wt%	+ 21%	+ 35%	+21%	[120]
				30 wt%	- 3%	- 3%	-39%	
	Octadecanoyl chloride (C18)			15 wt%	+ 41%	+ 55%	+66%	
				30 wt%	- 21%	- 8%	-22%	
	Hexanoyl chloride (C6), DS=0.42	Cellulose	LDPE	30 wt%	+ 51%	+ 73%	+30%	[121]
	Hexanoyl chloride (C6), DS=1.26				- 7%	+ 34%	+40%	
	Dodecanoyl chloride (C12), DS=0.61				- 11%	+ 4%	+180%	
	Dodecanoyl chloride (C12), DS=1.28				- 31%	+ 56%	+140%	
	Docosanoyl chloride (C22), DS=0.01				+ 37%	+ 3%	-60%	
	Docosanoyl chloride (C22), DS=1.01				+ 4%	+ 62%	+50%	
	Acetic anhydride, DS=1.6	Flax	PLA	16 vol%	+ 18%	-	-11%	[133]
	Acetylation	Flax	PHBH	25 vol%	-	+ 30%	-	[132]
	Propionic anhydride	Wood particles	PP	50 wt%	+ 18%	+ 12%	+61%	[144]
	Succinic anhydride	Wood particles	PP	50 wt%	+ 10%	+ 6%	+33%	
Silanization	3-Aminopropyltriethoxy silane	Ramie	PLA	30 wt%	-	+ 13%	+28%	[114]
	N-(n-butyl)-3-aminopropyltrimethoxy silane	Cellulose fiber	TPU/DAT A blend (80/20)	10 wt%	+ 16%	-	-	[113]
	Trimethoxy(octadecyl) silane	Wood flour	PHBV	20 wt%	+ 16%	+ 6%	-	[116]
	Mercaptopropyltrimethoxyl silane (MRPS)	Flax	PLA	20 wt%	+ 5%	+ 20%	-	[96]
Alkali + Silanization	Flax	PLA	20 wt%	+ 6%	+ 25%	-		
Carbamylation	Methylenediphenyl-diisocyanate (MDI)	Wood flour	PLA	20 wt%	0%	+ 6%	+12%	[181]
			PLA	40 wt%	+ 20%	+ 9%	+11%	
Grafting	PEG (350 g.mol <sup>-1</sup> )	Flax	PBSA	25 vol%	- 4%	+ 6%	+6%	[134]
		Flax	PLA	21 vol%	+ 18%	+ 15%	-8%	[133]

The addition of unmodified cellulose fiber leads to a reduction of the tensile strength that is less pronounced in case of modified cellulose [121]. This suggests a better interfacial adhesion matrix/filler for grafted fibers and an improved level of dispersion of the fillers in the matrix. Similarly, the elongation at break was higher for modified fiber-based composites. The results from Freire *et al.* [121] clearly demonstrate that the final properties of the composites also depends on the DS of the modified cellulose. A strong degradation of fillers can cancel the beneficial effect of improved interfacial adhesion on the mechanical properties [120].

Generally, the fibers functionalization improved the mechanical properties of the resulting composite materials. An improvement in the range of 40% for tensile strength and Young's modulus can be reasonably expected after surface treatment (Figure 19). The main limitation is related to potential alteration of the intrinsic properties of the fillers. The polymer matrices properties can be also altered by the fillers treatment. Indeed, the grafted chemical functions can diffuse within the matrix or interact with it.

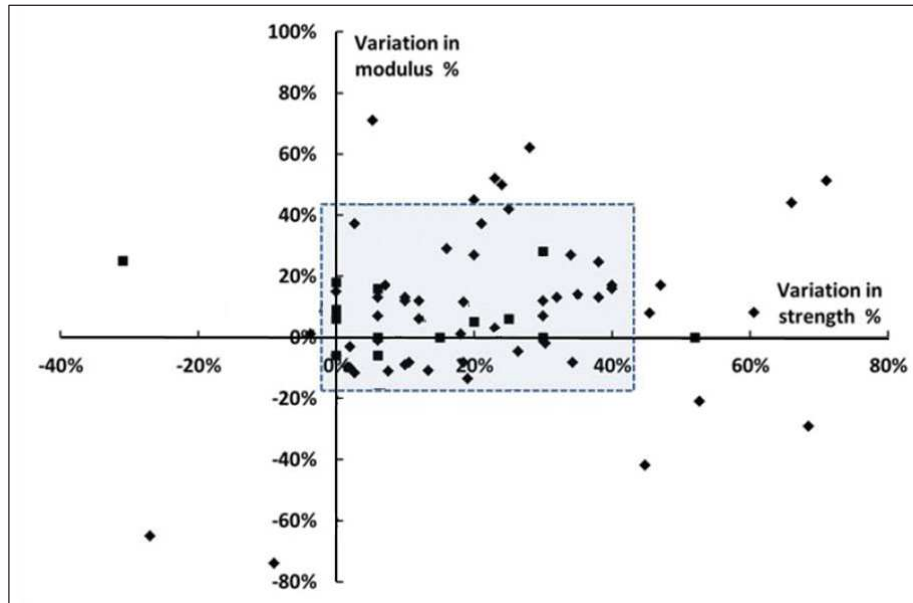


Figure 19. Ashby plot of variation of modulus versus variation in strength of composites reinforced with short natural fibers after their modifications (tensile properties). Non-exhaustive set of data, ■ for polyolefins based composites and ◆ for biopolyesters based composites adapted from [37].



### III. Eco-design of biocomposites

Up to now, the development of biocomposites has mainly been done by focusing on the improvement of their performance (technical properties), while decreasing as much as possible the overall economic cost of materials. Given the current environmental issues, biocomposites should also be designed in such a way to decrease their overall environmental impact. Indeed, the fact that the raw materials are biosourced and/or that the final materials are either biodegradable or recyclable is not enough to make it clean for the environment. The Brundtland Report presented for the first time in 1987 the idea of sustainable development [182]. It is defined as the “development that meets the needs of the present without compromising the ability of future generations to meet their own needs.”

First, the main bioplastic matrices, especially PHA are presented. Then, the main properties of PHA composites are discussed including the biodegradability. Finally, the principle of life cycle assessment and its application to composites are exposed.

#### III-1 Biosourced and biodegradable polymer matrices

##### III-1.1 Categories of bioplastics

Bioplastics are plastics that are either biosourced and/or biodegradable (Figure 20). They can be classified according to three characteristics: their origin (renewable vs. fossil), their synthesis (chemical or enzymatic) and their end of life (biodegradable or not). Here, only thermoplastic resins are considered.

A first category includes biodegradable/compostable biopolymers obtained by conventional polymerization of monomers derived from oil cracking. Among them, there are biodegradable copolyesters such as polybutylene co-apidate terephthalate (PBAT) available under the reference "Ecoflex" from BASF or poly(butylene succinate co-adipate) (PBSA) under the reference "Bionolle" by Showa Denko.

A second category includes biobased but non-biodegradable/compostable biopolymers (biopolyolefins, biopolyurethanes, biopolycarbonates, etc.) produced from monomers derived from agro-resources. This category is booming not to contribute to the depletion of fossil resources. There are bio-PET (Globio grade from Toyota Tsuho), bio-PA (EcoPaXX grade from DSM) and bio-PE (Braskem).

A third category includes biobased and biodegradable/compostable biopolymers, but synthesized by conventional polymerization of monomers from the deconstruction of biomass. The main advantage of this category of polymers is the ability to produce polymers with controlled properties. The poly(lactic acid) (PLA) is produced by polycondensation of lactic acid. Lactic acid is from fermentation from renewable carbon sources such as glucose or maltose

by *Lactobacillus sp.* in the presence of calcium hydroxide. The lactic acid can also be obtained from fossil resources. The properties of PLA are close to those of polyolefins, but their rigidity is much higher because of a glass transition temperature between 5°C and 60°C depending on the PLA grades. The main inconvenient of PLA is the fact that it is not a biodegradable in natural environments, but only compostable under industrial conditions. The main commercial grade is "IngeoTM" (Natureworks-Cargill, USA).

Finally, a fourth category includes biopolymers that meet all the "bio" criteria, produced by biosynthesis in plant cells or by bacterial fermentation. On the one hand, there are the agropolymers (proteins, starch, cellulose) which are directly derived from the plant, and which are generally available in very large quantities. But their intrinsic reactivity makes them very sensitive to environmental conditions (temperature and humidity), so unstable. It is the starch-based mixtures that dominate this category of biopolymers, notably with the Mater-Bi grade from Novamont. On the other hand, there are microbial biopolyesters, for example poly(hydroxyalkanoates) (PHA), produced by bacterial fermentation which have excellent barrier properties and high water resistance, but are very expensive (around 5 €/kg minimum). The major interest of these bacterial biopolyesters is the possibility of producing them from residues.

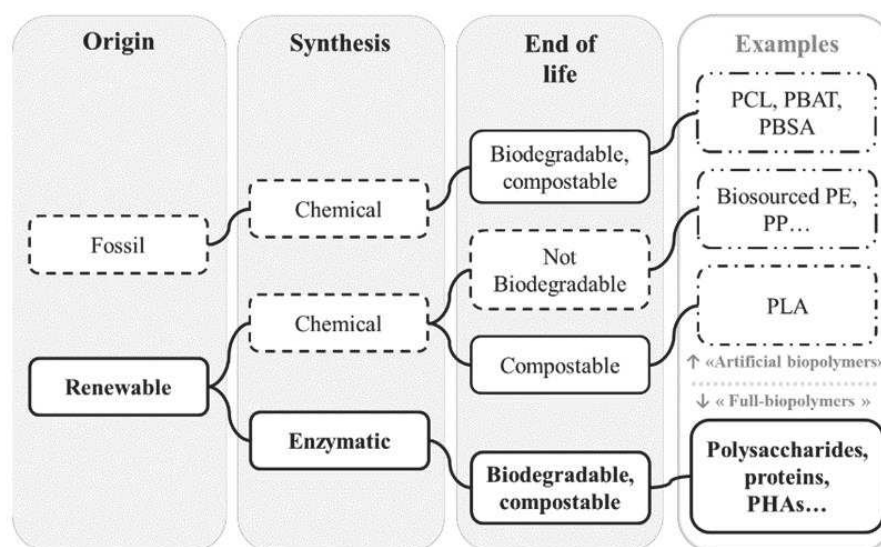


Figure 20. Main groups of bioplastics from [12]

The most promising bioplastic category for the future is the one that meets all three "bio" criteria, namely biosourced, biosynthesized and biodegradable biopolymers (fourth category). However, this category only represents 21% of the bioplastics market [183]. The term "biopolymer" should be only reserved for this category of bioplastics to avoid confusion.

Bioplastics (2.11 million tons in 2018) currently account for only 1% of the total annual production of plastics (350 million tons) [183]. But the demand is more and more important,

especially in the field of packaging. The latest predictions made by European Bioplastics and the Nova Institute thus estimate a production of about 2.62 million tons in 2023 [184]. Flexible or rigid packaging is the major field of application for bioplastics (58%). Other applications are textiles, agriculture, horticulture, construction, automotive, and consumer goods.

### III-1.2 Polyhydroxyalcanoates (PHAs)

Polyhydroxyalkanoates (PHAs) are the most well-known biosourced and biodegradable plastics. They are polyesters produced by microorganisms from glucidic or lipidic substrates, mostly as intracellular storage compounds for energy and carbon. A wide variety of different monomer compositions of PHAs has been described (Figure 21), that provide different properties and functionalities.

The copolymer of poly- $\beta$ -hydroxybutyrate-co- $\beta$ -hydroxyvalerate (PHBV) is one of the first high-profile biodegradable plastics to be used in packaging. It has generally properties close to polypropylene. It is possible to control the relative amounts of butyrate and valerate units in this copolymer by changing the diet fed to the bacteria. The homopolymer of poly- $\beta$ -hydroxybutyrate (PHB) is melt processable with a melting point at 185°C and a glass transition temperature at -4°C [185]. These characteristic temperatures are dependent on the valerate content and decrease when the HV content increases. PHBV with higher valerate content are easier to be used in melt process and the flexibility and elongation increase, whereas the tensile strength decreases. The HV makes the PHB more ductile and less brittle. PHBV has attracted great attention because of its improved thermomechanical properties as compared to PHB.

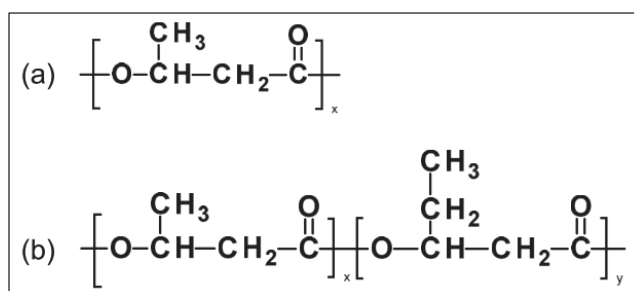


Figure 21. Chemical structures of (a) poly( $\beta$ -hydroxybutyrate) (PHB) and (b) poly(3-hydroxybutyrate-co-3-hydroxyvalerate) (PHBV)

Table 10 presents the main PHA providers in the world. The only grade commercially available in large quantities is the copolymer PHBV, supplied by the Chinese company Tianan under the reference EntMat. This PHBV is currently produced from a food resource, namely glucose syrup from maize, which contributes to its high price (5 €/kg). In addition, this commercial PHBV has a limited 3-hydroxyvalerate (3HV) content (3% for the EnMat grade), which limits their application because of a too low viscosity, too slow crystallization kinetics and a melting temperature very close to the degradation temperature. They are important disadvantages in

thermoplastic processes. Finally, the final material is also brittle (elongation at break around 2%) due to an excessive crystallinity ( $> 60\%$ ).

The EcoBioCAP project (2011-2015) demonstrated the feasibility of high-valerate (10-25%) PHBV production from agro-food residues and the use of mixed cultures (MMC) [186]. The ANR Valoria project has demonstrated that during the PHA biosynthesis step, the choice of raw materials and the control of the operating conditions are essential to ensure the accumulation of PHA in the cells and to control the composition in monomers [187]. Today, many projects focus on the use of non-food competitive resources for the production of PHAs, for example with agricultural residues (European NoAW project, <http://noaw2020.eu/>) or urban waste (European RESURBIS project, <http://www.resurbis.eu/>).

Table 10. Industrial scale PHA manufacturers currently active worldwide [188].

Company	Product (Trademark)	Substrate	Production capacity (t/year)
Biomer, Germany	PHB (Biomer)	Sugar (sucrose)	-
Bio-On Srl., Italy	PHB, PHBV (Minerv)	Sugar beets	10 000
Kaneka, Japan	P(3HB-co-3HH) (Aonilex)	Plant oils	3 500
PHB S.A., Brazil	PHB, PHBV (Biocycle)	Saccharose	3 000
TianAn, China	PHB, PHBV (EnMat)	Corn (glucose)	30 000
Tanjin GreenBio, China	PHB (Sogreen)	Sugar	10 000
Yield10 Bioscience (Metabolix), USA	PHB (P226)	-	-

## III-2 PHA/short fiber-based biocomposites

### III-2.1 Processing

It is important that agro-resourced materials, including biocomposites, can be used with conventional plastic processes (extrusion, injection, thermoforming, calendering) to consider their use at industrial scale. In some cases, and depending on the application, the solvent casting method can be used. The main limitation of some bioplastics is their thermal sensitivity due to a melting temperature close to the degradation temperature, which can lead to degradation of the polymer during the process of implementation [189]. Some problems related to the processing of these materials can be also due to the hydrophilic nature of the fillers.

Among the processing and production technologies for biocomposites; injection molding, extrusion, compression molding, sheet molding and resin transfer molding are the major manufacturing processes. In this thesis the extrusion will be used. The extrusion process is used by the plastics industry for the production of granules and also in the continuous production of semi-finished products (films, rods, tubes). Single screw or twin-screw extruders that run either co- or counter-rotating can be used for this process. It has a good mixing effect and the fillers are generally homogeneously distributed and wetted in the thermoplastic. When the

natural fillers undergo thermomechanical treatment, they can be altered and their size can be reduced. It highly depends on the process conditions: screw design, temperature profile, rotation speed and feed rate (residence time). A good dispersion of the fillers has to be obtained while preserving their integrity. Filler amount rarely exceeds 50–60 wt%.

### III-2.2 Properties of PHA-based biocomposites

The incorporation of natural fillers in PHBV allows to obtain cheaper materials that are still biodegradable. The functional properties are also modulated by the natural fillers.

The mechanical properties of different PHBV-based composites are presented in Table 11. The Young's modulus is often increased with the addition of natural fibers because of a mixing law (PHBV has a Young's modulus around 3 GPa whereas fibers range from 5 to 100 GPa). The increase of the Young's modulus is important for filler content higher than the percolation threshold. As regards the properties at break (tensile strength and strain), they are mainly dependent on the quality of interfacial fiber/matrix adhesion. Moreover, there is a critical limit threshold of fiber length and filler content below which the transfer of stress from the matrix to the fibers is not done efficiently. Mechanical properties decrease with increasing filler content and increasing filler size (for low aspect fillers) [190]. This negative impact of fillers is mainly due to poor filler/matrix affinity, agglomeration and the occurrence of defects in the presence of fillers.

Table 11. Mechanical properties of PHBV-based composites (the neat PHBV properties are written in brackets to allow comparison).

Fillers	Filler content (wt%)	Young's modulus (GPa)	Tensile Strength (MPa)	Elongation at break (%)	Source
Bamboo (fibers)	40	2.9 (1.1)	16.1 (21.0)	-	[191]
Coir (particles)	30	3.9 (2.5)	6.2 (11.8)	2.1 (2.8)	[192]
Corn straw (short fibers)	30	3.6 (1.1)	23.3 (23.0)	1.1 (5.5)	[193]
Flax (fibers)	30	6.8 (3.0)	31.5 (40.0)	1.5 (3.5)	[194]
Hemp (fibers)	30	3.5 (2.4)	27.0 (25.9)	1.1 (1.4)	[195]
Jute (fibers)	30	7.0 (2.1)	35.2 (27.3)	0.8 (7.0)	[196]
Olive pomace (stone particles)	30	2.2 (2.7)	7.7 (34.2)	0.6 (2.3)	[30]
Olive pomace (pulp particles)	30	2.4 (2.7)	21.7 (34.2)	1.5 (2.3)	[30]
Spruce (particles)	40	0.5 (0.5)	20.2 (32.0)	6.6 (17)	[197]
Spruce (short fibers)	40	0.5 (0.5)	17.4 (32.0)	5.5 (17)	[197]
Soy stalk (short fibers)	30	2.5 (1.1)	20.2 (23.0)	2.1 (5.5)	[193]
Wheat straw (short fibers)	30	3.8 (1.1)	24.9 (23.0)	1.4 (5.5)	[193]
	20	2.6 (2.8)	16.9 (36.4)	1.1 (1.8)	[190]

The impact of the introduction of plant fibers on the transfer properties depends on the rate of charge, the fiber morphology, their intrinsic characteristics (e.g. crystallinity and composition) and their state of dispersion within the polymer matrix. An increase in permeability is systematically observed for filler content higher than 10 wt%. It is due to the fact that plant fibers are more permeable than PHBV matrix. Another explanation is the creation of macroscopic defects within the biocomposite resulting from the agglomeration of the fibers and/or by a low interfacial filler/matrix adhesion.

### III-2.3 Thermal stability of PHAs upon processing

PHAs have their melting temperature close to the degradation temperature, which can lead to degradation of the polymer during the process of implementation. The two main thermal degradation reactions of PHBV are well described in the literature: a random cleavage of the polymer chains by cis-elimination, leading to a drastic reduction in the molecular mass, and in to a lesser extent, a trans-esterification reaction leading to the crosslinking of the polymer chains [198]. This thermal sensitivity can be mitigated by playing on the constituent monomers of the polymer.

Thermal degradation reactions were even more important when incorporating lignocellulosic fibers due to an increase in shear forces during extrusion. It has been shown that incorporation of lignocellulosic fibers also induces PHBV degradation reactions by (i) hydrolysis due to the presence of residual water molecules adsorbed on the fibers and (ii) alcoholysis due to the presence of surface hydroxyl groups [199].

## III-3 Biodegradability of biocomposites

### III-3.1 Assessment the biodegradability of materials

Lignocellulosic fillers are particularly interesting because they potentially allow improving the performance of the material without compromising its biodegradability. By definition, biodegradation is a biological process of degradation of organic materials into molecules simpler and smaller ( $\text{CO}_2$ ,  $\text{H}_2\text{O}$  for example). Biodegradation in presence of oxygen (aerobic) can be differentiated from biodegradation without oxygen (anaerobic).

It must be noted that the (bio)degradation of a product varies from one environment to another. In most cases it is the temperature and the microbial activity which determines the rate and level of (bio)degradation (Figure 22). Compost is considered as the most aggressive environment, while landfill is considered as the least aggressive environment [200]. It is therefore not possible to extrapolate positive biodegradation results from one environment to another.

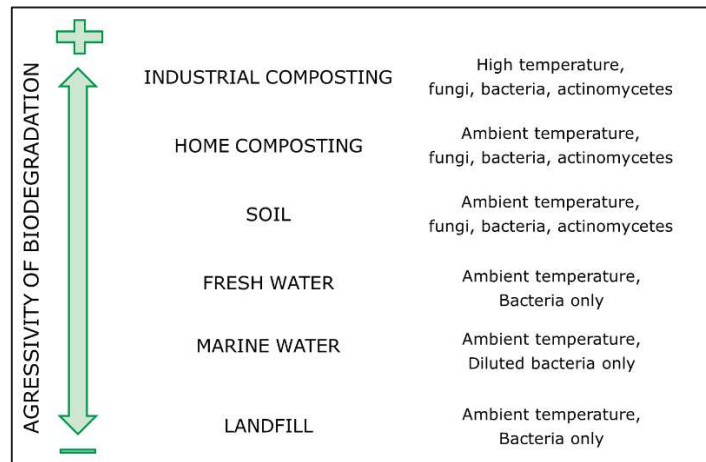





Figure 22. Biodegradation in different environments

There are standards to describe the biodegradability of materials. In case of respirometric test, at 58°C (industrial composting) the released CO<sub>2</sub> should be higher or equal to 90% of CO<sub>2</sub> produced by the biodegradation of the cellulose (reference) in less than 6 months in aerobic (EN 13342) or anaerobic (EN 14995) conditions. For home composting, at 28°C the released CO<sub>2</sub> should be higher or equal to 90% of CO<sub>2</sub> produced by the biodegradation of the cellulose (reference) in less than 2 years (NF EN 17033). There are labels that certify the conformity with the standards (Table 12).

Table 12. Existing biodegradation labels.

Label	Logo
OK compost Certification label of ISO 18606, NF EN 13432 et CAN-BNQ 0017-088-4 standards	
Ok compost Home Certification label of NFT51-800 standard	
OK Biodegradable Soil Certification label of NF U 52-001 standard	

### III-3.2 Biodegradability of lignocellulosic-based biocomposites

Plastics are solid materials where biodegradation happens on the surface. Chinaglia et al. explored the role of particle size on biodegradability by milling and sieving polybutylene sebacate (PBS) pellets to obtain different specific surface areas [201]. It was showed the materials displaying high specific area were biodegraded faster than the others.

PHAs are fully biodegradable by the breakage of the ester from the end of the chain. The biodegradation of polyhydroxyalkanoates (PHAs) takes place either under, anaerobic conditions to produce carbon dioxide (CO<sub>2</sub>), water (H<sub>2</sub>O) and methane or under aerobic

conditions to produce CO<sub>2</sub> and H<sub>2</sub>O. The biodegradability property of PHBV has been demonstrated in soil, water, and compost [202,203]. The copolymer PHBV tended to be degraded faster than PHB. The degradation rates were very different depending on the environment and increased with temperature.

The biodegradability of a lignocellulosic composite mainly depends on its polymer matrix. Many studies have shown that lignocellulosic composites are biodegradable if they are made up of a biodegradable polymer matrix. The composition of lignocellulosic fibers used as fillers also influences the biodegradation behavior of their composites. Indeed, a high content of lignin will slow down the biodegradation [204]. The use of compatibilizers in biocomposites may affect the rate of biodegradability as shown in PLA/coir fibers composites with maleic anhydride as coupling agent [205]. The compatibilized composite had lower biodegradation (53%) than the uncompatibilized composite (which showed 60% biodegradation) in a 90 days test period.

In PHBV/wheat straw composite, the presence of straw did not affect biodegradation rate evaluated in liquid environment and in long term soil burial tests [179]. It was also noticed that PHBV or composites degraded slower than cellulose reference materials (Whatman) but faster than neat straw. Lignocellulosic materials biodegrade usually slowly due to their structural complexity and presence of lignin which is quite recalcitrant to microbial degradation.

The biodegradation of a wood flour/Mater-Bi composite was studied in a sewage sludge reactor [206]. Wood flour enhanced the biodegradability of the material. In addition, results indicated the biodegradation also depends on the processing method. Higher roughness leads to wider bacterial attack and effective packing of matrix and filler together reduced the biodegradation.

Therefore, these results support the hypothesis that some physical, chemical, and/or biological properties of PHBV can be enhanced without hardly impairing its original biodegradability.

## III-4 Life cycle assessment

### III-4.1 General principle

Life cycle assessment (LCA) is a technique to assess environmental impacts associated with all the stages of a product's life from cradle-to-grave. It assesses the environmental impact of a product, a service or a system in relation to a specific function and this by considering all the steps of its life cycle (Figure 23). All the points on which a product can be improved are identified and it contributes to the development of new products. Thus, LCA is useful for industrial companies to know which strategies of improvement are the best, knowing the distribution of the impacts. Environmental regulations can be anticipated and respected, allowing to be in the vanguard and have a good reputation among consumers. It is generally done *a posteriori* on an existing product or from the design step and constitutes a decision-making tool such as a cost study or feasibility study.



An LCA consists of determining all the exchanges between the product system (technosphere) and the environment (ecosphere) and calculating the environmental impacts associated with these elementary flows. Human activities withdraw “primary resources” (oil, minerals, etc) and release pollutants (waste, gas, etc). The whole life cycle of the product is thus considered and makes possible to arbitrate pollution displacements related to the various alternatives. The different steps of the cycle can be condensed as followed: raw material acquisition, manufacturing, distribution use/maintenance/re-use and end-of-life activities.

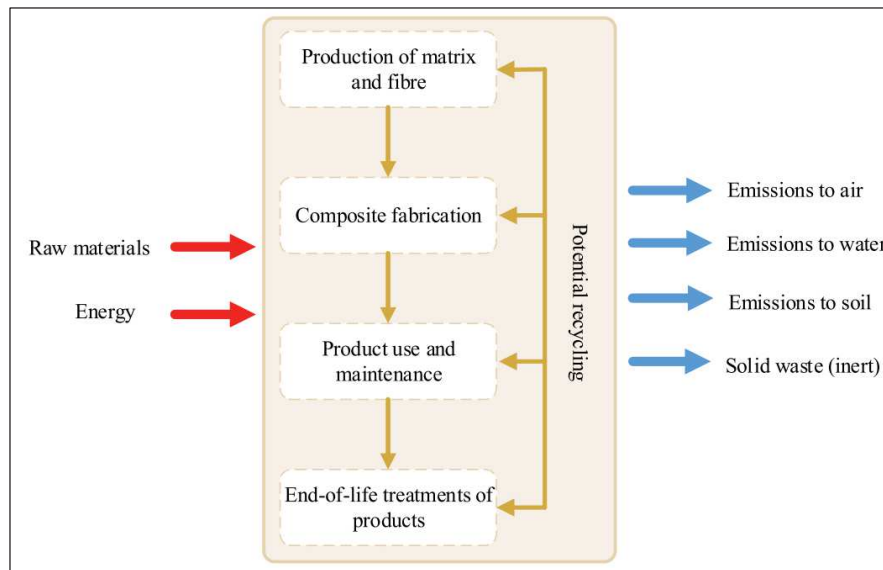


Figure 23. Life cycle steps for composite materials [207]

LCA has been described and explained by two main international standards: ISO 14040-14044 [208,209]. ISO 14040 describes the principles and framework for life cycle assessment whereas ISO 14044 provides more details about the technique itself. According to these references, the method can be divided in four steps: the definition of the goal and the scope, the inventory, the impact assessment and finally the interpretation (Figure 24).

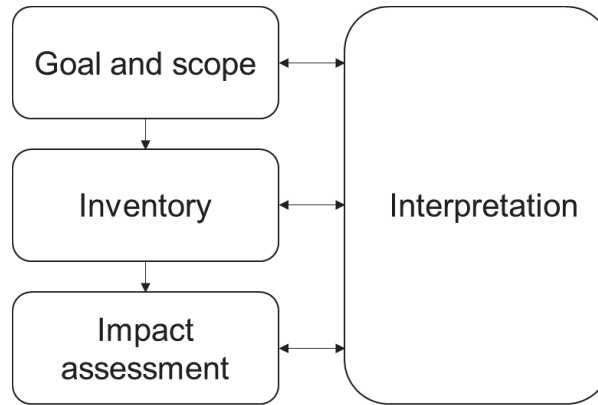


Figure 24. The main steps of an LCA

The first step consists of describing precisely the study, identifying the product, why it is performed, who the target audience is, and what the study intends to answer. Once, the objectives and the context are defined, the scope is determined. It is a clear description of what is included/excluded from the study, what is the functional unit. The functional unit provides a reference to which inputs and outputs are related. The validity of the study and its conclusions highly depends on it [210]. Finally, the boundaries of the system are set, the possible scenarios described and the assumptions made.

The inventory consists of making a quantitative description of the flows of matter, of energy and pollutants involved in the previously defined system. Data are collected for all elements related to the unit processes. It compiles and quantifies inputs and outputs relative to the system. The reference flows which is the amount of product necessary to fulfill the function, are calculated for each unit process. The data collection is often a difficult task because of the data availability. A review and comparison of life cycle inventory was studied by Shu et al. [211]. Data bases, such as Ecoinvent [212], help the inventory work including inputs and outputs for numerous process and products, even if a customized collect is necessary.

The life cycle assessment highly depends on the choices made in the first two phases. Three steps must be followed according to the ISO 14040 standard: selection, classification, characterization. First, the impact categories are selected in accordance with the scope. Then, the different elementary flows are classified in the respective category. Lastly, the elementary flows are translated and aggregated into indicator scores which represent the extent of the total impact for each category. Moving from inventory to impact assessment is a delicate step of LCA largely discussed, this is why different methodologies have been developed for impact analysis: Eco-indicator 99, CML 2001 [213], IMPACT 2002+ [214], etc. The ILCD 2011 Midpoint method was released by the European Commission, Joint Research Centre in 2011. It supports the correct use of the characterization factors for impact assessment as recommended in the ILCD guidance document [215]. ReCiPe method is the most recent and harmonized indicator approach available. The choice of the ReCiPe method is also supported by the International Reference Life Cycle Data System (ILCD) Handbook [216]. It transforms

the inventory into a limited number of indicator scores. Factors are included depending on the chosen perspective: individualist, hierarchist and egalitarian. Individualist perspective is a short term method, stating that technology can avoid many problems in future, whereas egalitarian model is based on the precautionary principle thinking in long term. Hierarchist method is the consensus model often encountered in scientific models that can be considered to be the default model [217]. Impact assessment can be done at two levels depending on the degree of analysis along a cause-effect chain: midpoints (middle of the causal chain) or endpoints (end of causal chain) (Figure 25). Midpoint indicators are generally preferred because they are more scientifically robust even if they are less evocative. Endpoint indicators are calculated from results of Midpoint with new factors that add uncertainties to the impact values.

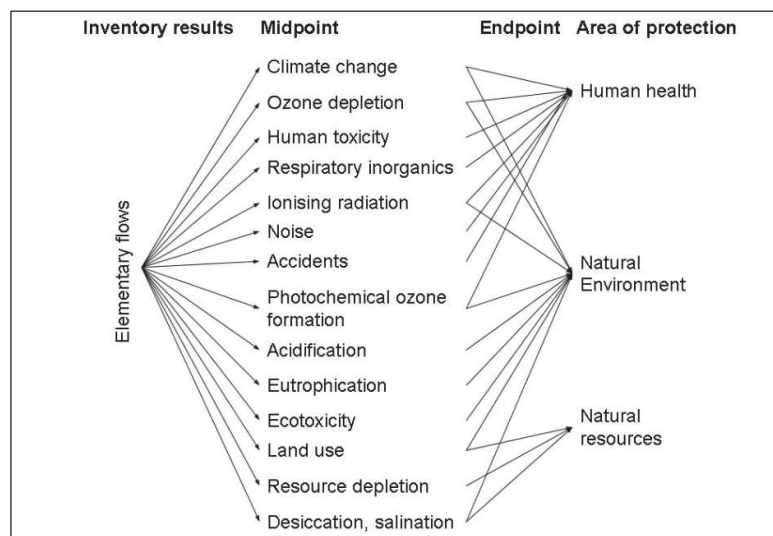


Figure 25. Framework of impact categories for characterization modelling at midpoint and endpoint levels (adapted from [218])

The interpretation is the last phase of the LCA. It makes possible to analyze the results provided by the impact assessment according to the objectives and the scope of the study previously defined. Conclusions are thus made, and improvement can be suggested for decision-making. The results need to be reviewed with sensitivity study. These interpretations may cause LCA to be an iterative procedure, until an inventory model and satisfying impact assessment is found.

It was shown that most of the LCA consider the unit processes as black boxes without taking account different operating conditions [219]. Most of LCA target the product rather than the process because the process is considered as the part of the product life cycle. The inventory used usually literature or industrial data at fixed operating conditions without other precisions. This last decade, an estimation of missing data was done by the use of process simulation for the production of biomass-derived polypropylene [220].

There are some limits to use LCA. The first one is the difficulty to collect data that are the more adapted to the studied product.

### III-4.2 LCA of biocomposites

Le Duigou et al. compared the production of flax and glass fibers [221]. They showed the ecological advantages of flax fibers for most of the environmental indicators. The only drawbacks were the eutrophication remains high mainly due to the use of fertilizers and the land use for its cultivation. Natural fibers have generally less impact than most of the petroleum-based matrices which encourages high filler content [222].

Sometimes, in order to have the same performance and to satisfy the same functional unit, the thickness and weight of the biocomposite must be higher than that of the synthetic composites or neat matrix and thus environmental impacts increase. This was, for example, observed in the case of composite lighting columns where jute was used to substitute the glass fiber reinforcement [223]. In case of composite for automotive application, the use phase represents the main energy consumption of the life cycle. Thus, the reduction of the material mass is very important [224]. The comparison between wood-fiber polypropylene composites (30 % wt) and polypropylene produced by compression molding showed that for the same mass, composite displayed superior environmental friendliness compared to the neat matrix [225].

#### *Concerning packaging materials*

Mango packaging made from PE/natural fiber composite or cardboard were studied through LCA approach [226]. When single use was considered, the cardboard tray had less impact for almost all the considered categories, mainly due to the higher weight of the composite packaging, inducing a higher fuel consumption for transportation and a higher electricity input. The impact of the composite trays was lower than that of cardboard packaging after 4 reuses for the Brazilian scenario and 30 for the European one. The different end of life treatment in Brazil and Europe explained largely this discrepancy. Wikström et al. demonstrated the influence of the user behavior on the environmental impact of food packaging [227]. In a study about biodegradable food packaging, it was concluded that conventional packaging, multilayer film of PP and PA6, display a 90% higher impact than biodegradable one, multilayer film based on starch and PLA [228].

It is worth to note that in case of packaging, the product, such as fresh fruit, can often travel several thousand miles before reaching end-consumers. These long travel distances make lightweight materials interesting from an environmental perspective, as they could help reduce the fuel consumption per transported unit of food [229].

### III-4.3 Consideration of the end of life of materials

Different factors motivate the choice of the waste management system: composition, application, volume on the market and available infrastructure (technical and legislative) for collection and processing. The results of the LCA will be influenced by the selected recovery or final disposal option.

In France, 28% of the municipal waste are landfilled, 30% are incinerated, 24% are recycled, 16% are used in compost and 2% in anaerobic digestion [230].

#### III-4.3.1 Landfilling

Landfilling is the only waste management that does not recover useful material or energy from waste.

#### III-4.3.2 Incineration

Incineration of natural fibers results in recovered energy and carbon credits [222]. In incineration, the natural fibers have a lower calorific value 20 MJ/kg compared to matrix such as PP 48.7 MJ/kg but it is better than glass fibers with a negative energy balance (-1.7 MJ/kg) [231]. Plants stock carbon dioxide thanks to photosynthesis [232]. During their incineration, the CO<sub>2</sub> emitted is biogenic in case of fibers or bio-sourced plastics which induced a lower impact.

#### III-4.3.3 Recycling

In theory, one of the best ways to reduce the impact of a composite is to be able to recycle it, because in this case, the production of virgin material is avoided for the next life cycle. However, no all composites are recyclable, for example thermoset composites. Moreover, the mechanical properties of a recycled material may change and the recycled materials may be not able to fulfill the functional unit.

Numerous studies demonstrate a considerable advantage of recycling over landfill disposal or incineration [233]. The use of thermoplastic matrix allows to consider an end of life by mechanical recycling. Concerning composites with short fibers, several works have studied their recyclability. A biocomposite wood particles/MaterBi (biopolyester from Novamont) with a filler content of 30 %wt was recycled 10 times and their mechanical properties were not significantly altered [234]. The mechanical properties of wood/PP-MA composites were slightly decreased by reprocessing mainly due to the decrease of filler size and the decrease of the matrix molecular weight [235]. In another study, Soccalingame et al. showed also that the composite mechanical properties remain quite stable after 7 processing cycles despite wood flour degradation and PP degradation [236]. The recycling of flax/PLLA composites resulted in the same conclusion than for the other articles: the fiber size decreased as well as the stress and strain at break of the materials [237]. After 3 cycles of injection, the properties rapidly were

declined partly because of the progressive hydrolytic degradation at high temperature of the matrix.

Thus, the choice of the matrix and the filler type has an important concerning the recyclability of the composite materials. There are a large range of types of thermoplastic polymers on the market which does not facilitate the sorting. The treatment of materials made of combination of several resins, such as multilayer packaging, is often technically challenging and can increase significantly the cost. In addition, substances can be added to develop specific properties: plasticizers to modify the rheological characteristics and additives such as dyes, flames retardants, antifungals, etc. In case of composites, fillers are added to modify properties of the materials and reduce the cost. At the end the complexity of the product increases and thus it may hinder the end-of-life treatment. The complexity of packaging contributes to a high level of contamination of the collected waste that reaches the sorting and recycling facilities. Another loss of material can occur with dark or black products that cannot be identified in the optical sorting process [238].

Results from LCA cannot be summarized in generalizations such as “bioplastics are better or worse than other materials”, details and nuances are needed. As bioplastics are still in development and produced in small scale, the different stage of their life cycle are not well optimized. A biased comparison often happens with mature materials. LCA should not restricted innovation to its early stage of development. A balance of view should be provided, with projections of improvements. Indeed, the enhancement of bioplastics are varied. The input biomass can be from non-food crop or agricultural waste streams. The efficiency of processes can be improved with new technologies or larger production scale. In order to develop the idea of the “cradle-to-cradle” idea, the end-of-life options can be rethought with new possibilities such as composting, anaerobic digestion or chemical recycling. Moreover, cascades of successive valorizations in a biorefinery logic be set up.

### III-5 Towards early design

Nevertheless, this expansion will be possible only if constraints are addressed during all the life cycle (Figure 26). From the cradle, with environmentally friendly growing methods, in the middle of the chain with industrially processable materials, and at the end of life with product in accordance with waste management. The eco-conception is a major challenge in the context of circular economy. It is the consideration of the environment during the conception of products. Here a product is in broad sense, it represents a good or a service.

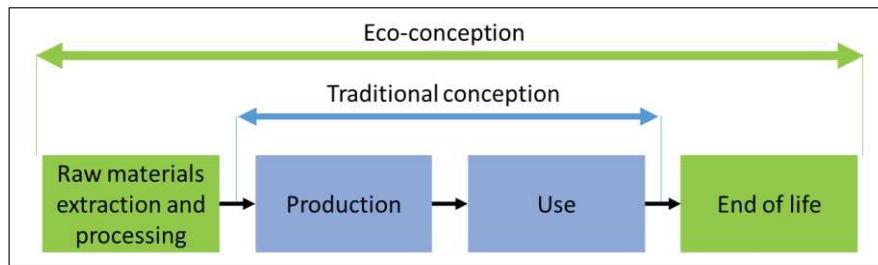


Figure 26. Eco-conception in the life cycle of the product (adapted from [239])

In conception, there are generally three criteria to take into account: the consumer expectation, the technical feasibility and the cost. In eco-conception, a fourth criteria about the environment is added. The solution should be an overlap of all the criteria. Eco-conception (standard XP ISO/TR 14062 2003) aims to improve the ecological quality of a product. Whatever the product, it has negative impacts on the environment, thus the objective is to try to reduce these impacts while keeping its functionalities.

Environment is a new factor in the classical product development processes, it represents only one “piece of the cake” as shown in Figure 27. Indeed, many other pressures appears during the conception, each demands need to be addressed to get a viable product without overstating one factor. The eco-design is defined more specifically as “the systematic integration of environmental considerations into product and process design”.

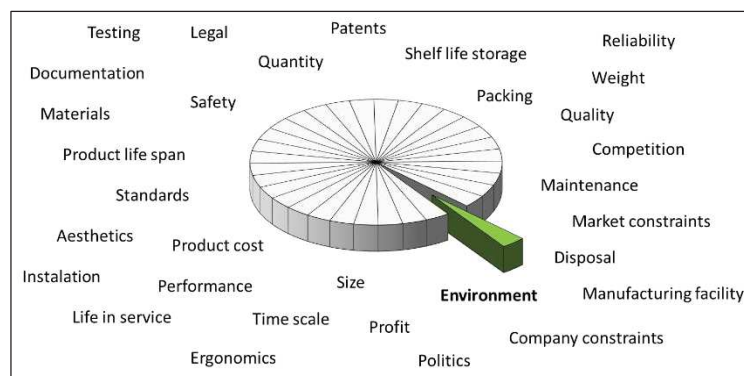


Figure 27. The product development ‘cake’ (Adapted from [240], p 1398).

According to Charter and Chick [241], there are 4 types of strategies :

- Re-pair: transform a negative externality generated by the product into valuable function (example: convert a waste into a product).
- Re-fine: improvement of existing product with integration of the environment in the specifications, synergy with preexisting constraints (example: change materials to improve the technical and environmental performance)

- Re-design: design a product including the environment from the beginning, in conflict with preexisting constraints (example: change of technology to have power and clean engine)
- Re-think: completely rethink the product (example: walking bus for schoolchildren for short distance)

The optimization and improvement of products and processes are possible but in the long run the eco-conception is linked to innovation.

The ideal system is the system that does not exist physically but every functions operate properly [242]. The total “re-think” is dematerialization. An example of dematerialization is the car-sharing; the need is not anymore to buy a car but to have a service that allows to move. Car-sharing adapts to the use, with more flexibility to the needs (small car for city and large car for family). Thus the reformulation of the problematic could lead to the awareness that the best solution is the elimination of the product that we want to green.

Even if the design process itself consumes only a small part of manufacturing costs, it might be considered responsible for most, if not all, environmental impacts a product.

Life cycle assessment (LCA) was described as the “scientific response” for eco-design and as key asset to quantify the environmental impacts. Nevertheless, LCA can be too complicated and time costing. It is based on models and requires significant amounts of highly qualitative data, which, in general, are not available in the earlier phases of the product development process.



## Conclusion Chapitre I.

Il existe une grande diversité de charges de renfort végétales. Des fibres techniques sont issues de cultures dédiées comme le lin et le chanvre. Les résidus forestiers et agricoles représentent aussi une source intéressante de lignocellulose. Les sarments de vigne font partie des agro-résidus mal exploités dont la gestion doit être améliorée. Leur taille chaque année génère de grandes quantités de bois, particulièrement en région Occitanie avec environ 2 tonnes de sarments par hectare. Malgré des extractibles d'intérêts tels que les polyphénols, les sarments de vigne sont aujourd'hui peu valorisés. Par ailleurs, la variabilité de la biomasse lignocellulosique, et notamment des sarments de vigne, reste une donnée peu connue qui doit être déterminée et prise en compte afin d'assurer un sourcing régulier auprès des industriels et ainsi permettre un usage plus large dans le domaine des matériaux biocomposites. Les fibres naturelles, composées de lignocellulose, possèdent une structure complexe. Les propriétés de renfort des charges lignocellulosiques dépendent principalement de leur morphologie, de leur composition chimique, et de leurs propriétés de surface, ces dernières influençant leur compatibilité avec la matrice polymère.

Les modifications des charges naturelles afin d'améliorer les propriétés finales des composites ont été largement étudiées. L'enjeu est désormais de dégager des techniques respectueuses de l'environnement à moindre coût. De plus, la transposition industrielle est primordiale pour pouvoir appliquer ces traitements sur des matériaux à faible valeur ajoutée. L'estérification en voie gazeuse semble remplir ces critères en greffant des molécules hydrophobes à la surface des fibres naturelles.

Dans la logique d'obtention des matériaux entièrement bio-sourcés et biodégradables, les polyhydroxyalcanoates (PHAs) sont des bons candidats en tant que matrice. Leur biodégradabilité en conditions naturelles et en milieu marin a été prouvée. Les biocomposites s'affichent comme respectueux de l'environnement grâce à leur origine naturelle et leur biodégradabilité. Mais encore faut-il le quantifier pour s'en assurer. L'analyse de cycle de vie (ACV) est un outil qui permet de cela, malheureusement la plupart des études publiées s'intéressent à la comparaison fibres naturelles/fibres synthétiques ou à la comparaison bioplastiques/plastiques fossiles. La fin de vie est un enjeu important qui est difficilement quantifiable en ACV. Il existe un manque de connaissance sur la quantification de l'intérêt environnemental des biocomposites. Les enjeux environnementaux se faisant de plus en plus pressants, la recherche pour produire de nouveaux matériaux est stimulée. L'addition de biomasse dans les matériaux peut satisfaire ces enjeux tout en réduisant la dépendance aux ressources fossiles.

Très peu d'études portent sur la valorisation des sarments de vigne en tant que charges de renforts. Les études publiées sur l'usage de résidus agricoles dans les composites sont principalement axées sur les propriétés mécaniques.

# Chapter II. Materials and Methods

## Chapter II. Materials and Methods

This part aims at describing all the materials and methods used during this thesis. Its reading is not necessary to the good understanding of the Chapter III, IV and V. Indeed, each articles already contains a specific “Materials and Methods” part. This chapter gives more details in order to enable future researchers to use the described methods easily. First, the composite components: PHBV, cellulose and vine shoots are described. Then, the filler modifications and the processes used to produce composite materials are explained. Finally, the different techniques to characterize the fillers and the resulting materials are presented.

### I. Materials

#### I-1 Polymer matrix

The polymer used was poly(3-hydroxybutyrate-co-3-hydroxyvalerate) commonly known as PHBV (Figure 28). The polymer pellets were supplied by NaturePlast under the grade PHI002. In fact, it corresponds to the ENMAT grade of Tianan (China), containing 1 wt% of boron nitride as nucleating agent. It is worth noting that two batches were used during this thesis: EDW 2152 for the production of cellulose-based composites and EDW 2267 for the production of vine shoots-based composites. A control (processing and characterization of material properties) was systematically performed to interpret as much as possible differences between batches. The main properties given by the supplier are presented in Table 13.

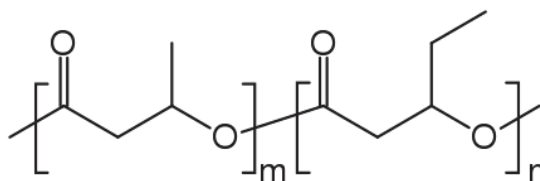


Figure 28. Formula of PHBV

Table 13. Main characteristics of the PHBV grade (PHI 002) given by the supplier NaturePlast.

	Method	Unity	Value
<b>General Properties</b>			
Density	ISO 1183	/	1.23
MFI (190°C ; 2,16 kg)	ISO 1133	g/10min	5 – 10
Hardness (15s)	ISO 868	Shore D	76
Optical properties	/	/	Opaque
<b>Thermal Properties</b>			
Melting temperature	DSC	°C	170 – 176
<b>Mechanical Properties</b>			
Stress at elastic limit	ISO 527	MPa	18.7
Strain at elastic limit	ISO 527	%	1
Stress at break	ISO 527	MPa	39,6
Strain at break	ISO 527	%	3.2
Young's modulus	ISO 527	MPa	4200
Flexural modulus	ISO 178	MPa	3800
Charpy shock (unnotched)	ISO 179	kJ/m <sup>2</sup>	5

The polymer granules were stored away from air and light as well as from source of heat. The packaging was kept sealed until it is ready to be used and resealed quickly to prevent any contamination or moisture regain. Before transformation of the polymer plastic, the granules were dried overnight at 50°C.

## I-2 Fillers

### Cellulose particles

Pure cellulose particles were supplied by J. Rettenmaier & Söhne (JRS) under the commercial name of Arbocel® BE 600-10 TG. The particles were obtained after bleaching and successive grinding of pine cellulose. They were in the form of a fine white powder, with an average particle length of 18 µm (Table 14). The shape of the particles and their morphology were characterized by image analysis from picture taken with a macroscope and SEM observations(see paragraph 0 and 0).

Table 14. Main characteristics of BE 600-10 TG cellulose particles given by Arbocel.

Chemical and physical properties	Value
Cellulose content	99.5%
Average fiber length	18 µm
Average fiber thickness	15 µm
Bulk density (DIN EN ISO 60)	0.23 – 0.30 g·cm <sup>-3</sup>

## Vine shoot particles

Vine shoots were collected in 2017 from Syrah (Figure 29). This choice has been done as it is the most common vine species in Languedoc-Roussillon and in France.



Figure 29. Syrah vine shoots collected in Gruissan (France).

In order to study the impact of both the seasonality and the species on the intrinsic properties of vine shoots, three additional vine species were studied over three years (2017-2019), i.e. another red species (Grenache) and two white species (Chardonnay and Viognier). These pruning woods were collected every year in the same parcels of land in Gruissan (Languedoc-Roussillon) in collaboration with Jean-Michel Salmon (UEPR, INRA). In all cases the pruning mode was “single Guyot cane pruning”, keeping one cane and one-two spurs per vine (Figure 30).

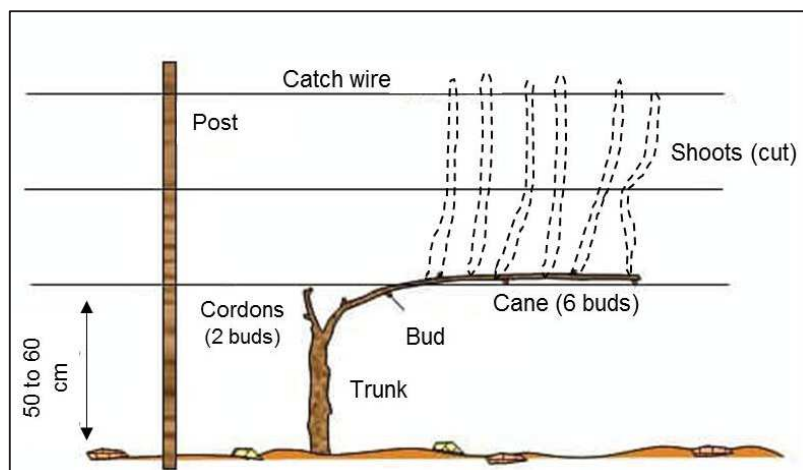


Figure 30. Single Guyot pruning method of the vine

The fresh vine shoots were first air dried outside during 2 months, then they dried 24 h at 60°C in an oven. In order to get particles displaying an apparent median diameter of 50  $\mu\text{m}$ , the milling involved several steps (Figure 31). First, organ dissociation (from meter to centimeter) was realized by applying cutting and crushing forces in a coarse shredder (170  $\text{kg}\cdot\text{h}^{-1}$ , AXT 22D, Bosch, Germany). Then, an intermediate comminution (from cm down to 0.5 mm) at the tissue scale was realized by applying shearing and impact forces in a knife mill (1.5  $\text{kg}^{-1}$ , 2000 rpm, SM 300, Retch, Germany). A first pass was performed with a 4.0 mm sieve, followed by a second pass with a 2.0 mm sieve. Afterwards, an impact mill type 100 UPZ (1.5 $\text{kg}/\text{h}$ , 18 000 rpm, Hosokawa Alpine, Germany), implying impact and shearing processes, was used with a 0.3 mm grid (trapezoid holes) with an output recovery by cyclone. At this stage the median particle apparent diameter ( $d_{50}$ ) was 150  $\mu\text{m}$ . Finally, an ultra-fine ball milling (5L Faure type ball mill) was performed with compression and attrition as mechanical stresses. This mill was filled with 3 kg of metallic balls (1/3 of balls with 15 mm diameter, 1/3 of balls with 20 mm diameter and 1/3 of balls with 25 mm diameter) to occupy 25% of the internal volume. 150 g of biomass were milled by batch, the speed was set at 50 rpm to avoid centrifugation and a residence time was 10 h to get particles around 50  $\mu\text{m}$ . If the different milling steps could not be carried out the same day, the vine shoots particles were stored in hermetic drums at room temperature and dried again at 60°C the day before the scheduled grinding.

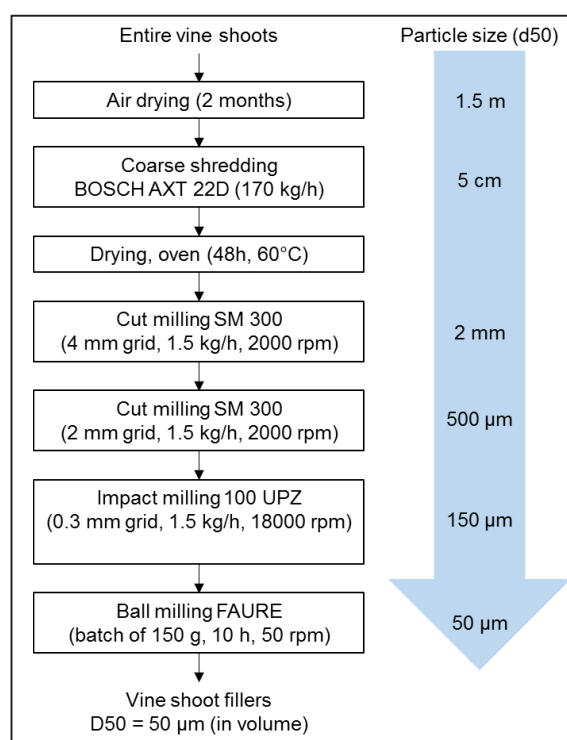


Figure 31. Process diagram for the milling of vine shoots to obtain particles displaying a median particle apparent diameter below 50  $\mu\text{m}$ .

Particles were used as fillers as they are, with no sorting after successive milling processes. The particle size distribution was measured with a laser granulometer (Figure 32) according to the protocol described in paragraph.

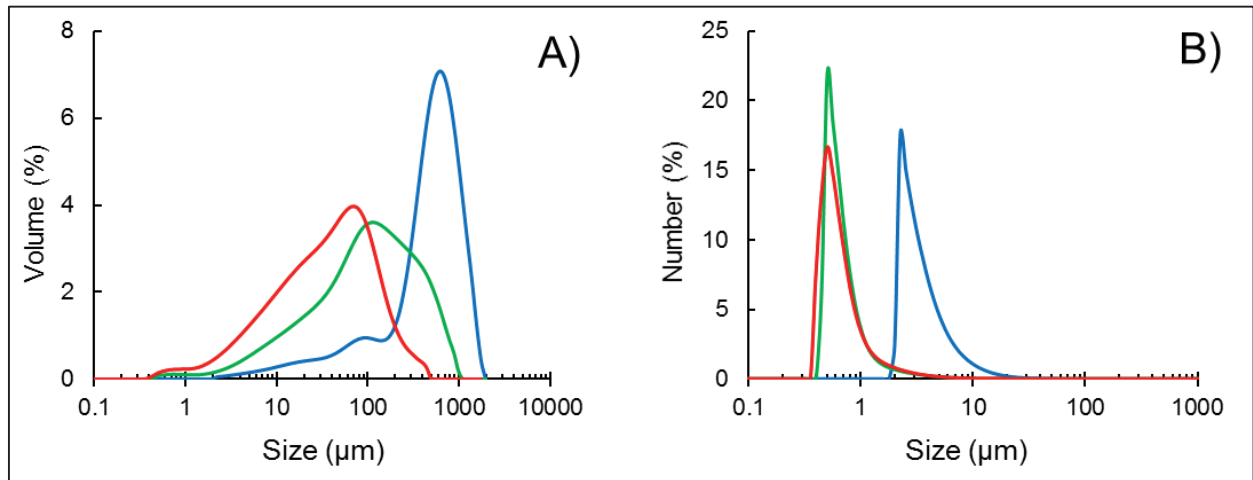


Figure 32. Particle size distribution in volume (A) and in number (B) for milled vine shoots: knife 2 mm (—); UPZ 0.3 mm (—) and ball (—).

## II. Methods

### II-1 Filler modifications

In order to improve the filler-matrix interfacial adhesion in the composite materials, two strategies have been investigated in the frame of this PhD thesis. A part of this thesis was devoted to the study of a gas-phase esterification of the filler surface (surface chemical treatment) in collaboration with CTP (Centre Technique du Papier) and CERMAV (Centre de Recherches sur les Macromolécules Végétales) in Grenoble. Then the impact of a pre-extraction of polyphenols using a solvent-based process (mass chemical treatment) was studied in collaboration with the University of Bologna (Italy), partner of the NoAW project. A very first exploratory work on gamma irradiation was started to create reactive free radicals at the interface (physical treatment) in collaboration with the C2MA team in Alès.

#### Gas-phase esterification

Gas-phase esterification of hydroxyl groups of cellulose substrates was first developed in CTP and CERMAV laboratories on papers and aerogels respectively. The reagent was palmitoyl chloride (C16), it was purchased from Sigma-Aldrich (92% of purity). The experimental set-up used in this study was developed at CERMAV laboratory in Grenoble. It had been optimized for the grafting of cellulosic aerogels especially during the PhD thesis of Matthieu Fumagalli who worked on the reinforcement of elastomers with nanocellulose. In the present study, the

set-up was applied to graft hundred grams of micrometric particles of cellulose and lignocellulose, which was never done before. As shown in Figure 33, it consisted in a jacketed glass reactor with controlled temperature thanks to an oil bath. The reagent was poured in a glass Petri dish that was first placed at the very bottom of the reactor. Cellulose or lignocellulose particles were initially dried at 60°C overnight. Then, they were introduced in nylon mesh bags with a pore size of 7  $\mu\text{m}$  (PA 7/2, Saati, Italy) that were sealed. 4 bags of about 25 g each were put on a Teflon grid just above the reagent, so that there was not direct contact between the reagent and the substrate.

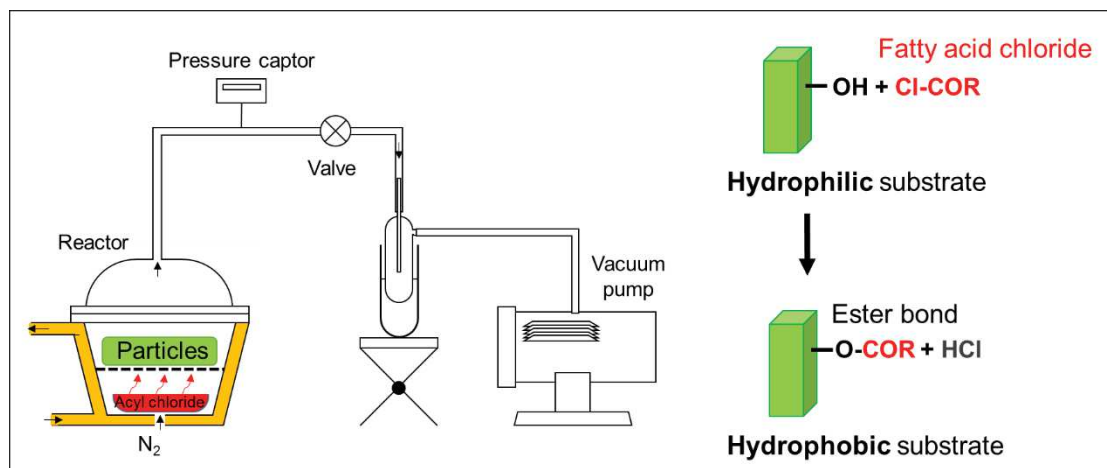


Figure 33. Principle of the gas-phase esterification

The reactor was closed with a greased glass lid in order to have a hermetic system. A constant nitrogen flow was introduced from the bottom of the reactor to diffuse the reagent and also to evacuate by-products that were then trapped before the vacuum pump. A manometer was placed at the output of the reactor to measure the pressure, which could be regulated by a fine control valve. At the end of the reaction, atmospheric pressure and room temperature were reached by stopping the pump, opening the valve and turning the oil bath off. Finally, the grafted substrate and the rest of the reagent were recovered. The grafted sample was then purified with a Soxhlet extraction during 6 hours at 60°C with acetone. No Soxhlet thimble was used, the bags filled with the substrate were directly introduced in the extraction chamber. Lastly, the bags were opened and the grafted particles were dried in oven at 60°C.





Figure 34. Experimental set-up of the gas-phase esterification

The progress of the reaction is characterized by the degree of substitution (DS), which is defined as the molar ratio of the grafting reagent per glucose unit for the cellulose (Eq. 1). It is therefore between 0 and 3.

$$DS = \frac{\text{number of grafted fatty acids}}{\text{number of anhydroglucose unit}} \quad \text{Eq. 1}$$

Several parameters monitor the grafting: temperature, reaction time, pressure, quantity of reagent, quantity of substrate. Experimental conditions of the gas-phase esterification were adapted from works of Berlioz et al. and Fumagalli et al. [160,243]. The pressure was set at 2 mbars, the quantity of reagent was 0.2 eq in order to be in excess compared to surface hydroxyl groups of the cellulose and the quantity of substrate was 100 g for each reaction. By changing the reaction time (from 3 h to 15 h) and the temperature (100°C and 120°C), DS between 0.01 and 0.14 were obtained.

### Polyphenol extraction

Polyphenol extraction is not a “voluntary” filler modification. It is used in order to optimize de biorefinery scheme. The same protocol as the optimized solvent-based extraction with 75% (v/v) acetone from the University of Bologna (partner of the NoAW project) for wine pomace was used to extract polyphenols [244]. 10 g of sample were extracted with 50 mL of solvent (solid/liquid ratio of 1:5). The mixture was incubated at 50°C during 2 hours in a shaking water bath, in a close system to avoid solvent evaporation. At the end of the incubation, liquid extract was separated from solid residue by centrifugation (5 min, 5000 rpm) and then dried at 60°C during 48 h.

## II-2 Production of composite materials

### Compounding using melt extrusion

Compounding or melt extrusion is the process that is used for melt-mixing polymers with additional materials (fillers, additives, pigments...). It is one of the most widespread technologies in plastic, rubber and food industries. Typically, it is carried out using a twin extruder that is a barrel containing two rotating screws which transport materials down the barrel. The materials are heated and undergo shearing between the rotating screws as they are conveyed. The aim is to have a good dispersion of the filler within the matrix. It is a continuous process that forces the materials through an exit die that will give the shape of the extrudate.

Composites were prepared by melt extrusion using a lab-scale co-rotating twin screw extruder Prism Eurolab 16 XL (Thermo Scientific, Germany) (Figure 35). The 8-shaped chamber barrel has a centerline distance of 15.6 mm and two 624 mm long screws were used with length to diameter ratio of  $L/D = 40$ . Different types of dies were used: a flat die of 300  $\mu\text{m}$  with calendering unit to produce plane sheet or a filament die of 3 mm of diameter and a pelletizer to produce granules. In the second case, samples were cooled in a water bath and air-dried at room temperature before being cut by the pelletizer. The screw speed was 300 rpm and the flow rate was  $1.0 \text{ kg}\cdot\text{h}^{-1}$ . PHBV-based composites with cellulose and vine shoots particles as filler had been made. The matrix and the fillers were previously dried at  $60 \text{ }^\circ\text{C}$  overnight before extrusion. PHBV pellets were introduced with a volumetric single screw feeder (Brabender DSR28). A loss-in-weight twin screw feeder (Brabender DDW-MD1-MT2) was used to control fillers feed rate. The combination of these two feeders with the global flow rate of the extruder allows to get different formulation (from 5 to 40% wt%) that would be then checked by a thermogravimetric method.



Figure 35. Melt extrusion set-up (here with a filament die)

Figure 36 displays the different zones in the melt extrusion process : the polymer and fillers were introduced zone 1 and zone 4 respectively. Zone 9 shows a passive vent unit to degas

residual water present in the materials and avoid air bubbles. The screw profiles can be divided in three main parts: melting zone, mixing zone and conveying zone. The screw was assembled by combining feed screw elements (in blue), mixing elements (in green), reverse elements (in red) and discharge elements (in light blue). The aims of this screw profile is to get a short residence time of filler to avoid temperature degradation or breakage while ensuring a good mixing.

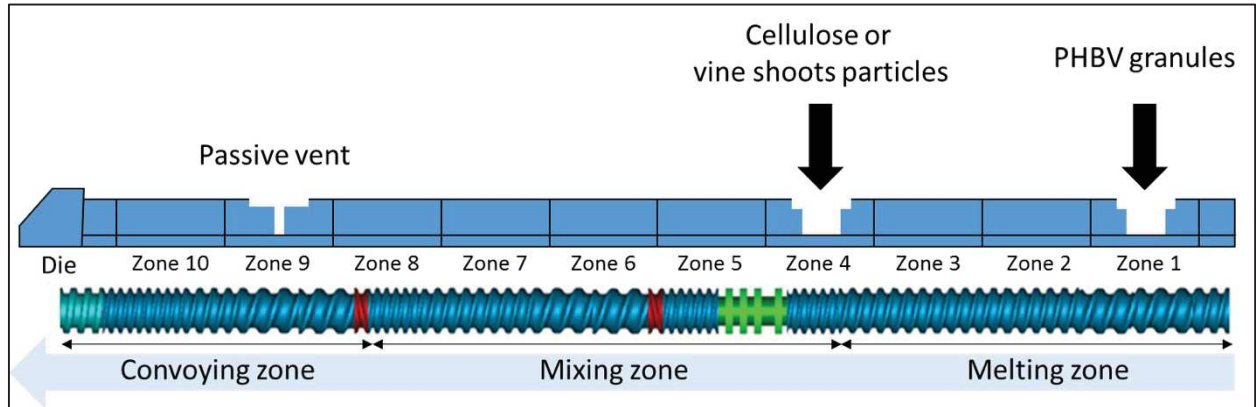


Figure 36. Presentation the melt extrusion process.

The temperature profile, described Table 15, was set up regarding the material melting point and thermal properties of the polymer matrix. The temperatures were optimized so that the viscosity of the melt materials is low enough to allow conveying down the barrel and mixing while keeping temperatures low enough to avoid thermal degradation and to get a usable output. In order to melt the polymer, a constant increase of the temperature was set, followed by a constant temperature zone until the die. The first zone (feeding) started as low as 80°C to avoid plugging phenomenon.

Table 15. Temperature profile used for PHBV-based composite processing.

Zone	1	2	3	4	5	6	7	8	9	10	Die
Temperature (°C)	80	140	160	160	160	170	170	180	180	180	175

Specific Mechanical Energy (SME) is the mechanical energy given to the fluid during extrusion per unit of mass ( $\text{J}\cdot\text{kg}^{-1}$ ). It is the product of the couple  $C$  ( $\text{N}\cdot\text{m}$ ) by the speed of the screws ( $\text{rad}\cdot\text{h}^{-1} = 2\pi\cdot\text{rpm}\cdot 60$ ), divided by the flow of the matter ( $\text{kg}\cdot\text{h}^{-1}$ ). It can be calculated with the following equation (Eq. 2):

$$\text{SME} = \frac{C \times v}{q} \quad \text{Eq. 2}$$

Residence time distribution characterizes the flux in the extruder. Indeed, the macromolecules do not stay the same time in the extruder. Experimentally, a tracer (for example a dye) is rapidly injected in the input of the extruder (Dirac injection) and the evolution of the tracer concentration is measured output.

Two representations can be used: the cumulative frequencies,  $F(t=x)$ , which corresponds to the fraction of the fluid remained during a shorter than  $x$  in the extruder and the derivative of  $F$ ,  $E(t=x)$ , which represents the density of frequency of the different possible residence times for all macromolecules ( $E(t) = dF/dt$ ).  $F(t) = \int_0^t E(t).dt$ , thus the fraction of macromolecules that remained during a time between  $t = x$  and  $t = x + dt$  is equal to  $E(t=x).dt$ . If  $dt$  tends to zero,  $E(t=x)$  is the fraction of macromolecules staying a time  $x$  in the extruder.  $E(t)$  is normalized, so  $\int_0^{+\infty} E(t).dt = 1$  can be written.

The intensity of the color of the extrudate is followed. The average residence time is determined by the following equation (Eq. 3):

$$\bar{t} = \int_0^{+\infty} t.E(t).dt \quad \text{Eq. 3}$$

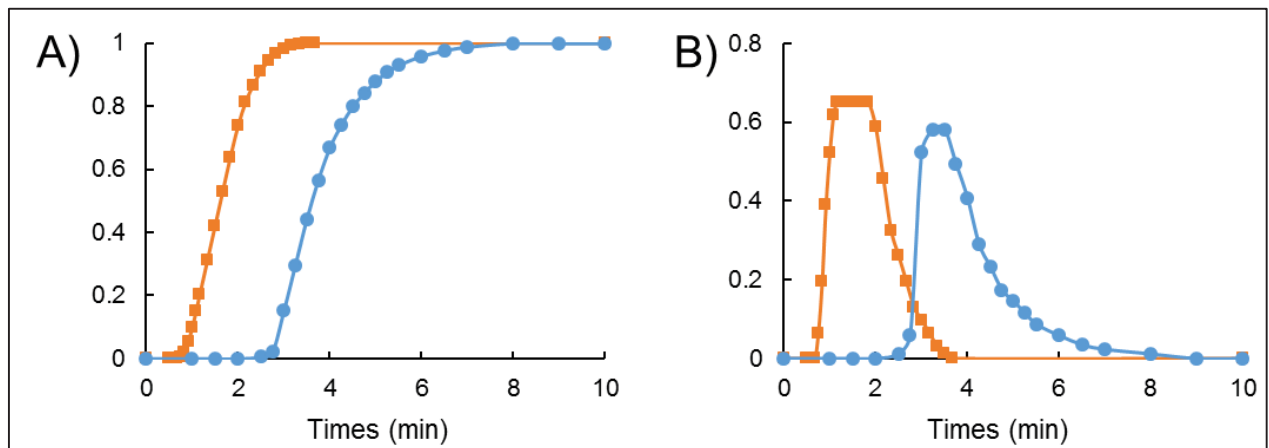


Figure 37. Theoretical representation of the residential time distribution (■ for filament die, ● for flat die): (a) cumulative frequencies curves and (b) frequency densities curves.

At 300 rpm, 1 kg/h with the flat die 300  $\mu\text{m}$  of thickness:

- $SME = (5 \times 2.\pi.300.60) / 1 = 565.5 \text{ kJ.kg}^{-1}$ .
- $\bar{t} = 4.0 \text{ min}$

At 300 rpm, 1 kg/h with the filament die 3 mm of diameter:

- $SME = (5 \times 2.\pi.300.60) / 1 = 565.5 \text{ kJ.kg}^{-1}$ .
- $\bar{t} = 1.75 \text{ min}$

## Calendering

A calendering equipment (Thermo Scientific) is used output the extrusion equipped with a flat die. The temperature of the rollers was set at 50°C.

## Heating press

A heated hydraulic press (20T, Pinette Emidecau Industries, Chalon-sur-Saône, France) was used to produce composite films (300  $\mu\text{m}$  thick and 12 x 12 cm) from granules previously produced by melt extrusion. Compounds were first heated during 5 min at 178 °C by putting the heating plates at the contact of granules and then compressed between two Teflon-coated plates (Taconic, France) for 4 min at 178°C by increasing gradually the pressure from 20 bar to 150 bars. Films were then allowed to cool between the two Teflon-coated plates at room temperature for 5 min under a weight (around 1 kg). All composite films were stored in hermetic drum with silica gel (around 0%RH) at room temperature.



Figure 12. Hydraulic thermal press

## Shaping of massive samples using injection molding

The extruded compounds were dried at 60 °C overnight before using them for shaping process. The extruded composite pellets were injection-molded with a Minijetpro Haake machine (Thermo-Fischer) for tensile (bar according to ISO527-2-1BA). Respectively, the cylinder and mold temperature were 185 °C and 70 °C, and the injection and holding pressure were 400 and 100 bar, respectively. The injection and holding times were 20 s and 10 s, respectively.

## II-3 Characterization of fillers and biocomposites

### Scanning electron microscopy (SEM)

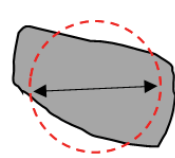
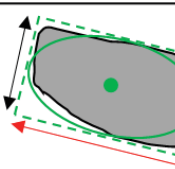
The surface of the particles and their morphology were observed using a scanning electron microscopy (SEM). It was also used to qualitatively characterized the state of dispersion as well as the interfacial interaction in case of composites cross section. It produces images of a

sample by scanning a focused electron beam over a surface. The electrons in the beam interact with the sample, producing various signals. The samples were examined with a Hitachi S4800 Scanning electron microscope (Technology platform of IEM Laboratory of the Balard Chemistry pole) with an acceleration voltage of 2 kV after a coating with Pt by cathode pulverization. Observations were realized by the help of Didier Cot (IEM, Montpellier). For particles, a solution of 1.0 g·L<sup>-1</sup> of particles in pure ethanol was first prepared, then 50 µL of this solution was dropped on brass support. This solution was preferred to a direct spray of the particles. In case of composite films, the cross-section was observed after tensile test or after cryo-fracture in liquid nitrogen.

### Macroscopy coupled to image analysis

The morphology and the dimensions of the fillers were assessed by optical microscopy coupled to image analysis. Observations were realized by using a Multizoom AZ100 macroscope (Nikon, Japan) equipped with a RGB DS-Ri1 camera (Nikon, Japon) in the light transmission mode. The magnification was set at ×40 combining the lens AZ-Plan ×5 and setting the optical zoom at ×8. For each sample, mosaic images were assembled by reconstructing 5 × 5 images using the imaging software NIS-Elements (Nikon, Japon). Particles were dispersed in ethanol (0.35 g·L<sup>-1</sup>) and dropped on glass slides. Image analysis was performed on mosaic images using the ImageJ software. For each particle, different 2D morphological parameters were calculated, i.e. the circularity, the major axis, the minor axis and the aspect ratio (Table 16). Each image analysis was performed around one thousand particles. For each analysis, it was verified that the mean of minor axis and the mean of major axis were stabilized with a variation lower than 5%. They were stabilized from 200 particles for cellulose and 350 particles for vine shoot particles.

Table 16. Circularity and aspect ratio as measured with ImageJ software

Parameter	Explanatory scheme	Equation
Circularity	 <ul style="list-style-type: none"> <li>-- Circle with the same area as particle</li> <li>— Perimeter of the particle</li> <li>↔ Diameter of the circle of same area</li> </ul>	$\text{Circularity} = \left( \frac{\text{Perimeter of circle}}{\text{Perimeter of particle}} \right)^2$ $= \frac{4\pi \cdot \text{Area}}{\text{Perimeter}^2}$
Aspect ratio	 <ul style="list-style-type: none"> <li>— Perimeter of the particle</li> <li>— Inertial ellipse</li> <li>↔ Major axis (length of inertial ellipse)</li> <li>↔ Minor axis (width of inertial ellipse)</li> </ul>	$\text{Aspect ratio} = \frac{\text{Major axis}}{\text{Minor axis}}$

The circularity is a shape descriptor ranging from 0 to 1 for a perfect disc. It is calculated as square of the ratio between the perimeter of the particle and the circumference of a circle with the same area. Sometimes this value is also called sphericity.

To get volume distributions, the particles were considered as cylinder with minor axis as diameter and major axis as length of the cylinder. This assumption lead to a slight overestimation of the volume of the particles. The volume was calculated as follow (Eq. 4):

$$\text{Volume of particle} = \pi \times \left(\frac{\text{minor axis}}{2}\right)^2 \times \text{major axis} \quad \text{Eq. 4}$$

### Laser Granulometry

The apparent diameter of the particles was measured using a laser granulometer in the wet mode (Malvern Mastersizer 2000 Instrument Ltd, United Kingdom), by dispersing particles in ethanol 95%. Laser diffraction is a widely used particle sizing technique for materials ranging from hundreds of nanometers up to several millimeters in size. It measures particle size distributions by measuring the angular variation in intensity of light scattered as a laser beam passes through a dispersed particulate sample. The small particles give larger diffraction angle than large partilces. The results given by the granulometer were the particle size distributions in volume by assuming that each particle occupied the same volume as an equivalent sphere. The particles size distribution in number can be calculated from particle size distribution in volume as followed (Eq. 5):

$$\text{Number distribution} = \frac{\text{Volume distribution}}{\text{Volume of sphere}} \quad \text{Eq. 5}$$

From the particle size distribution, four values were identified to characterize the sample and allow comparison. The value of  $d_{10}$  represents the particle size diameter for which 10% of particles (in volume or number) have a diameter below. Similarly,  $d_{50}$  represents de median and  $d_{90}$  the diameter from where the cumulative distribution of particles is 90%. The span value gives an idea of the width of the size distribution, the spread of the particles size (Eq. 6).

$$\text{Span} = \frac{d_{90} - d_{10}}{d_{50}} \quad \text{Eq. 6}$$

### Pycnometer

The true density ( $\rho^*$ ) of the particles was measured with gas pycnometer (ULTRAPYC 1200e, Quatachrom). It consists of measuring the difference of pressure between a reference volume ( $V_R$ ) and the volume of the sample cell ( $V_C$ ). Nitrogen was the gas used to fill reference and samples cells, the pressure was set at 40 kPa. The volume of the cellulose sample ( $V_S$ ) was calculated as followed (Eq. 7):

$$V_S = V_C - V_R \cdot \left(\frac{P_1}{P_2} - 1\right) \quad \text{Eq. 7}$$

where  $P_1$  is the pressure in the reference cell and  $P_2$  the pressure after expansion of the gas into reference cell and the sample chamber. Knowing the mass of the sample ( $M_S$ ), the true density was deduced from the particle volume by the equation (Eq. 8):

$$\text{True density } (\rho^*) = \frac{M_S}{V_S} \quad \text{Eq. 8}$$

### Colorimeter

The color of the materials was measured with a colorimeter (Minolta CR-410, Nieuwegein, Netherlands), using the CIELAB color space (Figure 38). It describes a color in three parameters  $L^*$  for the luminance and  $a^*$  and  $b^*$  for green-red and blue-yellow color components. The total change in color ( $\Delta E$ ) was calculated following Euclidean distance equation Eq. 9:

$$\Delta E = [(L^* - L_0^*)^2 + (a^* - a_0^*)^2 + (b^* - b_0^*)^2]^{0.5} \quad \text{Eq. 9}$$

An increase in  $L$  means that the sample is lighter than the reference. Looking at the  $L^*$ ,  $a^*$ ,  $b^*$  values for each sample, we can objectively determine the difference in color. Five replicates per sample were measured different locations after a calibration. In case of powder, sample was put in a crystallizer with a thickness of at least of 0.5 cm in order to have an opaque layer. Virgin cellulose was used as reference for  $L_0^*$ ,  $a_0^*$  and  $b_0^*$  in case of particles. Neat PHBV film was reference for composite films.

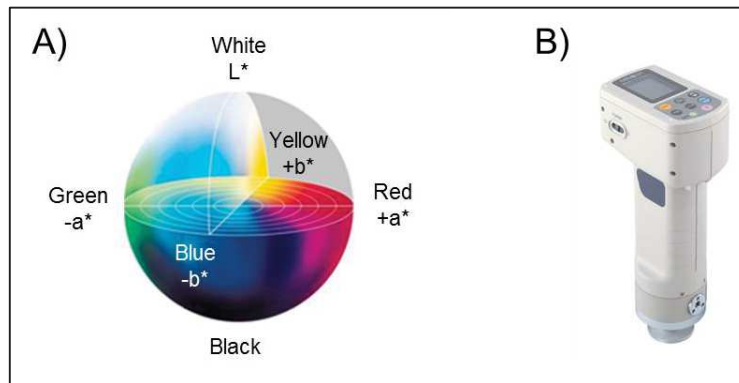


Figure 38. Representation of the CIELAB color space (A), chromameter CR-410 Minolta (B).

### Biochemical composition

The biochemical composition of vine shoots and other wine by-products (i.e. vine pomace) was characterized to study its variability through the species and the years. This biochemical composition is also important to explain possible differences in the performance of final composite materials and to be able to implement a biorefinery concept for a given biomass.



Dry matter was determined calculating the difference of mass after drying around 2 g of sample at 103°C in air-oven, in triplicate. Samples were dry when the weight was constant for two consecutive readings.

Ash content was determined in triplicate from the residue after thermogravimetric analysis (Mettler TGA2, Schwerzebach, Switzerland) at 800°C under air. Analysis was carried out on samples of about 40 mg.

Protein content was determined from elemental analysis. Nitrogen content was multiplied by a factor of 6.25 to obtain the protein content. Indeed, the average nitrogen (N) content of vine shoots proteins was found to be about 16 percent, which led to use of the calculation  $N \times 6.25$  ( $1/0.16 = 6.25$ ) to convert nitrogen content into protein content. This approach is based on the assumption that all of the nitrogen in the material is present as amino acids in proteins.

Extractive content was determined as the difference in weight between the raw biomass and the extractive-free biomass after a Soxhlet extraction with acetone at 70°C for 4 hours.

Lignin content. Klason lignin was determined by mass deduction after double hydrolysis in acidic conditions. 80 mg of dry extracted biomass was put in 0.85 mL of sulfuric acid 72% and stirred manually for 1 h at room temperature. 23.8 mL of ultrapure water was then added, and the mixture was heated and stirred at 121°C during 1h in a sealed flask. Then the hydrolysates were filtered (10 µm), washed by water, and dried at 105°C overnight. The ash also contained in the residues were subtracted to know the lignin content.

### Determination of the phenolic composition

Analytical mercaptolyses developed by Roumeas et al. [245] were conducted to determine the phenolic composition of ground vine shoots with help of H el ene Fulcrand and Guillaume Billerach (UMR-IATE). A mercaptolysis solution was of a 5% (v/v) mercaptoethanol and 0.1 M HCl prepared by adding 1.5 mL of 2-mercaptoethanol (Sigma-Aldrich, France) and 0.25 mL of hydrochloric acid (37%) to 28.25 mL of methanol (VWR, France). 20 mg of ground vine shoots ( $d_{50} = 500 \mu\text{m}$ ) were suspended in 1 mL of the previously prepared mercaptolysis solution. The samples were stirred 10 seconds and sonicated 30 seconds, then placed in a bath thermostatted at 40°C for two hours. Then, the samples were centrifugated 5 min (3000 rpm) and the supernatant was analysed by an UPLC-DAD-MS system (see [245]). The quantification was done according to the UV absorbance at 280 nm. The quantified compounds were catechin, epicatechin, epicatechin gallate, resveratrol and viniferin.

All the previously described results were reported on dry weight basis.

## Infrared Spectroscopy (FT-IR)

Infrared spectroscopy (FT-IR) was used to evidence the efficiency of the gas-phase esterification treatment. FT-IR allows to identify the vibrations of covalent bonds of the particles and of the grafted moiety.

The infrared spectroscopy exploits the fact that molecules are in rotation or vibrate at specific frequencies corresponding to discrete levels of energy. The infrared radiation can be used to study these absorbed frequencies that are characteristic of the molecules structures. With the Fourier transform infrared spectroscopy, a data-processing technique called Fourier transform turns this raw data into the sample spectrum. In attenuated total reflectance (ATR) spectroscopy, the sample is pressed against the face of a single crystal and the infrared radiation interacts with the sample surface with a penetration depth between 0.5 and 2  $\mu\text{m}$ .

The infrared spectrum from attenuated total reflectance-Fourier transform infrared analysis (ATR-FTIR) of cellulose was recorded using a Nexus 6700 spectrophotometer (ThermoElectron Corp.) equipped with a laser source HeNe and a nitrogen-cooled MCT detector. The spectra were obtained by accumulation of 32 scans with a resolution of 2  $\text{cm}^{-1}$  in the 500-4000  $\text{cm}^{-1}$  range. The data processing was performed using the Omnic v7.3 software. The spectra were normalized with respect to the cellulose backbone peak height, which was invariant from one sample to another.

## Solid state $^{13}\text{C}$ -NMR

This technique was used to study the evolution of the cellulose signals and the appearance grafted moiety signals according to the experimental conditions. The degree of substitution was calculated from these results as the integration of the spectra gives quantitative information.

Nuclear Magnetic Resonance spectroscopy (NMR) is a technique used to determine the molecular structure of a compound. The principle is that atoms with nonzero nuclear spin ( $^1\text{H}$ ,  $^{13}\text{C}$ ...) placed in a strong static magnetic field produce a characteristic electromagnetic signal after absorption and relaxation. This information can be converted in chemical shift specific to the environment of the nuclei. In solid state, the chemical shifts depend on the chemical binding but also on the structure.  $^{13}\text{C}$ -NMR detects only the  $^{13}\text{C}$  isotope of carbon which is not naturally abundant (1.1%), thus the signal need to be amplified by cross polarization (CP). The resolution can be improved by the technique of magic angle spinning (MAS) that average the anisotropy. The combination of the techniques CP and MAS on rigid molecules allows quantitative measures.

The measured were performed using a Bruker Avance DSX 400 MHz spectrometer operating at 100.6 MHz for  $^{13}\text{C}$ . The combination of cross-polarization and magic angle spinning (CP-MAS) method was used. Standard conditions were 2000 scans with 2 ms of contact and 2 s of recycle delay. The acquisition time was 35 ms and the sweep width was 29400 Hz.

The spectra were then studied with MestreNova software. The baseline was corrected and the integrals of the different peaks were measured. For DS determination, integrals were normalized with respect to area of cellulose C1 resonance peak.

The crystallinity of the cellulose can be also determined from solid-state  $^{13}\text{C}$ -NMR analysis. The ratio of the integrals of the crystalline core signals ( $\text{C4}_{\text{crys}}$ , 87-90 ppm) and amorphous chain signals ( $\text{C4}_{\text{am}}$ , 80-87 ppm).

### X-ray Photoelectron Spectroscopy (XPS)

XPS is a surface sensitive spectroscopic technique used to characterize the surface chemistry of materials. This nondestructive and quantitative technique allows determining the chemical composition of a sample, in particular the chemical bonds. All the elements are detected except hydrogen and helium. XPS is based on the photoelectric effect which is the phenomenon that occurs when a photon with a specific frequency is able to eject photoelectron from the surface of a material (Figure 39 [246]). The X-ray penetrates only 1-10 nm under the surface (depending on the inelastic mean free paths of electrons and the tilting angle of sample). The ejected electron ( $e^-$ ) has a kinetic energy ( $E_{\text{kinetic}}$ ) that is related to the energy of the incident beam ( $h\nu$ ), the electron binding energy ( $E_{\text{binding}}$ ) and the work function ( $\phi$ ) of the spectrometer.  $E_{\text{kinetic}}$  is measured by the spectrometer. Thus, the XPS detector identifies the number of electrons ( $e^-$ ) with the same binding energy that is proportional to the number of corresponding atoms in the sample.

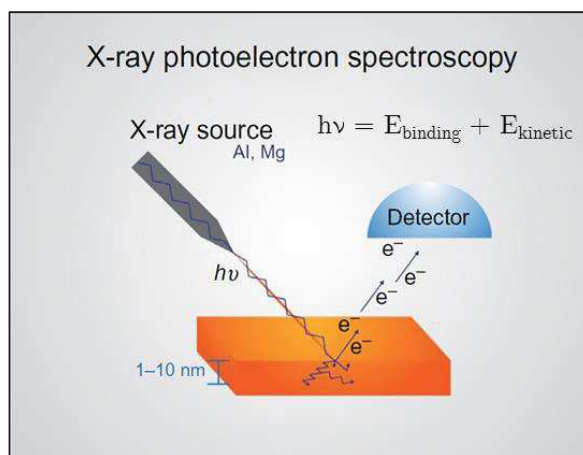


Figure 39. Diagram of X-ray photoelectron spectrometer.

X-ray photoelectron spectra were obtained with a Thermo Electron ESCALAB 250 instrument (ICGM, France), using monochromatised Al-K $\alpha$  ( $h\nu= 1486.6$  eV) radiation. The analyzed area was approximately  $0.2$  mm $^2$ . The binding energy scale was established by referencing the C 1s value of C-C carbon (284.8 eV). The charge is compensated by a low energy electron beam (-2eV). The photoelectron peaks were analyzed by Gaussian/Lorentzian (G/L= 50) peak fitting. XPS was performed on the tablets of cellulose previously made.

## Contact angle measurements

The contact angle method is one of the most established technique for determining the surface free energy of a solid material. The principle is based on the fact that a liquid with a surface tension of  $\gamma_{LV}$  placed on a solid surface displaying a surface tension of  $\gamma_{SV}$  will spontaneously form a droplet or spread out onto the material. A relationship between the solid and the liquid surface tension is described by the Young equation (Eq. 10) for over two hundred years :

$$\gamma_{SV} = \gamma_{SL} + \gamma_{LV} \cos \theta \quad \text{Eq. 10}$$

where  $\theta$  is the contact angle between the solid and the measuring liquid and  $\gamma_s$  the surface free energy of the solid. Depending on the  $\theta$  value obtained, the liquid is considered as wetting ( $\theta < 90^\circ$ ) or non-wetting ( $\theta > 90^\circ$ ) (Figure 40). In case of water, an angle higher than  $90^\circ$  demonstrates the hydrophobicity of the materials.

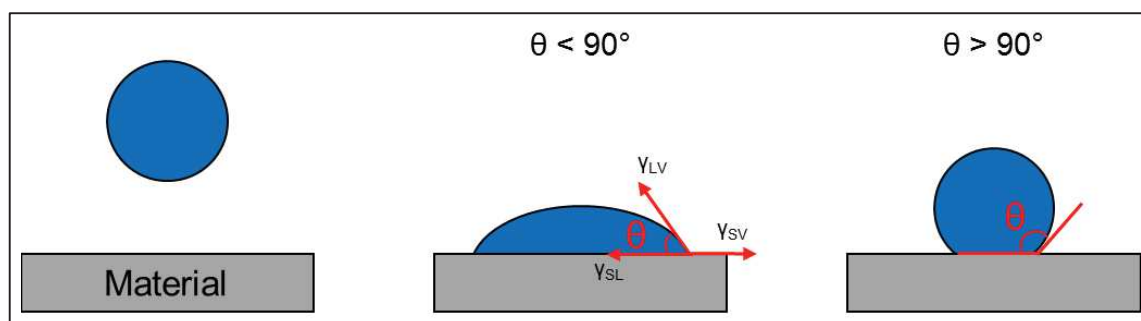


Figure 40. Schematic representation of the contact angle and its surface free energy components.

Different reference liquids with known polar and dispersive components of the surface tension were used (Table 17). Thus, the different contact angles, the regression of the Owens-Wendt model can be applied (Figure 41).

Table 17. Reference liquids used for the determination of the surface free energy with Owens-Wendt model.

Liquids	Surface free energy (mJ·m <sup>-2</sup> )			
	$\gamma_{L^p}$	$\gamma_{L^d}$	$\gamma_L$	$\sqrt{\gamma_{L^p}/\gamma_{L^d}}$
Water	51	21.8	72.8	1.53
Glycerol	30	34	64	0.94
Ethylene glycol	19	29	48	0.81
Formamide	19	39	58	0.70
Diiodomethane	0	50.8	50.8	0.00

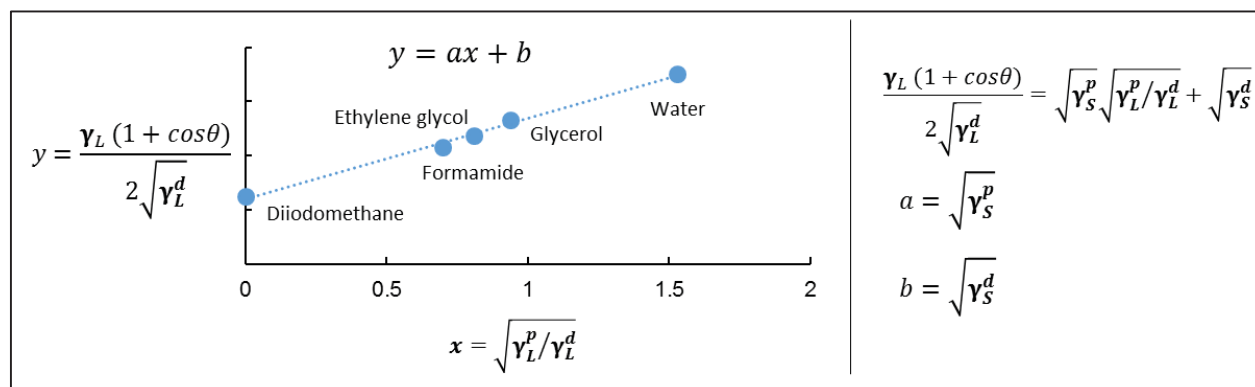


Figure 41. Owens-Wendt regression.

Particle surface free energy was evaluated by contact angle measurements on tablets (about 0.7 mm thick and 13 mm in diameter) obtained by compacting fibers in a Specac Atlas Evacuatable Pellet mold using a hydraulic press (Perkin-Elmer) at a pressure of 150 MPa (Figure 42). The idea is to get the smoothest surface possible. The resulting tablets were dried over  $P_2O_5$  under vacuum for 1h before analysis. Contact angles were measured at 23°C using a goniometer instrument (Digidrop, GBX, France) equipped with a CCD camera (25 frames·s<sup>-1</sup>) and the GBX software (Windrop, GBX, France). A drop of 3  $\mu$ L was deposited on the surface of the tablets or film and contact angles were measured at equilibrium using “Contour” mode. The dispersive ( $\gamma^d$ ) and polar ( $\gamma^p$ ) components of the solid surface tension were evaluated by applying the Owens-Wendt approach [247] by using five reference liquids, i.e. distilled water, diiodomethane (Acros organics, Geel, Belgium), formamide (Acros organics, Geel, Belgium), ethylene glycol (Sigma-Aldrich, Milwaukee, USA) and glycerol (Merk, Darmstadt, Germany).

Some limits of this method have to be kept in mind as the surface roughness and the porosity of the tablets can influence the contact angles, as shown by Blancher et al. [248] in the case of non-ideal material surfaces. The equilibrium angles are generally underestimated on rough surfaces. It was checked that the porosity of the tablets was always the same, so that this technique could be used at least comparatively.

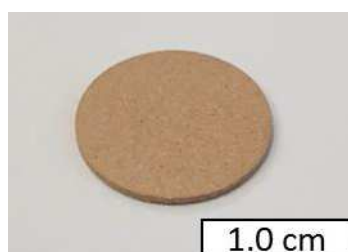


Figure 42. Compressed tablets of vine shoots particles used for contact angle measurements

## Wide-angle X-ray diffraction analysis (WAXS)

Wide angle X-ray diffraction analysis was applied to assess the crystallinity and the crystalline structure of cellulose and vine shoots particles. The method consists of constraining the sample in a monochromatic X-ray beam and measuring the diffraction spectrum emitted by the sample. WAXS analysis was performed in collaboration with Philippe Dieudonné-George at the L2C lab (CNRS, Montpellier), using an 'in-house' setup in which samples were in glass capillaries [249]. A high brightness low power X-ray tube, coupled with aspheric multilayer optic (GeniX<sup>3D</sup> from Xenocs with Cu K $\alpha$  radiation  $\lambda=1.54 \text{ \AA}$ ) was used delivering an ultralow divergent beam (0.5 mrad). The experiments were done in the transmission configuration and the scattered intensity was measured by a Schneider 2D image plate "Pilatus" detector, at a distance of 1.9 m. The signals were then analyzed with the software Fit2D. The measurements were carried out in  $2\theta$  ranges between  $5^\circ$  and  $25^\circ$  with a step size of  $0.047^\circ$ . The crystallinity index (CrI) of the cellulose was calculated (Eq. 11) according to the Segal method [250]:

$$\text{Crystallinity index (CI)} = \frac{I_{002} - I_{\text{am}}}{I_{002}} \quad \text{Eq. 11}$$

where  $I_{002}$  is the maximum intensity of the 002 lattice reflection of the cellulose crystallographic form ( $I_{002}$ ) at  $2\theta = 22^\circ$  and  $I_{\text{am}}$  the diffraction intensity of the amorphous material at  $2\theta = 18^\circ$ . Sample were conditioned at 50 %RH before the analysis.

## Molecular weight

Molecular weight was studied by gel permeation chromatography (GPC) that is a technique which separates molecules by their sizes. The small molecules are delayed as they flow in and out of pores in the gel while larger molecules flow in the solvent stream and elute first (Figure 43). It is also called size-exclusion chromatography (SEC). This technique is used to determine the average molecular weight distribution of PHBV.

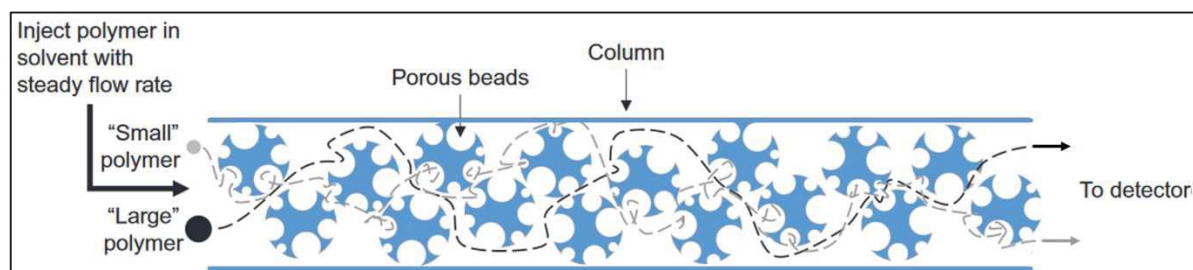


Figure 43. Gel permeation chromatography principle (adapted from [251])

A gel permeation chromatograph GPC PL-50 Plus system equipped with two columns of 300 mm PL-gel 5  $\mu\text{m}$  mixed-C (200–2,000,000  $\text{g}\cdot\text{mol}^{-1}$ ) (Polymer Laboratories, Church Stretton, UK), and a refractive index detector was used to measure the molecular weight of PHBV. The

eluent was chloroform, the flow was set at  $1.0 \text{ mL}\cdot\text{min}^{-1}$  and the volume of injection was  $20 \text{ }\mu\text{L}$ . PHBV samples (10 mg) were previously dissolved in 2 mL of chloroform in a closed tube under stirring at  $50 \text{ }^\circ\text{C}$ . Samples were filtered on Macherey–Nagel Chromafil Xtra syringe filter (PTFE-45/25, Düren, Germany) with  $0.45 \text{ }\mu\text{m}$  pore size. The GPC equipment was calibrated with polystyrene standards. To measure the broadness of the molecular weight distribution of the matrix, the polydispersity index ( $I_p$ ) was calculated as follows (Eq. 12):

$$I_p = \frac{M_w}{M_n} \quad \text{Eq. 12}$$

### Differential scanning calorimetry (DSC)

The thermal properties of the composite materials were determined by differential scanning calorimetry (DSC). It was used to characterize the thermal transition temperatures (melting and crystallization) and the crystallinity of the different composites. It is a technique in which the difference in the amount of heat required to increase the temperature of a sample and reference is measured as a function of temperature.

Analysis were realized using a Q200 modulated DSC from TA Instruments (New Castle, USA). Tzero Aluminium Hermetic pans (TA Instruments New Castle, USA) were filled with approximately 10 mg of sample and hermetically sealed. DSC was performed under nitrogen gas at a heating and cooling rate of  $10 \text{ }^\circ\text{C}\cdot\text{min}^{-1}$ . Samples were first heated to  $200^\circ\text{C}$ , then kept at  $200^\circ\text{C}$  for 5 min before being cooled from 200 to  $-30^\circ\text{C}$ , and heated again from  $-30$  to  $200^\circ\text{C}$ . The first heat ramp was to erase any thermal history in the samples. Analyses were performed in triplicate. An empty hermetical aluminium pan was used as a reference. Melting enthalpy  $\Delta H_m$  was calculated by integrating the area of the melting peak. The crystallinity ( $X_c$ ) of composites was evaluated by Eq. 13:

$$X_c = \frac{\Delta H_m}{\Delta H_m^0 \left(1 - \frac{\% \text{wt filler}}{100}\right)} \times 100 \quad \text{Eq. 13}$$

where  $\Delta H_m$  is the enthalpy of melting in  $\text{J}\cdot\text{g}^{-1}$ ,  $\Delta H_m^0$  is the enthalpy of melting 100% crystalline polymer. The  $\Delta H_m$  100% of PHB equal to  $146 \text{ J}\cdot\text{g}^{-1}$  was used to estimate the crystallinity [252].

### Thermogravimetric analysis (TGA)

The thermal stability of the sample was investigated using thermogravimetric analysis (TGA), which consists of measuring the mass loss of a sample as a function of increasing temperature under a controlled atmosphere of nitrogen or air. Mass loss and first derivate of mass loss were recorded as a function of temperature for each sample.

Analyses were carried out using a Mettler TGA2 apparatus (Schwerzebbach, Switzerland) equipped with a XP5U balance (precision of  $0.0001 \text{ mg}$ ). For each measurement, about 40 mg

of materials were used, and the heating rate was  $10\text{ }^{\circ}\text{C}\cdot\text{min}^{-1}$  from  $25\text{ }^{\circ}\text{C}$  to  $800\text{ }^{\circ}\text{C}$  under nitrogen flow ( $50\text{ mL}\cdot\text{min}^{-1}$ ). The maximum degradation temperature ( $T_{\text{deg}}$ ) corresponded to the temperature at which the degradation rate was maximum (Figure 44, A). The onset and offset degradation temperatures ( $T_{\text{onset}}$  and  $T_{\text{offset}}$ , respectively) were measured respectively when the first derivative of the weight loss became higher than  $0.1\text{ }\% \cdot ^{\circ}\text{C}^{-1}$  and lower than  $0.1\text{ }\% \cdot ^{\circ}\text{C}^{-1}$ . Analyses were done in triplicate.

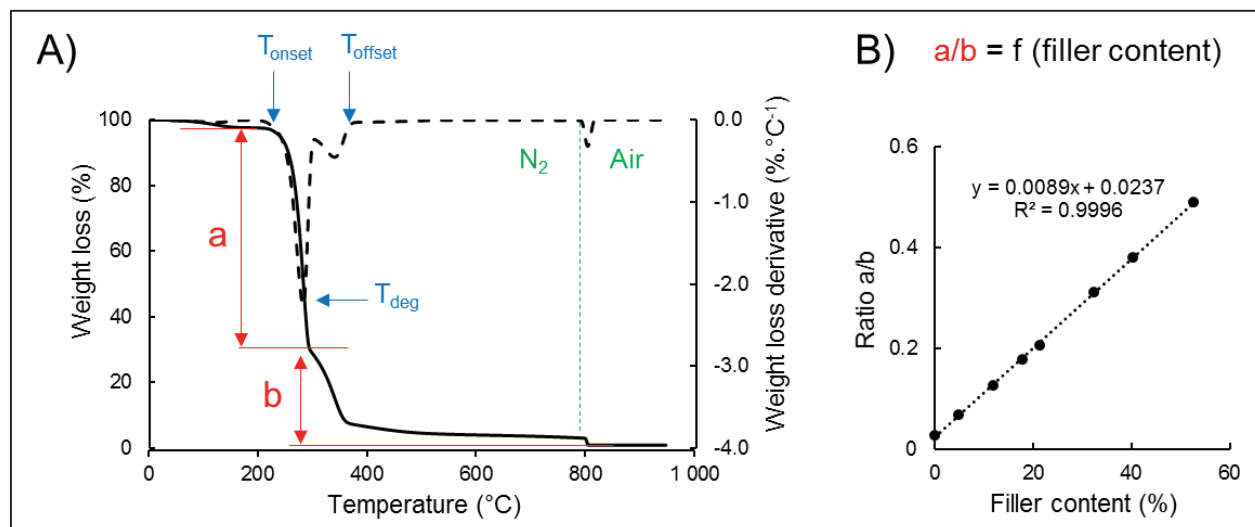


Figure 44. Example of the method: A) TG and DTG curves of a PHBV-20VC; B) Standard curve obtained for PHBV composite with virgin cellulose.

The PHBV and cellulose degradation windows overlap. Thus, the weight filler content of the composite was determined from inflection point between  $280\text{ }^{\circ}\text{C}$  and  $300\text{ }^{\circ}\text{C}$  corresponding to the end of PHBV degradation and beginning of cellulose degradation. To correct the overlapping thermal degradation, standard curves for virgin and grafted cellulose in PHBV were used ( $R^2 = 0.999$ ). These standard curves were obtained with samples (40 mg) for which the amount of PHBV and cellulose were exactly known. The ratio  $a/b$  was calculated for different filler content from 0 to 60%. A linear curve was get when ratio  $a/b$  was plotted in function of the filler content (Figure 44, B). Similarly, the filler content for composite with lignocellulose was measured. The deconvolution method of the peaks of the weight loss derivative were not used because, the peak of fillers degradation, especially in case of lignocellulose, was not symmetric. The volume filler content was deduced from the weight filler content based on knowledge of the true density of both composite constituents.

### Dynamic Vapor Sorption (DVS)

Vapor water sorption kinetics of lignocellulosic fillers and biocomposites were measured with a Dynamic Vapor Sorption equipment (Surface Measurement System, London, UK) (Figure 45). It includes a Cahn D-200 microbalance with a  $0.1\text{ }\mu\text{g}$  precision of mass variation. This type of balance is adapted for vapor sorption measurements from few minutes to several weeks. The



device ensures a regulation of the relative humidity and is placed in a controlled temperature enclosure. The mixture of dry air and air saturated with water streams generates the water vapor flow desired. This air with the controlled relative humidity circulates in the “reference” and “sample” pathways. It is the difference of weight between reference and sample pans that gives the water vapor uptake.

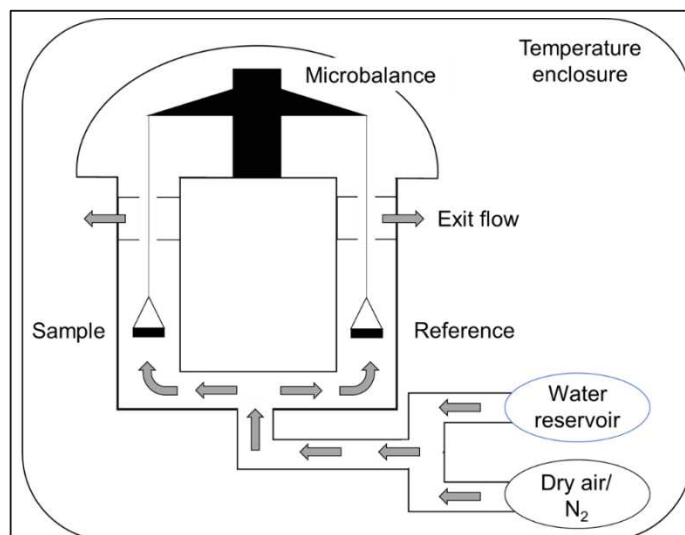


Figure 45. Sorption micro-balance of DVS apparatus

This device enables recording the water vapor uptake of the materials as a function of time for successive relative humidity (RH) steps (0, 10, 20, 30, 40, 50, 60, 70, 80, 90 and 95%). It is automatically controlled by a computer by DVS-Win software. Water vapor sorption isotherms were established from the equilibrium moisture contents at each RH step. The sample was first dried at 60°C in an oven and then dried over P<sub>2</sub>O<sub>5</sub> in a desiccator and finally placed in the DVS apparatus at 0% RH for 5 h at 20°C. In case of fillers, around 1 mg of particles were deposited in the form of a monolayer powder bed in a DSC pan itself placed in DVS pan [253]. For composite films, discs were cut by using a puncher with a diameter of 7.5 mm and were placed in DVS pan.

The estimation of the diffusion coefficient was adapted from the work of Valentin Thoury during his thesis (UMR-IATE, Montpellier) [253]. According to the Fick’s first law (1855), the mass flux  $F$  ( $\text{g}\cdot\text{m}^{-2}\cdot\text{s}^{-1}$ ), corresponding to the rate of mass transfer of diffusing compound through a unit area, is proportional to the concentration gradient normal to the surface and can be written as followed (Eq. 14):

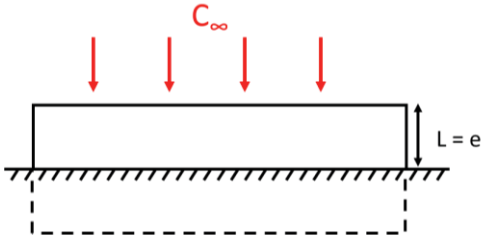
$$\mathbf{F} = -D \frac{\partial C}{\partial z} \quad \text{Eq. 14}$$

where  $D$  is the diffusion coefficient ( $\text{m}^2\cdot\text{s}^{-1}$ ),  $C$  is the concentration ( $\text{g}\cdot\text{m}^{-3}$ ) and  $x$  is the coordinate of normal space at the surface section (m). For that purpose, it was assumed that the diffusion in the material was isotropic and independent of time and space. In addition, the

possible swelling of the sample with increasing relative humidity was considered negligible. It was assumed that the polymer phase was immobile, only water molecules are in movement. Diffusion in an infinite plane sheet was used to describe water vapor diffusion of fillers and composite films. The apparent diffusion coefficient was estimated using the analytical solutions provided by Crank [254]. Considering an isotropic diffusion, the diffusion could be reduced to a pure axial diffusion that occurs in an infinite plane sheet of thickness  $L$  (m). The diffusion equation at time  $t$ , at position  $z$ , and for film of thickness  $L$  is given in Eq. 15, where  $D$  ( $\text{m}^2\cdot\text{s}^{-1}$ ) corresponds to the water's apparent diffusivity in the material.

$$\frac{\partial C}{\partial t}(t, z) = D \left( \frac{\partial^2 C(t, z)}{\partial z^2} \right) \quad \text{Eq. 15}$$

Table 18. Information of infinite plane sheet to estimate the diffusion coefficient of water vapor

INFINITE PLANE SHEET (axial diffusion) water vapor sorption	
Geometry	 <p>In case of water vapor sorption (deposition of the sample in a DVS pan), the plane sheet was insulated at its bottom, and defined by <math>z \in [0, L]</math></p>
Initial conditions	<p>Initial concentration <math>C_0</math> is uniform</p> $C(t = 0, z) = C_0 \quad \forall z \in [0, L]$
Boundary conditions	<p>Sample surface is kept at a constant concentration <math>C_\infty</math></p> $\frac{\partial C}{\partial z}(t, z = 0) = 0 \quad \forall t \geq 0$ $C(t, z = L) = C_\infty \quad \forall t \geq 0$

The analytical solution for an infinite plane sheet of thickness  $L$  (m) in both cases was described by Eq. 16:

$$\frac{M_t}{M_\infty} = 1 - \sum_{n=0}^{\infty} \frac{8}{(2n+1)^2 \pi^2} \exp\left(\frac{-D(2n+1)^2 \pi^2 t}{4L^2}\right) \quad \text{Eq. 16}$$

where  $M_t$  and  $M_\infty$  denote, respectively, the water mass uptake at time  $t$  and the corresponding value for infinite time.

Water's apparent diffusivity  $D$  was determined using the `lsqnonlin` function that solved the corresponding nonlinear least squared problem in MATLAB<sup>®</sup> R2015b software. The idea was to minimize the root mean square error (RMSE) between experimental sorption kinetics and simulated ones.  $N$  is the number of experimental data points from DVS,  $m_{\text{sim}}(t)$  and  $m_{\text{exp}}(t)$  are, respectively, the estimate and the experimental mass uptake at time  $t$ . Simulations were performed by using Eq. 17:

$$\text{RMSE} = \sqrt{\frac{\sum_{i=1}^N (m_{\text{sim}}(t_i) - m_{\text{exp}}(t_i))^2}{N}} \quad \text{Eq. 17}$$

### Liquid water uptake and estimation of liquid water diffusivity

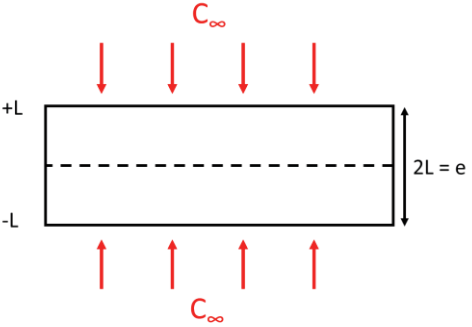
Liquid water uptake kinetics were measured on discs of 25 mm diameter cut from composite films. The films were 300  $\mu\text{m}$  thick allowing to assume that water diffusion was unidirectional. After drying overnight at 60  $^{\circ}\text{C}$ , the specimens were weighted using a balance with  $\pm 0.001$  mg precision and then immersed into distilled water at 20  $^{\circ}\text{C}$ . At various time intervals, the samples were removed, blotted to remove free water on their surface, and immediately weighed. Experiments were performed in triplicate until reaching the water uptake equilibrium for each sample. Water uptake (WU) was calculated as followed:

$$\text{WU} = \frac{m_t - m_0}{m_0} \quad \text{Eq. 18}$$

where  $m_0$  and  $m_t$  are respectively the initial sample mass and the sample mass after a time  $t$  of immersion.

The estimation of the diffusion coefficient was similarly determined as for water vapor. Only the geometry model, initial and boundary conditions were adapted as follow (Table 19):

Table 19. Information of infinite plane sheet to estimate the diffusion coefficient of liquid water

	INFINITE PLANE SHEET (axial diffusion) liquid water sorption
Geometry	

	In case of liquid water sorption (immersion of the samples in water), it was considered that the plane sheet was not insulated and that it was defined by $z \in \left[ \frac{-L}{2}, \frac{L}{2} \right]$ .
Initial conditions	Initial concentration $C_0$ is uniform $C(t = 0, z) = C_0 \quad \forall z \in \left[ \frac{-L}{2}, \frac{L}{2} \right]$
Boundary conditions	Sample surface is kept at a constant concentration $C_\infty$ $\frac{\partial C}{\partial z}(t, z = 0) = 0; \quad \forall t \geq 0$ $C\left(t, z = \pm \frac{L}{2}\right) = C_\infty \quad \forall t \geq 0$

### Water vapor permeability (WVP)

Moisture barrier properties need to be known for packaging application. Water vapor permeability (WVP) of films were gravimetrically determined at room temperature with a relative humidity gradient from 0 to 100% using a modified ASTM procedure (ASTM E96). The free film surface was 9.08 cm<sup>2</sup> per sample. Films samples (five repetitions) were hermetically sealed with Teflon seal in glass permeation cells containing distilled water. Cells were placed in a desiccator containing silica gel to have 0% of relative humidity (Figure 46).

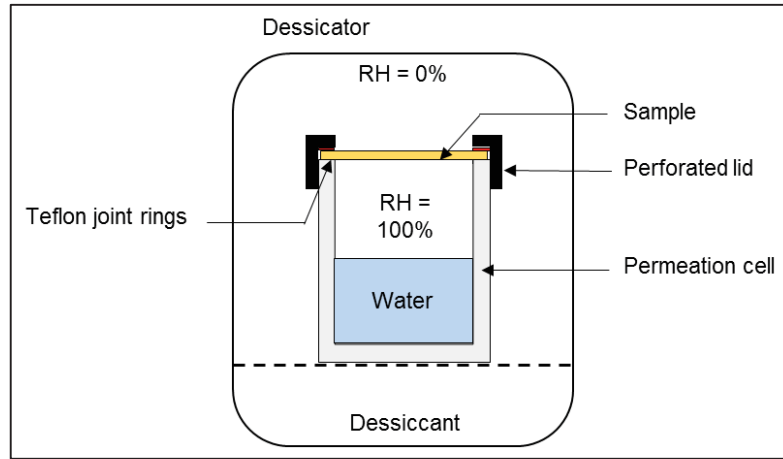


Figure 46. Water vapor permeability measurements set-up

A relative humidity (RH) gradient equal to 0–100% was obtained (i.e.,  $\Delta P = P_{\text{sat}} = 2809$  Pa at 23 °C, assuming that RH on the silica gel is negligible). Periodic weightings determined the rate of water vapor movement through the films. WVP ( $\text{mol}\cdot\text{s}^{-1}\cdot\text{Pa}^{-1}\cdot\text{m}^{-1}$ ) values were calculated from Eq. 19, where  $S$  is the slope of the weight change from the straight line ( $\text{g}\cdot\text{h}^{-1}$ ),  $A$  is the permeation area ( $\text{m}^2$ ),  $e$  is the average specimen thickness (m),  $\Delta P$  is the water vapor pressure differential (Pa), and  $M_{\text{H}_2\text{O}}$  is the molar mass of water ( $\text{g}\cdot\text{mol}^{-1}$ ).

$$WVP = \frac{S \times e}{3600 \times A \times \Delta P \times M_{H_2O}} \quad \text{Eq. 19}$$

### Tensile properties

Maintaining physical material integrity is essential to consider different applications. The mechanical properties were evaluated through tensile tests conducted at room temperature by a texture analyzer (Zwick BZ2.5/TN1S, Metz, France) equipped with a force transducer (KAF-S, A.S.T., Dresden, Germany). Tests were performed on dog-bone shaped film specimens (width of 4 mm and initial distance between clamps of 45 mm) that had been cut in 300  $\mu\text{m}$  composite films (Figure 47, A). The specimens were previously stored in a closed chamber at 23 °C and 50% RH. Stress–strain curves obtained with a cross-head speed of 1  $\text{mm}\cdot\text{min}^{-1}$  helped determine Young’s modulus ( $E$ ), nominal stress at break ( $\sigma$ ), and nominal strain at break ( $\epsilon$ ) (Figure 47, B). The energy at break was calculated from the total area under the stress–strain curve. Ten replicates were realized for each formulation of composites.

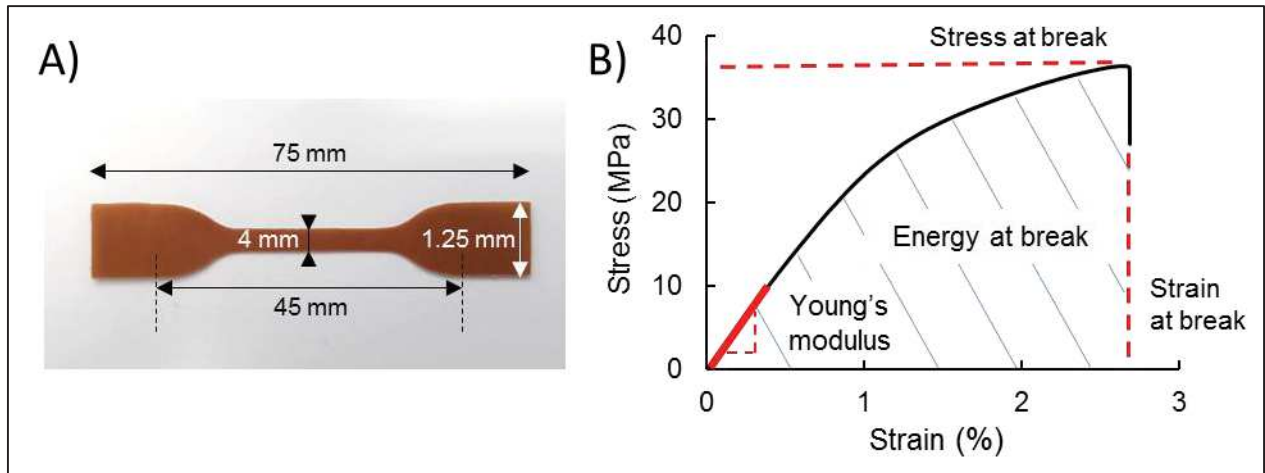


Figure 47. A) Specimen used for tensile tests; B) Stress-strain curves after tensile tests

### Biodegradability

The biodegradability of the composite materials was studied in soil in order to demonstrate their sustainability compared to common plastic existing on the market.

Respirometric tests were conducted in soil at 28°C under aerobic conditions to evaluate the biodegradability of composite materials during 73 days. The method was adapted from the US standard ASTM D5988-96, which describes the method for determining aerobic biodegradation in soil of plastic materials. The released  $\text{CO}_2$  is proportional to the amount of biodegraded substrate. The measure of  $\text{CO}_2$  gives information about the ultimate degradation step, namely the mineralization, during which the substrate is broken down to final products.

First, the samples were milled with a coffee grinder (Moulinex type DPA1, France) then sieved at 0.5 mm to get the same size of particles between the different samples. The carbon contents were measured by elemental analysis (ThermoQuest NA 2500) for each sample. Thus, exactly 50 mg of equivalent carbon were introduced into 25 g of soil. The soil used in this study was a top soil (Verve, pH = 7.5). The soil was air dried during one week then it was sieved through a sieve of 2 mm. The dry matter content was determined by drying the soil at 105°C until constant weight, 97% was found. The biodegradation tests were carried out in hermetic glass jars (1 L, Le Parfait, France) which contained three open polypropylene vials (60 mL). One vial contained 25 g of dry soil mixed with 50 mg equivalent carbon of samples. The water content of soil was adjusted to reach 80 % of the water holding capacity of the soil. A second vial of 15 mL of NaOH (0.2 M) trapped the CO<sub>2</sub> released by the microorganisms. The relative humidity was maintained at 100% inside the jar thanks to a third vial filled with distilled water. The jars were hermetically closed and incubated in the dark at 28 ± 1°C.

At selected time, the glass jars were open to determine the amount of CO<sub>2</sub> trapped by the NaOH solution by back titration with a HCl solution (0.1 M) in the presence of thymophthaleine 0.10% in ethanol 95, 5 mL of barium chloride solution (20% in water) was added in each flask to precipitate carbonate ions (Eq. 20).

$$m_{\text{CO}_2} = (C_{\text{NaOH}}V_{\text{NaOH}} - C_{\text{HCl}}V_{\text{HCl}}) \times \frac{M_{\text{CO}_2}}{2} \quad \text{Eq. 20}$$

where  $m_{\text{CO}_2}$  is the mass of CO<sub>2</sub> trapped (mg),  $C_{\text{NaOH}}$  and  $C_{\text{HCl}}$  the concentration (mol·L<sup>-1</sup>) of NaOH and HCl solutions,  $V_{\text{NaOH}}$  and  $V_{\text{HCl}}$  are the volume (L) of NaOH and HCl solutions at equivalence.  $M_{\text{CO}_2}$  is the molecular mass of CO<sub>2</sub> (g·mol<sup>-1</sup>). It is divided by 2 because two NaOH are neutralized by one CO<sub>2</sub>.

Table 20. Chemical equation involved in the biodegradation test.

Biodegradation	$C_{\text{material}} \rightarrow \text{CO}_2 + \text{H}_2\text{O} + \text{biomass}$
Dissolution of CO <sub>2</sub> by the sodium hydroxyde	$2 \text{NaOH} + \text{CO}_2 \rightarrow \text{Na}_2\text{CO}_3 + \text{H}_2\text{O}$
Precipitation of Na <sub>2</sub> CO <sub>3</sub> by BaCl <sub>2</sub>	$\text{Na}_2\text{CO}_3 + \text{BaCl}_2 \rightarrow \text{NaCl} + \text{BaCO}_3$
Titration of remaining NaOH by HCl	$\text{NaOH} + \text{HCl} \rightarrow \text{NaCl} + \text{H}_2\text{O}$

The vials containing soil were weighted and if necessary appropriate amount of water was added to stay at 80% of the soil water retention capacity. A new vial containing a NaOH solution (0.2 M) replace the one which was titrated.

The biodegradation tests included a control and a blank. For the control, the reference was cellulose because of its well-known degradation. For the blank, the experiment was conducted without addition of carbon source in the soil to be able to measure the CO<sub>2</sub> produced naturally by the soil and the CO<sub>2</sub> present in the air of the glass jar. The tests were measured in triplicate. Results were calculated by subtracting the CO<sub>2</sub> production of the blank.

The percentage of biodegradation  $D_t$  for each test jar  $J_i$  from the amount of carbon dioxide evolved during each measurement interval using Eq. 21:

$$D_t = \frac{\Sigma m_i - \Sigma m_b}{ThCO_2} \times 100 \quad \text{Eq. 21}$$

where  $\Sigma m_i$  and  $\Sigma m_b$  are the amount of carbon dioxide (mg) evolved in the test jar  $J_i$  and in the blank control jar respectively between the start of the test and time  $t$ .  $ThCO_2$  is the theoretical amount of carbon dioxide (mg) produced by total oxidation of the tested material. In the same way the percentage of biodegradation of the reference material is calculated to check in the soil activity.

The test is considered valid if a) the degree of biodegradation of the reference material is more than 60 % at the end of the test; b) the difference of biodegradation between jars of the same repetition is within 20 % of the mean at the end of the test.

The experimental degradation data were modeled with the Hill equation (Eq. 22):

$$Deg = \frac{Deg_{max} \times t^n}{k^n + t^n} \quad \text{Eq. 22}$$

where  $Deg$  is the percentage of degradation at time  $t$  (day),  $Deg_{max}$  the percentage of degradation at infinite time,  $k$  (days), the time for which  $Deg = \frac{1}{2} Deg_{max}$  and  $n$  the curve radius of the sigmoid function.

## Life Cycle Analysis (LCA)

In order to get an unbiased point of view on the real environmental performance of the resulting materials a comparative life cycle assessment was performed. All background data used in the assessment were obtained from the Ecoinvent v.3.4 database with the Cut-off system model and processed using the LCA software Simapro v.8.4. The ReCiPe 2016 Midpoint Hierarchist (H) methodology was used in the interpretation phase of the assessment. In accordance with the geographical boundary, all the electricity used in the system was assumed to conform to the French energy mix.

Chapter III. Modulating  
filler/matrix interactions in  
biocomposites



## Chapter III. Modulating filler/matrix interactions in biocomposites

L'état de l'art a montré l'importance de l'affinité charge/matrice pour améliorer les propriétés mécaniques et de transfert des composites à charge végétale. L'addition des charges naturelles dans les matrices polymères présente une limite majeure liée à leur caractère hydrophile. Dans ce chapitre, afin de pouvoir moduler l'interface charge/matrice, l'étude d'une modification des charges, sera réalisée puis les effets de leur incorporation dans une matrice PHBV seront évalués.

Dans un premier article (Article 1), un procédé d'estérification en phase gaz est appliqué sur les particules micrométriques de cellulose destinées à servir de charge de renfort pour composites. La cellulose est choisie en tant que composé modèle pour appréhender cette technique, la lignocellulose étant plus complexe. Historiquement, la modification de la cellulose visait à transformer cette ressource abondante en matériaux thermoplastiques ou soluble dans les solvants courants. Désormais, l'objectif n'est pas la substitution intégrale des chaînes cellulosiques, mais la modification contrôlée de la surface pour permettre leur dispersion et renforcer l'interface avec la matrice. Afin de contrôler cette modification différentes conditions expérimentales sont testées et leurs effets sur les particules sont évalués. La réaction se fait sur une centaine de grammes de particules micrométriques afin de pouvoir obtenir suffisamment de matière pour une application composite.

Un deuxième article (Article 2) évaluera les effets de cette modification des particules de cellulose sur les propriétés fonctionnelles des composites à base de PHBV. Pour ce faire, les composites avec différents taux de charges sont préparés par extrusion en utilisant des charges de cellulose à la fois vierges et modifiées. Premièrement, les changements structuraux provoqués par l'addition de telles charges sont étudiés. La masse moléculaire, la cristallinité du PHBV et la microstructure de l'interface par observation au MEB sont déterminées afin d'expliquer les propriétés fonctionnelles. Les changements de stabilité thermique, les propriétés de tractions et les propriétés de transfert de vapeur d'eau et d'eau liquide des composites sont discutés en relation avec le type de charges.

I. Exploring the potential of gas-phase esterification to hydrophobize the surface of micrometric cellulose particles  
(Article 1)

Grégoire David <sup>a</sup>, Nathalie Gontard <sup>a</sup>, David Guérin <sup>b</sup>, Laurent Heux <sup>c</sup>, Jérôme Lecomte <sup>a,d</sup>,  
Sonia Molina-Boisseau <sup>c</sup>, Hélène Angellier-Coussy <sup>a</sup>

<sup>a</sup> JRU IATE 1208 – Univ. Montpellier, CIRAD, INRA, Montpellier SupAgro, 2 Place Pierre Viala, Bat 31, F-34060 Montpellier 01, France

<sup>b</sup> CTP, Centre Technique du Papier, CS90251, Domaine Universitaire, Grenoble, France

<sup>c</sup> CNRS, CERMAV, Univ. Grenoble Alpes, 38000 Grenoble, France

<sup>d</sup> CIRAD, UMR IATE, F-34398 Montpellier, France

Published in European Polymer Journal. 05 March 2019. 10.1016/j.eurpolymj.2019.03.002

Abstract

In order to lift the barrier of a poor interfacial interaction between cellulosic plant fibers and polymeric matrices in biocomposites, an eco-friendly surface modification of fibers was explored. A solvent-free gas-phase esterification applied to cellulose particles allowed to graft palmitoyl moieties on their surface in order to make them more compatible with non-polar polymers for composite applications. The efficiency of the treatment was evidenced from FT-IR analysis, and the degree of substitution (DS) was quantified by solid-state <sup>13</sup>C NMR spectroscopy. The effect of surface grafting on resulting intrinsic characteristics of cellulose particles, i.e. crystallinity, thermal stability, morphology, surface free energy and water vapor sorption were investigated respectively by X-ray diffraction, thermogravimetric analysis, SEM observations coupled with image analysis, contact angle measurements and dynamic vapor sorption system (DVS). It was shown that a DS as low as 0.01 was enough to drastically increase the hydrophobicity of cellulose particles without affecting the inner properties of cellulose.

Keywords: Cellulose; gas-phase esterification; degree of substitution; surface free energy; crystallinity; water vapor sorption

## I-1 Introduction

The research on composite materials filled with vegetal particles has sharply increased to meet the society demand for more sustainable materials. Nowadays, biocomposites combining polymers and fibers that are both bio-sourced and biodegradable are becoming serious candidates to replace conventional plastics [255]. In addition to being largely available and renewable, cellulose resources provide many benefits due to their inherent characteristics such as low density, non-abrasivity and high availability at low cost [5]. The incorporation of cellulose-based fillers in polymer matrices has one major technical bottleneck, namely the hydrophilic nature of fillers that contrasts with the more hydrophobic nature of most polymer matrices. This strong hydrophilic character leads to two main limitations: a high moisture sensitivity and a poor compatibility between the filler and the matrix. This latter results in a weak interfacial adhesion and in a low wettability of the fillers by the matrix, making difficult the dispersion of fillers in the polymer matrices due to agglomeration into knotty masses [14,90,256]. Therefore, the achievement of a good filler/matrix interfacial adhesion is essential to get materials with enhanced properties, especially mechanical properties and life span [257].

To address this problem, many strategies aiming at increasing the similarity of the surface properties of the composite components have been already largely investigated. They include physical and chemical modifications of either the filler surface or the polymer matrix, or the introduction of coupling agents such as maleic anhydride [99]. The modification of the filler surface is very easy due to the presence of surface hydroxyl groups and well-known grafting reactions. Possible chemical treatments of cellulose are numerous, including esterification with carboxylic acids, anhydrides, alkyl ketene dimers, acid chlorides, transesterification with triglycerides of fatty acids, etherification with epoxides, silanization with trialkoxysilane, and carbamylation with isocyanates [5,22,98,145,258]. Modifications with covalent linkages are favored to get significant and long-lasting changes of hydrophobicity. Esterification is the most common reaction used for grafting carbon chains on hydroxyl groups and the resulting cellulose is among the more biodegradable cellulose derivatives [175]. The reaction between the hydroxyl groups present at the surface of cellulose and long chain fatty acid chloride has been known in chemistry for decades [259]. Reactions can be implemented either in homogeneous or heterogeneous phase. In homogenous conditions, cellulose is dissolved in suitable solvents, which damage the supramolecular structure of the cellulose resulting in the loss of its intrinsic properties [127,260]. In heterogeneous systems, a partial modification of cellulose may occur but without significant effect on its characteristics [146,156,261]. However, the cost and the potential toxicity of aprotic organic solvents, the implementation of such reaction in anhydrous conditions as well as the use of HCl scavengers such as pyridine, have prevented large-scale sustainable applications.

Thus there is an increasing interest for solvent-free treatments. Esterification reactions were explored by mixing directly cellulose or sawdust with fatty acids, with a displacement of the equilibrium under vacuum [148] or nitrogen flow [149]. Vapor-phase esterification with

trifluoroacetic anhydrides mixed with acetic acid was first successfully applied to filter paper and tunicate cellulose film hydrophobation, thus demonstrating its interest in the paper industry [135]. Chromatogenic chemistry, also called chromatografting, is based on the propagation of long chain fatty acid chlorides vapors within porous structures, akin to the diffusion conditions encountered in gas chromatography. The residual water molecules and the generated by-products of the reaction (HCl in the case of acid chloride) are continuously removed by the gas flow, which limits the possible degradation of the substrate and the reverse hydrolysis reaction. The reaction can thus be performed without any solvent and without the need of strict anhydrous conditions or HCl scavengers. This technique was first applied on paper surfaces [161,262] and then on cellulose-based aerogels using fatty acid chloride such as palmitoyl chloride [150,157,263]. Degrees of substitution (DS) between 0.1 and 2.5 were reported, but grafting was restricted to the surface of cellulose only for DS values lower than 0.4. Fumagalli et al. also showed that different reagents could be used for this process and that bi-functional reagents, such as sebacoyl chloride, reacted exclusively on nanocellulose surface [151]. Up to now, such technology has never been applied to a hundred gram batch of micrometric size cellulose particles in the form of powder. In the overall context of developing high performance biocomposites by increasing the compatibility of cellulose particles with an apolar matrix, the potential interest of such an eco-friendly gas-phase esterification has been investigated in a recent study [264]. It has been shown that this process significantly improved the hydrophobicity of the cellulosic fillers resulting in a stronger filler/matrix interfacial adhesion in the PHBV-based composite. The negative effects resulting from the incorporation of cellulose in PHBV were limited when cellulose was modified by gas-phase esterification, making possible the use of higher filler contents [264].

The present paper aims at achieving deeper knowledge on the relationships between the gas-phase esterification conditions, the degree of substitution and the resulting intrinsic properties of cellulose. For that purpose, a well-known and largely available reagent, namely palmitoyl chloride, was used. Fumagalli et al. experimental conditions [157] were adapted so that a large amount of cellulose particles (100g) could be treated. The efficiency of the treatment was evaluated by spectroscopy technics ( $^{13}\text{C}$  NMR, FT-IR). The impact on the hydrophobicity of cellulose particles was evaluated from the measurements of contact angle with different solvents and from dynamic water vapor absorption. Key intrinsic properties of cellulose particles were also monitored (thermal stability, crystallinity, morphology) in order to assess whether bulk properties were affected by the surface grafting.

## I-2 Materials and methods.

### I-2.1 Materials

Cellulose was supplied by Arbocel J. Rettenmaier & Söhne (France) under the reference Arbocel<sup>®</sup> (grade BE 600-10 TG) in the form of a fine powder obtained after milling and sorting from pine cellulose. Particles were characterized by a cellulose content of 99.5%, a bulk density of 0.23 – 0.30 g.cm<sup>-3</sup> (in accordance with DIN EN ISO 60), a skeletal density of 1.56 g.cm<sup>-3</sup>, an average thickness of 15 μm and an average length of 18 μm (data given by the supplier). The specific surface, measured by the BET method, was 1.33 ± 0.02 m<sup>2</sup>.g<sup>-1</sup>.

Palmitoyl chloride (92% of purity) was purchased from Sigma-Aldrich. Absolute ethanol (99.9% of purity) was supplied by Meridis, and acetone (99.8% of purity) was obtained from Biosolve Chimie. All chemicals were used without any further purification.

### I-2.2 Methods

#### I-2.2.1 Gas-phase esterification of cellulose

Before treatment, cellulose was previously dried at 60°C overnight. Cellulose (around 100 g) was placed in nylon mesh bags that were sealed and put on a grid above the reagent in a heated vacuum reactor. The reagent, palmitoyl chloride, was introduced at 0.2 eq compared to anhydroglucose units (AGU) and so in excess compared to surface hydroxyl groups. The 2 L reactor was connected to a vacuum pump through a cold trap to reach a pressure of 2 mbar. A constant nitrogen flow was introduced in order to evacuate the by-products of the reaction, mainly gaseous hydrochloric acid. The temperature varied between 100°C and 120°C, and the reaction time between 3 hours and 15 hours. After the grafting step (Figure 48), a Soxhlet extraction with acetone was undertaken in order to remove palmitic acid and unreacted palmitoyl chloride, and to get clean grafted cellulose samples. Resulting grafted cellulose (called C-G1, C-G2, C-G3 or C-G4 depending on the grafting conditions) was finally dried overnight at 60°C to remove residual acetone. A control sample (called C-control) was prepared without palmitoyl chloride following the same procedure including the washing step.

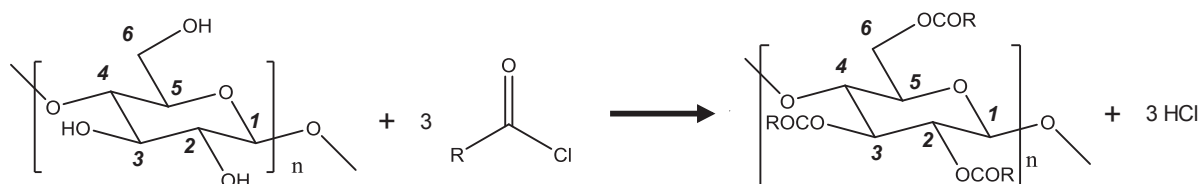


Figure 48. Esterification of cellulose with an acyl chloride

## I-2.2.2 Characterization of cellulose particles

Degree of substitution. The degree of substitution (DS) represents the number of palmitoyl moieties grafted per anhydroglucose unit (AGU). As each AGU unit has 3 hydroxyl groups, the DS can thus theoretically range between 0 and 3. Here, the DS of the grafted cellulose was determined by  $^{13}\text{C}$  NMR and confirmed by FT-IR analysis. Samples were analyzed in triplicate. Solid-state  $^{13}\text{C}$  NMR analyses were performed using a Bruker Avance DSX 400 MHz spectrometer operating at 100.6 MHz for  $^{13}\text{C}$ . The combination of cross-polarization, high-power proton decoupling and magic angle spinning (CP/MAS) method was used. Standard conditions were 2000 scans with 2 ms of contact and 2 s of recycle delay. The acquisition time was 35 ms and the sweep width was 29400 Hz. For DS determination, integrals were normalized with respect to area of cellulose C1 resonance peak. The infrared spectrum from attenuated total reflectance-Fourier transform infrared analysis (ATR-FTIR) of cellulose was recorded using a Nexus 6700 spectrophotometer (ThermoElectron Corp.) equipped with a laser source HeNe and a nitrogen-cooled MCT detector. The spectra were obtained by accumulation of 32 scans with a resolution of  $2\text{ cm}^{-1}$  in the  $500\text{-}4000\text{ cm}^{-1}$  range. The data processing was performed using the Omnic v7.3 software. The spectra were normalized with respect to the cellulose backbone peak height, which was invariant from one sample to another.

## X-ray diffraction analysis

Wide angle X-ray diffraction analysis was applied to assess the impact of the treatment on the crystallinity of cellulose, using an in-house setup of the laboratory Charles Coulomb, University Montpellier 2, France. An ultralow divergent beam ( $0.5\text{ mrad}$ ; flux:  $20\text{ MPhotons/s}$ ; size at sample:  $0.36\text{ mm}^2$ ) was delivered by a high brightness low power X-ray tube coupled with aspheric multilayer optic (GeniX<sup>3D</sup> from Xenocs). The samples were in glass capillaries. In transmission configuration, scattered intensity was measured by a 2D pixel “Pilatus” detector. The signals were then analyzed with the software Fit2D. The measurements were carried out in  $2\theta$  ranges between  $5^\circ$  and  $25^\circ$  with a step size of  $0.047^\circ$ . The crystallinity index (CrI) of the cellulose was calculated (Eq. 23) according to the Segal method [250]:

$$\text{CrI} = \frac{I_{002} - I_{\text{am}}}{I_{002}} \times 100 \quad \text{Eq. 23}$$

where  $I_{002}$  is the maximum intensity of the 002 lattice reflection of the cellulose crystallographic form ( $I_{002}$ ) at  $2\theta = 22^\circ$  and  $I_{\text{am}}$  the diffraction intensity of the amorphous material at  $2\theta = 18^\circ$ .

### Thermogravimetric analysis

Thermogravimetric analysis (TGA) was carried out with a Mettler TGA2 apparatus equipped with a XP5U balance with a 0.1  $\mu\text{g}$  resolution. Experiments were performed in triplicate. Samples (40 mg) were heated from 25°C up to 800°C at a rate of 10°C.min<sup>-1</sup> under a nitrogen flow (50 mL.min<sup>-1</sup>). The temperature of thermal decomposition ( $T_{\text{deg}}$ ) corresponded to the temperature at which the degradation rate was maximum. The temperature corresponding to the beginning of the main thermal degradation ( $T_{\text{onset}}$ ) was measured when the first derivative of the weight loss became higher than 0.1 %·°C<sup>-1</sup>. Likewise, the offset temperature ( $T_{\text{offset}}$ ) was taken at the end of derivative weight loss degradation peak when the first derivative of the weight loss became lower than 0.1 %·°C<sup>-1</sup>.

### Scanning electron microscopy (SEM)

SEM was performed with a high-resolution field emission gun (SEM S-4800, Hitachi, Japan) with an acceleration voltage of 2 kV. The samples were coated with Pt by cathode pulverization.

### Cellulose particle morphology

Cellulose particles were dispersed in ethanol (0.35 g.L<sup>-1</sup>) and dropped on glass slides. Observations were done with an AZ100 microscope (Nikon, JP) operating in the light transmission mode. Mosaic images were assembled with 5×5 images using NIS-Elements software (Nikon, JP). Images were treated using the Image J software to evaluate the polydispersity of the particles size. The software viewed each particle as an ellipse and measured major and minor axes from which  $d_{10}$ ,  $d_{50}$ ,  $d_{90}$  and span values were calculated. Circularity was calculated as square of the ratio between the perimeter of the particle and the circumference of a circle with the same area. A circularity value of 1.0 indicates a perfect circle.

### Contact angle measurements and surface free energy

A hydraulic press (Perkin-Elmer) was used to form 13 mm diameter compact disc tablets of 0.1 g of cellulose and about 700  $\mu\text{m}$  thickness, with a disc mold under pressure. Cellulose tablets were dried over P<sub>2</sub>O<sub>5</sub> under vacuum for 1 hour before analysis. Contact angle measurements were carried out at 23°C using a goniometer instrument (Digidrop, GBX, France) coupled to the Windrop software (GBX, France). Five reference liquids (distilled water, ethylene glycol, diiodomethane, formamide and glycerol) were used. A drop of 3  $\mu\text{L}$  was deposited on the surface of tablets and contact angles were measured as soon as the drop spreading was stabilized. Five measurements were done for each sample and each liquid. Surface free energy values were calculated using the Owens-Wendt model [247].

## Dynamic vapor sorption

Water vapor sorption kinetics were performed at 20°C using a controlled atmosphere microbalance (DVS, Surface Measurement System Ltd., London, UK), which enables recording the water vapor uptake of the materials as a function of time for successive relative humidity (RH) steps (0, 10, 20, 30, 40, 50, 60, 70, 80, 90 and 95%). The sample was first dried at 60°C in an oven and then dried over P<sub>2</sub>O<sub>5</sub> in a desiccator and finally placed in the DVS apparatus at 0% RH for 5 h at 20°C. Around 1 mg of cellulose particles were deposited in the form of a monolayer powder bed. Water vapor sorption isotherms were established from the equilibrium moisture contents at each RH step. Tests were performed in duplicate.

## I-3 Results and Discussion

### I-3.1 Quantification of the gas-phase esterification efficiency

On the basis of what was already done on aerogels using this esterification method [150,157], different conditions of temperature and reaction time were tested (Table 21). The aim was not to optimize this reaction, but to understand its effect on micro-sized cellulosic particles. The occurrence of the grafting was quantified by the calculation of the degree of substitution (DS) from solid-state <sup>13</sup>C NMR results and it was further confirmed by FT-IR analysis. Results are gathered in Table 21.

Table 21. Degree of substitution calculated from <sup>13</sup>C NMR and FT-IR experiments for different experimental conditions (duration and temperature).

Codification	Experimental conditions (duration, temperature)	DS <sub>C=O</sub> ( <sup>13</sup> C NMR)	DS <sub>C-H</sub> ( <sup>13</sup> C NMR)	DS <sub>estimated</sub> (FT-IR)
C-virgin	No grafting	-	-	-
C-control	3 h - 100°C without reagent	-	-	-
C-G1	3 h - 100°C	0.01	0.01	0.01 ± 0.00
C-G2	15 h - 100°C	0.02	0.02	0.04 ± 0.00
C-G3	7 h - 120°C	0.07	0.09	0.13 ± 0.01
C-G4	15 h - 120°C	0.13	0.14	0.23 ± 0.01

DS values were calculated by solid-state <sup>13</sup>C NMR spectroscopy (Figure 49) from peaks assigned according to the literature data [124]. The occurrence of the grafting was evidenced by the appearance of new peaks in the spectra of the modified cellulose, i.e. carboxylic carbons at 172 ppm and aliphatic carbons between 10 and 40 ppm. The degree of substitution was calculated



from Eq. 24 and Eq. 25 using these two features and the integral of carbon C1 as cellulose reference:

$$DS_{C-H} = \frac{I_{C-H}}{15 \times I_{C1}} \quad \text{Eq. 24}$$

$$DS_{C=O} = \frac{I_{C=O}}{1 \times I_{C1}} \quad \text{Eq. 25}$$

There were only slight differences between  $DS_{C-H}$  and  $DS_{C=O}$ . For low DS,  $DS_{C-H}$  was likely more suitable since integral of carboxylic resonance signal was very low and might lead to approximations. Results from Table 21 showed that DS displayed some proportionality to reaction time and temperature, as already described in such reactions [150,157]. Grafted celluloses were obtained with DS varying from 0.01 to 0.14. These DS were lower than the ones reported by previous works: 0.15-2.7 [150] and 0.04-2.36 [157] using a similar vapor treatment. This was explained by the fact that the specific surface area of cellulose particles considered in the present study ( $1.33 \text{ m}^2 \cdot \text{g}^{-1}$ ) was much lower than that of aerogel ( $100 \text{ m}^2 \cdot \text{g}^{-1}$ ), resulting in a lower availability of surface hydroxyl groups. The comparison with DS values obtained from other treatments was delicate because of the absence of specific surface data of the substrate.

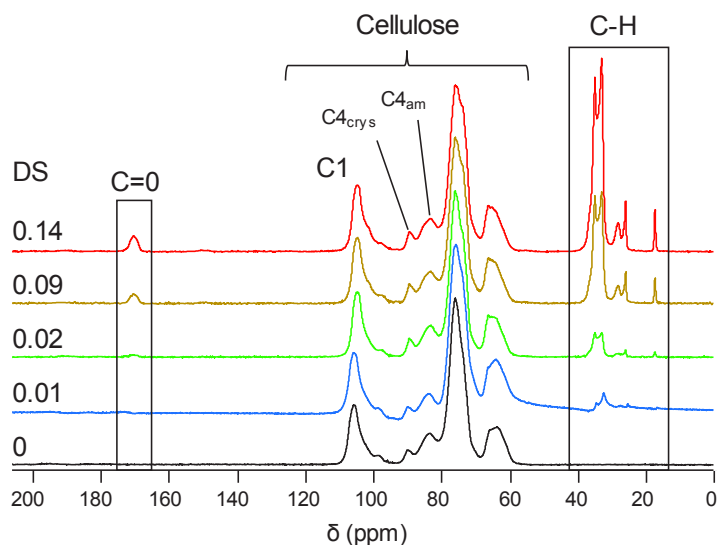


Figure 49. Solid  $^{13}\text{C}$  NMR spectra of virgin cellulose ( $DS = 0$ ) and modified cellulose ( $DS = 0.01-0.14$ ).

DS values were corroborated by FT-IR analysis. Virgin cellulose displayed a typical IR spectrum, which was mainly characterized by a broad band between  $3000$  and  $3600 \text{ cm}^{-1}$  corresponding to O-H groups, a peak around  $2900 \text{ cm}^{-1}$  corresponding to C-H bonds and a series of peaks between  $950-1200 \text{ cm}^{-1}$  corresponding to C-O bonds of the cellulose skeleton [265] (Figure 50). The grafting of cellulose by esterification was clearly visible with the appearance of the ester carboxyl signal at  $1745 \text{ cm}^{-1}$  together with the intensity decrease of the hydroxyl

parts ( $3000\text{-}3600\text{ cm}^{-1}$ ). This highlighted that hydroxyl groups of cellulose reacted with palmitoyl chloride to form covalent ester bonds [151,157]. Palmitoyl chloride being a sixteen carbons compound, its grafting on cellulose also resulted in an increase of the intensity of the peaks around  $2900\text{ cm}^{-1}$  and in the appearance of a new band around  $710\text{ cm}^{-1}$  ascribed to  $\text{CH}_2$  vibrations of aliphatic chains. An estimation of the degree of substitution was calculated from the intensity of the  $\text{C}=\text{O}$  stretching band ( $I_{1745}$ ) and the intensity of the  $\text{C}-\text{O}$  stretching of cellulose backbone ( $I_{1030}$ ) measured at  $1745\text{ cm}^{-1}$  and  $1030\text{ cm}^{-1}$ , respectively (Eq. 26).

$$DS_{\text{estimated}} = \frac{I_{1745}}{I_{1030}} \quad \text{Eq. 26}$$

As expected, DS from FT-IR analysis were higher than those from  $^{13}\text{C}$  NMR, especially for the highest DS because ATR technique allows the analysis of the sample surface and does not take into account the ungrafted cellulose bulk. That is the reason why FT-IR is more used as a qualitative rather than a quantitative method.

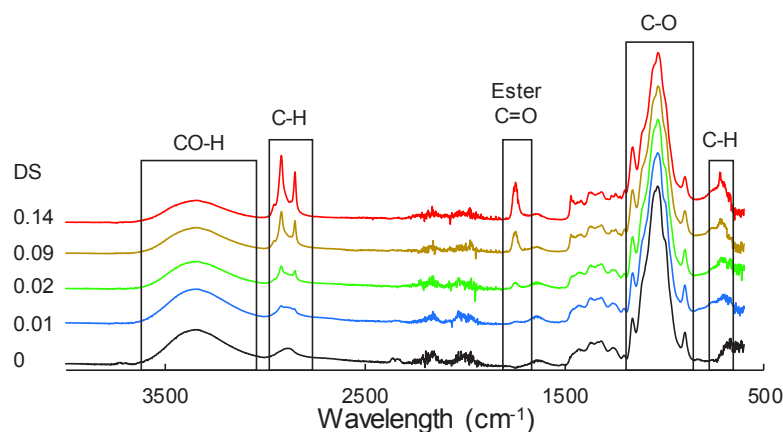


Figure 50. FT-IR spectra of the modified celluloses with different DS.

Knowing native cellulose dimensions, it can be assumed that there is one hydroxyl group every  $0.5 \times 0.5\text{ nm}$  at the surface [266]. So,  $4.10^{18}\text{ m}^{-2}$  is the density of hydroxyl groups ( $d_{\text{OH}}$ ), namely the number of OH groups per unit of surface. Knowing the specific surface area of cellulose particles (SSA), the molecular mass of anhydroglucose unit ( $M_{\text{AGU}}$ ) and the Avogadro number ( $N_{\text{A}}$ ), a theoretical  $DS_{\text{Surface}}$  can be calculated as follows (Eq. 27):

$$DS_{\text{Surface}} = \frac{\text{SSA} \times d_{\text{OH}} \times M_{\text{AGU}}}{N_{\text{A}}} \quad \text{Eq. 27}$$

Using values of respectively  $1.33\text{ m}^2\cdot\text{g}^{-1}$ ,  $162\text{ g}\cdot\text{mol}^{-1}$  and  $6.022 \times 10^{23}\text{ mol}^{-1}$ , a  $DS_{\text{Surface}}$  value of 0.0014 was obtained. Acylation of cellulose occurring from the surface to the core [123] and all the DS obtained (Table 1) being higher than  $DS_{\text{Surface}}$ , it was deduced that all the OH groups available at the surface of cellulose particles were grafted even under the mildest conditions

tested (C-G1). As  $DS_{\text{Surface}}$  strongly depends on SSA, the obtained value was obviously lower than the one from cellulose aerogels [157].

## I-3.2 Impact of gas-phase esterification on cellulose particles intrinsic characteristics

### I-3.2.1 Crystallinity

The crystallinity is a key intrinsic characteristic influencing the cellulose properties. XRD (Figure 51), as well as solid-state  $^{13}\text{C}$  NMR analyses were used to study the treatment effect on the cellulose crystalline structure. The Segal method is useful for quickly comparing differences between cellulose samples [250]. It is also the most usual method to determine the crystallinity index of cellulose [267]. For virgin cellulose, the typical pattern of cellulose I was displayed with  $2\theta$  peaks at  $14.9$ ,  $16.3$  and  $22.3^\circ$  that correspond to the diffraction planes  $101$ ,  $10\bar{1}$ , and  $002$ , respectively [146,268]. The cellulose considered in the present study showed a low crystallinity index, of  $35 \pm 3\%$ , as compared to common cellulose fibers which usually display a crystallinity index higher than  $50\%$ . This was ascribed to the fact that the cellulose sample was obtained after successive dry grinding steps, which are well known to induce amorphization [269]. Results showed that gas-phase esterification conducted under the most drastic conditions of the present study (C-G4) did not alter significantly the crystallinity. In general, esterified cellulose with higher DS showed a progressive decrease of crystallinity [124,146]. This suggested that most of the substitutions occurred at the surface of the amorphous regions without modifying the inner structure of cellulose. This was in accordance with what was observed on  $^{13}\text{C}$  NMR spectra (Figure 2): the amorphous chains signal ( $C_{4\text{am}}$ , 80-87 ppm) and crystalline core signal ( $C_{4\text{crys}}$ , 87-90 ppm) did not vary within the present range of DS. The ratio of the two integrals also confirmed that the used cellulose was semi-crystalline with an important amorphous phase. The  $C_{4\text{am}}$  peak gave a broader resonance due to the higher disorder and molecular mobility in the non-crystalline regions [270]. On the X-ray diffractogram of C-G4, the very slight shoulder observed at around  $21^\circ$  was attributed to the presence of grafted fatty chains [271].

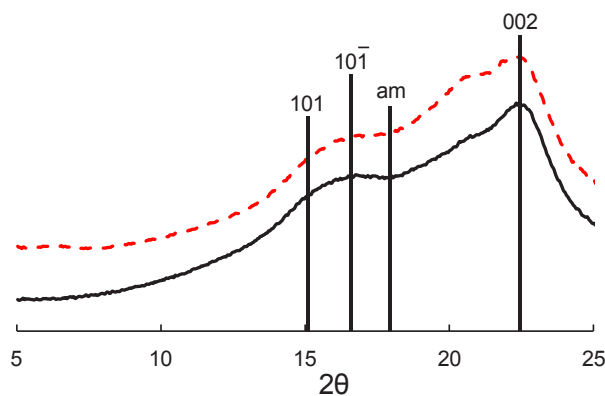


Figure 51. X-ray diffractograms of C-virgin (—) and C-G4 (---).

### I-3.2.2 Thermal stability

The thermal degradation behavior of virgin, control and grafted celluloses was investigated by thermogravimetric analysis (TGA) under nitrogen flow (Figure 52 and Table 22). All the samples displayed a main thermal degradation step with a maximum decomposition temperature around  $346 \pm 1^\circ\text{C}$  for virgin and control celluloses, and  $341 \pm 1^\circ\text{C}$  for grafted samples. Virgin cellulose started to decompose at  $260.4 \pm 0.1^\circ\text{C}$  and control cellulose at  $258.0 \pm 0.1^\circ\text{C}$  showing a very low degradation due to the experimental conditions. Except for C-G4, which started to decompose at  $251.3 \pm 0.8^\circ\text{C}$ , the  $T_{\text{onset}}$  values of all grafted celluloses were around  $246.5 \pm 0.5^\circ\text{C}$ . Thus, there was a slight reduction of the thermal stability induced by esterification with a decrease of  $T_{\text{onset}}$  and  $T_{\text{deg}}$  for grafted celluloses compared to ungrafted celluloses (C-virgin and C-control). Normally, a small decrease of crystallinity after treatment could explain this behavior [261], which was not evidenced in section I-3.2.1. The earlier thermal degradation of grafted cellulose could be thus attributed to the high lability of ester bonds [272]. However, the onset of thermal degradation temperature remained high enough, so that cellulose will not be thermally degraded during a possible future melt extrusion. It is worth noting that the thermal degradation of grafted celluloses occurred on a larger range of temperature, with  $T_{\text{offset}}$  values up to  $405^\circ\text{C}$  instead of  $337^\circ\text{C}$  for virgin cellulose. The degree of substitution had only a minor influence on the thermal stability.

In the case of grafted cellulose, DTG curves showed a second degradation peak at around  $380^\circ\text{C}$ , the integral of which was proportional to the DS of the sample. This second degradation peak was therefore related to esterified aliphatic chains, as previously observed by Uschanov et al. [156].

Additionally, the enhancement of the hydrophobicity of grafted celluloses was confirmed by the decrease of the weight loss around  $70^\circ\text{C}$  corresponding to the evaporation of absorbed water [273]. Thermogravimetric analysis showed that the differences between samples did not raise any concern about thermal stability, this validated the gas-phase esterification as a potential pre-treatment of cellulose for fillers in composite materials.

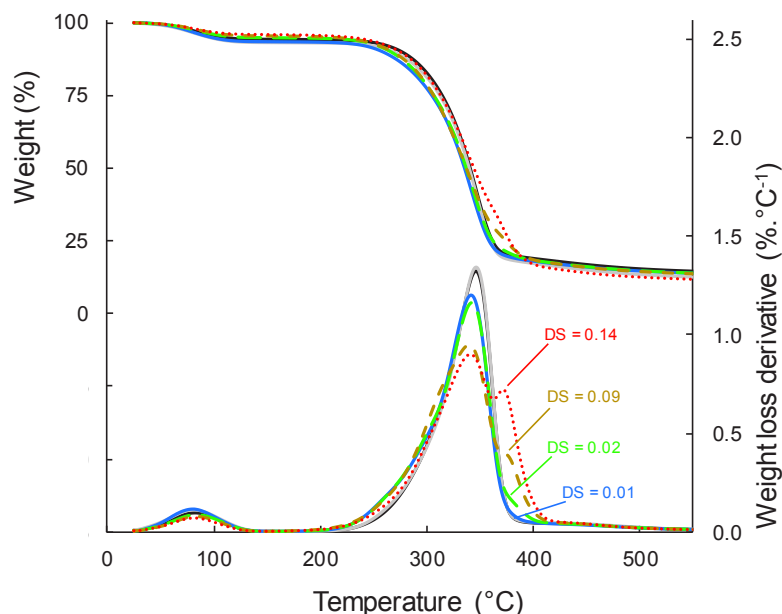


Figure 52. TG and DTG curves of C-virgin (—), C-control (···) and grafted celluloses: C-G1, DS=0.01 (—); C-G2, DS=0.02 (—); C-G3, DS=0.09 (—); and C-G4, DS=0.14 (···) under N<sub>2</sub>.

Table 22. Results of the thermogravimetric analysis.

	T <sub>deg</sub> (°C)	T <sub>onset</sub> (0.1%/°C)	T <sub>offset</sub> (0.1%/°C)
C-virgin	345.9 ± 0.3	260.4 ± 0.1	377.3 ± 0.1
C-control	346.5 ± 0.1	258.0 ± 0.1	377.0 ± 0.6
C-G1	341.1 ± 0.8	246.0 ± 0.3	378.3 ± 0.1
C-G2	342.4 ± 0.1	246.8 ± 0.4	390.3 ± 0.1
C-G3	340.5 ± 1.0	246.8 ± 0.2	400.7 ± 0.1
C-G4	341.0 ± 0.1	251.3 ± 0.8	405.6 ± 0.3

### I-3.2.3 Cellulose particle morphology

The appearance of modified particles was observed by SEM and compared to virgin cellulose (Figure 53). No clear difference between grafted and virgin celluloses was visible on SEM images, suggesting that no significant degradation of the macroscopic structure occurred during the treatment. This was in agreement with TGA results. At high resolution, a surface smoothness could be observed on C-G4 particles (C3) as compared to virgin cellulose (A3) or C-G1 cellulose (B3). This looked like depositions on particles; the particles seemed to be embedded in a kind of snow layer. Similar phenomenon was observed on bacterial cellulose microfibrils by Berlioz et al. [150]. It was confirmed by 2D image analysis (Table 23) that the dimensions of the particles were not significantly affected.

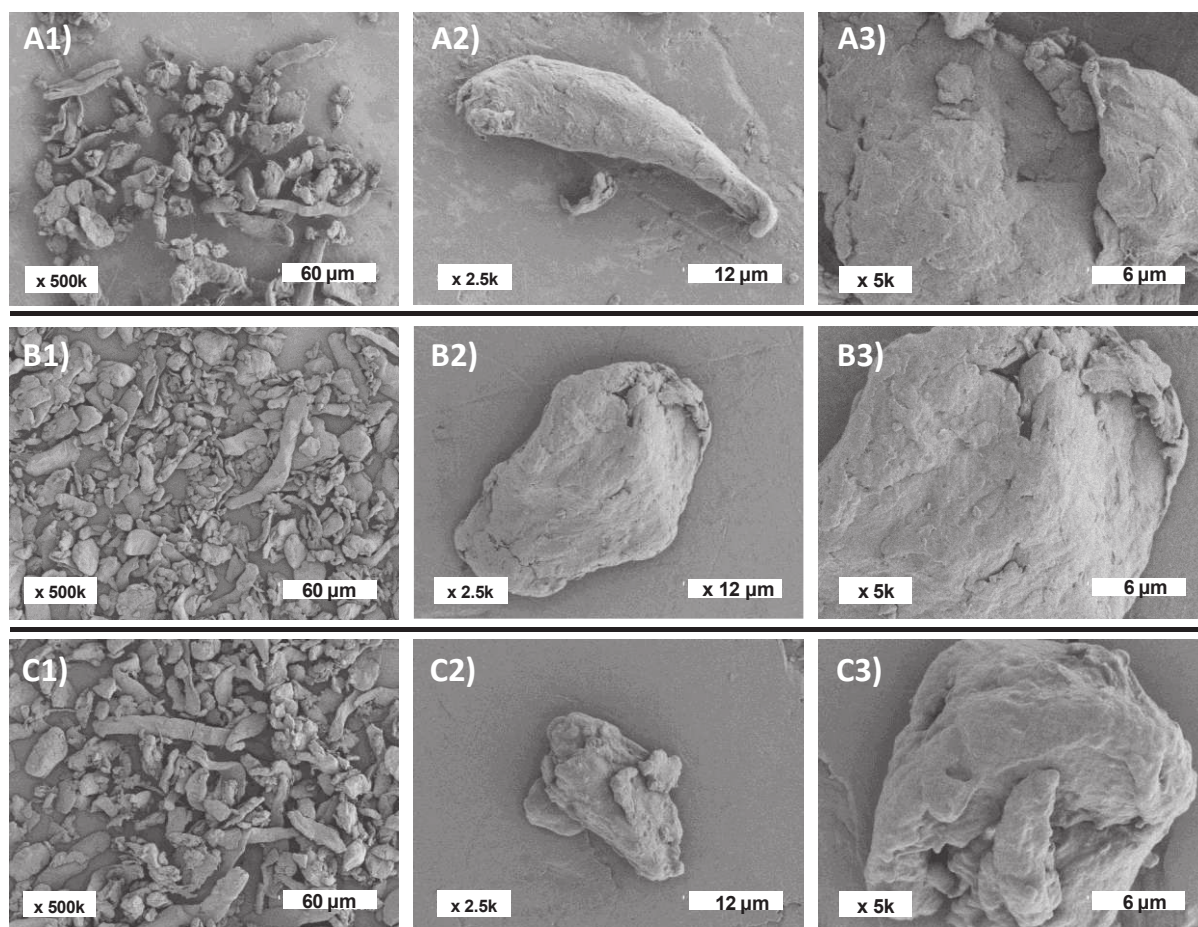


Figure 53. SEM pictures of (A1-3) virgin cellulose C-virgin and grafted cellulose (B1-3) C-G1 and (C1-3) C-G4 particles at different magnifications.

Table 23. Morphological parameters in volume of C-virgin and C-G4 cellulose particles.

		d10 ( $\mu\text{m}$ )	d50 ( $\mu\text{m}$ )	d90 ( $\mu\text{m}$ )	Span	Circularity
C-virgin	Major axis	$17 \pm 3$	$40 \pm 4$	$71 \pm 5$	$1.4 \pm 0.3$	$0.71 \pm 0.02$
	Minor axis	$11 \pm 2$	$23 \pm 2$	$34 \pm 3$	$1.0 \pm 0.1$	
C-G4	Major axis	$19 \pm 4$	$43 \pm 2$	$65 \pm 4$	$1.0 \pm 0.1$	$0.71 \pm 0.02$
	Minor axis	$12 \pm 2$	$24 \pm 2$	$36 \pm 1$	$1.0 \pm 0.2$	

#### I-3.2.4 Wettability of grafted cellulose

The effect of gas-phase esterification on the cellulose surface hydrophobicity was clearly and visually evidenced by the observation of a drop of water on either the virgin or grafted cellulose (Figure 54) and quantified by contact angle measurements (Table 24). Whatever experimental conditions used, gas-phase esterification resulted in a drastic increase of the water contact angle value, highlighting the expected targeted increase of hydrophobicity induced by the grafting. Water contact angle values increased from  $44^\circ$  for the virgin cellulose up to  $97^\circ$ - $109^\circ$  for grafted cellulose. Obtaining water contact angle values higher than  $90^\circ$  corroborated concluding on the hydrophobic character of grafted cellulose [274], this was confirmed with other polar liquids.

Grafted cellulose displayed a hydrophobic surface even with modest DS of 0.01. The increasing values of the contact angle with non-polar solvents such as diiodomethane indicated that the particles became slightly lipophobic. This double phobic character is generally found with perfluorinated materials [275]. The macroscopic behavior of the water drop on cellulose tablets depended on the nature of the cellulose surface. Grafted cellulose tablets exhibited a water repellence, with a water contact angle very stable over time, whereas the drop of water was rapidly absorbed by virgin cellulose tablets due to capillarity effects. However, no correlation between the degree of substitution and water contact angle values could be established, as already reported for long chain cellulose esters [126].

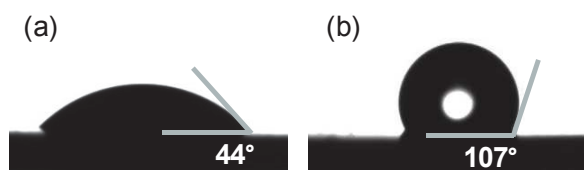


Figure 54. Pictures of a drop of water deposited on compressed tablets constituted of (a) virgin cellulose and (b) grafted cellulose.

Contact angle measurements with solvents of different polarities allowed the estimation of the polar ( $\gamma^P$ ) and dispersive ( $\gamma^d$ ) components of the solid surface free energy ( $\gamma$ ) of virgin and grafted celluloses using the Owens-Wendt's approach (Table 24). In all cases, the substitution of the surface hydroxyl groups by long-chain aliphatic esters after gas-phase esterification resulted in a drastic decrease of the polar component from 17.7 mJ.m<sup>-2</sup> down to nearly zero. This decrease might be too sharp since the objective was to reduce the polar component of cellulose to be the closest to the polymer one and not necessary to reach zero. The dispersive components of grafted celluloses exhibited a lower  $\gamma^d$  value (around 22 mJ.m<sup>-2</sup>) than the virgin cellulose (32 mJ.m<sup>-2</sup>). Such phenomenon was observed with octadecyl-silanated cellulose [276]. This is rather unexpected compared with the literature data [146,277,278] but could be explained by the low surface energy of grafted alkyl chain. The extent of grafting, reflected by the DS value, did not have a significant impact on surface free energy values, suggesting that the mildest experimental conditions used were sufficient to reach a complete hydrophobization of the cellulose surface. Since the hydrophobic character was the main target, low DS values were enough to achieve our primary goal. The DS threshold was  $3 \times 10^{-4}$  for acetic-oleic cellulose esters [279]. This value may change with the length of the grafted fatty chain.

Table 24. Contact angle values ( $^{\circ}$ ), polar ( $\gamma^p$ ) and dispersive ( $\gamma^d$ ) components of the surface free energy ( $\gamma$ ) of virgin cellulose (C-virgin) and grafted cellulose (C-GX) with different reference liquids.

	Contact angle ( $^{\circ}$ )					Surface free energy ( $\text{mJ.m}^{-2}$ )		
	Water	Ethylene glycol	Diiodom ethane	Formamide	Glycerol	$\gamma^p$	$\gamma^d$	$\gamma$
C-virgin	$44 \pm 2$	$35 \pm 2$	$33 \pm 3$	$28 \pm 3$	$59 \pm 5$	17.7	32.1	49.8
C-G1	$98 \pm 1$	$51 \pm 1$	$36 \pm 2$	$52 \pm 0$	$91 \pm 7$	0.2	22.2	22.4
C-G2	$107 \pm 2$	$87 \pm 3$	$64 \pm 5$	$94 \pm 2$	$103 \pm 2$	0.2	23.5	23.7
C-G3	$109 \pm 3$	$87 \pm 1$	$57 \pm 4$	$99 \pm 2$	$105 \pm 2$	0.1	21.5	21.6
C-G4	$103 \pm 4$	$95 \pm 4$	$57 \pm 4$	$103 \pm 4$	$100 \pm 3$	0.1	20.1	20.2

### I-3.2.5 Water vapor sorption of grafted cellulose

The impact of chemical grafting on water vapor sorption in cellulose particles was investigated by dynamic vapor sorption (DVS) measurements (Figure 55). Similar water sorption patterns were observed for all samples, esterified or not. Water vapor isotherms displayed a sigmoidal curve typical of cellulose-based materials [280]. The water vapor uptake gradually increased with the relative humidity, reaching at 95% RH a water vapor uptake of  $0.227 \pm 0.004 \text{ g.g}^{-1}$  dry basis (d.b.) for virgin cellulose and  $0.162 \pm 0.005 \text{ g.g}^{-1}$  d.b. for C-G4. The virgin cellulose values were in accordance with water vapor sorption uptake measured using a QCM device [281]. From the Park's model that usually well describes such experimental results, the isotherm curves can be divided in three parts: at  $\text{RH} < 10\%$  water is sorbed by hydrogen bonding onto specific sites at the surface (part I), then at  $10\% < \text{RH} < 60\%$  the water concentration increases linearly with water activity by capillarity due to the porous structure of cellulose. Finally, at  $\text{RH} > 60\%$ , the water sorption increases more dramatically as a power function likely due to the capillary condensation in cellulose and to water vapor clustering effect [282,283].

Globally, except for a RH of 10%, lower equilibrium moisture uptakes were recorded for grafted samples as compared to virgin cellulose. This means that the hydrophobic carbon moieties on grafted celluloses prevented the adsorption of water vapor. It is worth noting that esterification mainly affected water vapor sorption behavior on zone II. In fact, at the beginning of this zone ( $\text{RH} = 10\%$ ), water uptake was the same for all cellulose samples whereas toward at the end of this zone ( $\text{RH} = 60\%$ ), water vapor uptake was  $0.102 \text{ g.g}^{-1}$  d.b. and  $0.055 \text{ g.g}^{-1}$  d.b. for C-virgin and for C-G4 respectively. Moisture sorption was significantly affected by the degree of substitution, with decreasing water sorption values at each RH step for increasing DS values. The difference of water sorption could not be explained by the crystallinity that remained the same, as shown previously. This result could rather be explained by the pore volume modification of the cellulose particles due to the esterification step. Similar results were previously observed on cellulose nanofibrils [139] and agave fibers [284]. This effect was more pronounced than the one already observed by Peydecastaing et al. for acetic-fatty cellulose esters [279]. In the present case, this could be explained by a longer alkyl chain grafted to the cellulose as suggested by the study of Sehaqui et al. which showed a relation between the



moisture absorption and the alkyl chain length grafted. The effect of grafting was more DS dependent in the case of vapor water than with liquid water (water contact angle), because of their physical state. As explained in the study by Peydecastaing et al. [279], individual vapor water molecules could more easily reach free remaining hydroxyl groups of the cellulose than a drop of water which is a cluster of hydrogen bonded molecules.

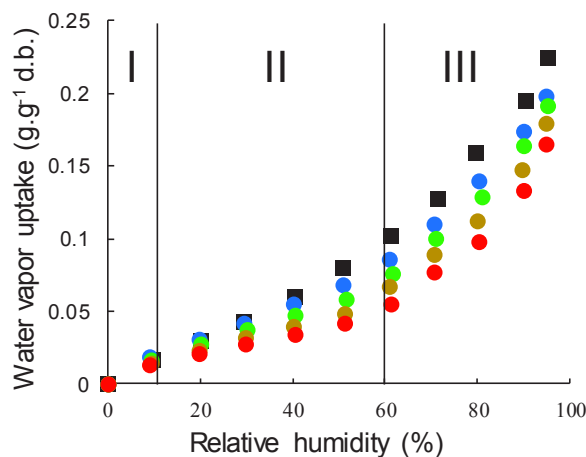


Figure 55. Water vapor sorption isotherm of virgin cellulose: C-virgin (■) and grafted cellulose: C-G1 (●), C-G2 (●), C-G3 (●), C-G4 (●).

## I-4 Conclusion

Gas-phase esterification of cellulose particles by fatty acid chlorides seems to be a promising approach to produce bio-based fillers tailored for the biocomposite market. The gas-phase esterification was first used on micron-size cellulose particles. This treatment was carried out to make them more hydrophobic and to avoid the main drawbacks of cellulose as fillers namely, poor compatibility with non-polar matrix and moisture absorption. The reagent was palmitoyl chloride, a well-known bio-based long-chain aliphatic acid chloride. The chosen conditions enabled the grafting of palmitoyl moieties onto the surface without degrading the intrinsic structure of cellulose. Surface free energy of grafted celluloses calculated from contact angles showed a fall of the polar component even for the lowest DS, whereas moisture sorption was significantly decreased by the cellulose DS. Cellulose integrity was checked through macroscopic observations, thermogravimetric analyses, SEM, XRD and spectrometric methods. The backbone of cellulose was not altered. Next steps would be the study of these fillers in composite materials. Overall, it can be concluded that gas-phase esterification is an adequate reaction to tailor the interfacial adhesion of micrometric size cellulose particles with an apolar matrix, therefore offering new perspectives in the development of novel biocomposite materials.

### Acknowledgments

This work was carried out in the framework of the NoAW project, which is supported by the European Commission through the Horizon 2020 research and innovation program under the Grant Agreement No 688338. The authors would like to acknowledge Emilie Ressouche for her help and advices on the use of the reactor for gas-phase esterification.

### Data availability

The data that support the findings of this study are openly available in “Exploring the potential of gas-phase esterification to hydrophobize the surface of micrometric cellulose particles \_ Raw data”. at <https://doi.org/10.15454/6VQ9JA>.

## II. Mitigating the impact of cellulose particles on the performance of biopolyester-based composites by gas-phase esterification (Article 2)

*Grégoire David, Nathalie Gontard and H el ene Angellier-Coussy \**

*JRU IATE 1208—CIRAD/INRA/Montpellier Supagro/University of Montpellier, 2 Place Pierre Viala, Bat 31, CEDEX 01, F-34060 Montpellier, France; gregoire.david@supagro.fr (G.D.); nathalie.gontard@inra.fr (N.G.)*

Published in *Polymers*. 24 January 2019. doi:10.3390/polym11020200

### Abstract

Materials that are both biodegradable and bio-sourced are becoming serious candidates for substituting traditional petro-sourced plastics that accumulate in natural systems. New biocomposites have been produced by melt extrusion, using bacterial polyester (poly(3-hydroxybutyrate-*co*-3-hydroxyvalerate)) as a matrix and cellulose particles as fillers. In this study, gas-phase esterified cellulose particles, with palmitoyl chloride, were used to improve filler-matrix compatibility and reduce moisture sensitivity. Structural analysis demonstrated that intrinsic properties of the polymer matrix (crystallinity, and molecular weight) were not more significantly affected by the incorporation of cellulose, either virgin or grafted. Only a little decrease in matrix thermal stability was noticed, this being limited by cellulose grafting. Gas-phase esterification of cellulose improved the filler's dispersion state and filler/matrix interfacial adhesion, as shown by SEM cross-section observations, and limiting the degradation of tensile properties (stress and strain at break). Water vapor permeability, moisture, and liquid water uptake of biocomposites were increased compared to the neat matrix. The increase in thermodynamic parameters was limited in the case of grafted cellulose, principally ascribed to their increased hydrophobicity. However, no significant effect of grafting was noticed regarding diffusion parameters.

Keywords: poly(hydroxybutyrate-*co*-valerate) (PHBV); biocomposite; gas-phase esterification; cellulose; water transfer

## II-1 Introduction

Cellulose is the most abundantly available renewable polymer on earth [38]. Its use as a filler in polymer matrices for the production of biocomposites has interested scientists and industries for decades, and even more so now with the will for developing new sustainable, biodegradable, light, and functional materials [5,14,21,22,98,142,285–287]. Compared to common industrial fillers, such as glass or carbon fibers, cellulose presents huge advantages, including its renewable character, low density, low cost, large availability throughout the world, non-abrasive behavior towards process equipment, high stiffness and tensile strength, and full biodegradability under natural conditions [14,288]. Unfortunately, cellulosic fillers also display some drawbacks due to their strong polar character, giving rise to three major limitations when used in composite materials. The first one is their poor compatibility with hydrophobic polymer matrices generally used, resulting in weak interfacial adhesion. The final properties of composite materials strongly depend on the intrinsic properties of the filler and matrix, and on the interface area, i.e., the compatibility between the two constituents. The quality of the filler–matrix interface is crucial since the load transfer from the matrix to the filler should be efficient enough to allow the material to stand up to the external mechanical solicitation [37]. The second one is their poor dispersion state within aforesaid matrices, due to the formation of cellulose aggregates through hydrogen bondings. The third limitation is associated with their strong sensitivity to water and even moisture, which induce swelling and loss of mechanical properties under ageing conditions [37,91]. To overcome these limitations, cellulosic fillers are generally submitted to various surface modifications to minimize the interfacial energy between the fillers and non-polar polymer matrix. These modifications present an opportunity for developing biocomposites with new functional properties.

The literature describes several strategies for developing biocomposites, including physical and chemical treatments [91,99,258,289–292]. Among them, esterification with fatty acids, from hexanoic (C6) to dodecanoic acids (C22), is a common treatment applied to decrease the surface hydrophilicity of cellulose fibers used in composite materials [113,120,121,271,293,294]. Le Moigne et al. [37] reported that in most studies, chemical surface functionalization of natural fibers enhanced the mechanical properties of biocomposites. Concerning pure cellulosic reinforcements, Pasquini et al. showed that their surface modification with octadecanoyl and dodecanoyl chloride in heterogeneous conditions led to improved interfacial adhesion with a polyethylene-based matrix, a higher filler dispersion level, and better water resistance [120]. However, mechanical performances of biocomposites were not improved due to the degradation of cellulose with the treatments. In a study by Freire et al. [121], where they focused on the impact of the degree of substitution (DS) and fatty chain length on the properties of acylated cellulose low-density polyethylene-based composites. The study showed that water resistance, interfacial adhesion, and mechanical properties were enhanced, especially for composites displaying low DS-modified cellulose. De Menezes et al. [271] detected an increased dispersion

state of esterified cellulose whiskers, and improved elongation at break with increasing lengths of the grafted chains.

With the objective of developing greener processes of cellulose surface modification, a gas-phase esterification with palmitoyl chloride was previously studied [295]. This process was adapted from work by Berlioz et al. and Fumagalli et al. [150,157], who in both cases used this reagent derived from one of the most common fatty acids of vegetable origin. The occurrence of the chemical modification of micrometric cellulose particles was evidenced by solid-phase  $^{13}\text{C}$  NMR, with DS values ranging between 0.01 and 0.14. It was shown, by contact angle measurements, that the treatment made cellulose particles drastically more hydrophobic, without altering their bulk properties, i.e., morphology, crystallinity, and thermal stability.

Mechanical and thermal properties of esterified cellulose-based biocomposites have been already investigated and presented in some literature reviews [37,99,296], however, very few studies are available on mass transfer properties in such biocomposites [297–301]. When mass transfers are evaluated, it is essentially at the macroscopic scale via permeability measurements. Little interested is focused on the evaluation of diffusion and sorption phenomena, which are absolutely necessary to correctly formalize the structure/mass properties relationships. Furthermore, to the best of our knowledge, transfer properties of both moisture and liquid water in esterified cellulose composites have not been yet investigated. Besides, research still needs to ascertain these materials by selecting appropriate polymer matrices. In order to benefit from the fully biosourced and biodegradable character of cellulose, increasing interest is being given to biopolymers that are biosourced and fully biodegradable in natural conditions, i.e., polyhydroxyalkanoates (PHAs). Among PHAs, poly(hydroxybutyrate-*co*-valerate) (PHBV) is a very promising polymer, because its easily processable and displays similar properties to common polyolefins [299,302–309].

In this context, the objective of the present study was to investigate the effects of gas-phase esterification of cellulose on the functional properties of PHBV/cellulose biocomposites. For that purpose, PHBV/cellulose biocomposites with different filler contents were prepared by melt extrusion using either virgin or gas-phase esterified cellulose. Changes in thermal stability, tensile properties, water vapor, and liquid water transfer properties of biocomposites were discussed in relation to some molecular structural parameters, including PHBV molecular weight and crystallinity, and to the microstructure of materials qualitatively assessed by SEM observations.

## II-2 Materials and Methods

### Materials

Cellulose, in powder form, was supplied by Arbocel J. Rettenmaier & Söhne (Rosenberg, Germany) under the reference Arbocel<sup>®</sup> (grade BE 600-10 TG). Cellulose particles were characterized by a true density of  $1.59\text{ g}\cdot\text{cm}^{-3}$ , a cellulose content of 99.5%, and a median

apparent diameter ( $d_{50}$ ) of 18  $\mu\text{m}$ . In a previous study dealing with exactly the same grade of cellulose [310], particles were assimilated to cylinders with the length and diameter corresponding to the major and the minor axis, respectively. These two shape descriptors were determined in volume, and the median values were respectively  $32 \pm 2 \mu\text{m}$  and  $19 \pm 1 \mu\text{m}$ .

PHBV was purchased from NaturePlast (Iffs, France) under the reference PHI 002. As reported by the manufacturer, PHBV contained 1–3 mol % of valerate and had a true density of  $1.24 \text{ g}\cdot\text{cm}^{-3}$ .

## Methods

### II-2.1 Grafting of Cellulose

Cellulose particles were subjected to a gas-phase esterification using palmitoyl chloride, as described by David et al. [295]. After a drying step at  $60 \text{ }^\circ\text{C}$  overnight, the reaction was conducted in a 2 L reactor, on a 100 g batch at  $100 \text{ }^\circ\text{C}$ , and 2 mbar during 15 h. The cellulose particles were inserted in nylon mesh bags, which were positioned on a Teflon grid above the liquid reagent. The reagent was used in excess compared to surface hydroxyl groups (0.2 eq compared to total anhydroglucose units). A nitrogen flow was used to evacuate the reaction by-products that were vacuum-pumped. The resulting grafted cellulose sample was purified using acetone and finally dried at  $60 \text{ }^\circ\text{C}$ . The grafted cellulose (noted C-grafted in the following article) was characterized by a degree of substitution (DS) of 0.02, as measured by  $^{13}\text{C}$  solid-state NMR spectroscopy [295]. The virgin cellulose, without treatment, was noted C-virgin. The covalent grafting of cellulose by esterification was evidenced by FT-IR analysis (ATR-FTIR, VERTEX 70v Bruker, Ettlingen, Germany), with the appearance of the ester carboxyl signal at  $1745 \text{ cm}^{-1}$  together with the intensity decrease of the hydroxyl parts ( $3000\text{--}3600 \text{ cm}^{-1}$ ) (Figure 56). FT-IR spectra were normalized with respect to the peak height at  $1030 \text{ cm}^{-1}$ , considered as an invariant for the cellulose backbone.

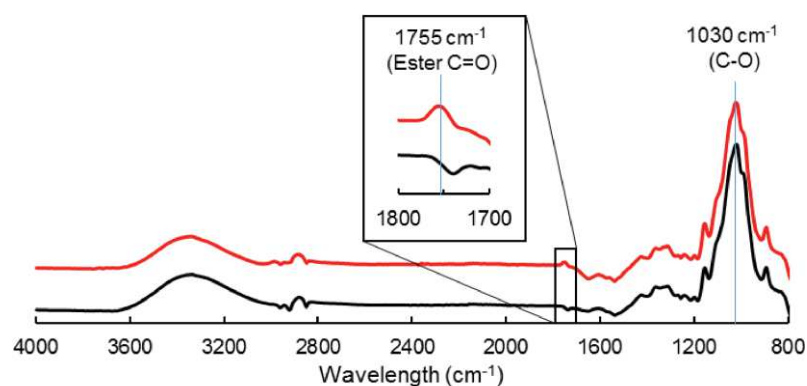


Figure 56. FT-IR spectra of C-virgin (—) and C-grafted (—).

## II-2.2 Preparation of Composite Materials

Composite films displaying an average thickness of 300  $\mu\text{m}$  were prepared using a lab-scale twin screw extruder, with a L/D ratio of 40 and a screw diameter of 16 mm (Eurolab, Thermo Scientific, Karlsruhe, Germany), equipped with a flat die of 300  $\mu\text{m}$  of thickness and a calendering unit. Raw PHBV pellets and cellulose particles (either virgin or esterified) were previously dried at 60  $^{\circ}\text{C}$  overnight before extrusion. Cellulose and PHBV pellets were introduced with a loss-in-weight twin screw feeder (Brabender, Duisburg, Germany) and a volumetric single screw feeder (Brabender), respectively. The temperature profile from the feeding to the die varied from 80  $^{\circ}\text{C}$  to 180  $^{\circ}\text{C}$  (80–160–160–160–160–170–170–180–180–160  $^{\circ}\text{C}$ ). The screw speed was set to 300 rpm and the total flow rate was 1.0  $\text{kg}\cdot\text{h}^{-1}$ . The average residence time was 4.0 min. Three filler contents were produced, i.e., 10, 20, and 33 wt %, respectively named PHBV-10VC, PHBV-20VC and PHBV-33VC, for composite with virgin cellulose as filler or PHBV-10GC, PHBV-20GC and PHBV-33GC for composite containing grafted cellulose.

## II-2.3 Characterization of Films

For each sample, film thickness was systematically measured using a precision gauge (Hanatek-model FT3, East Sussex, UK) on at least five different positions. Thickness mean values were considered for all following calculations (mechanical properties, water vapor sorption kinetics, water vapor permeability, and liquid water uptake). Samples were stored in a hermetic drum at 23  $^{\circ}\text{C}$  in presence of silica gel (around 0% RH) before further analysis.

A gel permeation chromatograph GPC PL-50 Plus system equipped with two columns of 300 mm PL-gel 5  $\mu\text{m}$  mixed-C (200–2,000,000  $\text{g}\cdot\text{mol}^{-1}$ ) (Polymer Laboratories, Church Stretton, UK), and a refractive index detector was used to measure the molecular weight of PHBV. The eluent was chloroform, the flow was set at 1.0  $\text{mL}\cdot\text{min}^{-1}$  and the volume of injection was 20  $\mu\text{L}$ . PHBV samples (10 mg) were previously dissolved in 2 mL of chloroform in a closed tube under stirring at 50  $^{\circ}\text{C}$ . Samples were filtered on Macherey–Nagel Chromafil Xtra syringe filter (PTFE-45/25, Düren, Germany) with 0.45  $\mu\text{m}$  pore size. The GPC equipment was calibrated with polystyrene standards. To measure the broadness of the molecular weight distribution of the matrix, the polydispersity index ( $I_p$ ) was calculated as follows (Eq. 28):

$$I_p = \frac{M_w}{M_n} \quad \text{Eq. 28}$$

Differential scanning calorimetry (DSC) analysis was carried out using a thermo-modulated calorimeter (Q200 modulated DSC, TA Instruments, New Castle, DE, USA). Aluminium pans (Tzero Aluminium Hermetic pan, TA Instruments New Castle, DE, USA) were filled with approximately 10 mg of sample and hermetically sealed. Analyses were performed in triplicate. The purge gas was nitrogen, with a flow rate of 50  $\text{mL}\cdot\text{min}^{-1}$ . Each sample was first heated up to 200  $^{\circ}\text{C}$  at 10  $^{\circ}\text{C}\cdot\text{min}^{-1}$ , then cooled at 10  $^{\circ}\text{C}\cdot\text{min}^{-1}$  until temperatures reached  $-30$   $^{\circ}\text{C}$ , and

finally heated again from  $-30\text{ }^{\circ}\text{C}$  to  $200\text{ }^{\circ}\text{C}$  at a heating rate of  $10\text{ }^{\circ}\text{C}\cdot\text{min}^{-1}$ . The resultant thermogram displayed the variation of heat flow per gram of sample ( $\text{W}\cdot\text{g}^{-1}$ ) towards temperature ( $^{\circ}\text{C}$ ). From this thermogram, crystallization temperature ( $T_c$ ) and melting temperature ( $T_m$ ) were measured respectively from peaks of the cooling ramp and second heating ramp, respectively. Melting enthalpy ( $\Delta H_m$ ) was calculated from the area under the peak observed on the 1st and 2nd heating ramps.  $\Delta H_m^0 = 146\text{ J}\cdot\text{g}^{-1}$  was taken for 100% crystalline PHBV matrix from [252], and  $w$  is the weight fraction of the matrix in the composite calculated from TGA analysis. Crystallinity of the materials was calculated as follow (Eq. 29):

$$X_c = \left( \frac{\Delta H_m}{\Delta H_m^0} \right) \times \left( \frac{100}{w} \right) \quad \text{Eq. 29}$$

Thermogravimetric analysis (TGA) under nitrogen flow ( $50\text{ mL}\cdot\text{min}^{-1}$ ) was carried out using a Mettler TGA2 apparatus (Schwerzebbach, Switzerland) equipped with a XP5U balance (precision of  $0.0001\text{ mg}$ ). For each measurement, about  $40\text{ mg}$  of materials were used, and the heating rate was  $10\text{ }^{\circ}\text{C}\cdot\text{min}^{-1}$  from  $25\text{ }^{\circ}\text{C}$  to  $800\text{ }^{\circ}\text{C}$ . The maximum degradation temperature ( $T_{\text{deg}}$ ) corresponded to the temperature at which the degradation rate was maximum. The onset and offset degradation temperatures ( $T_{\text{onset}}$  and  $T_{\text{offset}}$ , respectively) were measured respectively when the first derivative of the weight loss became higher than  $0.1\text{ }\%\cdot^{\circ}\text{C}^{-1}$  and lower than  $0.1\text{ }\%\cdot^{\circ}\text{C}^{-1}$ . Analyses were done in triplicate. The weight filler content of the composite was determined from inflection point between  $280\text{ }^{\circ}\text{C}$  and  $300\text{ }^{\circ}\text{C}$  corresponding to the end of PHBV degradation and beginning of cellulose degradation. To correct the overlapping thermal degradation, standard curves for virgin and grafted cellulose in PHBV were used ( $R^2 = 0.999$ ). The volume filler content was deduced from the weight filler content based on knowledge of the true density of both biocomposite constituents.

Scanning electron microscopy (SEM) observations were performed with a S-4800 microscope (Hitachi, Japan) after coating the sample with Pt by cathode pulverization. In case of cryo-fractured section observations, the specimens were frozen in liquid nitrogen then fractured before coating.

Tensile tests. Mechanical properties were evaluated through tensile tests conducted at room temperature by a texture analyzer (Zwick BZ5/TN1S, Metz, France) on dog-bone shaped film specimens (width of  $4\text{ mm}$  and gauge length of  $45\text{ mm}$ ). The specimens were previously stored in a closed chamber at  $23\text{ }^{\circ}\text{C}$  and  $50\%\text{ RH}$ . Stress–strain curves obtained with a cross-head speed of  $1\text{ mm}\cdot\text{min}^{-1}$  helped determine Young’s modulus ( $E$ ), nominal stress at break ( $\sigma$ ), and nominal strain at break ( $\epsilon$ ). The energy at break was calculated from the total area under the stress–strain curve. Ten replicates were realized for each formulation ( $10\text{ wt } \%$ ,  $20\text{ wt } \%$ , and  $33\text{ wt } \%$ ).

Water vapor sorption kinetics were measured at  $20\text{ }^{\circ}\text{C}$  using a controlled atmosphere microbalance (DVS, Surface Measurement System Ltd., London, UK). The mass evolution of the material was recorded using a Cahn D-200 microbalance with a precision of  $0.1\text{ }\mu\text{g}$ . The relative humidity was also followed over time. A pre-drying step was first run at  $60\text{ }^{\circ}\text{C}$  in an oven, then



the sample was dried over P<sub>2</sub>O<sub>5</sub> in a desiccator, and finally placed in the DVS equipment at 0% RH for 5 h at 20 °C. In the case of cellulose, 1 mg of cellulose was deposited in an aluminum pan (DSC Tzero® pans provided by TA Instruments), which was placed in the DVS nacelle, as previously described by Thoury et al. [311]. In the case of biocomposite films, circular pieces of a 7.5 mm diameter were cut and deposited directly in the DVS nacelle. Increasing relative humidity steps (0, 20, 40, 60, 80, and 95%) were performed for the same sample, and each step time was adjusted to insure equilibrium. Water vapor sorption isotherms were determined from the equilibrium moisture contents at each RH step. Tests were performed at least in duplicate.

Water vapor permeability (WVP) were gravimetrically determined at 23 °C using an adapted ASTM E96/E96M procedure. Discs of films (five repetitions) were sealed in permeation cells filled with distilled water that were put into a desiccator containing silica gel. A relative humidity (RH) gradient equal to 0–100% was obtained (i.e.,  $\Delta P = 2809$  Pa at 23 °C, assuming that RH on the silica gel is negligible). The permeation area was 9.08 cm<sup>2</sup>. Periodic weightings determined the rate of water vapor movement through the films. WVP (mol·s<sup>-1</sup>·Pa<sup>-1</sup>·m<sup>-1</sup>) values were calculated from Equation (3), where  $S$  is the slope of the weight change from the straight line (g·h<sup>-1</sup>),  $A$  is the permeation area (m<sup>2</sup>),  $t$  is the average specimen thickness (m),  $P_{\text{sat}}$  is the saturation vapor pressure at 23 °C (Pa), and  $M_{\text{H}_2\text{O}}$  is the molar mass of water (g·mol<sup>-1</sup>).

$$\text{WVP} = \frac{S \times t}{3600 \times A \times P_{\text{sat}} \times M_{\text{H}_2\text{O}}} \quad \text{Eq. 30}$$

Liquid water uptake kinetics were measured on discs of 25 mm diameter cut from composite films. After drying overnight at 60 °C, the specimens were weighted using a balance with  $\pm 0.001$  mg precision and then immersed into distilled water at 20 °C. At various time intervals, the samples were removed, blotted to remove free water on their surface, and immediately weighed using an analytical balance. Experiments were performed in triplicate until reaching the water uptake equilibrium for each sample.

### II-2.3.1 Modeling

Diffusion in an infinite plane sheet was used to describe water vapor diffusion of fillers, matrix, and composite. It was assumed that the diffusion in the material was isotropic and independent of time and space. In addition, the possible swelling of the sample with increasing relative humidity was considered negligible. The apparent diffusion coefficient was estimated using the analytical solutions provided by Crank [254]. Considering an isotropic diffusion, the diffusion can be reduced to a pure axial diffusion that occurs in an infinite plane sheet of thickness  $L$  (m). The diffusion equation at time  $t$ , at position  $z$ , and for film of thickness  $L$  is given in Eq. 31, where  $D$  (m<sup>2</sup>·s<sup>-1</sup>) corresponds to the water's apparent diffusivity in the material.

$$\frac{\partial C}{\partial t}(t, z) = D \left( \frac{\partial^2 C(t, z)}{\partial z^2} \right) \quad \text{Eq. 31}$$

In case of water vapor sorption (deposition of the sample in a DVS pan), the plane sheet was insulated at its bottom, and defined by  $z \in [0, L]$ , with initial and boundary conditions given in Eq. 32.

$$\begin{aligned} C(t = 0, z) &= C_0 \quad \forall z \in [0, L] \\ \frac{\partial C}{\partial z}(t, z = 0) &= 0 \quad \forall t \geq 0 \\ C(t, z = L) &= C_\infty \quad \forall t \geq 0 \end{aligned} \quad \text{Eq. 32}$$

In case of liquid water sorption (immersion of the samples in water), it was considered that the plane sheet was not insulated and that it was defined by  $z \in \left[-\frac{L}{2}, \frac{L}{2}\right]$ . Eq. 31 was kept by considering boundary conditions given in Eq. 33.

$$\begin{aligned} C(t = 0, z) &= C_0 \quad \forall z \in \left[-\frac{L}{2}, \frac{L}{2}\right] \\ \frac{\partial C}{\partial z}(t, z = 0) &= 0; \quad \forall t \geq 0 \\ C\left(t, z = \pm \frac{L}{2}\right) &= C_\infty; \quad \forall t \geq 0 \end{aligned} \quad \text{Eq. 33}$$

The analytical solution for an infinite plane sheet of thickness  $L$  (m) in both cases was described by Eq. 34 [254]:

$$\frac{M_t}{M_\infty} = 1 - \sum_{n=0}^{\infty} \frac{8}{(2n+1)^2 \pi^2} \exp\left(\frac{-D(2n+1)^2 \pi^2 t}{4L^2}\right) \quad \text{Eq. 34}$$

where  $M_t$  and  $M_\infty$  denote, respectively, the water mass uptake at time  $t$  and the corresponding value for infinite time.

Water's apparent diffusivity  $D$  was determined using the `lsqnonlin` function that solved the corresponding nonlinear least squared problem in MATLAB<sup>®</sup> R2015b software. The idea was to minimize the root mean square error (RMSE) between experimental sorption kinetics and simulated ones, as shown in Eq. 34.  $N$  is the number of experimental data points from DVS,  $m_{\text{sim}}(t)$  and  $m_{\text{exp}}(t)$  are, respectively, the estimate and the experimental mass uptake at time  $t$ . Simulations were performed by using Eq. 35.

$$\text{RMSE} = \sqrt{\frac{\sum_{i=1}^N (m_{\text{sim}}(t_i) - m_{\text{exp}}(t_i))^2}{N}} \quad \text{Eq. 35}$$

## II-3 Results and Discussion

### II-3.1 Impact of Gas-Phase Esterification on Some Macromolecular Parameters of PHBV

Functional properties of biocomposites, e.g., mechanical and mass transfer properties, are known to be strongly dependent on the polymer's macromolecular parameters, including mainly molecular weight and crystallinity, that influence properties of cellulose grafting on PHBV.

#### II-3.1.1 Molecular Weight

Table 1 shows PHBV's molecular weight after processing by melt extrusion. The introduction of cellulose fillers resulted in a very slight decrease in the polymer's molecular weight, without a significant effect of grafting or filler content. It could be concluded that the thermal degradation of polymer chains was not promoted by the presence of cellulosic particles, either virgin or grafted, as already described for plasticized PHBV [312] or lignocellulosic-based biocomposites [190]. In any case, the molecular chains of PHBV are still considered as long chains because they are larger than 150 kDa [16].

#### II-3.1.2 Differential Scanning Calorimetry

A heat-cool-heat cycle was performed using differential scanning calorimetry (DSC) in order to investigate the crystallization behavior of "as produced" composites, as well as the intrinsic crystallization behavior after having erased the thermal history of materials. Virgin PHBV (extruded under the same conditions as biocomposites) presented a crystallinity degree ( $X_c$ ) of  $73 \pm 1\%$  (measured during the second heating ramp). As previously reported [190], this high crystallinity was ascribed to the addition of boron nitride as a nucleating agent (1 wt%) in the commercial formulation (Table 25). This value was in agreement with results reported in previous studies using the same grade of PHBV [30]. It is worth noting that lower crystallinity values were found in the work of Berthet et al. [16,190], probably due to the differences in processing conditions and lower molecular weight. The addition of cellulosic fillers, either virgin or grafted, decreased the crystallinity degree to  $66 \pm 1\%$  for all samples, except for PHBV-20VC for which the crystallinity remained constant. This decrease could be attributable to a hindered motion of the polymer segments due to the presence of fillers. Fillers could interact with the matrix or act as local defects, inhibiting the growth of PHBV crystals. The fact that the crystallinity of PHBV-20VC remained constant would indicate that the mobility of polymer chains was not affected. In the present study, the little effect of filler on crystallinity could be explained by the presence of boron nitride that masked the potential nucleating effects of cellulose [308].

Regarding the melting temperature, it was not significantly impacted by the addition of either virgin or esterified cellulose [120,121], even for high filler contents, which could be due to the unchanged polymer molecular weight. However, the crystallization temperature significantly decreased with the addition of esterified cellulose, while it remained unchanged in the case of

virgin cellulose. This highlighted that the presence of fatty acids on the surface of cellulose, which inhibited the initiation of the crystallization growth of the surrounding matrix.

Table 25. Molecular weight ( $M_w$ ) with polydispersity index ( $I_p$ ), thermal properties (melting temperature ( $T_m$ ) and crystallization temperature ( $T_c$ )), and degree of crystallinity ( $X_c$ ) of PHBV-based composites.

Materials	$M_w$ <sup>1</sup> (kDa)	$I_p$	$T_m$ <sup>2</sup> (°C)	$T_m$ <sup>3</sup> (°C)	$T_c$ (°C)	$X_c$ <sup>2</sup> (%)	$X_c$ <sup>3</sup> (%)
PHBV	241	3.2	177 ± 1	172 ± 1	124 ± 1	63 ± 1	73 ± 1
PHBV-20VC	245	2.7	173 ± 1	171 ± 1	124 ± 1	64 ± 1	74 ± 1
PHBV-20GC	231	3.2	171 ± 3	169 ± 1	111 ± 1	59 ± 1	66 ± 1
PHBV-33VC	230	3.6	170 ± 1	169 ± 1	120 ± 1	62 ± 9	67 ± 1
PHBV-33GC	230	3.2	172 ± 4	171 ± 1	108 ± 1	69 ± 2	66 ± 1

<sup>1</sup> The uncertainty was estimated at 5 kDa. <sup>2</sup> Measured at the first heating scan. <sup>3</sup> Measured at the second heating scan.

### II-3.1.3 Thermal Stability

The thermal stability of the composites and their separated constituents was examined by thermogravimetric analysis (TGA) under inert atmosphere (Figure 57). Neat PHBV was characterized by one main sharp thermal degradation occurring between 260 °C and 310 °C, due to the chain scission reaction mechanism. The temperature at the maximal rate of degradation ( $T_{deg}$ ) was 297 °C (Table 26). The degradation of virgin cellulose and esterified cellulose occurred on a larger temperature range than that of PHBV, with  $T_{deg}$  of respectively 343 °C and 336 °C. The temperature range was even more important for esterified cellulose, with  $T_{onset}$  and  $T_{offset}$  values of 247 °C and 398 °C, respectively, against 259 °C and 375 °C for virgin cellulose. As already showed by David et al. [295], the earlier thermal degradation of grafted cellulose could be ascribed to the high lability of ester bonds. It is worth noting that a second degradation peak of low intensity was observed on the first derivative curve (DTG) for grafted cellulose (around 375 °C), which was related to the palmitoyl moiety David et al. [295]. The weight loss around 100 °C, which was observed for both C-virgin and C-grafted, was due to the water loss contained in the samples.

TGA curves of composite materials showed two degradation steps, the first one corresponding to the degradation of the PHBV matrix, and the second one to the filler degradation, with a small overlap. The introduction of cellulose fillers resulted in a slight decrease in the thermal stability of PHBV, which was attributed to the interactions between cellulose and PHBV, as already reported in Reference [308]. The thermal degradation of cellulose produced small polar molecules that likely facilitated breaking of PHBV chains. This negative effect was even more important by increasing the content of virgin cellulose, while the filler content had no impact in the case of esterified cellulose. Indeed,  $T_{deg}$  decreased from 296.8 °C for the neat PHBV down to 294.4 °C for PHBV-33GC, and 287.1 °C for PHBV-33CV. The second degradation corresponding to cellulose decomposition was much less steep for composites filled with esterified cellulose than with virgin cellulose. It was shown that this effect could not be explained only by a simple rule of mixing the respective effects of each constituent, meaning that the degradation of grafted cellulose was slowed while embedded in the PHBV matrix. It was thus assumed that the interactions at the filler/matrix interface could also play a role

[121]. Regarding temperatures at the maximal rate of degradation, differences between materials filled with virgin cellulose or grafted cellulose were only significant for a filler content of 10 wt %. Nevertheless, it is worth noting that  $T_{deg(2)}$  of composites filled with grafted cellulose were not any lower than  $T_{deg(2)}$  of composites filled with virgin cellulose. This phenomenon could be explained by the fact that stronger filler/matrix interactions occurred in the case of composites filled with grafted cellulose, thereby hindering the thermal degradation of the filler. This has been previously observed by Freire et al. [121].

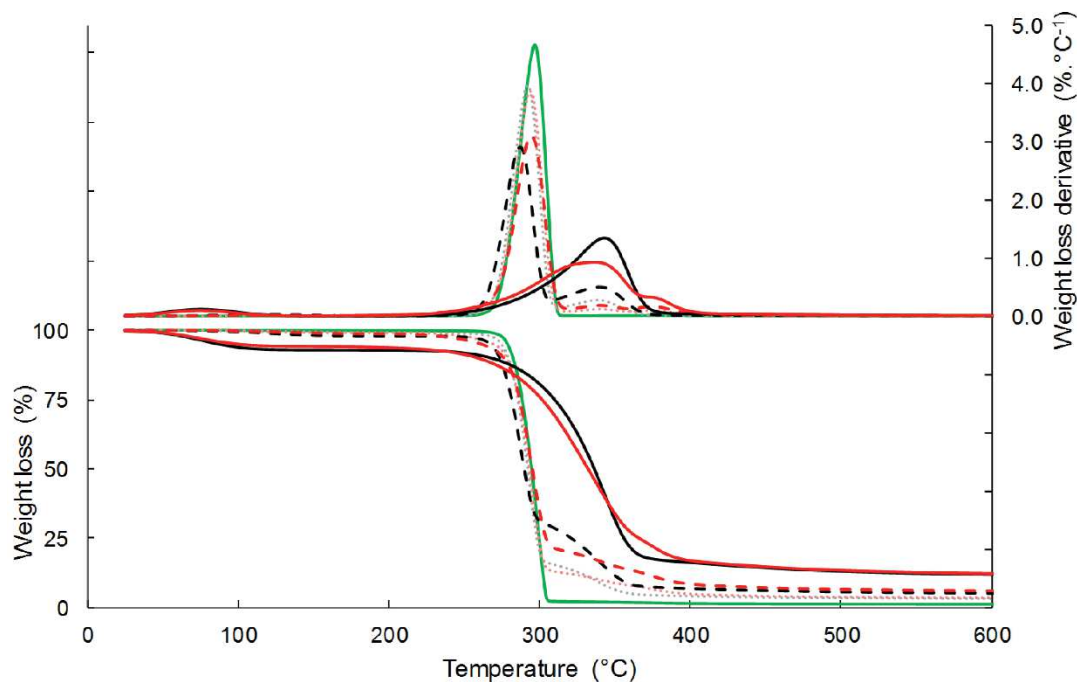


Figure 57. TG and DTG curves of C-virgin (—), C-grafted (—), PHBV (—), PHBV-20CV (···), PHBV-20CG (···), PHBV-33CV (---), and PHBV-33CG (---) under  $N_2$ .

Table 26. Thermal degradation temperature of PHBV-based composites.

Materials	$T_{deg(1)}$ (°C)	$T_{deg(2)}$ (°C)	$T_{onset}$ (°C)	$T_{offset}$ (°C)
PHBV	$297 \pm 1$	-	$267 \pm 1$	$312 \pm 1$
C-virgin	-	$343 \pm 1$	$259 \pm 1$	$375 \pm 0$
C-grafted	-	$336 \pm 1$	$247 \pm 1$	$398 \pm 0$
PHBV-10CV	$295 \pm 5$	$335 \pm 1$	$248 \pm 4$	$380 \pm 4$
PHBV-10CG	$298 \pm 1$	$339 \pm 1$	$237 \pm 1$	$413 \pm 2$
PHBV-20CV	$292 \pm 1$	$336 \pm 4$	$264 \pm 2$	$357 \pm 4$
PHBV-20CG	$294 \pm 1$	$340 \pm 1$	$254 \pm 1$	$377 \pm 0$
PHBV-33CV	$287 \pm 1$	$339 \pm 1$	$256 \pm 1$	$365 \pm 1$
PHBV-33CG	$294 \pm 1$	$339 \pm 2$	$248 \pm 1$	$389 \pm 0$

$T_{deg(1)}$ : Temperature of maximal degradation of the PHBV (matrix).

$T_{deg(2)}$ : Temperature of maximal degradation of the cellulose (filler).

### II-3.2 Impact of Gas-Phase Esterification on Interfacial Adhesion: Qualitative Evaluation

The impact of gas-phase esterification on the filler/matrix interfacial adhesion was qualitatively assessed by SEM observations of cryo-fractured cross-sections (Figure 58). Neat PHBV displayed a smooth surface with the inclusion of boron nitride used as a nucleating agent (Figure 58A). In the case of virgin cellulose, the distinction between cellulose particles and the matrix was obvious, with clear gaps at the filler/matrix interface (Figure 58B). In the case of composites filled with grafted cellulose, fillers were intimately embedded in the matrix, with particles perfectly coated by the polymer (Figure 58C). Such an improved wetting of fillers by the surrounding PHBV matrix would be ascribed to the increased hydrophobicity of grafted cellulose, as previously demonstrated by contact angle measurements in previous work by David et al. [295]. Contrary to Pasquini et al. [120] who obtained similar results for LDPE filled with esterified cellulose, an improvement of the filler's dispersion state was not significantly observed in the present study.

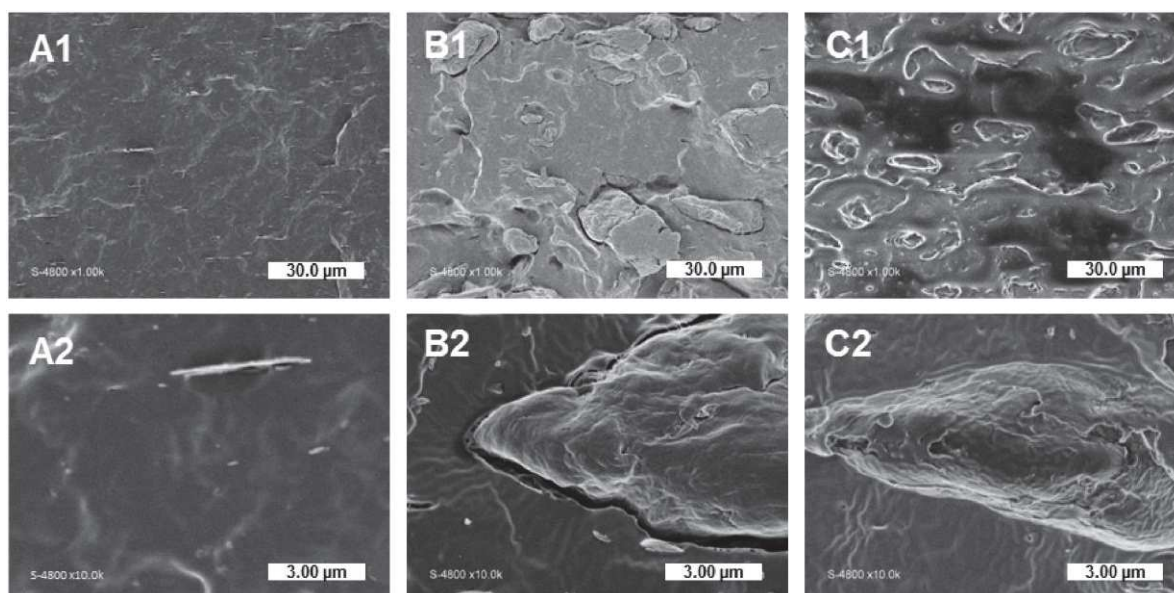


Figure 58. SEM pictures of cryo-fractured sections: (A1,A2) neat PHBV, (B1,B2) PHBV-20VC, and (C1,C2) PHBV-20CG.

### II-3.3 Impact on Water Transfer Properties in Resulting Composites

Moisture and liquid water transfer properties of biocomposites are important aspects that must be assessed, because they govern many other functional properties of usage conditions, including material stability. They are particularly important when materials are used for packaging applications since they ensure the preservation of packed goods that are sensitive to hydration or dehydration.

## II-3.3.1 Water Vapor Sorption Kinetics

Water vapor sorption kinetics at successive relative humidity (RH) steps allowed the assessment of moisture sorption isotherms and estimating moisture's apparent diffusivity. Water vapor sorption isotherms of cellulose samples, neat PHBV, and biocomposite films are shown in Figure 59. Cellulose absorbed much more water vapor than PHBV, with moisture uptake at the equilibrium at 95% of RH of  $0.5 \pm 0.0 \text{ g}\cdot\text{g}^{-1} \text{ d.b.}$ ,  $22.7 \pm 0.0 \text{ g}\cdot\text{g}^{-1} \text{ d.b.}$ , and  $19.0 \pm 0.2 \text{ g}\cdot\text{g}^{-1} \text{ d.b.}$  for PHBV, virgin cellulose, and esterified cellulose, respectively. This corroborated the high hydrophobic character of PHBV compared to cellulose samples, even esterified. In the case of cellulose samples, a classical sigmoidal shape was observed for water vapor isotherms. The region until 20% of RH was ascribed to the absorption of a monolayer of water onto specific sites of the material's surface, with no difference in sorption behavior between the two samples of cellulose. Then, a linear portion between 20% and 60% RH corresponded to the dissolution of water vapor in the materials due to the porous structure of cellulose and to the stacking of water layers. Finally, for high relative humidity the water vapor uptake increased abruptly due to the formation of water cluster and capillarity [282]. As previously reported, esterification hindered water sorption behavior on the two last zones, due to the modification of pore volume of cellulose particles [295].

The addition of cellulose particles in PHBV led to a significant increase in water vapor sorption, with water vapor uptake at 95% of RH of  $6.6 \pm 0.0 \text{ g}\cdot\text{g}^{-1} \text{ d.b.}$  and  $6.1 \pm 0.0 \text{ g}\cdot\text{g}^{-1} \text{ d.b.}$  for PHBV-33VC and PHBV-33GC, respectively.

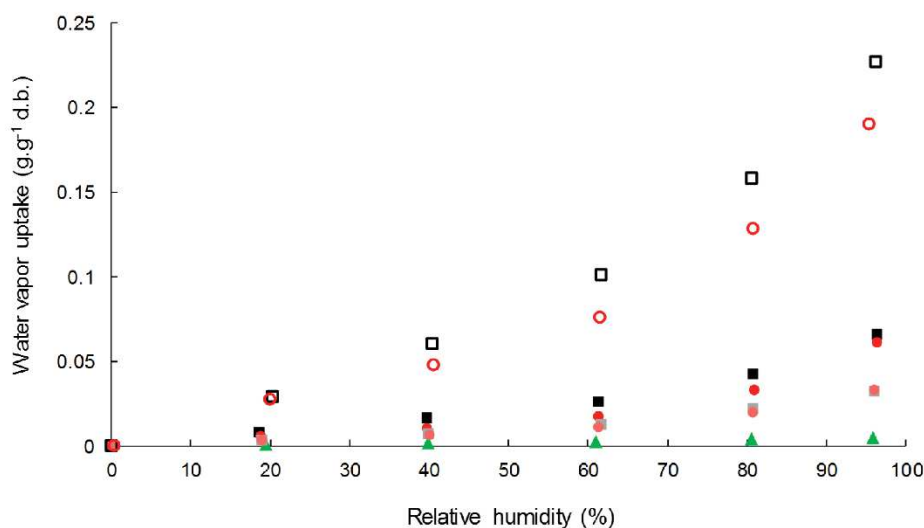


Figure 59. Water vapor sorption isotherm of C-virgin (□), C-grafted (○), PHBV (▲), PHBV-20VC (■), PHBV-20GC (●), PHBV-33VC (■) and PHBV-33GC (●).

In order to understand the contribution of each constituent in the composites, experimental data were compared to values predicted using a simple rule of mixture by considering weight fractions ( $w$ ) and the water vapor content ( $M$ ) of each constituent at each RH (Eq. 36).

$$M_{\text{composite}} = M_{\text{filler}} \times w_{\text{filler}} + M_{\text{matrix}} \times w_{\text{matrix}} \quad \text{Eq. 36}$$

It was shown that the rule of mixture over-estimated the water sorption in the biocomposites for the two types of fillers, especially for high RH (Figure 60). It can be concluded that water vapor sorption of composites was not a simple addition of the contribution of cellulose and PHBV, as already shown by Wolf et al. [301] in PHBV/wheat straw fiber composites. It is worth noting that the slight decrease of crystallinity would have been in favor of a higher water vapor uptake. Furthermore, since no significant changes in PHBV's molecular weight was evidenced by GPC, such results could be explained by structural changes of the polymer matrix not evidenced in the present paper, e.g., the formation of rigid amorphous regions within the PHBV matrix [313], or by hindered water vapor sorption of cellulose due to the surrounding matrix.

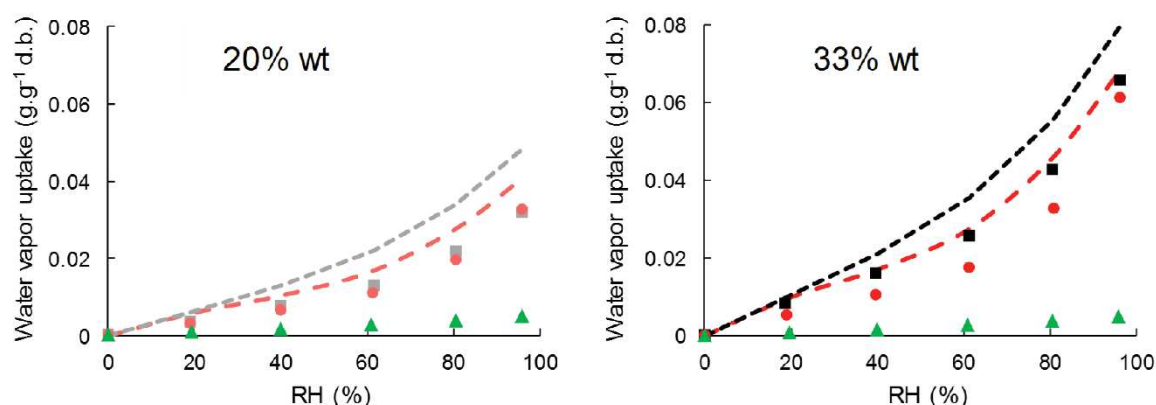


Figure 60. Simulated sorption isotherms from Equation (9) for PHBV-based composites: PHBV ( $\blacktriangle$ ), PHBV-20VC (- -), PHBV-20GC (- -), PHBV-33VC (- -), PHBV-33GC (- -).

Apparent diffusivity values were identified at each RH step by fitting a mathematical model to the experimental data from water vapor sorption kinetics (Figure 61). Apparent diffusivity of water vapor was lower in composites than in the neat matrix, even though the two types of cellulose displayed higher diffusivity values. The diffusivity slightly decreased with the filler content. This unexpected behavior was also reported by Wolf et al. [301] for PHBV/wheat straw biocomposites. This could be ascribed to a tortuosity effect that would be emphasized by the formation of a barrier interphase.



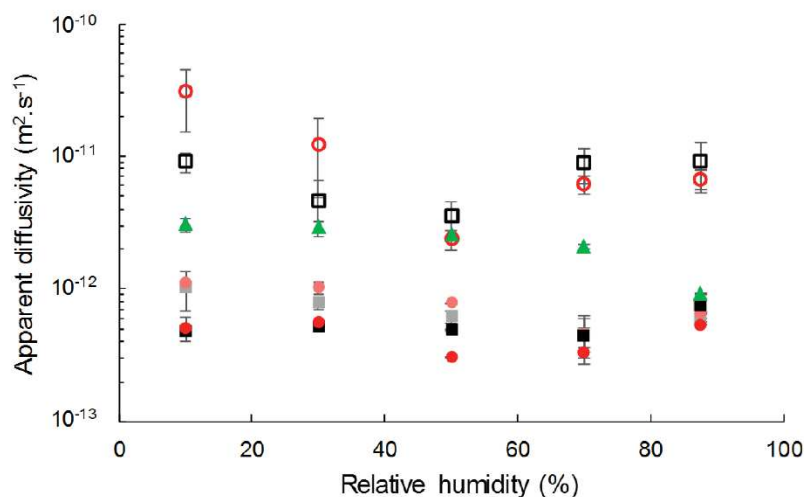


Figure 61. Apparent diffusivity of C-virgin ( $\square$ ), C-grafted ( $\circ$ ), PHBV ( $\blacktriangle$ ), PHBV-20VC ( $\blacksquare$ ), PHBV-20GC ( $\bullet$ ), PHBV-33VC ( $\blacksquare$ ) and PHBV-33GC ( $\bullet$ ).

Grafting did not affect the water vapor diffusivity in the composite, but had an impact on the diffusivity of the insulated cellulose. For relative humidity lower than 50% of RH, the diffusion coefficient of water in grafted cellulose was higher than in virgin cellulose. It could not be explained by a difference in crystallinity since it has been shown in a previous paper that it was not affected [295]. For RH higher than 50%, the diffusivity of water vapor in grafted cellulose became lower than in virgin cellulose, probably due to a water clustering effect emphasized by the hydrophobic character of esterified cellulose, as already observed in hydrophobic polymers [314]. A recrystallization phenomenon of the cellulose hindered by the grafting could also be possible.

It is worth noting that for a given filler content, moisture's apparent diffusivity values were the same for composites filled with grafted or virgin cellulose. The difference in behavior between grafted and virgin cellulose was annihilated when they were incorporated in PHBV.

### II-3.3.2 Water Vapor Permeability (WVP)

Water vapor permeability (WVP) of the PHBV matrix was found to be  $3.7 \pm 1.0 \times 10^{-13} \text{ mol}\cdot\text{m}^{-1}\cdot\text{s}^{-1}\cdot\text{Pa}^{-1}$ , which was slightly lower than other values mentioned in the literature [190,315]. This difference could be explained by a small change in valerate content. The incorporation of cellulose, either virgin or grafted, increased WVP up to  $36 \pm 3.2 \times 10^{-13} \text{ mol}\cdot\text{m}^{-1}\cdot\text{s}^{-1}\cdot\text{Pa}^{-1}$  for PHBV-33VC (Table 27). Knowing that the permeability coefficient combines the effects of diffusion and solubility according to the relation  $P = D \times S$ , the increase in WVP could be ascribed to an increase in diffusion (kinetic parameter) and/or solubility (thermodynamic parameter), with the possibility of competitive effects. In the present study, we can conclude that WVP of cellulose-based biocomposites was governed by a solubility phenomenon since the effect of the previously demonstrated decreased diffusion was drastically compensated by the increased solubility.

The increase in WVP was limited by esterification for high filler contents. For a filler content of 33 wt %, esterification reduced WVP by more than a factor of two compared to virgin cellulose. This could be ascribed to the slight decrease in the diffusion parameter, induced by a possible better dispersion state of fillers and filler/matrix adhesion, but more likely to the decreased solubility.

Water vapor permeability (WVP) is a key feature for food packaging. Obtaining a range of WVP values is very interesting since it could fulfill the requirements of different kinds of food products. As an example, composites with high filler contents could be used for packaging respiring products.

Table 27. Water vapor permeability (WVP), water vapor and liquid water diffusivity, and equilibrium uptake in PHBV-based biocomposites.

Materials	Water vapor					Liquid water	
	WVP ( $\times 10^{13}$ mol·m/(m <sup>2</sup> ·s·Pa)	Apparent diffusivity at 50% of RH ( $\times 10^{-13}$ ·m <sup>2</sup> · s <sup>-1</sup> )	Equilibriu m uptake at 50% RH (%)	Apparent diffusivity at 95% of RH ( $\times 10^{-13}$ ·m <sup>2</sup> · s <sup>-1</sup> )	Equilibriu m uptake at 95% RH (%)	Apparent diffusivity ( $\times 10^{-13}$ ·m <sup>2</sup> · s <sup>-1</sup> )	Equilibriu m uptake (%)
C-virgin	-	42 ± 16	8.1 ± 0.0	70.2 ± 10.1	22.7 ± 0.0	-	-
C-grafted	-	63 ± 36	6.2 ± 0.0	115 ± 62	19.0 ± 0.2	-	-
PHBV	3.7 ± 1.0	25.9 ± 6.2	0.2 ± 0.0	23.3 ± 8.7	0.5 ± 0.0	4.1 ± 0.2	0.6 ± 0.0
PHBV-20VC	5.6 ± 1.0	6.1 ± 0.6	1.0 ± 0.1	6.9 ± 2.2	3.2 ± 0.1	1.7 ± 0.1	3.7 ± 0.1
PHBV-20GC	5.0 ± 0.8	7.8 ± 0.0	0.9 ± 0.0	8.0 ± 2.7	3.3 ± 0.0	1.2 ± 0.0	3.8 ± 0.1
PHBV-33VC	36 ± 3.2	4.9 ± 0.1	2.1 ± 0.1	5.3 ± 1.2	6.6 ± 0.0	8.7 ± 0.6	6.3 ± 0.1
PHBV-33GC	15 ± 2.0	3.0 ± 0.0	1.4 ± 0.1	4.5 ± 1.2	6.1 ± 0.0	1.9 ± 0.1	5.5 ± 0.1

### II-3.3.3 Liquid Water Absorption

Liquid water absorption was assessed as a function of time for the different composites (Figure 62). Water was absorbed by all the composites during the experiments following a two-step pattern, with significant differences in both the initial diffusion rate and water uptake at equilibrium. A fast water uptake step preceded an equilibrium plateau suggesting a Fickian behavior.

PHBV, due to its hydrophobic nature, showed low liquid water uptake with a value at equilibrium of 0.58 g·g<sup>-1</sup> d.b. The introduction of cellulose fillers led to an increase in water uptake, which was proportional to the filler content, as already described for cellulose in LDPE or PLA [121,316]. As observed for WVP, the effect of gas-phase esterification was only significant for high filler content (33 wt %). It is worth noting that liquid water uptakes at equilibrium were similar to those of moisture at 95% of RH (Table 27).

The time to reach the equilibrium was around 50 h for all materials, this duration being related to the thickness of the films (around 300 µm in the present study). However, a slight but significant decrease in apparent diffusivity was noticed in the case of biocomposites, which was in agreement with the results obtained for moisture (Table 27). This could be ascribed to an

increased diffusion pathway induced by the introduction of filler. For a virgin cellulose content of 33 wt %, this tortuosity phenomenon competed with the formation of cellulose aggregates and poor interfacial adhesion that would be in favor of water diffusion. Logically, esterification induced a reduction of apparent diffusivity.

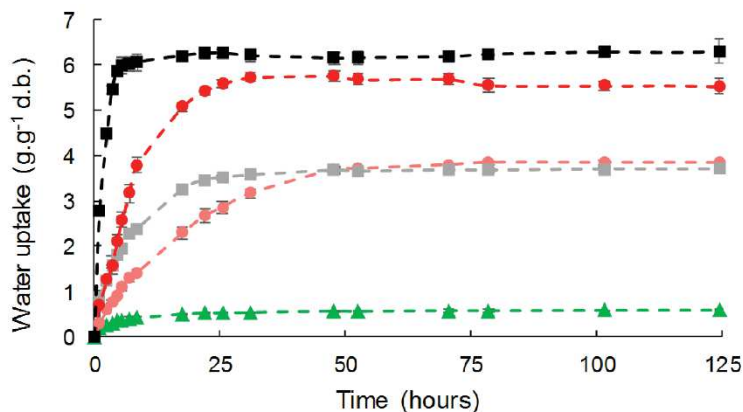


Figure 62. Water liquid sorption kinetics for PHBV-based composites: PHBV (▲), PHBV-20VC (■), PHBV-20GC (●), PHBV-33VC (■), PHBV-33GC (●). Points were linked for more visibility.

### II-3.4 Impact on Gas-Phase Esterification on Mechanical Properties of the Resulting Composites

PHBV-based composites displayed the common behavior of a rigid and fragile thermoplastic, as previously observed in similar studies [30,190] (Figure 63). The neat PHBV matrix was characterized by a Young's modulus of  $2.9 \pm 0.1$  GPa, a stress at break of  $39.7 \pm 0.1$  MPa, and strain at break of  $2.4 \pm 0.2\%$  (Table 28). The Young's modulus was not deeply impacted by the incorporation of cellulose. An increase in Young's modulus with the filler content could be expected when the rigidity of fillers is higher than the matrix's [179,180,197,317], which is not the case in the present study [190]. The low aspect ratio of the studied cellulose particles could explain this phenomenon.

The incorporation of fillers resulted in a decrease in the stress at break, which was limited in the case of grafted cellulose. As an example, the stress at break of PHBV-10GC was 23% higher than PHBV-10VC. The better filler/matrix interfacial adhesion and thinner interphase observed in SEM could explain it. A better filler dispersion state could also be in favor of a limited decrease in strength at break, even if it was not clearly evidenced by SEM observations of film cross-sections.

Similarly, the strain at break dramatically decreased with filler content, especially with virgin cellulose. The decrease in elongation at break for composite with rigid fillers is explained by the fact that the proportion of stretchability is lower in composite [120]. Interestingly, this decrease was lower in the case of grafted cellulose. The grafting improved the elongation by around 30% for all the studied filler contents.

Table 28. Tensile properties (Young's modulus, nominal stress at break, nominal strain at break, and energy at break) of PHBV-based biocomposites.

Materials	Young's modulus (GPa)	Stress at break (MPa)	Strain at break (%)	Energy at break (mJ·cm <sup>-3</sup> )
PHBV	2.9 ± 0.2	39.7 ± 0.1	2.40 ± 0.15	626 ± 68
PHBV-10CV	3.2 ± 0.2	25.1 ± 1.3	0.90 ± 0.07	124 ± 15
PHBV-10CG	3.3 ± 0.1	31.0 ± 1.5	1.23 ± 0.21	229 ± 56
PHBV-20CV	3.1 ± 0.1	23.6 ± 1.3	0.91 ± 0.05	122 ± 12
PHBV-20CG	2.6 ± 0.1	25.1 ± 1.1	1.15 ± 0.05	164 ± 13
PHBV-33CV	2.6 ± 0.2	15.8 ± 2.4	0.70 ± 0.10	62 ± 17
PHBV-33CG	2.5 ± 0.2	19.0 ± 0.8	0.93 ± 0.06	101 ± 8

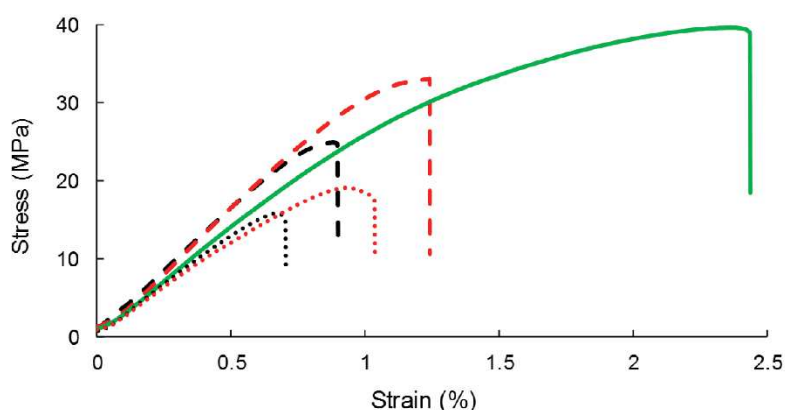


Figure 63. Representative stress–strain curves of the composite materials: PHBV (—), PHBV-10VC (---), PHBV-10GC (···), PHBV-33VC (···), PHBV-33GC (···).

As described by Pukánszky [318], an interfacial adhesion model can be used to predict the tensile strength of composites as a function of the filler content:

$$\sigma_c = \sigma_m \lambda^n \left( \frac{1 - xf}{1 + 2.5xf} \right) e^{(Bxf)} \quad \text{Eq. 37}$$

where  $\sigma_c$  and  $\sigma_m$  are the stress at break of the composite and matrix, respectively;  $xf$ , the filler volume fraction; and  $B$  the empirical parameter describing the quality of the filler/matrix interface.  $\lambda$  is relative elongation and  $n$  accounts for to the strain hardening of the matrix. Because of the small elongation of the composite,  $\lambda^n$  can be neglected [35]. The model provides information about the filler/matrix interface thanks to the parameter  $B$ : a low  $B$  corresponds to a low adhesion. In the present study, experimental data were well fitted with  $B = -0.8$  for composites with virgin cellulose (Figure 64), confirming the poor adhesion observed in SEM. A low but positive value of  $B$  ( $B = 0.5$ ) was obtained for PHBV-grafted cellulose, meaning a better interfacial adhesion. Thus, this model confirmed the idea that grafting only limited the negative impact of cellulose incorporation.

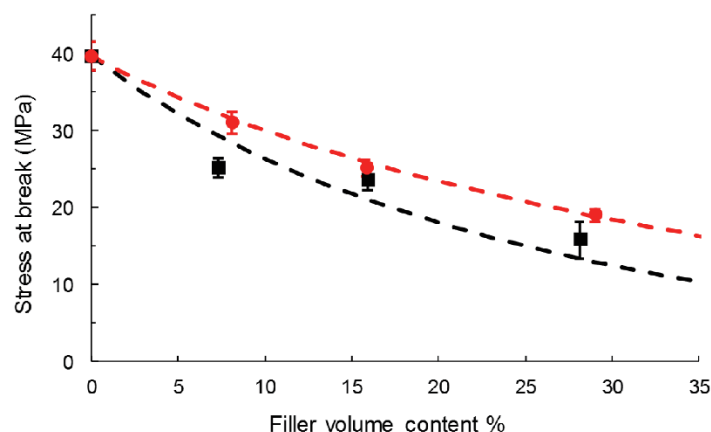


Figure 64. Pukánszky's model applied for virgin cellulose (- -, ■),  $B = -0.8$  and grafted cellulose (- -, ●),  $B = 0.5$  based composites.

The energy at break decreased with increasing filler content (Table 28). Logically, this decrease was lower in the case of grafted cellulose. The addition of cellulose made the materials more brittle (decrease of stress and stress at break) and less tough (decrease of the energy at break). Similar results with esterified fillers in LDPE-based composites were measured by Pasquini et al. [120].

SEM observations of film cross-sections after tensile tests were also carried out (Figure 65). When samples were subjected to high mechanical deformation, no difference of breaking sections between composites filled with grafted cellulose or virgin cellulose was noticed. In both cases, cellulose particles were pulled out from the matrix with the evidence of interfacial voids. Thus, when composites were mechanically solicited at high deformations, the break occurred at the filler/matrix interface even for treated cellulose. The adhesion was not sufficiently high to make the break happening in the bulk of the matrix or of the fibers.

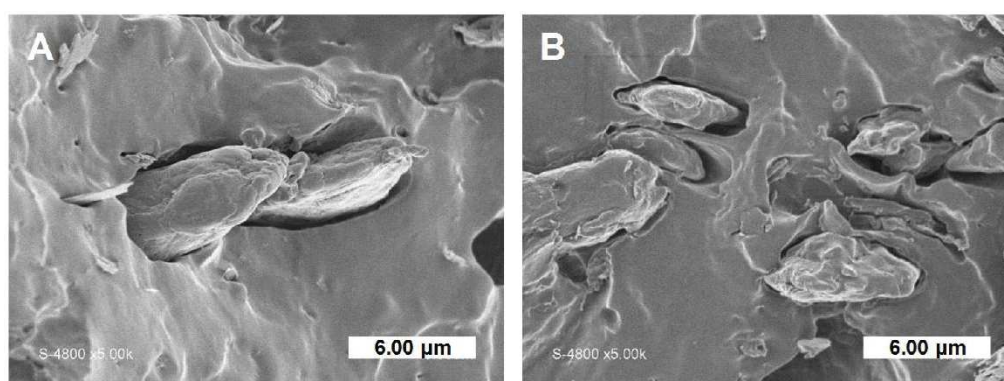


Figure 65. SEM pictures of fracture sections after tensile test: (A) PHBV-20VC and (B) PHBV-20CG.

## II-4 Conclusions

In this work, we studied the structure/functional properties of biocomposites constituted of PHBV and cellulose particles either pre-treated or not. The pre-treatment consisted in gas-

phase esterification using palmitoyl chloride. It was shown that gas-phase esterification of cellulosic particles allowed significant improvement to their hydrophobicity, resulting in a stronger filler/matrix interfacial adhesion and a decrease in water vapor permeability compared to virgin cellulose. The better compatibility of the esterified filler with the apolar PHBV matrix was confirmed by SEM observations of the cryo-fractured cross-sections of composite films. The gas-phase esterification of cellulose particles significantly slowed and limited the negative effects of cellulose incorporation into the composite, which offers hope for using high filler contents. However, the enhanced adhesion was not sufficient to largely improve interfacial adherence, which would be necessary to improve mechanical properties at high deformations. In conclusion, the surface grafting of cellulose particles with long aliphatic chains might be an easy and versatile tool for designing fully organic biocomposites with tailored properties.

Author Contributions: Conceptualization, G.D. and H.A.-C.; methodology, G.D. and H.A.-C.; software, G.D.; validation, G.D. and H.A.-C.; formal analysis, G.D.; investigation, G.D.; data curation, G.D.; writing—original draft preparation, G.D.; writing—review and editing, G.D., H.A.-C., and N.G.; supervision, H.A.-C and N.G.; project administration, H.A.-C. and N.G.; funding acquisition, N.G.

Funding: This work was carried out in the framework of the NoAW project, which is supported by the European Commission through the Horizon 2020 research and innovation program under the Grant Agreement No. 688338.

Acknowledgments: The authors would like to acknowledge Valentin Thoury-Monbrun for his help and advices on the estimation of the diffusion coefficients.

Conflicts of Interest: The authors declare no conflict of interest. The funders had no role in the design of the study; in the collection, analyses, or interpretation of data, in the writing of the manuscript, and in the decision to publish the results.

### III. Complementary results

#### III-1 XPS: X-ray Photoelectron Spectroscopy

Concerning the gas-phase esterification, all the used characterizations tended to confirm the surface grafting of the materials. However, the FTIR technique can have a depth of analyses superior to 1 mm, the  $^{13}\text{C}$  NMR is a bulk analysis and contact angle is an indirect measurement. In order to directly check the surface grafting, X-ray photoelectron spectroscopy (XPS) analyses were performed.

XPS was performed in collaboration with ICGM laboratory. The surface elemental concentrations of the virgin and grafted cellulose (C-G2 sample) were investigated with XPS.

The deconvolution of the C1s peak showed the different carbon signal peaks (Figure 1). The XPS analysis of virgin cellulose reveals three C1s peaks at 284.6, 286.4 and 287.8 eV, arising from C1 (C-C and/or C-H), C2 (C-O) and C3 (O-C-O and/or C=O), respectively. An additional peak, namely C4 (O-C=O), at 288.9 eV appeared for grafted cellulose. A peak at 285.49 eV for binding C-C-O can be also noticed. the first carbon is a C1 close to C-C but shifted because of the oxygen (2<sup>nd</sup> neighbor), and the second carbon is a C2. The signal for C3 was not longer visible because certainly having a very low intensity.

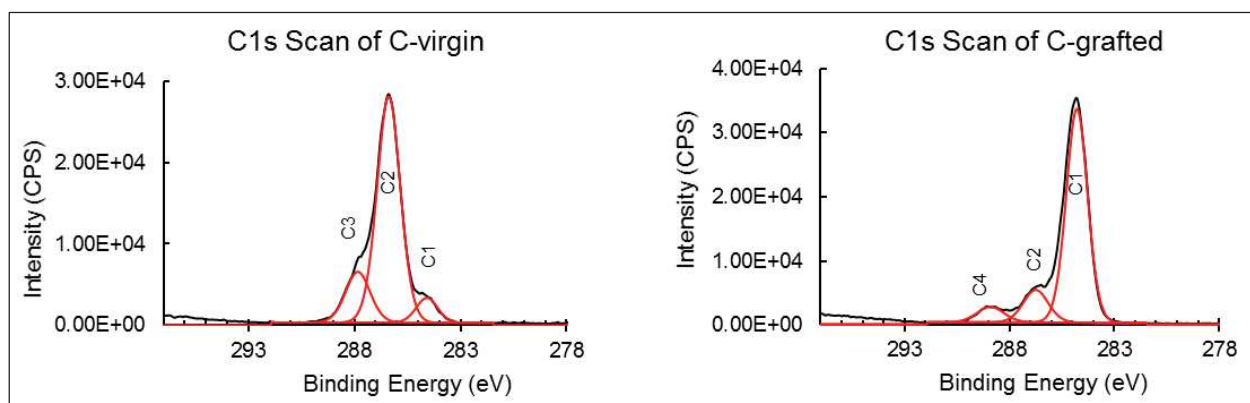


Figure 66. XPS high-resolution spectra for C-virgin and C-grafted

The surface O/C ratio for pure cellulose is theoretically 0.83 (5 oxygen for 6 carbons in an AGU). This ratio is systematically lower because of the presence of C-rich molecular segments at the surface of the sample. In our case, O/C ratio found for virgin cellulose is 0.77 (Table 29), there would be a slight pollution with hydrocarbons adsorbed to the surface [138]. The

O/C ratio decreased significantly after grafting, from 0.77 to 0.17, indicating the presence of fatty acid chains and thus confirming the esterification reactions.

It worth notice that the ratio of C1/C3 increased dramatically after grafting. This ratio reflects the number of aliphatic carbons per AGU and shows the presence of palmitate moiety at the cellulose surface.

Table 29. Mass concentration of each element for virgin and grafted cellulose correlated to deconvolution C 1s.

Samples	Experimental values			Deconvolution of C 1s				
	%C	%O	O/C	C1%	C2%	C3%	C4%	C1/C3
C-virgin	56.4	43.6	0.77	7.7	74.8	17.6	0	0.44
C-grafted	85.6	14.4	0.17	70.6	22.6	0	6.7	$\infty$

The degree of substitution of the surface (DSS) can be deduced from XPS data. The DSS is similar to DS localized at the extreme surface layer (1 - 10 nm). The DSS was determined with a method based on Andresen et al. [319] who defined the DSS as follows (Eq. 38):

$$\text{DSS} = \frac{\%C4 \times M_{\text{AGU}}}{\%C4 \times M_{\text{grafts}} - M_{\text{C}}} \quad \text{Eq. 38}$$

where %C4 is the intensity of the signal attributed to O–C=O moieties,  $M_{\text{AGU}}$  the molecular mass of an anhydroglucose unit (162.14 g.mol<sup>-1</sup>),  $M_{\text{grafts}}$  the molecular weight of the grafted moiety (239.4 g.mol<sup>-1</sup>) and  $M_{\text{C}}$  the molecular weight of one carbon atom. The DSS was 2.67 for grafted cellulose (C-G2). This value confirmed that the grafting happens first at the surface and then in the core of the cellulose because it is higher than DS of the bulk cellulose (DS = 0.02) determined with <sup>13</sup>C NMR. DSS was close to the theoretical full esterification of the surface which is DSS = 3.



### III-3 Homogeneity and repeatability of the gas-phase esterification of cellulose.

The experimental condition of “C-G2” were chosen to produce cellulose fillers of the second article. Same experimental conditions were used for each batch of 100 g: 100 °C, 15 hours, 2 mbars.

In order to get enough materials to use as fillers in composites during the melt extrusion, four nylon mesh bags filled with 50 g of cellulose were used per reaction. As shown in Figure 67, the bags were put on top of each other.

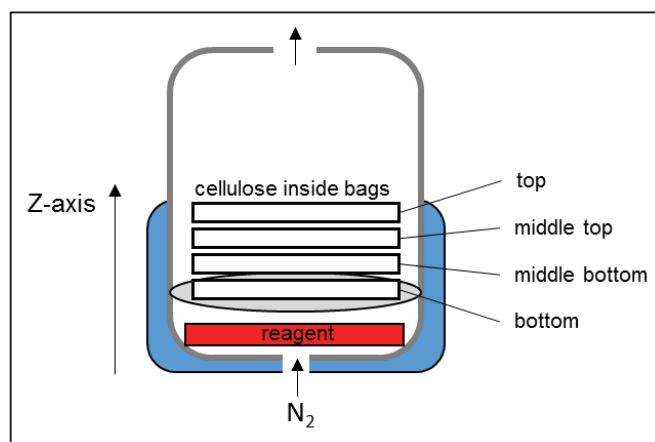


Figure 67. Scheme of the experimental set-up.

The reagent being at the bottom of the reactor and nitrogen flow with the vacuum pump inducing a vertical flow, it was important to know the homogeneity of the reaction between these four bags according to Z-axis. Thus, the DS of each bag was determined by FT-IR and <sup>13</sup>C NMR analysis (Figure 68). It is worth noting that the samples measured by FT-IR were from a different reaction than the ones measured by <sup>13</sup>C NMR analysis. As already explained in the article 1, the DS from FT-IR, which were only estimation, were higher than DS from NMR. The results from <sup>13</sup>C NMR (Figure 68A) showed that the cellulose from the first bag was twice more grafted than the cellulose from the three bags on top. Those three bags were grafted almost equally.

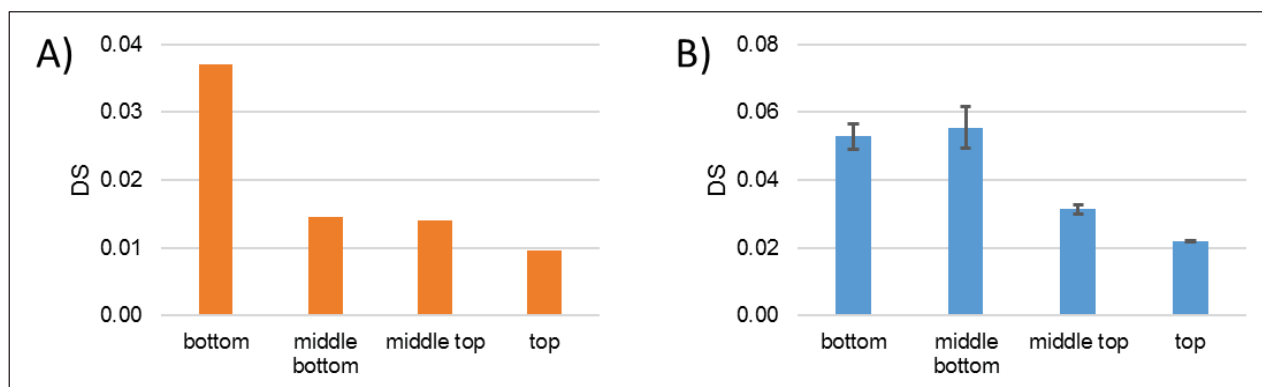


Figure 68. DS of C-G2 samples according to the Z-axis, determined by  $^{13}\text{C}$  NMR analysis (A) or by FT-IR (B).

In the article 1 and 2, the cellulose from the different bags of the same reaction were mixed in order to get a homogeneous DS. Interestingly, if the DS calculated from FT-IR are weighted with the mass of each bags, a  $\text{DS}_{\text{avg}}$  (FT-IR) of 0.046 can be calculated. This value is close to the one found for C-G2 in the first article  $\text{DS}_{\text{estimated}}$  (FT-IR)=0.04. Similarly, if the DS(NMR) are weighted by the mass of each bags, a  $\text{DS}_{\text{avg}}$  (NMR) of 0.020 can be calculated which was the value calculated from  $^{13}\text{C}$  NMR in the first article.

$^{13}\text{C}$  NMR analysis of grafted cellulose from three different reactions (A, B and C) using the same reaction conditions (C-G2) were performed to assess the repeatability of the esterification. As shown in Figure 69, the gas-phase esterification with C-G2 conditions was repeatable with a  $\text{DS}_{\text{C-H}}$  variation of 0.002. The  $\text{DS}_{\text{C=O}}$  calculated from the integrals of the carboxylic groups were also repeatable but slightly higher, the signal being very weak a small constant contribution to the integrals led to a limited overestimation.

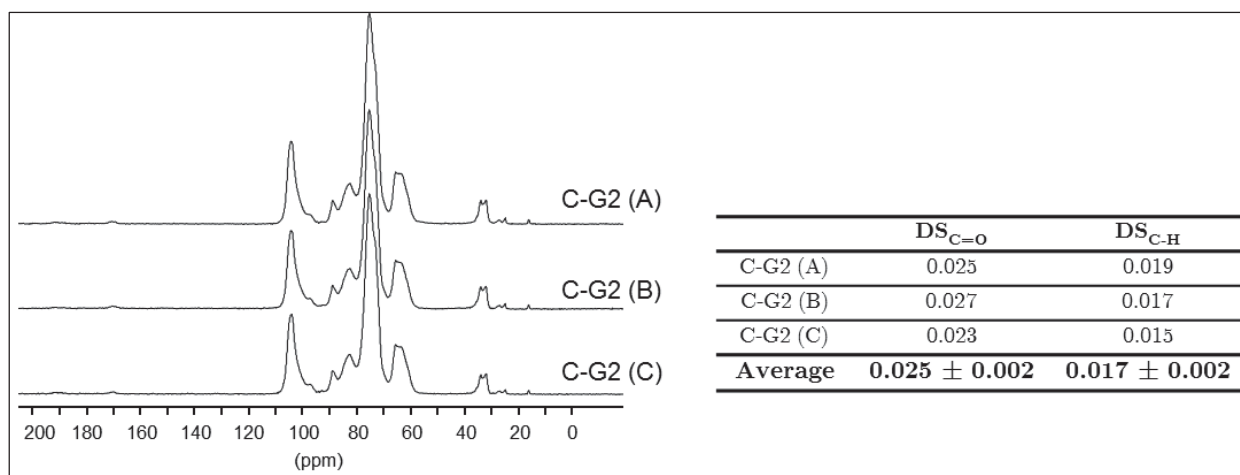


Figure 69. Cellulose  $^{13}\text{C}$  NMR spectra and calculated DS for the three repetition of the gas-phase esterification.

## III-5 Color of the samples

After the gas-phase esterification, a change in the color of the grafted cellulose was slightly observed. The difference of color ( $\Delta E$ ) calculated the measured color parameters  $L^*$ ,  $a^*$  and  $b^*$  varied with the degree of substitution (Figure 70A). The main difference was concerning the parameter  $b^*$  representing the yellow/blue opponent and ranging from positive (yellow) to negative (blue) values trough zero (grey).  $b^*$  increased with the DS. This can be explained the more drastic experimental conditions with increasing DS. Temperature of reaction was higher and the reaction time was longer, thus, a superficial degradation may occur.

Similarly, the color parameters of composites materials were measured according to the filler content and the type of fillers (Figure 70B). Composites films with grafted particles were slightly more yellow than composite with virgin cellulose. In both case,  $b^*$  increases with the filler content.

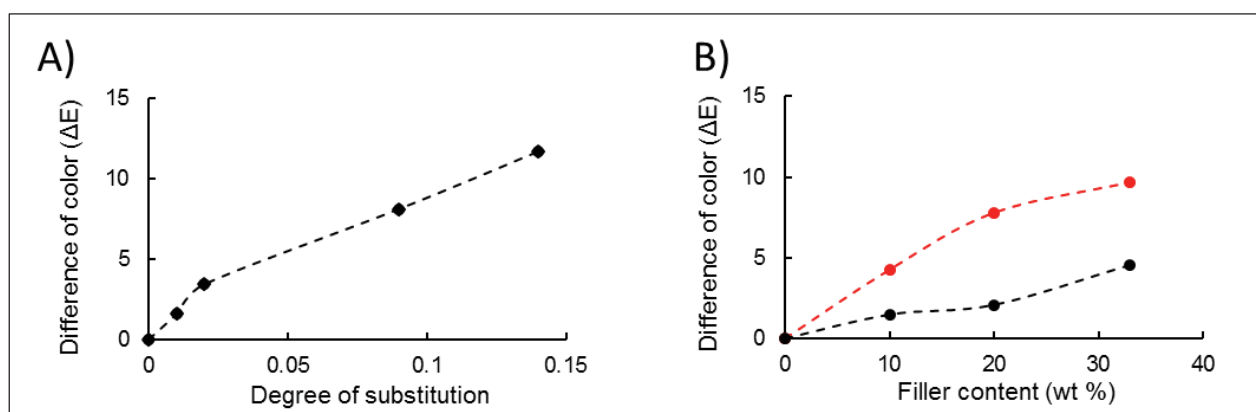


Figure 70. A) Effect of the degree of substitution on the color change ( $\Delta E$ ) of cellulose, B) Color change of the composite films according to the filler content C-virgin (---) and C-G2 (---).

Table 30. Color parameters of cellulose and PHBV-based composites

Sample	$L^*$	$a^*$	$b^*$	$\Delta E$	DS
C-virgin	56.77	1.29	5.11	0.00	0
C-G1	57.46	1.50	6.53	1.59	0.01
C-G2	59.87	1.52	6.54	3.42	0.02
C-G3	55.91	2.33	13.08	8.08	0.09
C-G4	59.96	2.70	16.21	11.63	0.14
PHBV	86.85	0.64	9.19	0.0	-
PHBV-10CV	86.31	0.61	10.57	1.5	-
PHBV-10CG	83.71	1.06	12.03	4.3	-
PHBV-20CV	86.19	0.26	11.12	2.1	-
PHBV-20CG	81.32	1.30	14.62	7.8	-
PHBV-33CV	84.99	0.17	13.29	4.5	-
PHBV-33CG	80.04	1.93	15.92	9.7	-

## Conclusion

Une centaine de grammes de cellulose par réaction a été greffée avec succès avec du chlorure d'acide palmitique en absence de solvant. L'estérification par voie gazeuse est donc transposable à des substrats de taille micrométrique (50  $\mu\text{m}$ ). Les degrés de substitution (DS) déterminés par RMN du  $^{13}\text{C}$  vont de 0.01 à 0.14.

Les conditions choisies ont permis le greffage sur les groupements hydroxyles de surface sans dégrader la structure intrinsèque de la cellulose. L'intégrité de la cellulose a été vérifiée par des observations macroscopiques, des analyses thermogravimétriques, des observations MEB, des méthodes DRX et spectrométriques. Le squelette de la cellulose n'a pas été altéré comme le montre les analyses de RMN solide du carbone. La taille des particules n'est pas modifiée de même que la cristallinité de la cellulose. Toutefois, une légère coloration jaune est notée à la suite du greffage.

Ce traitement rend les particules de cellulose plus hydrophobes. L'énergie libre de surface des celluloses greffées, calculée à partir des angles de contact, indique une chute de la composante polaire. Cette hydrophobicité de surface varie peu dans la gamme de DS obtenus. Au contraire, la sorption de vapeur d'eau est significativement réduite en augmentant le DS de la cellulose. Ainsi, le greffage de surface prévient la sorption d'eau liquide mais ne fait que limiter la sorption de la vapeur d'eau. Des analyses XPS démontrent le greffage quasi-total de la surface confirmant le modèle de progression du greffage de la surface vers le cœur du substrat.

Le principal inconvénient de la cellulose en tant que charge, à savoir son hydrophilicité, désormais atténuée par le greffage, la cellulose greffée avec un DS de 0.02 a été étudiée dans les matériaux composites. Ces conditions furent choisies car la température à 100 °C permet de ne pas altérer la cellulose tout en assurant un greffage efficace.

Les propriétés structurales et fonctionnelles des composites de PHBV et de particules de cellulose greffée ou non ont été étudiées. Une meilleure compatibilité de la charge estérifiée avec la matrice apolaire de PHBV a été confirmée par des observations au MEB des coupes transversales cryo-fracturées de films composites. Les particules de cellulose greffées sont sensiblement mieux imprégnées dans la matrice de PHBV. Les vides interfaciaux ne sont pas visibles, au contraire des composites contenant de la cellulose vierge. Une diminution de la perméabilité à la vapeur d'eau par rapport à la cellulose vierge a été observée.

Cependant, l'amélioration de l'adhésion interfaciale n'était pas suffisante pour améliorer les propriétés mécaniques à fortes déformations. Les propriétés de tractions sont légèrement améliorées par rapport aux composites avec cellulose vierge, avec notamment une elongation à la rupture 30% plus élevée. L'observation de fractures après essai de traction n'a pas montré d'amélioration de l'adhérence.

En conclusion, le greffage en surface de particules de cellulose avec de longues chaînes aliphatiques pourrait constituer un outil simple et polyvalent pour concevoir des biocomposites aux propriétés adaptées. L'incorporation des charges cellulosiques avec de faible rapport d'aspect s'accompagne généralement de perte de propriétés mécaniques du composite. L'estérification en phase gazeuse des particules de cellulose a considérablement ralenti et limité les effets négatifs de l'incorporation de la cellulose dans le composite, ce qui laisse entrevoir des possibilités d'utilisation de taux de charge élevés.

Globalement, on peut conclure que l'estérification en phase gazeuse est une réaction adéquate pour améliorer l'affinité de particules de cellulose de taille micrométrique à une matrice apolaire, offrant ainsi de nouvelles perspectives pour le développement de nouveaux matériaux biocomposites. Afin d'observer des effets d'amélioration de l'interface plus importants, cette technique de greffage devrait être envisagée avec un agent de couplage afin de créer des liaisons covalentes avec la matrice et ainsi d'améliorer de façon plus importante l'adhésion à l'interface dans le composite. La régiosélectivité de la réaction pourrait être également étudiée.

La réaction peut être maintenant appliquée sur des particules de sarments de vigne présentant une plus grande complexité (chapitre IV).

Chapter IV. Exploring the upcycling  
of vine shoots for the development of  
new biocomposites

## Chapter IV. Exploring the upcycling of vine shoots for the development of new biocomposites

Dans ce chapitre une nouvelle source de charge de renfort est explorée, les sarments de vigne. Ce résidu agricole est encore très peu valorisé et représente d'importants volumes dans les régions viticoles et en particulier en région Occitanie.

Tout d'abord, une courte étude sur la variabilité des sarments de vigne à l'échelle de la particule est réalisée (Article 3). La variabilité est un frein à l'utilisation de fibres naturelles pour l'application composite par les industriels. L'objectif de cet article 3 est de déterminer l'étendue de la variabilité des sarments de vigne entre quatre cépages différents sur trois années consécutives. La composition chimique, la stabilité thermique, la couleur et l'aptitude au broyage seront discutés en fonction des échantillons.

La Syrah est le cépage le plus répandu dans la région Occitanie, il a donc été choisi pour réaliser des composites dans les Articles 4 et 5.

Dans l'Article 4, des composites PHBV/sarments de vigne seront produits pour la première fois. L'objectif est l'évaluation du potentiel renfort de cet agro-résidu dans des composites entièrement biosourcés et biodégradables. Les propriétés finales des matériaux résultants dépendant en grande partie de l'interface charge/matrice, l'estérification en phase gazeuse présentée dans le chapitre III sera appliquée aux particules de sarments. Son effet sera étudié sur les particules elles-mêmes puis sur les propriétés des matériaux après extrusion. Les propriétés mécaniques et de perméabilité à la vapeur d'eau des composites préparés sont discutées.

Dans l'Article 5, deux résidus issus de l'activité viticoles, les sarments de vigne et le marc de raisin, seront comparés en tant que charge de renfort pour les composites à base de PHBV. Dans une logique de bioraffinerie, l'extraction préalable de molécules d'intérêt telles que les polyphénols est envisagée. L'objectif est de maximiser le potentiel des sarments ou du marc de raisin avant de les utiliser dans les matériaux. L'effet de cette extraction préalable sur les fibres et les composites est étudié à travers la stabilité thermique, la couleur, les propriétés mécaniques et de perméabilité à la vapeur d'eau.

## I. A quick view of vine shoots variability as regards biocomposite application: inter-varieties and inter-seasonality (Article 3)

*Grégoire David <sup>a</sup>, Nathalie Gontard <sup>a</sup>, H el ene Angellier-Coussy <sup>a</sup>*

*<sup>a</sup> JRU IATE 1208 – Univ Montpellier, CIRAD, INRA, Montpellier SupAgro, 2 Place Pierre Viala, Bat 31, F-34060 Montpellier 01, France*

### I-1 Introduction

Biocomposites with lignocellulosic fillers are gaining importance in various sectors. The most important market for biocomposites is currently the automotive industry with 150 000 tons produced in 2012 [320]. However other applications such as furniture, horticulture or packaging are also developed. The large range of possible applications offers the possibility to produce a panel of materials covering a large window of mechanical properties. Lignocellulosic fillers obtained by dry fractionation of the raw lignocellulosic biomass are rather used as filling materials than reinforcement even if technical natural fibers can reach high mechanical performances. Besides the common cited drawbacks about natural fillers, i.e. high moisture sensitivity and poor compatibility with mostly used polymer matrices, the innate variability of biomass resources and the inconsistency within one single resource also represents a brake to their use by industrials [321]. To boost the acceptance of biocomposites as a viable alternative to conventional materials, quality, consistency and standardization of the materials need to be ensured [255]. Thus, for a given couple of biomass and downstream processes, what is important is to characterize the variation of intrinsic characteristics of the biomass, to study its impact on targeted functional properties of biocomposites, and to develop strategies to standardize the overall process in such a way to provide consistent materials.

There are multiple causes responsible of the variability of the lignocellulosic biomass. The first obvious one is the genetics of the plants, which induces different varieties. Otherwise, there are natural factors: the seasonality (weather conditions), the geographical location (climate and soil composition), the ontogeny (evolution of plant properties during its lifespan) and the heterogeneity within the plant due to the different histological tissues. Variability can also come from possible biological attacks (bacterial, fungi or insect). Finally, artificial factors such as growth strategies and modes of cultivation, collection and storage conditions could also affect the characteristics of the lignocellulosic biomass. Some of these factors can be controlled



through standardization practices while other factors can be difficult to control. The influence of environmental conditions on biomass composition is particularly difficult to control because they are subject to variations in weather, including total supply and timing of water, daily and seasonal temperature swings, and variations in local soil conditions (e.g., clay, sand, rock, nutrient content, and pH). Variability is noticeable in inter-species because of the genetics, intra-species depending on environmental factors and there is even inter-individual variability.

Markers of variability are mainly the biochemical composition, the moisture content, the bulk density and the histological structure of the biomass, resulting in differences of intrinsic properties of fillers (composition, grindability, morphology, mechanical properties, surface properties...) and possibly in differences in the overall performance of the resulting composite materials. The biochemical composition has a strong impact on the intrinsic properties of lignocellulosic fillers, including mechanical properties and surface free energy. The tensile strength is known to evolve exponentially with cellulose content, while it decreases with increasing lignin content [4]. Elongation at break increases with lignin content, while it is not significantly affected by cellulose content. No clear relationship between Young's modulus and filler composition has been established. Mechanical properties also depends on the internal structure at the histological level, including mainly cellulose content, spiral angle of the cellulose microfibrils in the inner secondary cell walls along the fiber axis and cellulose crystals size [31]. The composition also influences the surface free energy of fillers because of the difference of surface free energy of each biopolymer constituting the biomass (i.e. cellulose, hemicelluloses, lignin, pectins...). In theory, it is possible to calculate the surface free energy of natural fibers based on the sum of those of their constituents [37]. The presence of lignin at the surface of particles is known to increase their surface hydrophobicity [37]. It also increases the thermal stability of the fillers. Finally, each biomass would exhibit a different grindability depending on their lignocellulosic structure [322]. The above cited factors are not independent from each other. However, variation in filler intrinsic properties did not necessarily imply discrepancy of the composites functional properties. As an example, Beaugrand et al. showed that variations was characterized along the height of the hemp stem, had no impact on the composite performances [323]. Extrusion and injection molding processes may have masked intrinsic particularities of the plant fillers. Concerning biocomposites, flax fibers and the influence of their properties on composites have been extensively studied [14,286,324].

Vine shoots (ViSh), which represent the annual growth units of the vineyard, are considered as agro-residues without yet convincing valorization. Their use as filler in composite materials is a potential good solution to their management [18,19]. Indeed, vines are woody perennial plants, which conserve and develop their root system and pursue the expansion of their aerial organs annually. More specifically, vine shoots develop and growth during spring and enter in a dormancy period at the end of autumn. Vine shoots are pruned in winter just after their lignification. After dormancy period, from march to august, the development of vine shoots is accompanied by the transformation and storage of available resources in the form of elaborated substances into fruits, seeds and perennial parts of the plants. The new tissues produced along

this process also need to meet the mechanical and hydraulic demands of the new grown structure at each moment [325]. The sampled material is therefore clearly dependent on the cultivation technique, environmental conditions and available resource of the correspondent year, resulting in a natural variability of its properties. Jimenez et al. investigated the influence of the variety and the growing method (goblet or espalier) on the composition of vine shoots [48]. No significant difference in composition among vine varieties (four) or between growing methods was noticed. Lignin content ranged from 19.3 to 21.8%, holocellulose content was between 64.2 and 69.6%, and ash content was from 3.0 to 3.8%. The impact of species on the biochemical composition and polyphenols contents in ViSh has already been investigated. However, to the best of our knowledge, studies about the seasonality are inexistent as well as the study of color, thermal stability and ability to be milled, which are key parameters for composite application.

In this context, the objective of the present study was to characterize four varieties of vine shoots (Syrah, Grenache, Chardonnay, Viognier) through three years (2016, 2017, 2018) from the same location and same cultivation method, in view of using ViSh as raw resources for the production of fillers.

## I-2 Materials and methods

### I-2.1 Raw materials

Vine shoots (ViSh) were kindly provided by INRA Pech Rouge (Gruissan, France) (Figure 71). Around 5 kg of them were collected at the same time on December 2016, 2017 and 2018. The pruning techniques and soils enrichments conditions were the same over the years. The vine varieties were Syrah, Grenache, Chardonnay and Viognier. They are part of the most common varieties in France. The shoots were first air dried during 2 months then dried 48 hours in oven at 60°C. It is worth noting that Grenache 2016 was let in the oven 2 weeks, which could explain further possible observed difference. Successive dry grinding steps were carried to get particles displaying an apparent median diameter of about 100-150  $\mu\text{m}$ . A first coarse milling using a shredder (AXT 22D, Bosch, Germany) gave fragments of about 5 cm that were then ground with a knife mill (SM 300, Retch, Germany) using successively grids of 4 and 2 mm. Finally, an impact mill (Fine Impact Mill UPZ, Germany) equipped with a 0.3 mm grid was used at 18 000 rpm.

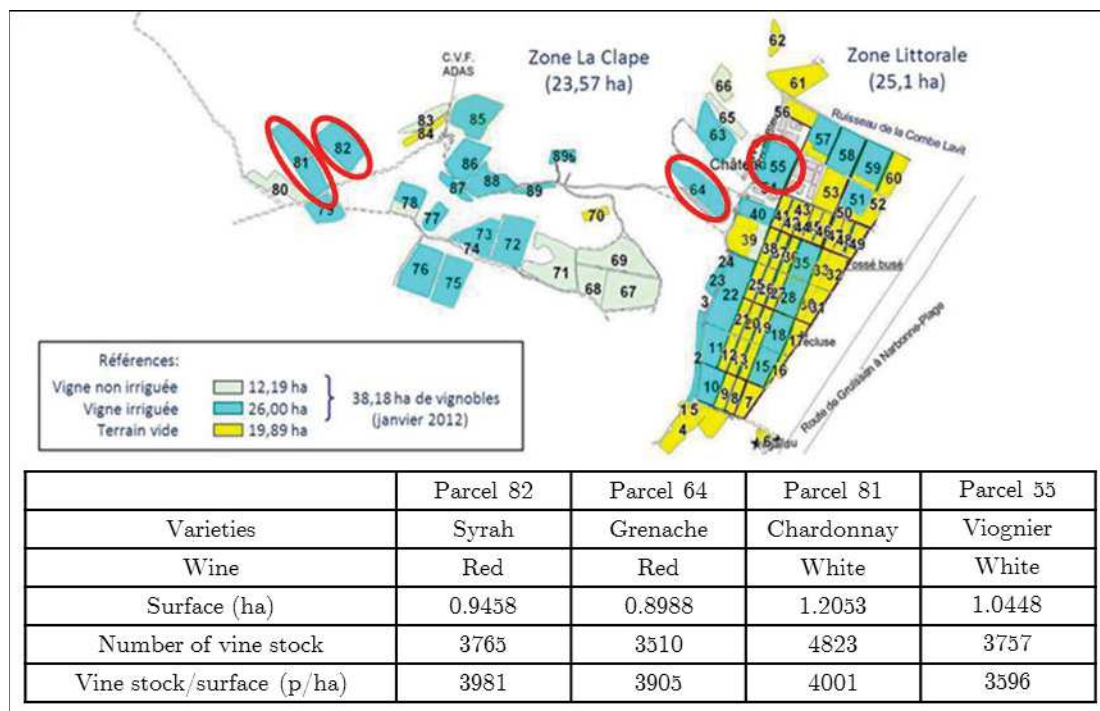


Figure 71. Map of the experimental unit in Gruissan (INRA Pech-Rouge). The parcels where vine shoots come from are encircled in red. Table recaps the characteristics of the vines from where vine shoots were collected.

Figure 72 recaps the annual precipitation and hours of sunshine (between March and December) during 2016, 2017 and 2018 in Gruissan, the location of the studied vines.

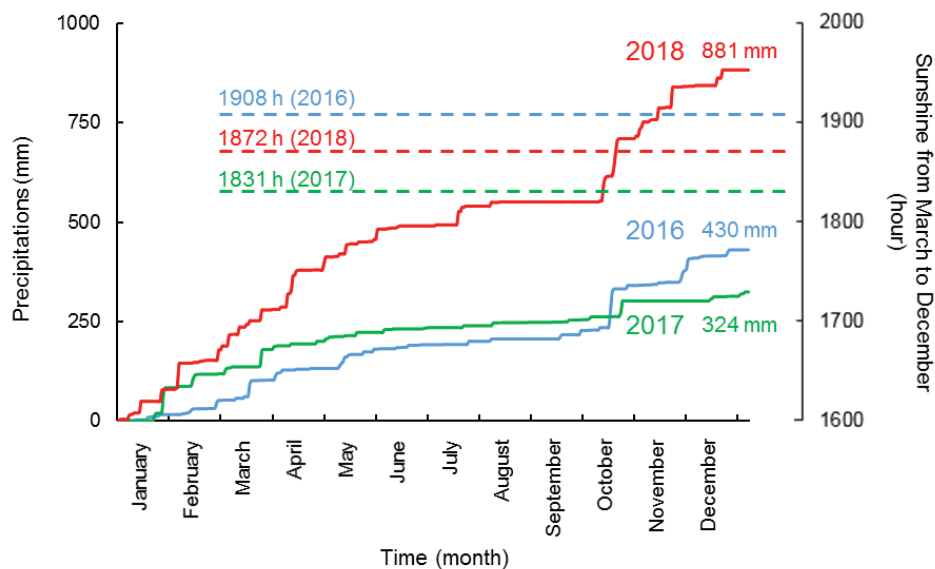


Figure 72. Precipitation and hours of sunshine during 2016, 2017 and 2018 in Gruissan (INRA Pech-Rouge).

### I-2.1.1 Biochemical composition

Klason lignin was determined by mass deduction after double hydrolysis in acidic conditions. 80 mg of dry finely milled ViSh (>1 mm) were put in 0.85 mL of sulfuric acid 72% and stirred manually for 1 h at room temperature. 23.8 mL of ultrapure water was then added, and the mixture was heated and stirred at 121°C during 1h in a sealed flask. Then the hydrolysates were filtered (10 µm), washed by water, and dried at 105°C overnight. The ash also contained in the residues were subtracted to know the lignin content.

Analytical mercaptolyses developed by Roumeas et al. [5] were conducted to determine the phenolic composition of ground vine shoots. The samples were then analyzed by an UPLC-DAD-MS system [5]. The quantification was done according to the UV absorbance at 280 nm.

It is worth noting that the biochemical characterization of ViSh, as for other vegetable materials, is not only related to the type of variety or time of pruning, but also significantly linked to their compounds extraction procedures according to the different techniques used [46]. That is why the same methods were strictly used to characterize the different varieties over the three years to allow comparisons.

### I-2.1.2 Thermogravimetric analysis (TGA)

TGA under nitrogen flow (50 mL·min<sup>-1</sup>) was carried out using a Mettler TGA2 apparatus (Schwerzebbach, Switzerland) equipped with a XP5U balance. The samples were heated at 10 °C·min<sup>-1</sup> from 25 °C to 600 °C under nitrogen flow of 50 mL·min<sup>-1</sup>. The results were analyzed using STARE software. The maximum degradation temperature (Tdeg) corresponded to the temperature at which the degradation rate was maximum. The onset and offset degradation temperatures (T<sub>onset</sub> and T<sub>offset</sub>, respectively) were measured respectively when the first derivative of the weight loss became higher than 0.1 %·C<sup>-1</sup> and lower than 0.1 %·C<sup>-1</sup>. Analyses were done in triplicate.

### I-2.1.3 Color

The color attributes of each ViSh fraction were measured with a colorimeter CR-410 (Minolta), using the CIELAB color system (L\*, a\*, b\*). The total color difference (ΔE) was calculated following the standard ASTM D2244 [326] (Eq. 39).

$$\Delta E = [(L^* - L_0^*)^2 + (a^* - a_0^*)^2 + (b^* - b_0^*)^2]^{0.5} \quad \text{Eq. 39}$$

where L\*, a\* and b\* the color components of each sample. The reference was a 99.5% pure cellulose BE 600-10TG (Arbocel, France). All measurements were carried out with 5 repetitions.

#### I-2.1.4 Laser granulometry

Particle size distribution was determined from 0.01  $\mu\text{m}$  to 10000  $\mu\text{m}$  using a Mastersizer 2000 laser granulometer in wet mode (Malvern Instruments Ltd., United Kingdom). Particles were suspended in ethanol 95% (v/v). From the particle size distribution, three values were identified to characterize the sample and allow comparison. The value of  $d_{50}$  represents the particle size diameter for which 50% of particles (in volume) have a diameter below. Measurements were done with at least 5 repetitions.

### I-3 Results and Discussion

#### I-3.1 Biochemical composition

Klason lignin ranged from 19.0 to 24.4 % according to the years and the varieties, with an average of  $21.0 \pm 1.7$  % considering all the samples and replicates (Table 31).

Vine shoots lignification occurs in autumn before the winter dormancy period. Since vine shoots were all sampled at the end of December, lignification should be complete for all samples. Moreover, the grinding process performed before characterizing biochemical composition enables higher homogeneity of the samples, thus limiting intra-species variability, which is by the way confirmed by the low standard deviation values reported. The variation in lignin content between samples result mainly from external stresses.

Results, detailed in Table 31, gave rise to the identification of different behaviors. Syrah and Viognier varieties showed the highest variability in term of lignin content (standard deviation per species of 2.5 and 1.7 respectively) and similar behaviors: lignification is more marked in 2017, followed by 2018 and 2016. It is worth noting here that 2017 was previously identified as the driest year. Anyhow, it can be inferred here the lignification process of these two species might be more sensitive to environment external stresses. On the contrary, the biochemical composition of Grenache and Chardonnay species was more stable, independently of the year (standard deviation per species of 0.5 and 0.2 respectively).

It is finally interesting to note that the driest year led to the highest rate of lignin content and to more variable results over species. Such observation tends to confirm the hypothesis that water stress can lead to the intensification of lignification process, which is even more pronounced for sensitive species. It is probable that lignification enabled here a better control of the efficiency and safety of water transport from roots to shoots, which is fundamental for plant survival under water stressed conditions [327].

Lignin deposition is observed in cells implicated in conductive or support functions along tissue maturation to adapt to the evolving structure requirements (age-dependent) but also in responses to changing growth conditions (stresses-dependent) [328]. Lignification of parietal cells results in more rigid and hydrophobic plants tissues [329]. It is therefore often reported that this natural process can contribute to the stiffening of the fibers in need of mechanical

support as well as to the healing of wounded tissues in need of protection against biological attacks.

To conclude regarding the composite application, variations of lignin contents were very low over the years and the varieties and should not induce drastic difference of mechanical properties or surface free energy of ViSh fillers.

Table 31. Klason lignin content (g/100g d.b.)

	2016	2017	2018	Average
Syrah	$19.4 \pm 1.3$	$24.4 \pm 0.2$	$21.8 \pm 0.9$	$21.9 \pm 2.5$
Grenache	$19.0 \pm 0.1$	$19.9 \pm 0.9$	$19.7 \pm 0.1$	$19.5 \pm 0.5$
Chardonnay	$21.5 \pm 2.2$	$21.6 \pm 0.8$	$21.2 \pm 0.2$	$21.4 \pm 0.2$
Viognier	$19.4 \pm 0.1$	$22.7 \pm 0.6$	$21.8 \pm 0.2$	$21.3 \pm 1.7$
Average	$19.8 \pm 1.1$	$22.2 \pm 1.9$	$21.1 \pm 1.0$	$21.0 \pm 1.7$

Variation of ash content is reported in Table 32. These results complement the previous analysis since ash content can give interesting information about vine growth conditions and be put in relation to soil quality and assimilative capacities of the plants.

Ash content ranged from 1.3 to 3.0 % according to the years and the varieties, with an average of  $2.3 \pm 0.5$  % considering all the samples and replicates.

Ash content highly depended on the year. The highest content was recorded in 2016 (2.8%), then in 2018 (2.2%) and finally in 2017 (1.8%). No trend could be drawn from the varieties. As observed for lignin, the cultivation year seems more impacting the ash content. No intensification of soil enrichment was reported during the three years.

Differences of sunshine hours (Figure 72) could explain the discrepancy of ash content over the three years. Indeed, sunshine induced an important photosynthesis activity and so a better assimilation of the resources. 2016 had the longest period with sun ahead of 2018 and finally 2017. The same order was observed concerning the ash content according to the years.

In the specific case of vine shoots, the references related to the mineral composition are rather limited. Çetin et al. studied ten Turkish cultivars and concluded that vine shoots are rich in some of the essential minerals including K, Ca, Fe, Mg, P, and Zn [330]. Ash content can also vary depending on the anatomical fraction of the plant as demonstrated in case of corncob and corn stover [331]. Environmental factor such as soil type or fertilization also affect the ash concentration of the biomass, but not in the present case.

Table 32. Ash content (g/100g d.b.)

	2016	2017	2018	Average
Syrah	$3.0 \pm 0.1$	$1.3 \pm 0.2$	$2.0 \pm 0.1$	$2.1 \pm 0.9$
Grenache	$2.7 \pm 0.2$	$2.1 \pm 0.2$	$2.4 \pm 0.1$	$2.3 \pm 0.5$
Chardonnay	$2.7 \pm 0.2$	$2.0 \pm 0.2$	$2.2 \pm 0.1$	$2.3 \pm 0.4$
Viognier	$2.8 \pm 0.3$	$1.8 \pm 0.2$	$2.4 \pm 0.1$	$2.4 \pm 0.3$
Average	$2.8 \pm 0.1$	$1.8 \pm 0.4$	$2.2 \pm 0.4$	$2.3 \pm 0.5$

As previously observed by Jimenez et al. [48], the biochemical composition of ViSh is poorly impacted by the varieties. However, the year of cultivation and collection seems to have a more significant impact. This was due to differences in climate (precipitations and sun exposition). Generally, the storage conditions are also responsible for variability. During storage, degradation of biomass constituents does not occur uniformly. Water-soluble components and structural components of cellulose and hemicellulose degrade first. Thus, generally residual biomass is enriched in lignin and ash. However, in the present study, the ViSh were stored in the same way.

Tannins are one family among the possible phenolic compounds. Interest for extracting them for cosmetic, pharmaceutical or materials applications. The average tannins content of ViSh in this study was 1.54 g/100g (d.b.). Tannins content was higher for 2017 samples and for white vine varieties (Chardonnay and Viognier) (Table 3). However, there are not general rules connecting the tannins content in ViSh and red or white varieties [50]. Controlling the storage time is required to investigate changes in the concentrations of polyphenols. Delgado-Torre et al. compared phenolic compounds from 18 vine shoots cultivars [50]. The total concentration of phenols was quite homogeneous among the different vine-shoot cultivars, the highest values was 5775  $\mu\text{g GAE/g}$  for Chardonnay and the lowest corresponding to Pedro Ximenez with 3323.70  $\mu\text{g GAE/g}$ .

Mossi et al. [332] reported that plants cultivated in complete sun exposure produce tannins as defense mechanism against UV-rays. The present results were in agreement with this previous paper as vine shoots of 2017 had the highest tannins content.

Resveratrol content seemed to be more complex from the years and the varieties. It was probably more influenced by the storage and the specific story of the vine with microorganisms as resveratrol is synthesized as a mechanism of defense. Storage is critical for the accumulation of bioactive compounds in vine shoots. In the case of *trans*-resveratrol it is known that their concentrations change during the storage of vine shoots [333]. A strong increase in the concentration of the monomer resveratrol (approximately 40-fold) was observed during the first 6 weeks of storage at 20 °C in eight different grape varieties (from 0.01 to 0.50 g/100g). Rodriguez-Cabo et al. showed differences in *trans*-resveratrol content depending on the vine variety from 0.06 to 0.45 g/100g. Another study described resveratrol value from 0.02 to 0.15 g/100g for 16 different ViSh varieties [53]. These concentrations match with the present results and also with previous results (0.35 g/100g for Pinot Noir) [51].

Table 33. Tannins and resveratrol contents (g/100g d.b.) for each species and year of cultivation.

	2016		2017		2018		Average	
	tannins	resveratrol	tannins	resveratrol	tannins	resveratrol	tannins	resveratrol
Syrah	1.25 ± 0.07	0.07 ± 0.01	1.65 ± 0.27	0.48 ± 0.09	1.36 ± 0.15	0.29 ± 0.03	1.42 ± 0.21	0.28 ± 0.21
Grenache	0.73 ± 0.06	0.18 ± 0.03	1.77 ± 0.11	0.29 ± 0.03	1.43 ± 0.07	0.15 ± 0.01	1.31 ± 0.53	0.21 ± 0.07
Chardonnay	1.54 ± 0.05	0.12 ± 0.02	2.07 ± 0.14	0.12 ± 0.03	1.70 ± 0.14	0.23 ± 0.01	1.77 ± 0.27	0.16 ± 0.06
Viognier	1.29 ± 0.03	0.07 ± 0.01	1.93 ± 0.10	0.17 ± 0.05	1.81 ± 0.04	0.27 ± 0.05	1.68 ± 0.34	0.17 ± 0.10
Average	1.20 ± 0.34	0.11 ± 0.05	1.86 ± 0.18	0.27 ± 0.16	1.57 ± 0.21	0.24 ± 0.06	1.54 ± 0.34	0.20 ± 0.12

### I-3.2 Thermal stability

$T_{\text{onset}}$ , corresponding to the temperature at which the thermal degradation begins, ranged from 226.5 °C and 236.3 °C according to the years and the varieties, with an average of  $230.3 \pm 2.4$  considering all the samples and replicates. These temperatures allow melt extrusion with most of the common polymer matrices.

In general, only little difference could be observed regarding thermal degradation. Nonetheless small differences could be observed between the species. First, red vine shoots varieties (Syrah and Grenache) had a better thermal stability than white vine shoots varieties (Chardonnay and Viognier), with higher overall  $T_{\text{onset}}$  and  $T_{\text{deg}}$  values, independently of the seasonality. Previous results obtained from biochemical composition did not correlate with this observation, proving that the higher thermal stability of red vine shoots biomass is probably more related to the quality rather than the quantity of macromolecules (crystallinity of cellulose for example).

It is also interesting to observe that, for all species, earlier thermal degradation (lower  $T_{\text{onset}}$ ) can be observed on dryer seasons. It is realistic to argue that the quality of the macromolecules produced could have been impacted in a context of scarcity of resource, leading structures more sensitive to temperature. The drought generally causes the production of more lignin and especially hemicellulose whereas the cellulose content is reduced [334,335] which could favor a lower  $T_{\text{onset}}$ .

Again Syrah and viognier display the highest standard deviation over years.

Table 34. Thermal stability of vine shoots.

	2016		2017		2018		Average	
	Tonset (°C)	Tdeg (°C)	Tonset (°C)	Tdeg (°C)	Tonset (°C)	Tdeg (°C)	Tonset (°C)	Tdeg (°C)
Syrah	236.3 ± 0.3	338.7 ± 0.2	230.8 ± 0.6	335.5 ± 0.3	232.3 ± 0.6	333.4 ± 0.2	233.1 ± 2.8	336.3 ± 2.1
Grenache	230.0 ± 0.3	331.6 ± 0.4	230.8 ± 0.6	334.0 ± 0.4	231.5 ± 0.4	333.3 ± 0.1	230.8 ± 0.8	333.0 ± 1.2
Chardonnay	229.9 ± 0.3	338.2 ± 0.3	227.9 ± 0.3	338.3 ± 0.3	229.0 ± 0.1	335.8 ± 0.2	228.9 ± 1.0	337.4 ± 1.4
Viognier	230.0 ± 0.3	333.4 ± 0.2	226.5 ± 0.4	332.8 ± 0.5	229.2 ± 0.2	331.2 ± 0.2	228.6 ± 1.8	332.5 ± 1.2
Average	231.5 ± 3.2	335.5 ± 3.5	229.0 ± 2.1	335.1 ± 2.4	230.5 ± 2.0	333.7 ± 3.0	230.3 ± 2.4	334.8 ± 2.5



Figure 73 displayed the thermal degradation behavior of the most contrasted samples according to Table 34: Syrah 2016 and Viognier 2017. It could be observed that both vine varieties display the same thermal degradation profile. Indeed, besides quantitative variations in biochemical composition, the biomass studied are composed of the same macromolecular building blocks, which degrade at similar temperatures. The first weight loss between 60 °C and 120 °C was attributed to the evaporation of absorbed water about 5% (w.m). Then, a main peak of degradation corresponding to cellulose with a shoulder attributed to hemicellulose were visible between 250 °C and 400 °C. This hypothesis could be supported by the results illustrated in Figure 3. Here, comparing TGA curves of Syrah 2016 and Viognier 2017, it can be observed that until 200 °C the two degradation curves overlapped perfectly. Viognier 2017 started to degrade first at 230 °C, probably due to the presence of small amount of unknown compounds not present in Syrah 2016. Curves overlapped again between 250 °C and 300 °C for the hemicellulose degradation. At 300 °C, a shifting of about 5-10 °C appeared. It was particularly visible at the maximum degradation rate around 330 °C. It corresponded to the cellulose degradation. It could be concluded that the cellulose in Syrah 2016 was more thermally stable than in Viognier 2017. It reinforced the idea of a more crystalline cellulose.

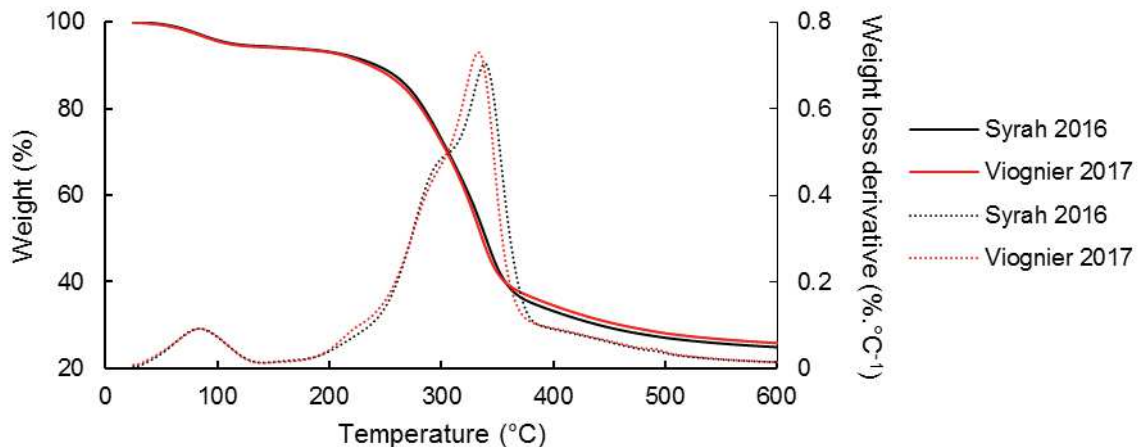


Figure 73. TG and DTG curves of Syrah 2016 and Viognier 2017.

### I-3.3 Color

For packaging applications, the color of materials can be an important criterion of choice.

Figure 74 shows vine shoots before (A1-B1) and after milling (A2-B2). Before grinding, there were “external” color differences which was then annihilated after grinding. It is assumed that ViSh surface chromophore groups lost their effect when assessing the color of particle powder. The filler color did not change with the year or the varieties as shown in Table 35.



Figure 74. Pictures of 2018 vine shoots: Chardonnay (A1) and Grenache (B1), and fillers after impact milling: Chardonnay (A2) and Grenache (B2).

Table 35. Color parameters of the different ViSh

Sample	L*	a*	b*	$\Delta E$
Cellulose	76.8	1.3	5.1	0.0
Syrah2016	63.9	6.7	22.4	22.2
Syrah2017	62.1	6.0	22.4	23.2
Syrah2018	62.6	5.7	22.0	22.4
Grenache2016	61.4	9.5	22.9	24.8
Grenache2017	62.1	6.5	22.1	23.0
Grenache2018	62.6	5.7	21.5	22.1
Chardonnay2016	62.7	6.0	21.4	22.1
Chardonnay2017	62.3	5.1	21.2	21.9
Chardonnay2018	63.3	5.3	21.4	21.5
Viognier2016	63.0	6.6	22.0	22.4
Viognier2017	61.9	5.9	21.8	22.8
Viognier2018	61.5	6.2	21.8	23.2

### I-3.4 Particles size

The choice of the milling equipment and parameters influences the properties of the produced powders for a given biomass. Particle morphology can be affected by initial moisture content. In aerobic storage, dry matter losses increase with moisture content [336]. Generally, moisture contents below 20% (wet basis) limit dry matter losses. In the present study, the vine shoots were dried and milled following the same procedure and were stored in hermetic conditions.

The ability to be milled, called grindability, of the different vine shoots was indirectly evaluated by the measurement of particle sizes after impact milling (Table 36). The median apparent diameter of the particles ( $d_{50}$ ) ranged from 91 to 159  $\mu\text{m}$ , with an average of  $123 \pm 23 \mu\text{m}$

considering all the samples and replicates. Here, differences were clearly visible according to the varieties and to the years. Viognier varieties and year 2017 gave the highest  $d_{50}$ . Grindability is intimately related to the mechanical properties of the different tissues. The most lignified structures are known to be more recalcitrant to grinding [337]. Silva et al. [322], who worked on the grinding of native wheat straw, reported that the lignocellulosic assembly was partially and unevenly dissociated during grinding steps, highlighting a non-homogeneous reduction behavior. Ashes and proteins were easily dissociated (more present in smaller fractions) while cellulose was more recalcitrant (more present in bigger fractions).

Table 36. Median apparent diameter of ViSh fillers ( $d_{50}$ ) after impact milling

	2016	2017	Average
Syrah	$111 \pm 7$	$116 \pm 6$	$116 \pm 7$
Grenache	$91 \pm 11$	$115 \pm 4$	$116 \pm 15$
Chardonnay	$113 \pm 7$	$120 \pm 5$	$120 \pm 7$
Viognier	$157 \pm 5$	$159 \pm 5$	$159 \pm 5$
Average	$118 \pm 26$	$130 \pm 19$	$123 \pm 23$

## I-4 Conclusion

Four ViSh varieties over three years from the same location were studied to assess the inter-seasonality and inter-species variability. The differences between years, mainly caused by difference of precipitation and sunlight, were globally more distinct than between varieties. Globally, the variability was low between the samples.

Lignin seems to be produced in case of water, and higher ash content are present in ViSh which grew with more sunlight. Tannin as a mechanism of defense also depends on the seasonality. Thermal stability was not corresponding to the lignin content probably due to the low difference and because it depends on the crystallinity more than in the quantity of cellulose. The color of fillers was very closed despite discrepancy of ViSh colors before milling.

Statistical comparison should be performed. In perspective of the present work, the effect of ViSh variability on the composite overall performance should be studied. In the future, composites will be produced with the more contrasted vine shoots to complete this work in order to determine if variations observed at the particle scale have an impact on composites properties.

Funding: This work was carried out in the framework of the NoAW project, which is supported by the European Commission through the Horizon 2020 research and innovation program under the Grant Agreement No. 688338.

## II. Upcycling vine shoots for biocomposites applications: About the interest of filler surface esterification to improve their performance (Article 4)

*Grégoire David<sup>a</sup>, Laurent Heux<sup>b</sup>, Stéphanie Pradeau<sup>b</sup>, Nathalie Gontard<sup>a</sup>, Hélène Angellier-Coussy<sup>a</sup>*

<sup>a</sup> *JRU IATE 1208 – Univ Montpellier, CIRAD, INRA, Montpellier SupAgro, 2 Place Pierre Viala, Bat 31, F-34060 Montpellier 01, France*

<sup>b</sup> *CNRS, CERMAV, Univ. Grenoble Alpes, 38000 Grenoble, France*

### Abstract

This paper aims at investigating the potential of using vine shoots (ViSh) as raw resources for their upcycling in micrometric size fillers by dry fractionation and their reinforcing effect in a PHBV matrix. A surface gas-phase esterification was applied to increase the hydrophobicity of ViSh fillers and improve their compatibility with the polymer matrix. The occurrence of the esterification reaction was quantified by <sup>13</sup>C-NMR spectroscopy, while changes in surface free energy were assessed by contact angles measurements. Biocomposites with increasing contents of either virgin or grafted ViSh particles were produced using melt extrusion. Mechanical, thermal and water vapor transfer properties of biocomposites were discussed in relation to their structure. The thermal and mechanical properties of resulting materials proved that ViSh could be used in thermoplastic composites. However, ViSh particles were as seen more as fillers than a reinforcing agents. It was shown that tensile properties were not significantly impacted by the filler treatment. Water vapor permeability of composite films filled with 30 wt% of ViSh was reduced by 27% in case of grafted fillers, which was the only significant effect of grafting on resulting functional properties. This was attributed to the absence of improvement of the filler/matrix interfacial adhesion, the wettability of the virgin ViSh particles being already quite good.

### II-1 Introduction

Biocomposite materials are a growing industry with a large potential of applications from automotive to packaging. The incorporation of lignocellulosic fillers into biosourced and biodegradable polymer matrices can offer economic and environmental benefits of a more 'circular' approach, with equivalent functional units [21]. Two main categories of lignocellulosic

biomass can be distinguished for the production of fillers, i.e. natural fibers grown or extracted for their high mechanical properties (e.g. hemp, flax, kenaf) and fillers derived from agricultural, forestry or food industries residues. The first type of fibers is the most commonly used as reinforcing agents. The second category allows adding value to residues while producing sustainable composites. Their mechanical performances are usually lower than dedicated grown plants but they can perfectly suit for applications with few constraints.

In the viticulture sector, huge amounts of waste and by-products are generated each year including, among organic solid residues, vine shoots, stalks and wine pomaces. Vine shoots (ViSh) correspond to the woody stems that are obtained after vine pruning that is essential to the vine cultivation. They are one of the most important primary agricultural residue being annually produced in large quantity (around 2 tons/ha/year) in wine regions [46]. Currently, these ViSh follow different fates depending on the region: They can either be collected and burnt, ground and let on the vineyards as soil amendment, or in a less extent collected and valorized for the extraction of polyphenols, the production of heating wood or compost. Given the biochemical and histological composition of ViSh, one other potential route could be their upcycling for biocomposites applications, as already investigated for other agricultural residues such as bagasse, wheat straw or corn stem [33,193,337,338]. However, very few papers deal with the use of ViSh as fillers in composites. ViSh were investigated as a raw materials to obtain a pulp potentially useable in composites [57]. In the study of Girones et al., ViSh (filler content of 30 wt%) were incorporated in LDPE and PP matrices [18]. It was concluded that composites displayed lower mechanical properties than neat matrices or composites reinforced with long technical fibers such as flax. This reduction was attributed to the low aspect ratio (1.8) of the ViSh fragments obtained by grinding in a granulator equipped with a 2.5 mm sieve. In another paper, Kilinc et al. [19] studied HDPE-based composites filled with 5, 10 and 20 wt% of ViSh powder displaying a volume median apparent diameter ( $d_{50}$ ) of 13.6  $\mu\text{m}$ . Materials containing 10 wt% of ViSh exhibited the highest tensile strength and flexural strength. The addition of ViSh allowed delaying the thermal decomposition of HDPE.

It was shown that successive dry milling processes could be successfully used to get lignocellulosic fractions with controlled size [337]. As an example, cut milling of native wheat straw allowed obtaining coarse fillers of around 0.5 mm ( $d_{50}$ ), that could be further ground to give fine particles with  $d_{50}$  around 100-150  $\mu\text{m}$  particles and finally ground using ball milling to reach ultra-fine particles with a size of 20-10  $\mu\text{m}$  [33,337]. In case of PHBV-based composites, Berthet et al. showed that decreasing wheat straw filler size allowed improving material processability and reaching higher filler contents due to a better filler dispersion within the polymer matrix and an improved filler/matrix adhesion [33]. Indeed, it was shown that grinding resulted in an increased hydrophobicity of the particle surface [337]. Besides, the best mechanical properties were obtained with ultra-fine particles ( $d_{50}$  of 20  $\mu\text{m}$ ). The thermal stability was decreased with increasing the filler content.

Among polymer matrices, polyhydroxy-co-3-butyrate-co-3-valerate (PHBV) has been reported to be bio-sourced and fully biodegradable. This thermoplastic has physical properties close to conventional polymers. However, PHBV has some limitations, such as, low crystallization rate, and higher production cost. High production cost of the PHBV can be minimized by incorporating the lignocellulose residues into the matrix [339].

The quality of the filler/matrix interface play an important role on the functional properties of composite materials. Lignocellulose (cellulose, hemicelluloses or lignin) are hydrophilic in nature because of their high content of hydroxyl groups. Most of the matrices used are mostly hydrophobic, including PHBV, and interfacial adhesion between such polymeric matrices and hydrophilic natural fibers are very poor. Besides, the hydrophilic character of natural fibers makes them sensitive to moisture uptake which induces reduced mechanical properties. For these reasons, natural fillers are generally subjected to surface modifications in order to achieve maximum compatibility and therefore good adhesion in the composite [91]. There are many different physical and chemical strategies described in the literature to enhance the filler-matrix adhesion [91,99,258,291]. Among them, in a previous study on PHBV-based composites, a gas-phase esterification with palmitoyl chloride gave recently promising results on cellulose fillers [264]. This solvent-free treatment allowed to significantly improve surface hydrophobicity, resulting in a better affinity between cellulose particles and the PHBV matrix. It substantially limited the negative effects observed for the incorporation of virgin cellulose into the composite. Furthermore, a low degree of substitution did not change the biodegradability of the esterified substrate [154]. Thiebaud and Borredon explored esterification of sawdust without organic solvents using fatty acid chlorides to improve thermoplastic properties of wood [149]. The reagent was in fact the solvent and the treatment was performed on low amount of wood. But to the best of our knowledge, such gas-phase esterification treatment has never been carried out on lignocellulosic particles targeting composite applications.

The objective of the present study was to assess the potential of a low-value agricultural residue from viticulture as reinforcing agents in fully biocomposite materials. In order to suit with the food packaging constraints, the ViSh were ground using the successive milling process until reaching an average size of 50  $\mu\text{m}$ . This relative low size of fillers will increase the ductility which has been identified as bottleneck for PHBV-based composite (low strain at break). Moreover, it would also allow the comparison with grafted cellulose from the previous study [264]. For the first time, the structure-properties relationships in PHBV/ViSh composites were studied. The present paper focused on tensile properties and water vapor permeability. The functional performance of composites depending largely on interfacial filler/matrix interactions, a gas-phase esterification of ViSh particles was performed and its effect on filler and composite properties was studied.

## II-2 Experimental

### II-2.1 Raw materials

Vine shoots (ViSh) were kindly provided by INRA Pech Rouge (Gruissan, France). They were collected on January 2017. The vine species was Syrah, which is the most common in France. The shoots were first air dried during 2 months then dried 48 hours in oven at 60°C. Successive dry grinding steps were carried to get particles displaying an apparent median diameter of about 50  $\mu\text{m}$ . A first coarse milling using a shredder (AXT 22D, Bosch, Germany) gave fragments of about 5 cm that were then ground with a knife mill (SM 300, Retch, Germany) using successively grids of 4 and 2 mm. Thereafter, an impact mill (Fine Impact Mill UPZ, Germany) equipped with a 0.3 mm grid was used at 18 000 rpm. Finally, resulting particles were ground in a ball mill (Faure Equipments, France) during 10 hours in jars filled with 3 kg of steel balls (25% of the internal volume) displaying diameters of 1.2, 1.6 and 2.6 cm diameter (ratio 1:1:1). 150 g of biomass were milled by batch and the speed was set at 50 rpm to avoid centrifugation. Once milled, ViSh particles were stored in a hermetic drum in presence of silica gel (around 0% RH) at room temperature. ViSh particles were used as they were for the preparation of composites, with no sieving.

A commercial poly(3-hydroxybutyrate-3-hydroxyvalerate) (PHBV) containing around 3% of valerate was purchased from NaturePlast (PHI002 grade).

### II-2.2 Gas-phase esterification of ViSh particles

Approximately 100 g of ViSh particles previously dried overnight at 60°C were subjected to a gas-phase esterification treatment using palmitoyl chloride (Sigma-Aldrich), as described by David et al. [340]. The experimental set-up used in this study was developed at CERMAV laboratory (Grenoble) [157]. The reaction was conducted in a 2 L reactor at 100 °C and 2 mbar during 15 h. ViSh particles were introduced in nylon mesh bags, which were positioned on a Teflon grid above the liquid reagent to avoid direct contact. The reagent was used in excess compared to surface hydroxyl groups (20 g). A constant nitrogen flow was used to evacuate the reaction by-products that were vacuum-pumped. At the end of the reaction time, grafted ViSh were purified by Soxhlet extraction with acetone reflux for 6 h. The final products were then oven dried at 60 °C overnight to remove any acetone leftover.

The same protocol was followed without reagent to obtain a control. Virgin, control and grafted ViSh particles were noted respectively ViSh-V, ViSh-C and ViSh-G.

## II-2.3 Preparation of composite materials

Composite compounds were first produced with a lab-scale twin screw extruder, with a L/D ratio of 40 and a screw diameter of 16 mm (Eurolab, Thermo Scientific, Karlsruhe, Germany). It was equipped with a rod die of 3 mm of diameter and a pelletizer to produce granules. The screw speed was 300 rpm and the flow rate was 1.0 kg.h<sup>-1</sup>. The temperature profile from the feeding to the die varied from 80 °C to 180 °C (80–160–160–160–160–170–170–180–180–160 °C). Virgin PHBV pellets and ViSh particles (either virgin or grafted) were previously dried at 60 °C before compounding. Four filler contents were used, i.e. 5, 10, 20 and 30 wt %. Composite films displaying a thickness of 300 µm were then prepared using a heated hydraulic press (20T, Pinette Emidecau Industries, Chalon-sur-Saône, France) from compounds previously produced by melt extrusion. Compounds were dried overnight at 60 °C before processing. Compounds were first heated during 5 min at 178 °C by putting the heating plates at the contact of granules and then compressed between two Teflon-coated plates (Taconic, France) for 4 min at 178°C by increasing gradually the pressure from 20 to 150 bars. Films were then allowed to cool between the two Teflon-coated plates at room temperature for 5 min under a weight (around 1 kg). All composite films were stored in a hermetic drum with silica gel (around 0%RH) at room temperature.

### II-2.3.1 Laser granulometry

Particle size distribution was determined from 0.01 µm to 10000 µm using a Mastersizer 2000 laser granulometer in wet mode (Malvern Instruments Ltd., United Kingdom). Particles were suspended in ethanol 95% (v/v). Three values were identified to characterize the sample and allow comparison. The value of d<sub>10</sub> represents the particle size diameter for which 10% of particles (in volume or number) have a diameter below. Similarly, d<sub>50</sub> represents de median and d<sub>90</sub> the diameter from where the cumulative distribution of particles is 90%. Measurements were done with at least 5 repetitions.

### II-2.3.2 Solid-state <sup>13</sup>C NMR

Solid-state <sup>13</sup>C NMR experiments were performed with a Bruker Avance DSX 400 MHz spectrometer operating at 100.6 MHz, using the combination of cross-polarization, high-power proton decoupling and magic angle spinning (CP/MAS). Standard conditions were 2000 scans with 2 ms of contact and 2 s of recycle delay. The acquisition time was 35 ms and the sweep width was 29400 Hz.

### II-2.3.3 Surface free energy

ViSh particles surface free energies were assessed by contact angle measurements, as already described by David et al. [340]. The dispersive ( $\gamma^d$ ) and polar ( $\gamma^p$ ) components were evaluated



by applying the Owens-Wendt approach [247] by using five reference liquids, namely distilled water, ethylene glycol, diiodomethane, formamide and glycerol.

#### II-2.3.4 Thermogravimetric analysis (TGA)

TGA under nitrogen flow ( $50 \text{ mL}\cdot\text{min}^{-1}$ ) was carried out using a Mettler TGA2 apparatus (Schwerzebbach, Switzerland) equipped with a XP5U balance. The samples were heated at  $10 \text{ }^\circ\text{C}\cdot\text{min}^{-1}$  from  $25 \text{ }^\circ\text{C}$  to  $600 \text{ }^\circ\text{C}$  under nitrogen flow of  $50 \text{ mL}\cdot\text{min}^{-1}$ . The results were analyzed using STARe software. The maximum degradation temperature ( $T_{\text{deg}}$ ) corresponded to the temperature at which the degradation rate was maximum. The onset and offset degradation temperatures ( $T_{\text{onset}}$  and  $T_{\text{offset}}$ , respectively) were measured respectively when the first derivative of the weight loss became higher than  $0.1 \text{ \%}\cdot\text{C}^{-1}$  and lower than  $0.1 \text{ \%}\cdot\text{C}^{-1}$ . Analyses were done in triplicate.

#### II-2.3.5 Scanning Electron Microscope (SEM)

The samples were examined with a Hitachi S4800 Scanning electron microscope (Technology platform of IEM Laboratory of the Balard Chemistry pole) with an acceleration voltage of 2 kV after a coating with Pt by cathode pulverization. Observations were realized by the help of Didier Cot (IEM, Montpellier). In case of cryo-fractured section observations, the specimens were frozen in liquid nitrogen then fractured before coating.

The aspect ratio of particles after milling was determined with a AZ100 macroscope (Nikon, JP). Images were treated using the Image J software that viewed each particle as an ellipse and measured major and minor axes. Average aspect ratio values (ratio between the major axis and the minor axis) were calculated from both the number and the volume distributions.

#### II-2.3.6 Differential Scanning Calorimetry (DSC)

The thermal properties of composites were investigated using a thermo-modulated calorimeter (Q200 modulated DSC, TA Instruments, New Castle, USA). Approximately 10 mg of sample were analyzed in hermetically sealed aluminium pans (Tzero Aluminium Hermetic pan, TA Instruments, New Castle, USA). Analyses were performed in triplicate. The purge gas was nitrogen, with a flow rate of  $50 \text{ mL}\cdot\text{min}^{-1}$ . Each sample was first heated up to  $200 \text{ }^\circ\text{C}$  at  $10 \text{ }^\circ\text{C}\cdot\text{min}^{-1}$ , then cooled at  $10 \text{ }^\circ\text{C}\cdot\text{min}^{-1}$  until temperatures reached  $-30 \text{ }^\circ\text{C}$ , and finally heated again from  $-30 \text{ }^\circ\text{C}$  to  $200 \text{ }^\circ\text{C}$  at a heating rate of  $10 \text{ }^\circ\text{C}\cdot\text{min}^{-1}$ . From the resultant thermogram, crystallization temperature ( $T_c$ ), melting temperature ( $T_m$ ) and melting enthalpy ( $\Delta H_m$ ) were measured. The polymer crystallinity was calculated as follows (Eq.40):

$$X_c = \frac{\Delta H_m}{\Delta H_m^0 \left(1 - \frac{w}{100}\right)} \times 100 \quad \text{Eq.40}$$

where  $\Delta H_m^0$  was the enthalpy of melting 100% crystalline polymer, (146 J·g<sup>-1</sup> for PHBV [252]), and  $w$  was the weight fraction of the matrix in the composite.

### II-2.3.7 Dynamic vapor sorption

Water vapor sorption was measured at 20 °C using a controlled atmosphere micro-balance (DVS, Surface Measurement System Ltd., London, UK). A Cahn D-200 microbalance, with a precision of 0.1 µg, recorded the mass evolution of the materials according to the relative humidity. A pre-drying step was first run at 60 °C in an oven, then the sample was placed in the DVS equipment at 0% RH for until reaching the equilibrium at 20 °C. In the case of cellulose, 1 mg of cellulose was deposited in an aluminum pan (DSC Tzero<sup>®</sup> pans provided by TA Instruments), which was placed in the DVS nacelle. Water vapor sorption isotherms were determined from the equilibrium moisture contents at each RH step. Tests were performed at least in duplicate.

### II-2.3.8 Water vapor permeability

Water vapor permeability (WVP) was gravimetrically determined at 23 °C using a modified ASTM E96 procedure. Discs of films (five repetitions) were sealed in permeation cells filled with distilled water that were put into a desiccator containing silica gel. A relative humidity (RH) gradient equal to 0–100% was obtained (assuming that RH on the silica gel is negligible). The permeation surface was 9.08 cm<sup>2</sup>. Periodic weightings determined the rate of water vapor movement through the films. WVP (mol·s<sup>-1</sup>·Pa<sup>-1</sup>·m<sup>-1</sup>) was calculated from Eq. 41 :

$$\text{WVP} = \frac{S \times e}{3600 \times A \times \Delta P \times M_{\text{H}_2\text{O}}} \quad \text{Eq. 41}$$

where  $S$  was the slope of the weight change from the straight line (g·h<sup>-1</sup>),  $A$  the permeation area (m<sup>2</sup>),  $e$  the average specimen thickness (m),  $\Delta P$  the saturation vapor pressure at 23 °C (2809 Pa), and  $M_{\text{H}_2\text{O}}$  the molar mass of water (g·mol<sup>-1</sup>).

### II-2.3.9 Tensile tests

Mechanical properties were evaluated through tensile tests conducted at 23°C by a tensile tester (Zwick BZ2.5/TN1S, Metz, France) on dog-bone shaped film specimens (width of 4 mm and

gauge length of 45 mm). Composite specimens were kept in a conditioned room at 23 °C and 50% humidity for at least 24 h before testing. Young's modulus ( $E$ ), nominal stress at break ( $\sigma$ ), nominal strain at break ( $\epsilon$ ) and energy at break were determined from stress–strain curves obtained with a cross-head speed of 1 mm·min<sup>-1</sup>. At least ten replicates were realized for each formulation (5, 10, 20, and 30 wt %).

## II-3 Results and discussion

### II-3.1 Impact of gas-phase esterification on ViSh particles intrinsic characteristics

#### II-3.1.1 Degree of substitution

The occurrence of the grafting and its extent was investigated by solid-state <sup>13</sup>C CP-MAS NMR. Figure 75 shows the spectra of the untreated, control and grafted ViSh particles. They all exhibit the characteristic signals of both cellulose and lignin. The assignment of the different carbon signals was achieved according to literature [124,341,342]. Concerning the virgin sample ViSh-V, the main peaks, between 60 and 115 ppm, corresponded to the polysaccharidic chains carbons that includes both cellulose and hemicelluloses, with the C1 peak at 105 ppm present in all polysaccharide and the C4 signal divided in two peaks, i.e. the first one at 83 ppm corresponding to amorphous regions (cellulose and hemicelluloses) and the second one at 89 ppm corresponding to crystalline regions of cellulose. These two latter peaks could be used to determine the crystallinity of the substrate according to the Newman method (Eq. 42) [343]:

$$X_C = \frac{I_{C4\ cry}}{I_{C4\ cry} + I_{C4\ am}} \quad \text{Eq. 42}$$

Using this method, all the samples had a crystallinity of 30 %, that includes the contribution of hemicelluloses [344]. This results confirmed that the reaction did not reduce the crystallinity staying at the surface of the particles.

The peak at 56 ppm was assigned to methoxy carbons of lignin while the broad signals between 130 and 160 ppm were assigned to aromatic ring carbons of lignin. Besides, peaks between 10 and 40 ppm could be assigned to methyl, methylene and alkyl carbons of lignin [345] but also to possible lipophilic components (aldehydes, sterol ester and ester waxes) [92]. These lipophilic components could also explain the carboxyl signals between 170 and 182 ppm. It is thus worth noting that the spectrum of virgin ViSh particles already revealed the presence of carboxylic carbons (peak at 172 ppm) and of aliphatic carbons (peaks between 10 and 40 ppm). The spectra of virgin and control ViSh-V and ViSh-C samples were very similar with no distinct difference. On the contrary, ViSh-G was characterized by a slight increased intensity of the carbonyl signal at 173 ppm but more visually with the higher intensity of the alkyl signal at

30 ppm compared to virgin particles (Figure 75). It evidenced the grafting of the fatty acid on the particles.

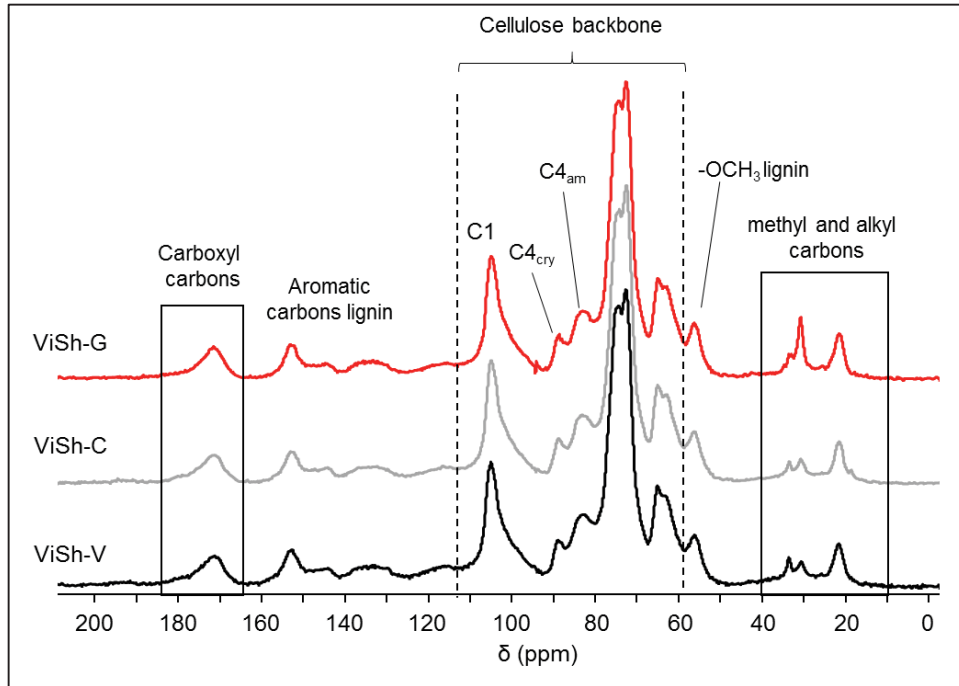


Figure 75. Solid  $^{13}\text{C}$  NMR spectra of ViSh-V (—), ViSh-C (—) and ViSh-G (—).

The esterification was quantified calculating the degree of substitution (DS) that is usually applied for cellulosic substrate. The lignocellulose being more complex than pure cellulose, the esterification product could be also difficult to be identified. Hydroxyl groups from lignin and hemicellulose can also react during the esterification. Thus, the DS was calculated by assuming that only hydroxyl groups of cellulose were the reaction sites, as already assumed in case of wood esterification [341]. The DS was calculated from Eq. 43 et Eq. 44 using the integral of carbon C1 as reference to normalize the integral of the carboxyl signal ( $I_{\text{C=O}}$ ) and integral of alkyl carbons ( $I_{\text{C-H}}$ ):

$$\text{DS}_{\text{C-H}} = \frac{I_{\text{C-H}}(\text{ViSh-G}) - I_{\text{C-H}}(\text{ViSh-C})}{15} \quad \text{Eq. 43}$$

$$\text{DS}_{\text{C=O}} = \frac{I_{\text{C=O}}(\text{ViSh-G}) - I_{\text{C=O}}(\text{ViSh-C})}{1} \quad \text{Eq. 44}$$

The DS of ViSh-G was calculated with respect to ViSh-C because during the Soxhlet extraction with acetone some extractives might be removed. The calculated values for  $\text{DS}_{\text{C-H}}$  and  $\text{DS}_{\text{C=O}}$

were respectively 0.007 and 0.011. The DS were lower than for the grafting of cellulose particles in the same experimental conditions (DS = 0.02) [340]. It was most probably due to the presence of lignin that has a different reactivity and a reduced density of hydroxyl groups.

The  $^{13}\text{C}$  NMR analysis proved the surface grafting with a fatty acid chloride of the ViSh particles without degrading their crystallinity.

### II-3.1.2 ViSh particle size and morphology

The particle size distribution was quantitatively assessed by laser granulometry, by assimilating particles to spheres of equivalent diameter (Table 37). It can be noted that the volume spans were high, reflecting the polydispersity of the ground ViSh sample. The  $d_{50}$  in number was very low because no sieving or sorting was performed in order to recover all the biomass and not generate waste. The grafting had no significant impact on the apparent median diameter of particles.

Table 37. ViSh particles apparent diameters (in volume/ in number)

Materials	d10 ( $\mu\text{m}$ )	d50 ( $\mu\text{m}$ )	d90 ( $\mu\text{m}$ )	Span*
ViSh-V	$7 \pm 1 / 0.5 \pm 0.1$	$49 \pm 1 / 0.6 \pm 0.1$	$191 \pm 10 / 1.2 \pm 0.1$	3.8 / 1.2
ViSh-C	$7 \pm 1 / 0.5 \pm 0.1$	$48 \pm 1 / 0.6 \pm 0.1$	$192 \pm 10 / 1.2 \pm 0.1$	3.8 / 1.2
ViSh-G	$6 \pm 1 / 0.5 \pm 0.1$	$48 \pm 1 / 0.6 \pm 0.1$	$197 \pm 14 / 1.3 \pm 0.1$	4.0 / 1.2

$$*\text{Span} = (d_{90}-d_{10})/d_{50}$$

Macroscopy and image analysis showed that ViSh particles were characterized by low aspect ratio values, ranging between 1.53 and 1.87 for number and volume averages respectively.

The morphology was qualitatively assessed by SEM observations (Figure 76). At low magnification, all the samples displayed a similar appearance. Zooming on particles, ViSh-V (A2), ViSh-C (B2) and ViSh-G (C2) did not displayed difference at their surface. They all have a moderately rough surface with residual dusts aggregated on particles. It could be concluded from these analyses that the macroscopic structure of particles was not affected by the chemical treatment.

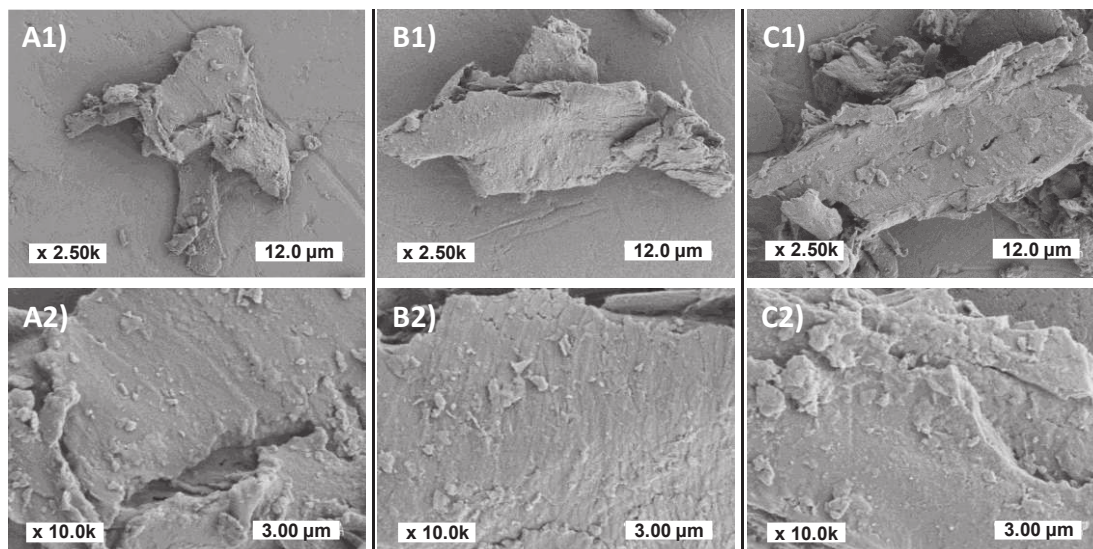


Figure 76. SEM pictures of (A1-2) S-virgin and grafted cellulose (B1-2) S-control and (C1-2) S-grafted particles at different magnifications.

### II-3.1.3 Wettability of grafted ViSh particles

The surface free energies of PHBV film and compressed tablets of ViSh particles were deduced from contact angles measurements (Table 38). Virgin ViSh particles had a relative low polar component ( $10.2 \text{ mJ}\cdot\text{m}^{-2}$ ). As expected, this value was lower than the polar component of cellulose particles due to the presence of lignin. However, common lignocellulosic fibers usually displayed polar component between 15 and  $25 \text{ mJ}\cdot\text{m}^{-2}$  and are considered as hydrophilic by nature [37]. Different reasons can explain this result. Lignocellulosic substrates are heterogeneous and it is often described that cellulose is mostly present in the bulk of particles or fibers. Thus non-cellulosic components can be present in a larger proportion at the surface and induce low polarity and low surface free energy. No data concerning the vine shoots surface free energy were found in the literature. In an overview of literature data for surface free energy of wood, it was reported that Douglas fir aspen or maple can display such value with polar component between 11.8 and  $16.4 \text{ mJ}\cdot\text{m}^{-2}$  and dispersive component between 36.2 and  $41.8 \text{ mJ}\cdot\text{m}^{-2}$  [346]. For example, Van Hazendonk et al. found that flax fibers were very hydrophobic with polar component lower than  $5 \text{ mJ}\cdot\text{m}^{-2}$ . The surface free energy of  $28.5\text{-}34.2 \text{ mJ}\cdot\text{m}^{-2}$  increased after fatty substances extraction to  $40.3\text{-}43.1 \text{ mJ}\cdot\text{m}^{-2}$  [347]. An additional extraction of pectins and hemicelluloses further raised the fiber surface tension to reach the one of pure cellulose.

Gas-phase esterification induced a drastic decrease of the polar component of vine shoot particles, from 10.2 down to  $2.2 \text{ mJ}\cdot\text{m}^{-2}$ , together with an increase of the dispersive component from 41.7 up to  $49.5 \text{ mJ}\cdot\text{m}^{-2}$ . The increase in hydrophobicity was clearly highlighted by the increase in contact angles formed with polar solvents, including water (increase from  $59^\circ$  for ViSh-V to  $114^\circ$  for ViSh-G), ethylene glycol, formamide and glycerol. Results obtained for the

ViSh-C demonstrated that such an increase in hydrophobicity was not ascribed to the experimental conditions notably the temperature treatment or the Soxhlet extraction. Interestingly, the ViSh-C sample that has been washed by Soxhlet displayed a slight increase of the polar component suggesting a partial removal of non-polar component. This result was consistent to the previously quoted work of Van Hazendonk et al. [347].

Table 38. Contact angle values ( $^{\circ}$ ) with different reference liquids, polar ( $\gamma^p$ ) and dispersive ( $\gamma^d$ ) components of the surface free energy ( $\gamma$ ) of PHBV, S-virgin, S-control and S-grafted.

Sample	Contact angle ( $^{\circ}$ )					Surface free energy ( $\text{mJ}\cdot\text{m}^{-2}$ )		
	Water	Ethylene glycol	Diiodom ethane	Formamide	Glycerol	$\gamma^p$	$\gamma^d$	$\gamma$
PHBV	$68 \pm 2$	$45 \pm 2$	$20 \pm 2$	$39 \pm 1$	$49 \pm 3$	6.2	42.6	48.8
S-Virgin	$59 \pm 4$	$27 \pm 3$	$24 \pm 3$	$30 \pm 3$	$46 \pm 4$	10.2	41.7	51.8
S-Control	$58 \pm 3$	$29 \pm 2$	$22 \pm 4$	$27 \pm 2$	$42 \pm 3$	10.7	42.2	52.9
S-Grafted	$114 \pm 3$	$73 \pm 1$	$25 \pm 4$	$62 \pm 2$	$93 \pm 3$	2.2	49.5	51.7

Finally, it is worth noticing that PHBV was not that hydrophobic displaying a water contact angle of  $68^{\circ}$ , i.e. lower than  $90^{\circ}$ . The measure has been carried out after stabilization of the drop on the surface of the film. Berthet et al. found PHBV with the same grade to be highly hydrophobic with almost null polar component and a water angle of  $100^{\circ}$  [13]. In another study with the same PHBV grade, the water contact angle measured was  $60^{\circ}$  [348]. Luo et al. reported a water contact angle of  $85.8^{\circ}$  although the surface energy was very closed to the present results [349]. Therefore, PHBV was less hydrophobic than PP, which had a water contact angle of  $97.2^{\circ}$  and a polar component of  $2.0 \text{ mJ}\cdot\text{m}^{-2}$ , due to the presence of ester bonds. In this sense, Ahankari et al. showed that wheat straw fillers had better compatibility with PHBV matrix as compared to PP matrix [193].

#### II-3.1.4 Water vapor sorption of ViSh particles

Dynamic vapor sorption (DVS) measurements were performed to investigate the impact of grafting on the water vapor sorption in ViSh particles (Figure 77). The water uptake of virgin ViSh increased with the relative humidity displaying a sigmoidal curve already observed for cellulosic materials [280]. In the first part, lower than 60 %RH, water was sorbed by hydrogen bonding then its concentration increased linearly in porous ViSh particles. In the second part, over 60 %RH, the water sorption increased exponentially that can be explained by a clustering effect and the capillarity of water in the material [282]. Compared to cellulose sample from [340], ViSh particles absorbed less water especially between 20 and 80 %RH. This can be explained by the presence of lignin that it known to have a lower water sensitivity.

ViSh-V and ViSh-C particles displayed identical isotherms that were very similar to the cellulosic substrate. The water uptake of ViSh-G was similar compared to particles without

treatment, however from 50 %RH a slight decrease (10%) was observed. This showed that the grafted hydrophobic moieties prevented the water vapor sorption. The slight decrease of crystallinity after grafting could explain the low difference in water vapor sorption since sorption occurs mainly in amorphous regions. Here, the grafting effect was less obvious than for water contact angles measurements because the water vapor reach more easily bulk remaining hydroxyl groups than liquid water. One has to remind that the very low grafting densities (DS=0.01 i.e. around 1% of the hydroxyl groups) is enough to modify the extreme surface [340] and hence change drastically the surface properties without changing the bulk properties.

These results showed an increase of moisture resistance of the ViSh after chemical treatment even if it was not drastic. According to these previous results [340], moisture sorption was significantly affected by the degree of substitution of such as reaction. Thus, with higher DS, it could be expected to reach lower water sorption.

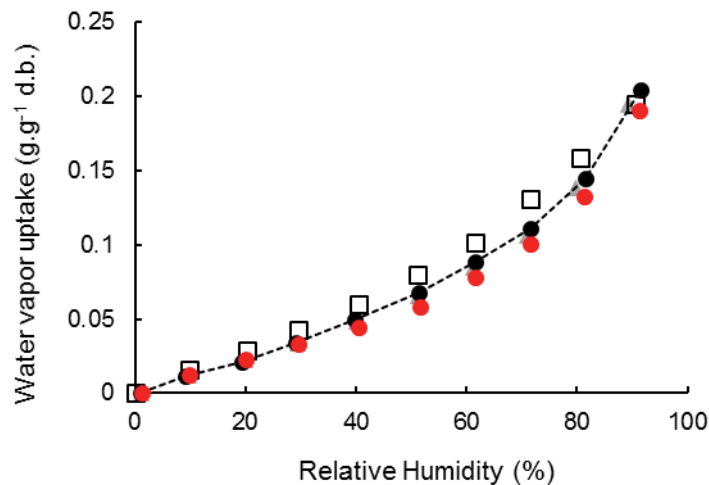


Figure 77. Water vapor sorption isotherm of ViSh-V (●), ViSh-C (▲), ViSh-G (●) and cellulose (□) from [340].

## II-3.2 Functional properties of PHBV/ViSh composites

### II-3.2.1 Morphology of composites: Qualitative evaluation of the filler/matrix interface

The morphology of composites was qualitatively assessed by SEM observations of the cross-section of cryo-fractured PHBV-based materials (Figure 78). Differences in interfacial filler/matrix adhesion were expected from the previous contact angle measurements (section II-3.1.3). In the case of a filler content of 20 wt%, fracture surfaces were rough and uneven. No difference of filler dispersion state was detected between the samples. Mechanical shearing forces induced during extrusion were probably enough to break potential particle aggregates.



ViSh fillers, even not grafted, were found to be quite well embedded within the PHBV matrix and only small voids were noticed at the filler/matrix interface. From these SEM observations, it was difficult to conclude in a better filler/matrix adhesion in the case of ViSh-G. Indeed, composites displayed similar facies (Figure 78A and Figure 78B). The increased hydrophobicity of ViSh-G did not seem to improve the wettability of the filler by the PHBV matrix that was already good.

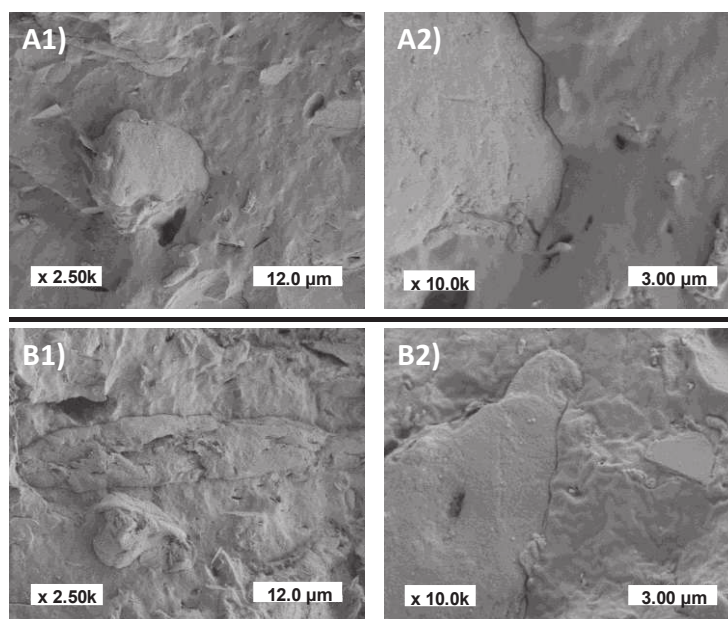


Figure 78. SEM pictures of cryo-fractured sections: (A1, A2) PHBV-20ViSh-V, (B1, B2) PHBV-20ViSh-G.

### II-3.2.2 Thermal properties

The degree of PHBV crystallinity in composite samples and their thermal properties were determined by DSC (Table 39). The PHBV matrix display a melting temperature of 174°C and a crystallization temperature of 123 °C. The relative high crystallinity of the matrix, 69%, was due to the presence of boron nitride as nucleating agents added by the supplier. The crystallinity ( $X_c$ ) gradually decreased with the filler content from 65 % to 59 % for PHBV-30ViSh-V and to 61 % for PHBV-30ViShG. The decrease in  $X_c$  was thus slightly limited by the gas-phase esterification.

Melting ( $T_m$ ) and crystallization ( $T_c$ ) temperatures followed the same trend towards filler content for both ViSh particles grafted or not. No nucleation of PHBV was induced by the fillers. The significant change due to the grafting in the thermal properties of composites were observed

Table 39. Melting temperature ( $T_m$ ), crystallization temperature ( $T_c$ ) and crystallinity of PHBV-based composites

	$T_m^1$	$T_m^2$	$T_c$	$X_c^1$	$X_c^2$
PHBV	$174 \pm 1$	$170 \pm 1$	$123 \pm 1$	$65 \pm 1$	$69 \pm 1$
PHBV-5ViSh-V	$173 \pm 1$	$169 \pm 1$	$120 \pm 1$	$64 \pm 2$	$68 \pm 1$
PHBV-5ViSh-G	$173 \pm 1$	$169 \pm 1$	$119 \pm 1$	$64 \pm 2$	$67 \pm 1$
PHBV-10ViSh-V	$172 \pm 1$	$169 \pm 1$	$118 \pm 1$	$63 \pm 2$	$67 \pm 1$
PHBV-10ViSh-G	$172 \pm 1$	$167 \pm 1$	$117 \pm 1$	$64 \pm 1$	$65 \pm 1$
PHBV-20ViSh-V	$170 \pm 1$	$167 \pm 2$	$115 \pm 2$	$61 \pm 2$	$63 \pm 3$
PHBV-20ViSh-G	$171 \pm 1$	$166 \pm 2$	$114 \pm 2$	$62 \pm 2$	$63 \pm 2$
PHBV-30ViSh-V	$169 \pm 1$	$166 \pm 3$	$113 \pm 3$	$59 \pm 1$	$63 \pm 2$
PHBV-30ViSh-G	$170 \pm 1$	$166 \pm 3$	$113 \pm 3$	$61 \pm 1$	$64 \pm 2$

<sup>1</sup>Measured at the first heating scan. <sup>2</sup>Measured at the second heating scan.

Figure 79 shows the TGA and DTGA curves of the PHBV, ViSh fillers and PHBV/ViSh composites (filler content of 30 wt%). The PHBV weight loss occurred in a one-step degradation process from 270 to 313 °C as proven by the single peak in DTG. The degradation temperature of PHBV was 298 °C (Table 40).

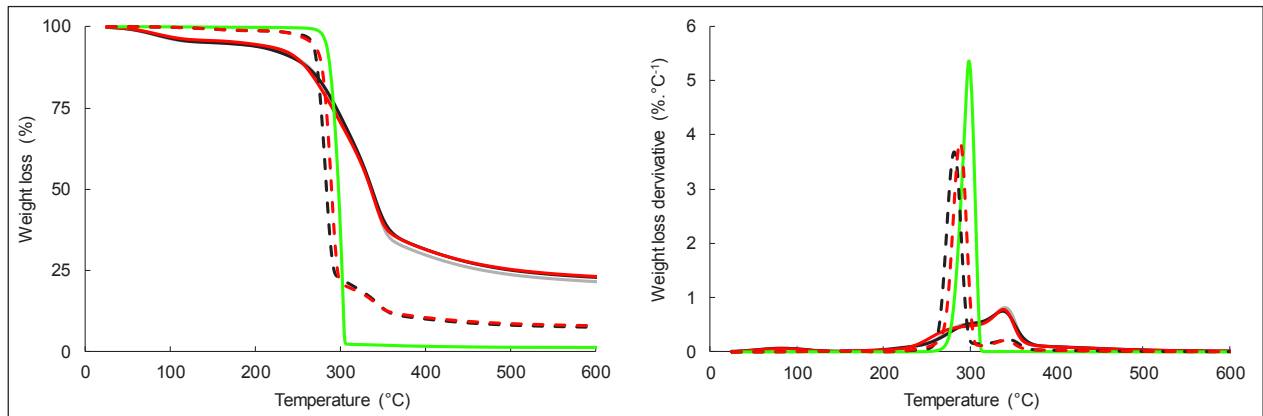


Figure 79. TG (right) and DTG (left) curves of PHBV (—), ViSh-V (—), S-control (—) and ViSh-G (—); PHBV-30ViSh-V (—); PHBV-30ViSh-G (—) under  $N_2$ .

Filler thermal stability is an important aspect to be considered regarding thermoplastic composites. If the studied filler has a low degradation temperature, it could be not suitable for producing composites with thermoplastics. In case of PHBV-based composite, the maximum processing temperature was 180°C.

The TGA curves displayed an initial decrease below 120 °C due to loss of moisture. Then, the decomposition of the ViSh filler started around 230 °C with the decomposition of pectin and non-structural hemicelluloses present in the ViSh. This suggests that these ViSh can be suitable for processing with polymers such as polyolefins having a melt temperature below 220 °C. The melt extrusion, used in the present study, did not thermally degraded ViSh fillers. The major

decomposition temperature of ViSh at 340 °C is due to the decomposition of cellulose. The ViSh residues at 600 °C under nitrogen represented 22% indicating a high amount of lignin [350]. The thermal stability of ViSh was close to the one of wood flour [351]. Gas-phase esterification had no significant effect on the thermal stability of ViSh particles.

The thermal degradation of PHBV-ViSh composites occurred in a two-step degradation process. The first thermal degradation step corresponded to the PHBV matrix, then the second degradation step was ascribed to degradation of ViSh fillers. The composite degradation maxima occurred at temperature a little lower than that of PHBV. A shifting was observed from 298 °C for neat PHBV to 282 °C for PHBV-30ViSh-V composites and 289°C for PHBV-30ViSh-G materials. The pro-degrading effect of ViSh was thus lower in the case of grafted ViSh.

Table 40. Results of thermogravimetric analysis

Materials	T <sub>deg(1)</sub> (°C)	T <sub>deg(2)</sub> (°C)	T <sub>onset</sub> (°C)	T <sub>offset</sub> (°C)
PHBV	298 ± 1	-	270 ± 1	313 ± 2
ViSh-V	-	338 ± 1	233 ± 1	387 ± 1
ViSh-C	-	341 ± 1	234 ± 1	387 ± 1
ViSh-G	-	338 ± 1	233 ± 1	390 ± 1
PHBV-5ViSh-V	293 ± 1	340 ± 2	268 ± 1	307 ± 2
PHBV-5ViSh-G	293 ± 1	341 ± 1	267 ± 1	307 ± 1
PHBV-10ViSh-V	287 ± 1	346 ± 3	263 ± 1	302 ± 1
PHBV-10ViSh-G	290 ± 1	342 ± 2	262 ± 1	304 ± 1
PHBV-20ViSh-V	282 ± 1	345 ± 1	259 ± 1	300 ± 1
PHBV-20ViSh-G	288 ± 1	342 ± 1	257 ± 1	302 ± 1
PHBV-30ViSh-V	282 ± 1	344 ± 1	256 ± 1	361 ± 1
PHBV-30ViSh-G	289 ± 1	341 ± 1	253 ± 1	356 ± 1

### II-3.2.3 Mechanical Properties

The properties of PHBV-based composites filled with ViSh grafted or not are summarized in Table 41. First, it can be noted was that composites had lower mechanical properties than PHBV matrix. As soon as ViSh particles were added the strain at break of the composite decreased, 38% reduction in case of PHBV-5ViSh-V. The strain decreased with the filler content reaching 1.14% for PHBV-30ViSh-V, which showed the brittle characteristic of the composite. The gas phase esterification did not impact significantly this property. Similarly, the effect of the grafting was studied on the stress at break. In both cases, for virgin and grafted ViSh, the composite stress at break was reduced with the filler content. Comparably, the addition of cellulose particles were shown to reduce the ultimate properties of the biocomposites [264]. However, the grafting had limited this negative impact which was not the case in the present study with lignocellulosic particles. It is worth noting that the decrease in stress and strain at break was slower in the ViSh particles than for the best case of cellulose particles or wheat straw [33]. The addition of ViSh fillers induced higher values of Young's moduli compared with

that from the neat PHBV. Modulus of the biocomposite was expected to be higher as the modulus of these natural fillers might be much higher than the matrix [338]. However, this increase was not higher than 30% because of the small particles size introduced.

Table 41. Tensile properties (Young's modulus, nominal stress at break, nominal strain at break, and energy at break) of PHBV-based biocomposites.

Materials	Young's modulus (GPa)	Stress at break (MPa)	Strain at break (%)	Energy at break (mJ.cm <sup>-3</sup> )
PHBV	2.6 ± 0.1	36.5 ± 0.4	2.65 ± 0.36	649 ± 110
PHBV-5ViSh-V	3.0 ± 0.1	35.1 ± 1.4	1.62 ± 0.19	344 ± 62
PHBV-5ViSh-G	3.0 ± 0.1	35.4 ± 1.3	1.71 ± 0.17	373 ± 54
PHBV-10ViSh-V	2.9 ± 0.1	31.4 ± 1.9	1.56 ± 0.12	299 ± 38
PHBV-10ViSh-G	2.9 ± 0.1	31.4 ± 1.2	1.55 ± 0.15	297 ± 38
PHBV-20ViSh-V	3.1 ± 0.1	29.6 ± 1.1	1.25 ± 0.06	218 ± 21
PHBV-20ViSh-G	3.2 ± 0.1	28.2 ± 0.7	1.14 ± 0.06	186 ± 15
PHBV-30ViSh-V	3.3 ± 0.2	27.3 ± 1.0	1.14 ± 0.07	186 ± 16
PHBV-30ViSh-G	3.2 ± 0.1	26.3 ± 0.4	1.08 ± 0.04	186 ± 9

As already explained in section II-3.1.3, PHBV was not as hydrophobic than polyolefins. This could also explain why the grafting effect was not visible for mechanical properties in PHBV-based composites. Therefore, from tensile tests, no improvement of interfacial adhesion or adherence was evidenced. Composites with 30 wt% of ViSh displayed acceptable tensile properties. An effort should be done concerning the strain at break.

#### II-3.2.4 Water Vapor Permeability (WVP)

Water vapor permeability (WVP) of PHBV-based materials was assessed for increasing ViSh filler content (Figure 80). The WVP value for PHBV film,  $3.8 \times 10^{13}$  mol.m/(m<sup>2</sup>.s.Pa), was in accordance with previous results [264]. The WVP of the present composites increased with the filler content. It was noticed that the crystallinity degree of the matrix decreased by the presence of the filler, thus the matrix was more permeable to water molecules. This increase was limited by the surface grafting of ViSh particles for high filler contents (20 and 30 wt%). As an example, the WVP value of the film containing 30 wt% of filler was 27 % lower with ViSh-G than with ViSh-V. It can be ascribed to the more hydrophobic character of grafted particles. Modified filler hydrophobic nature was evidenced by water contact angle and surface free energy. Voids at the interface were promoted by weak interfacial adhesion and agglomeration of fillers, facilitating the permeability for water. The grafting probably improved a little the wettability of the ViSh particles. Similar results were observed in the case of gas-phase esterified cellulose [264] or torrefied wheat straw [13] in PHBV films.

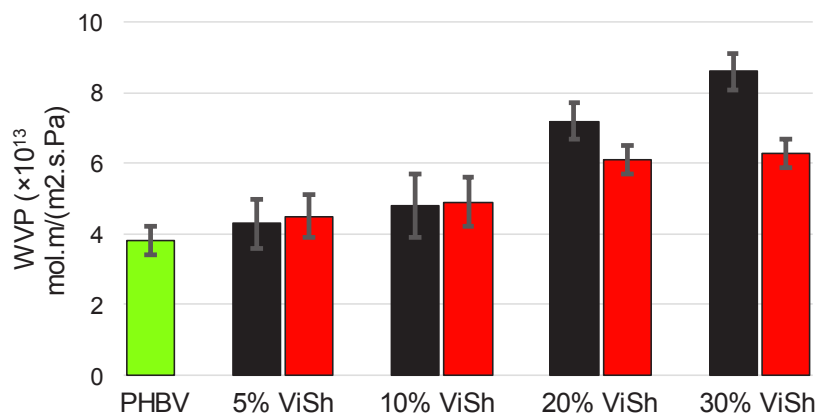


Figure 80. Water vapor permeability (WVP) in PHBV-based biocomposites with ViSh-V (■) and ViSh-G (■) fillers.

## II-4 Conclusion

Vine shoots particles of around 50  $\mu\text{m}$  were incorporated in PHBV-based materials. It was shown that this addition reduced the mechanical properties of PHBV. The thermal stability and the crystallinity PHBV also decreased for increasing filler content. However, these decreases were low and perfectly acceptable. Thus, green composites can surely provide a sustainable alternative to fossil sourced materials and a new way to manage agro-residues. Furthermore, at the economical point of view, the use of ViSh would decrease significantly the final cost of PHBV-based composites.

Besides, the surface compatibilization of ViSh particles with fatty chains via ester formation was achieved without solvent.  $^{13}\text{C}$ -NMR of the grafted particles revealed that the chemical modification was limited to the fiber surface. The backbone of lignocellulose was not altered with a constant crystallinity index. After grafting, the contact angle values jumped from  $59^\circ$  to more than  $114^\circ$ , which confirmed the hydrophobization of the ViSh particles. Mechanical properties of PHBV composites filled with 10, 20 and 30 wt% of particles revealed that the chemical grafting did not improved their reinforcing effect on the matrix. This results can be explained by the fact that PHBV is not such hydrophobic compared to polyolefins and the ViSh already less hydrophilic compared to virgin cellulose. The water vapor permeability of composite films with 30 wt% of ViSh was reduced was by 27% with grafted fillers. The gas phase esterification showed higher effect in cellulose-based composites than in lignocellulose-based composites.

Funding: This work was carried out in the framework of the NoAW project, which is supported by the European Commission through the Horizon 2020 research and innovation program under the Grant Agreement No. 688338.

### III. Eco-conversion of two winery lignocellulosic wastes into fillers for biocomposites (Article 5)

*Grégoire David<sup>a</sup>, Micaela Vannini<sup>b</sup>, Laura Sisti<sup>b</sup>, Anna-Maria Celli<sup>b</sup>, Nathalie Gontard<sup>a</sup>, Hélène Angellier-Coussy<sup>a</sup>*

<sup>a</sup> *JRU IATE 1208 – Univ Montpellier, CIRAD, INRA, Montpellier SupAgro, 2 Place Pierre Viala, Bat 31, F-34060 Montpellier 01, France*

<sup>b</sup> *Dept. of Civil, Chemical, Environmental, Materials Engineering, University of Bologna, Via Terracini 28, 40131, Bologna, Italy*

#### III-1 Introduction

The world plastic production is increasing every year, reaching 350 million tons in 2018 [7]. The growing associated environmental concerns, notably its accumulation in nature, and resulting new legislations push all the stakeholders to rethink plastic production and usage, including the search for more ecologically friendly materials. Among the different biosourced and biodegradable polymers commercially available, poly(hydroxy-3-butyrate-co-3-valerate) (PHBV), is a bacterial polyester presenting the advantage of being potentially prepared from agro-residues. Its mechanical properties are close to those of common fossil-based thermoplastic such as polypropylene (PP). However, as compared to conventional plastics, PHBV is still available at high price (around 5 €/kg), which limits its use to niche market applications. A larger use of PHBV would require to increase production capacities and to decrease its production cost and/or to find strategies to decrease the overall cost of developed materials. The incorporation of low cost lignocellulosic fillers constitutes one answer to this latter issue, while reducing the environmental impact of the materials and modulating their functional properties.

In parallel, agriculture is a huge generator of residues, including a large proportion of solid lignocellulosic biomass, which can be considered as the most highly available renewable resource on Earth at the lowest cost. Its upcycling as fillers in biocomposites is an attractive valorization route, avoiding the use of dedicated crops and proposing a new route of waste management [18,23]. In this context, the European project H2020 NoAW aimed at extending the state-of-the-art by developing eco-efficient products including biocomposites materials. Within the different agricultural activities, viticulture is one of the most spread crops in the world [58], producing a large amount of residues, such as wine pomaces and vine shoots.

Vine shoots (ViSh) are agricultural residues from vine pruning, with approximately 2 tons·ha<sup>-1</sup> (dry basis) generated per year, corresponding to an annual world production of 15 million tons [46]. They are usually ground and left in the field as organic amendment or burned to prevent proliferation of phytopathogens [352]. This is due to their very low economic value. The composition of ViSh is characterized by holocellulose (68%), lignin (20%), proteins (5%) and the rest includes small amounts of lipids, polyphenols and ashes [47,48]. Some studies explored the use of ViSh as a source of high added value products, such as polyphenols for their antioxidant properties [353] and especially resveratrol or viniferin [52]. Rayne et al. estimated that the extraction of resveratrol and viniferin from ViSh waste may reach a global economic value of over \$30 billion [51].

Wine pomace (WiPo) is one of the most abundant solid by-products generated during wine-making process. It corresponds to the solid residue from the pressing of fresh grapes, whether or not fermented [354] and are constituted of stems, skin and seeds. At least 20% of the grape weight become pomace, generating more than 10 million tons every year in the world [355]. A small portion of grape pomace follows the traditional ways of valorization, i.e. distillation to produce different types of spirits and liquors, or used as fertilizer after industrial or home composting, or as animal feed. However, the main part of pomaces is traditionally poorly exploited, due to decontaminating steps that are currently required from the environmental policies to remove heavy metals and phytotoxic compounds [71]. Wine pomaces is known to be rich in phenolic compounds, in particular flavonoids, phenolic acids and stilbenoids [356,357], many of which have shown biological activities and result to be beneficial to human health [358,359]. They therefore are an important feedstock exploitable to extract biomolecules for food, feed, cosmetic and pharmaceutical applications [357].

Very few papers deal with the use of residues stemming from the wine-making process in the preparation of composites. The studies are mainly considering fossil and non-biodegradable polymers as matrices, i.e. polyolefins [18,19,57], polystyrene ([360]) or poly(vinyl alcohol) [361], and in a lesser extend biosourced and biodegradable matrices such as soy four [361], and very recently poly(butylene succinate) [29] or PHBV [362]. Globally, the introduction of fillers derived from either ViSh, WiPo, grape stalks, skins or seeds resulted in a decrease of ultimate mechanical properties [18,29,362]. This reduction was attributed to a low aspect ratio of particles, e.g. 1.8 in the case of ViSh fragments obtained by grinding in a granulator equipped with a 2.5 mm sieve [18], or to a poor filler/matrix interface [18,29,363]. A treatment of lignocellulosic fillers, e.g. an alkaline treatment of grape stalks allowing to increase filler surface roughness and crystallinity [363], or the addition of compatibilizers, e.g. the use of maleic anhydride in the case of a HDPE-based system [18,29], could be useful to enlarge the overall performance of composites. As regards barrier properties, it was shown that the introduction of ViSh particles in PHBV allowed increasing water vapor permeability, which could be interesting for some applications, e.g. horticulture or packaging of respiring products [362]. A positive effect could also be noticed regarding the thermal stability, with a delaying of the thermal degradation, e.g. in the case of ViSh/HDPE [19] or WiPo/PBS [29] systems. It is worth

noting that the degradation of mechanical properties was relatively moderate (e.g. 25% of decrease for stress at break with 30% of filler content [362]), allowing to conclude on the interest of using such fillers to decrease the overall cost of materials while maintaining or modulating some functional properties.

The implementation of a biorefinery concept by developing cascading processes would be of great interest to give the highest possible value to winery lignocellulosic residues. As mentioned above, extraction of bioactive compounds is one of the most investigated valorization option for these two agro-residues since the extracted components can have a high market value. At the end, the process still leaves a solid residue, called either exhausted wine pomaces or exhausted vine shoots, that needs to be disposed of. Recently, some studies were devoted to the use of wine pomaces [29] and vine shoots [18,19] as reinforcing agents in polymer matrices. In a cascading logic, an interesting strategy would be to recover the exhausted solid residues and to use them as fillers in biocomposites. By the way, Krouit et al. showed that the solvent extraction of dry refined softwood fibers appeared as efficient as chemical grafting for compatibilisation treatment [364], meaning to think that the interest of polyphenols extraction before using the biomass for composite applications could be double.

The objective of the present paper was to assess and compare the reinforcing effect of fillers produced from two different winery solid residues, i.e. vine shoots and wine pomace, with fillers prepared either directly from the raw biomass or after polyphenol extraction. Fillers were characterized in terms of biochemical composition, density, morphology, thermal stability and color before being mixed with the PHBV matrix. The study focused on investigating the relationships between the main intrinsic characteristics of the constituents, the structure of resulting composites and their functional properties (tensile properties, water vapor permeability, thermal stability).

## III-2 Materials and Method

### III-2.1 Materials

A commercial grade of poly(3-hydroxybutyrate-co-hydroxyvalerate) (PHBV) under the reference PHI 002 was purchased from NaturePlast company (Iffs, France). In the form of pellets, this grade contained 1-3 mol% of valerate and had a true density of 1.24 g·cm<sup>-3</sup>.

Vine shoots (ViSh) of the Syrah variety (*Vitis vinifera L.*) was kindly provided by Jean-Michel Salmon (UEPR, INRA). They were from Gruissan, in the Languedoc-Roussillon region in the South of France. These residues displayed an initial moisture content of around 40 wt% when they were pruned in the field. Before dry fractionation, the fresh vine shoots were air dried during 2 months then they were dried in an oven at 60°C for 24 h.



Wine pomace (WiPo) of the Merlot variety (*Vitis vinifera L.*) was provided by InnovEn srl (Verona, Italy) and contained berry skins, seeds, petioles and stalks. Grape was harvested in the year 2016 and pomace was collected after pressing and wine fermentation. It was frozen and stored at -20°C the same day of wine production.

Acetone from (99.8% of purity) and ethanol (99.9% of purity) were respectively purchased from Biosolve Chimie and Meridis. Sodium hydroxide, sulfuric acid at (72%) was from Sigma Alrich. All chemicals were used without any further purification.

## III-2.2 Methods

### III-2.2.1 Extraction of polyphenols

Before extraction, wine pomaces and vine shoots were previously milled to obtain particle sizes ranging between 0.5 and 1 mm. This pre-milling conditions were different according to the biomass and adapted according the characteristics of the two residues. Dry pomaces were simply ground in a kitchen blender, while vine shoots were milled using a cutting mill type SM 300 (Retsch, Germany) with a 4.0 mm sieve and then 2.0 mm sieve.

Solvent-based extractions were carried out with the aim to recover the highest yield of phenolic compounds. Wine pomaces and vine shoots were extracted following the same protocol optimized in a previous study for grape pomaces [244]. Batches of 10 g of substrates were introduced in Pyrex glass reagent bottles with 50 mL of 75 % v/v acetone that were incubated 2 hours at 50 °C in a shaking bath. The bottles were closed to avoid solvent evaporation. After incubation, the liquid extract was separated from the solid residue by centrifugation (5 min, 5000 rpm). The solid residues were dried under the hood overnight then dried at 60 °C during 24 h. The liquid extracts were filtered with a 0.45 µm MF-Millipore filter (Merck) stored at -20 °C until further analyses. At the end, 60 g of substrate were extracted, with 6 batches of 10 g. ViSh and WiPo after extraction were named ViSh-E and WiPo-E, whereas virgin ViSh and WiPo (without extraction) were named ViSh-V and WiPo-V.

Such a protocol allowed to recover about 20 and 47 mg of polyphenols per gram of respectively dried ViSh and WiPo. Spectrophotometrical tests revealed that the extracted polyphenols mainly consisted of flavonoids, flavanols and hydroxycinnamic acids, molecules characterized by high antioxidant capacity [244]. After extraction, around 10% of weight loss (dry matter) was noticed for fillers.

### III-2.2.2 Production of fillers

After extraction, the exhausted pomace and shoots (dried solid residues) were milled with centrifugal mill ZM 200 (Retsch) at 14000 rpm with 0.5 mm sieve. Samples were stored in a hermetic drum at 23 °C in presence of silica gel (around 0% RH) before further analysis.

### III-2.2.3 Production of biocomposites

Compounding. Fillers (both virgin and exhausted fillers) and PHBV pellets were dried under vacuum at 60 °C overnight. Composites were prepared in a Brabender mixer at 180 °C for 6 min at 50 rpm. For each of the four types of fillers, three filler contents were considered, i.e. 5, 10 and 20 wt%. The samples were respectively named 5ViSh-V, 10ViSh-V, 20ViSh-V for composite with virgin ViSh and 5ViSh-E, 10ViSh-E, 20ViSh-E for composite with exhausted ViSh (after extraction). The same names were used for wine pomace with WiPo. The resulting composites were ground at low temperature. Compounds were dried at 60 °C overnight before using them for shaping process.

Preparation of films. 3.20 g of ground compounds were scattered on a Teflon foil (12x12 cm) within an aluminum frame (10x10 cm), 300 µm thick. A second Teflon foil was arranged on the first one and the resulting foils couple was placed between the plates of a Carver press, then heated at 190°C under 4.5 bars for 30 seconds. Then, films were quickly cooled to room temperature, led to room pressure and finally separated from the Teflon foils.

Preparation of dog-bone samples. Compounds were injection-molded using a Minijetpro Haake machine (Thermo-Fischer) for tensile tests (dog-bone shape ISO527-2-1BA). The cylinder and mold temperatures were respectively 185 °C and 70 °C. The injection and holding pressures were 400 and 100 bar, respectively. The injection and holding times were 20 s and 10 s, respectively.

Two control materials, PHBV ref1 and PHBV ref2, were used because the composite samples were not produced the same day. PHBV ref1 was the control for composites with ViSh and PHBV ref2, the control for the composites with WiPo.

### III-2.2.4 Scanning Electron Microscopy

SEM observations were done with a Hitachi S4800 Scanning electron microscope (Technology platform of IEM Laboratory of the Balard Chemistry pole) with an acceleration voltage of 2 kV after a coating with Pt by cathode pulverization. Observations were realized by the help of Didier Cot (IEM, Montpellier). For particles, a solution of 1.0 g·L<sup>-1</sup> of particles in pure ethanol was first prepared, then 50 µL of this solution was dropped on brass support. This solution was preferred to a direct spray of the particles. In case of composite films, the cross-section was observed after tensile tests or after cryo-fracture in liquid nitrogen.

### III-2.2.5 Laser granulometry

Filler size distribution (apparent diameter of particles), median apparent diameter and span values were determined using a laser granulometer in the wet mode (Malvern Mastersizer 2000 Instrument Ltd, United Kingdom), by dispersing particles in ethanol 95%. Measurements were done in triplicate.

## III-2.2.6 Color

The color attributes of each ViSh and WiPo-based fractions and biocomposites were measured with a colorimeter CR-410 (Minolta), using the CIELAB color system ( $L^*$ ,  $a^*$ ,  $b^*$ ). The total color difference ( $\Delta E$ ) was calculated following the standard ASTM D2244 [326] (Eq. 39).

$$\Delta E = [(L^* - L_0^*)^2 + (a^* - a_0^*)^2 + (b^* - b_0^*)^2]^{0.5} \quad \text{Eq. 45}$$

where  $L^*$ ,  $a^*$  and  $b^*$  the color components of each sample. The references were respectively a 99.5% pure cellulose BE 600-10TG (Arbocel, France) for fillers, and the neat polymer matrix for biocomposites. All measurements were carried out with 5 repetitions.

## III-2.2.7 Biochemical composition

The concentration of phenolic compounds in the extracts was determined by the Folin-Ciocalteu colorimetric method [365]. Estimations were carried out in triplicate and calculated from a calibration curve obtained with gallic acid. Total phenols were expressed results were expressed, in dry weight of pomace or vine shoot, as mg/g gallic acid equivalent (mg GA/gDW).

Double hydrolysis giving the Klason lignin. Analyses were done in duplicate. Ash content was determined in triplicate from the residue after thermogravimetric analysis (Mettler TGA2, Switzerland) at 800°C under air.

## III-2.2.8 Differential Scanning Calorimetry

Calorimetric analysis was carried out by means of a Perkin Elmer DSC6 calorimeter, calibrated with high-purity standards. The measurements were performed under a nitrogen flow. The thermal treatments used were as follows: first scan, from 30 to 210 °C at 20 °C·min<sup>-1</sup> and 1 min of isotherm at 210 °C; cooling scan, from 210 to 0 °C at 20 °C/min and 1 min of isotherm; second scan, from 0 to 210 °C at 20 °C·min<sup>-1</sup>.

The percentage of crystallinity ( $X_c$ ) was calculated by using the following equation Eq. 46:

$$X_c = \frac{\Delta H_m}{\Delta H_m \times (1 - w)} \times 100 \quad \text{Eq. 46}$$

where  $\Delta H_m = 146.6 \text{ J}\cdot\text{g}^{-1}$  is the enthalpy corresponding to the melting of a 100% crystalline PHB sample while the term  $1-w$  represents the biopolymer weight fraction in the composite [366].

### III-2.2.9 Thermogravimetric Analysis

A thermogravimetric analysis (TGA) under nitrogen flow (40 mL·min<sup>-1</sup>) was carried out by using a Mettler TGA2 apparatus (Switzerland) equipped with a XP5U balance (precision of 0.0001 mg). For each measurement, about 40 mg of material were heat from 40°C to 600°C at 10°C·min<sup>-1</sup>. The onset degradation temperature ( $T_{\text{onset}}$ ) was corresponding to the interception of the tangent drawn at the inflection point of the decomposition step with the horizontal zero-line of the TGA curve. The temperature of degradation ( $T_{\text{deg}}$ ) corresponded to the temperature at which the degradation rate was maximum.

### III-2.2.10 Mechanical properties

Tensile tests were conducted using an INSTRON 5966 series test apparatus equipped with a 10 kN load cell. The cross-head speed was set at 5 mm·min<sup>-1</sup>, the test was performed at room temperature. The reported data are the average values of at least ten determinations for each sample.

### III-2.2.11 Water vapor permeability (WVP)

Water vapor permeability of films (mol·m<sup>-1</sup>·s<sup>-1</sup>·Pa<sup>-1</sup>) was determined at 23 °C using a gravimetric method [367]. Composite films (five repetitions) were hermetically sealed with Teflon seal in glass permeation cells containing distilled water. These cells were placed in a desiccator containing silica gel (RH around 3%). They were weighed using a four-digit balance (BALCO – Type LX 220A, Switzerland) at regular interval during ten days. Water vapor permeability was calculated from the following equation (Eq. 47):

$$\text{WVP} = \frac{S \times e}{3600 \times A \times \Delta P \times M_{\text{H}_2\text{O}}} \quad \text{Eq. 47}$$

where  $S$  is the slope of the weight change from the straight line (g·h<sup>-1</sup>),  $A$  is the permeation area (m<sup>2</sup>),  $e$  is the average specimen thickness (m),  $\Delta P$  is the water vapor pressure differential (Pa), and  $M_{\text{H}_2\text{O}}$  is the molar mass of water (g·mol<sup>-1</sup>).

## III-3 Results and discussion

### III-3.1 Intrinsic properties of wine pomace and vine shoots particles

#### III-3.1.1 Particle biochemical composition

The content of Klason lignin as acid-insoluble residue was formally determined following a two-step hydrolysis (Table 42). The Klason lignin content was respectively of 19.4 % and 34.6% for ViSh and WiPo, which was common for such residues [46,368,369]. As suggested by Mendes et al., the high Klason lignin content in WiPo could be ascribed to structural polysaccharides

(cellulose, xylan, xyloglucan, etc.) that are embedded in a cuticle layer and thus inaccessible to acidic hydrolysis [370].

In the case of WiPo, the extraction treatment resulted in an increase of the Klason lignin content from 34.6% for WiPo-V up to 41.7% for WiPo-E. This could be explained by the fact that during extraction some sugars are also extracted, resulting in proportional increase of lignin content. This was not observed for ViSh-E, displaying a slightly lower value than ViSh-V. It was explained by the fact that vine shoots contain much less soluble sugars than pomace and condensed tannins were possibly extracted whereas they were included in lignin content for ViSh-V.

It is worth noting that ash content was higher in pomace than in vine shoots. In the literature, it was reported that skin pomace has a high mineral content, 14% (dry matter) whereas the seeds presents the lowest (3% dry matter) [371].

Such differences in biochemical composition may result in differences in intrinsic physical and physico-chemical properties of biomasses, including color, mechanical properties and capability to be milled, and thermal stability.

Table 42. Klason lignin and ash content and color attributes of fillers.

	Klason lignin (%)	Ash (%)	L*	a*	b*	$\Delta E$
Cellulose	-	-	76.8	1.3	5.1	0.0
ViSh-V	19.4 $\pm$ 0.5	3.9 $\pm$ 0.2	62.2	6.8	22.2	23.2
ViSh-E	17.7 $\pm$ 0.5	4.7 $\pm$ 0.5	65.1	7.0	22.8	21.9
WiPo-V	34.6 $\pm$ 0.9	5.5 $\pm$ 0.7	37.9	12.7	11.7	41.0
WiPo-E	41.7 $\pm$ 1.0	6.6 $\pm$ 0.2	35.9	11.7	12.0	42.7

### III-3.1.2 Particle color

ViSh particles were light brown whereas the pomaces were dark red (Figure 81-A1-B1). They were both derived from red wine varieties, however the red color is not visible in the vine shoots. The color was quantitatively assessed by the (L\*, a\*, b\*) values (Table 42). L\* represents the luminance, ranging from 0 (black) to 100 (white), while the two chromatic component a\* (from green to red) and b\* (from blue to yellow), range from -120 to +120. The gap  $\Delta E$  with pure cellulose was clearly more important for WiPo ( $\Delta E=41.0$ ) than for ViSh ( $\Delta E=23.2$ ). The darker color of wine pomaces was due to the higher content in polyphenols and lignin. The extraction step resulted in slightly lighter samples, highlighted by a small increase of L\*, but the color attributes were not significantly impacted (Table 42).

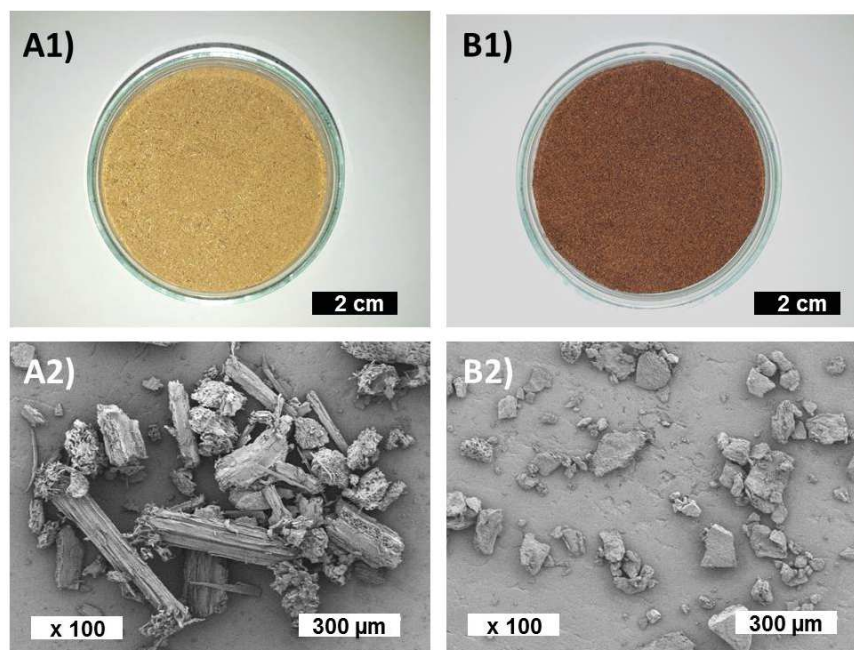


Figure 81. Visual aspect and SEM images of (A1 and A2) vine shoots and (B1 and B2) wine pomace fillers.

### III-3.1.3 Particle density, morphology and size

ViSh-V ( $1.449 \text{ g}\cdot\text{cm}^{-3}$ ) are a little denser than WiPo-V ( $1.420 \text{ g}\cdot\text{cm}^{-3}$ ). After extraction the density did not change or only very slightly in both cases (respectively  $1.445$  and  $1414 \text{ g}\cdot\text{cm}^{-3}$  for ViSh-E and WiPo-E).

The milled particles were poorly elongated with a low aspect ratio visually deduced from Figure 81. ViSh particles seems more elongated than WiPo with a more rectangular shape and a more fibrous structure. Numerous small and more spherical particles were also observed (Figure 81-A2). On the contrary, WiPo were close to square-like particles with an aspect ratio close to 1 (Figure 81-B2).

Despite the fact that the same grinding process was used, ViSh and WiPo particles did not display exactly the same size (Table 43), with a volume median equivalent diameter of respectively  $143 \mu\text{m}$  and  $114 \mu\text{m}$  for ViSh-V and WiPo-V. This highlighted that wine pomace was more fragile, or in other words less resistant to fractionation forces.

As already shown by SEM observations, particle size distributions were characterized by a high size polydispersity, even higher for the ViSh samples, with span values of 3.7 and 3.0 for ViSh and WiPo samples respectively. This was ascribed to the complex heterogeneous structure of the lignocellulosic biomass. Several populations can thus be seen within each sample size distribution (Figure 82). WiPo particles seems to be constituted of two fractions with respective median size of  $150 \mu\text{m}$  and  $50 \mu\text{m}$ . ViSh, on its side, displays slightly two fractions: a major one, centered on  $180 \mu\text{m}$ , and a major one, around  $10 \mu\text{m}$ . The repartition of these different fractions could be ascribed to differences of tissues grindability within the complex

lignocellulosic structures that are the studied fillers [322]. It was checked that the extraction process had no significant impact on the morphology nor on the size of particles (Table 43).

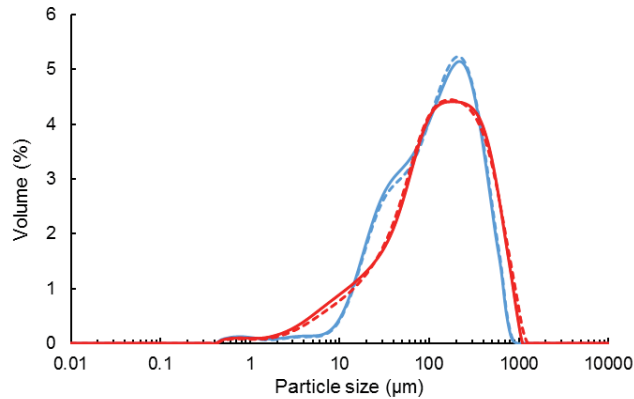


Figure 82. Particle size distribution for ViSh-V (—), ViSh-E (···), WiPo-V (—) and WiPo-E (···) in volume

Table 43. Filler apparent diameter, in volume

Sample	Density (g·cm <sup>-3</sup> )	d10 (μm)	d50 (μm)	d90 (μm)	Span
ViSh-V	1.449 ± 0.002	17 ± 1	143 ± 11	539 ± 67	3.7
ViSh-E	1.445 ± 0.002	20 ± 1	143 ± 9	569 ± 26	3.9
WiPo-V	1.420 ± 0.003	22 ± 1	114 ± 4	363 ± 15	3.0
WiPo-E	1.414 ± 0.002	21 ± 1	121 ± 5	370 ± 16	2.9

### III-3.1.4 Thermal stability

The thermal stability of the fillers is of great importance for biocomposites manufacturing, since it affects their processability and their overall thermal stability. For this reason, the thermal stability of produced ViSh and WiPo particles was evaluated under inert conditions by thermogravimetric analysis (TGA) in the temperature range from 20 °C to 600 °C. The thermograms of weight loss and derivative weight loss of both virgin and exhausted particles are displayed on Figure 83, while the degradation temperatures are summarized in Table 44. The two biomasses, i.e. ViSh and WiPo, exhibited a similar thermal degradation pattern, which was characteristic of lignocellulose [29,372]. The first degradation between 40 and 130 °C corresponded to the evaporation of water. The water amount was similar for all the samples, around 3.8 % (wet basis). The second step started around 170°C and extended to 500°C. It corresponded to the degradation of organic compounds, including extractives, hemicellulose, cellulose and lignin.

In the case of ViSh, the peaks associated respectively to the degradation of hemicellulose and cellulose were quite well distinguished, with a temperature of maximal rate of degradation of hemicellulose ( $T_{deg2}$ ) at 302 °C and a temperature of maximal rate of degradation of cellulose ( $T_{deg3}$ ) at 338 °C (Table 44). The last shoulder corresponded to the degradation of lignin that

is known to occur over a large range of temperature. From 500 °C, a passive pyrolysis step was characterized by a low and a continuous mass loss rate corresponds to the end of lignin degradation as well as char formation and rearrangement. The residue at 600 °C represented 26.5 % of the ViSh. This profile was similar to a stone-rich fraction of olive pomace [17].

In the case of WiPo, the TGA pattern displayed numerous degradation steps, showing that the biomass was more complex in term of composition. As compared to ViSh, the intensities of the peaks associated to the degradation of hemicellulose and cellulose were decreased by about 22% and 40% respectively, while the intensity of peak associated to the degradation of lignin was almost doubled (Figure 83), which was in accordance with the results of biochemical composition. A third peak was visible, with a maximum rate of degradation at 273 °C and a shoulder was around 240 °C. Both of them, peak and shoulder decreased after the extraction suggesting that they were probably associated with extractives.

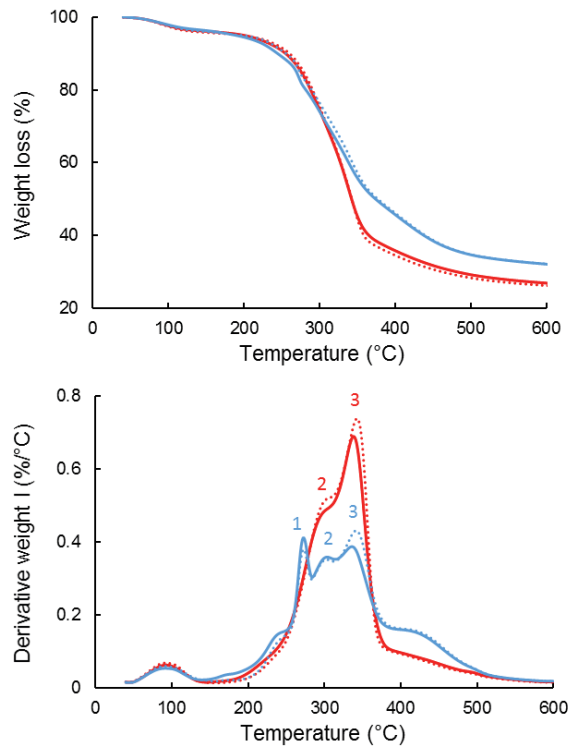


Figure 83. Thermogravimetric analysis of fillers under nitrogen: ViSh-V (—), ViSh-E (···), WiPo-V (—) and WiPo-E (···)

The polyphenol extraction did not change the thermal degradation profile of ViSh or WiPo. However, small differences could be observed regarding the intensities of the peaks on the derivative curves. The temperatures of maximal degradation rate of cellulose ( $T_{deg3}$ ) shifted to higher temperatures, i.e. from 337.9 to 342.4 °C for ViSh and from 336.3 to 341.3 °C for WiPo fillers. The increase of the peak intensity shows that they are more cellulose in proportion. The extraction moderately improved the material stability, with onset temperatures 7 and 8°C



higher than the virgin fillers, respectively for ViSh-E and WiPo-E. Same results were observed on enzymatically-treated rice endosperm [373].

Table 44. Results from thermogravimetric analysis under N<sub>2</sub> of ViSh and WiPo fillers

Sample	T <sub>onset</sub> (°C)	T <sub>deg1</sub> (°C)	T <sub>deg2</sub> (°C)	T <sub>deg3</sub> (°C)	Residues at 600°C (%)
ViSh-V	206 ± 1	-	302.4 ± 0.4	337.9 ± 0.3	26.5 ± 0.7
ViSh-E	218 ± 1	-	305.6 ± 0.6	342.4 ± 0.3	26.2 ± 0.1
WiPo-V	198 ± 1	272.9 ± 0.3	303.6 ± 0.1	336.3 ± 0.3	32.2 ± 0.1
WiPo-E	215 ± 1	272.7 ± 0.1	302.6 ± 0.3	341.3 ± 0.2	32.2 ± 0.1

### III-3.2 Impact of biomass origin and exhaustion on the properties of biocomposites

#### III-3.2.1 Visual appearance of films

The color of materials could be an important parameter for consumer acceptability. PHBV films were translucent and were characterized by a light beige color. The introduction of ViSh or WiPo particles resulted in darker and more brown materials, highlighted by a significant decrease in L\*, an increase in a\* and a decrease in b\* (Table 45). This evolution was even more pronounced in the case of WiPo particles, with even more brown and darker composite materials. As expected, the resulting color of biocomposites was dependent on the color of fillers. However, it is worth noting that differences in color ( $\Delta E$  values) observed for ViSh and WiPo fillers were less marked when incorporated in the PHBV matrix (Table 45).

As expected also, increasing the filler content also resulted in a continuous decrease in L\*, increase in a\* and decrease in b\*. As regards the effect of extraction, films were a little bit lighter (increase of L\*, related to higher values of L\* in case of exhausted samples).

Table 45. Color attributes of PHBV-based composite films.

	L*	a*	b*	$\Delta E$
PHBV	82.1	1.9	10.4	0.0
5ViSh-V	68.8	7.8	10.1	14.5
10ViSh-V	63.6	8.6	7.1	19.9
20ViSh-V	59.5	9.0	3.8	24.6
5ViSh-E	70.9	7.4	11.5	12.5
10ViSh-E	65.9	8.6	10.0	17.5
20ViSh-E	61.5	9.4	6.0	22.3
5WiPo-V	63.4	8.1	5.1	20.4
10WiPo-V	57.6	7.8	1.9	26.5
20WiPo-V	55.3	5.6	-1.7	29.6
5WiPo-E	66.4	8.4	6.1	17.5
10WiPo-E	60.4	8.7	2.8	23.9
20WiPo-E	56.1	7.1	-1.0	28.8

## III-3.2.2 Observation of the microstructure by SEM

Cryo-fractured surfaces of composite films were observed by SEM (Figure 84). Neat PHBV (Figure 84A) displayed a quite smooth surface with the presence of boron nitride used as nucleating agent in the PHBV grade PHI002. The incorporation of fillers led to a rough section, with the evidence of well-embedded fillers. No large interfacial holes or voids were visible, whatever the filler type and treatment, which allowed assuming that the filler/matrix interfacial adhesion was not too bad.

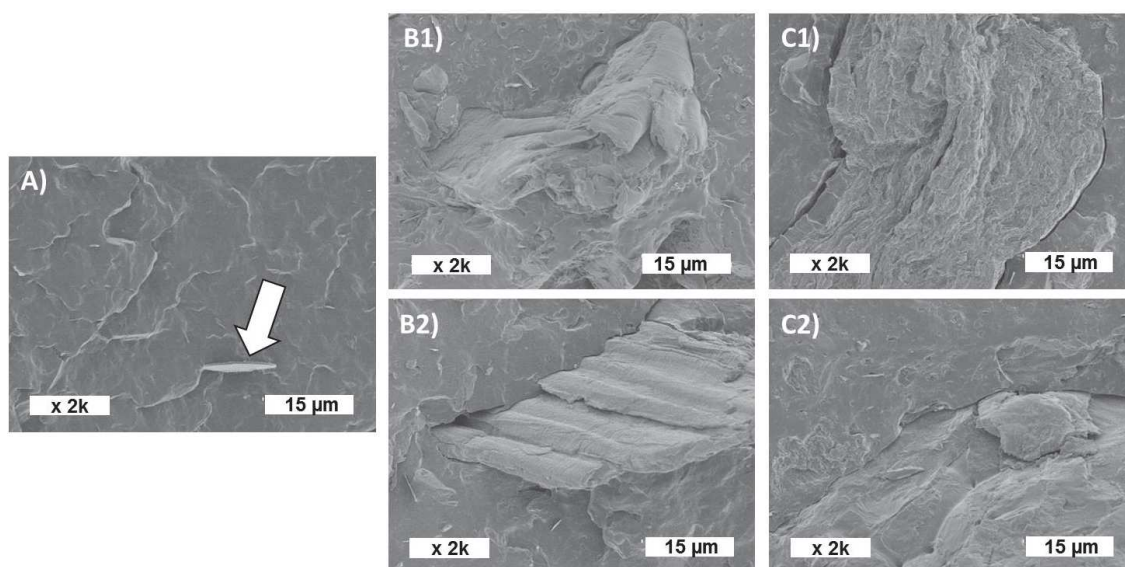


Figure 84. SEM observation of cross section of composites: (A) neat PHBV, (B1) 20ViSh-V, (B2) 20ViSh-E, (C1) 20WiPo-V and (C2) 20WiPo-E.

## III-3.2.3 Melting behavior

DSC analysis was carried out on all samples. Melting and crystallization temperatures, as well as crystallinity, were deduced from curves (Table 46). PHBV is a semi-crystalline polymer characterized by a noteworthy crystallinity: the crystallization and melting enthalpies are particularly high as shown in the Table 46 ( $\Delta H_c = 72-74 \text{ J}\cdot\text{g}^{-1}$ ;  $\Delta H_m = 82-83$  and  $83-85 \text{ J}\cdot\text{g}^{-1}$  in the first and in the second heating scan, respectively). Moreover, the polymer shows a high crystallization capability and crystallizes completely during the cooling step, due to the presence of inorganic nucleating agents (boron nitride) in the formulation.

The addition of the lignocellulosic residues into the PHBV matrix entailed a slight decrement in the crystallization temperatures during the cooling scan. In particular,  $T_c$  went from  $113 \text{ }^\circ\text{C}$  for PHBV to  $108 \text{ }^\circ\text{C}$  for the sample containing 20 wt% of WiPo (either virgin or exhausted). This behavior indicated that the wine pomaces acted as physical hindrances to the chain mobility, slightly slowing down the crystallization process. In the case of ViSh, such delaying in crystallization was not observed. In any cases, the polymeric matrix completely crystallized during the cooling step from the melt and the subsequent melting was very similar to that of

the sample without additives. As expected, the melting and crystallization enthalpies decreased in the composites, proportionally to the filler content.

The filler introduction did not significantly impact the PHBV crystallinity, except for those containing the exhausted pomaces. In that case, the  $X_c$  mildly increased, indicating a slight nucleating effect imparted by these fibers [366].

Table 46. Thermal properties of ViSh and WiPo-based composite films

Samples	$T_m^a$ (°C)	$\Delta H_m^a$ (J/g)	$T_c^b$ (°C)	$\Delta H_c^b$ (J/g)	$T_m^c$ (°C)	$\Delta H_m^c$ (J/g)	$X_c^c$ (%)	$T_{onset}^d$ (°C)	$T_{deg}^d$ (°C)
PHBV ref 1	176	82	113	72	172	83	56.6	276	291
5ViSh-V	174	74	113	68	171	78	56.0	258	274
10ViSh-V	175	81	112	65	170	75	56.8	271	281
20ViSh-V	173	60	111	56	170	65	55.4	248	268
5ViSh-E	173	74	113	68	171	79	56.7	272	283
10ViSh-E	174	78	112	66	171	76	57.6	276	284
20ViSh-E	173	65	112	58	170	66	56.2	256	271
PHBV ref 2	172	83	113	74	171	85	58.0	284	299
5WiPo-V	175	78	111	69	172	79	56.7	283	293
10WiPo-V	174	70	110	64	172	74	56.1	273	282
20WiPo-V	174	64	108	57	170	67	57.1	272	280
5WiPo-E	174	86	111	71	172	83	59.6	276	290
10WiPo-E	174	71	110	65	171	75	56.8	275	287
20WiPo-E	173	71	108	58	170	69	58.8	265	276

<sup>a</sup> determined by DSC during the first heating scan; <sup>b</sup> determined by DSC during the cooling scan; <sup>c</sup> determined by DSC during the second heating scan; <sup>d</sup> determined by TGA under N<sub>2</sub> flux, by heating at 10°C/min

### III-3.2.4 Thermal stability

Thermal stability of materials is an important criterion since they can be submitted to heating cycles during their service use or end-of-life treatment. The thermogravimetric analyses carried out on the samples are reported in Table 46 and Figure 85 shows the TGA curves for composites filled with 20 wt% of particles. The PHBV matrix degraded in a single step, with a thermal degradation beginning around 280 °C and a maximal rate of degradation between 291 and 299°C depending on the batch. The accepted mechanism for PHBV degradation consists in a random breakage of ester bonds to vinyl ester and carboxyl groups through a single step [374,375]. PHBV ref1 and ref2 displayed significant difference concerning the temperatures of

degradation with 8 °C of deviation for  $T_{\text{onset}}$  and  $T_{\text{deg}}$ , demonstrating the necessity of systematically using a reference at each production.

The biocomposites presented a second degradation stage, due to the filler decomposition. The extent of this step additional degradation was proportional to the filler content. In both case, the addition of vine shoots or wine pomaces decreased the thermal stability of the materials. Due to lower initial decomposition temperature ( $T_{\text{onset}}$ ) of fillers (206 °C for the ViSh and 198°C for WiPo), all the PHBV composites showed  $T_{\text{onset}}$  lower than that of PHBV. This reduced thermal stability could also be ascribed to a pro-degrading effect of fillers, promoting the PHBV chain scission. Composites with ViSh degraded at temperature lower than composites with WiPo. ViSh seems to favor the polymer degradation shifting the  $T_{\text{deg}}$  to lower values than those of composites with WiPo. A different slope for 20ViSh-V was noticed compared to 20WiPo-V.

The extraction step had a different effect on the composite thermal stability depending on the nature of the residue. In the case of ViSh, the thermal stability of ViSh-E-based composites was improved compared to ViSh-V-based composites. This was completely logical, due to the higher thermal stability of ViSh-E particles. In the case of WiPo, WiPo-E-based composites degraded at lower temperatures than WiPo-V-based composites, in spite of the higher thermal stability of WiPo-E fillers. This would mean that these fillers had a pro-degrading effect. This may be put in relation with the increased crystallinity previously observed for these composites. A favored polymer chain scission upon thermal treatment would be in favor of increased polymer mobility and ability to crystallize.

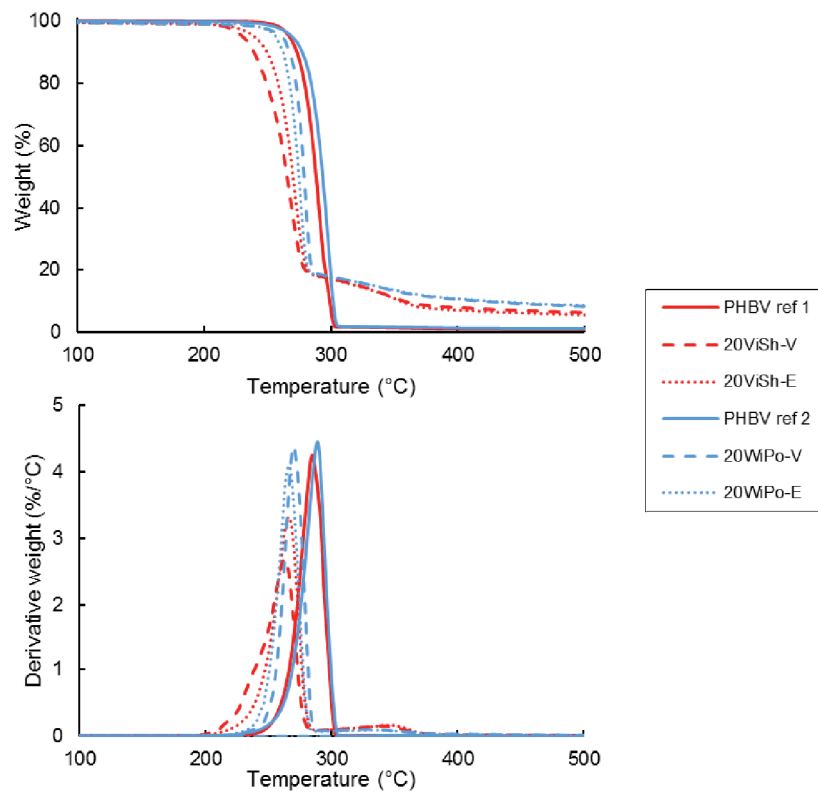


Figure 85. TGA curves of PHBV and 20 wt% composites.

## III-3.2.5 Mechanical properties

Results of the tensile tests on biocomposites with increasing filler content are presented in Table 47. PHBV exhibited a rigid behavior with a tensile strength of around 40 MPa, a Young's modulus of 2.2 GPa and an elongation at break lower than 5% (3.5 and 4.1% depending on the reference).

The addition of fillers led to a reduction of both tensile strength and strain at break. Similar evolution of mechanical properties is commonly noticed in all studies dealing with biocomposites. In the present work, this reduction is moderated. The strain at break decrease of 37% for 20WiPo-V and of 25% for 20ViSh-V. The degradation was more drastic concerning the stress at break. The stress at break value of 20ViSh-V was only reduced by 12% compared to control PHBV, whereas with 20WiPo-V had a value 41% lower. Thus, ViSh seemed to display a better reinforcing effect than WiPo. This could be ascribed to a better affinity with the polymer matrix (but not evidenced on SEM pictures), a more elongated shape of ViSh particles compared to WiPo and/or higher intrinsic mechanical properties of ViSh particles due to a higher content of holocellulose.

The rigidity of materials was slightly increased by the addition of ViSh fillers, probably due to a higher stiffness than the matrix. On the contrary, the addition of pomaces did not change Young's modulus of corresponding materials.

No significant impact of the extraction on composites materials was observed, meaning that extractives did not significantly impact the overall mechanical behavior of composites. It can be concluded that exhaustion of agro-residues particles to extract of high value-biomolecules could be an interesting strategy since it did alter the mechanical properties of resulting composites.

Table 47. Mechanical of ViSh and WiPo-based composite injected molded samples

Samples	Young's Modulus (MPa)	Tensile Strength (MPa)	Strain at break (%)
PHBV ref 1	2160 ± 20	40.4 ± 1.6	3.5 ± 0.3
5ViSh-V	2212 ± 40	40.3 ± 0.9	3.7 ± 0.1
10ViSh-V	2300 ± 42	38.3 ± 0.3	3.0 ± 0.2
20ViSh-V	2500 ± 29	35.5 ± 0.6	2.6 ± 0.1
5ViSh-E	2234 ± 33	39.2 ± 1.1	3.5 ± 0.3
10ViSh-E	2264 ± 58	37.3 ± 0.9	3.1 ± 0.2
20ViSh-E	2433 ± 43	34.9 ± 0.6	2.6 ± 0.2

PHBV ref 2	2182 ± 55	41.6 ± 1.1	4.1 ± 0.2
5WiPo-V	2259 ± 24	37.2 ± 1.1	3.1 ± 0.2
10WiPo-V	2260 ± 24	34.4 ± 0.6	2.9 ± 0.1
20WiPo-V	2162 ± 83	24.7 ± 1.5	2.6 ± 0.2
5WiPo-E	2197 ± 100	37.4 ± 1.2	3.5 ± 0.1
10WiPo-E	2207 ± 66	33.0 ± 1.5	3.1 ± 0.2
20WiPo-E	2187 ± 43	26.2 ± 0.6	2.5 ± 0.2

### III-3.2.6 Water vapor permeability

The water vapor permeability of the neat PHBV film,  $4.3 \pm 1.3 \times 10^{13}$  mol·m/(m<sup>2</sup>·s·Pa) was close to previous results in the literature [264,362] (Figure 86). The two controls, i.e. PHBV ref1 and ref2, gave the same results, meaning that the previously observed variability of mechanical and thermal properties did not impact water vapor permeability. The introduction of 20 wt% of ViSh or WiPo fillers led to an increase in the water vapor permeability. The water vapor permeability of 20ViSh-V and 20WiPo-V were respectively  $14 \pm 1.6$  and  $8.9 \pm 1.3$  mol·m/(m<sup>2</sup>·s·Pa). In case of composites with 20 wt% of ViSh fillers, the WVP was twice higher compared to previously composites observed by David et al. [362]. This was due to the higher size of the fillers, i.e. with a d50 of 150 µm instead of 50 µm (aggregation, more defects, edge effects even more favored by a lower thickness of the films [33]).

The increase in WVP was more important with ViSh fillers, with an increase of more than 3 times for 20ViSh-V. The increase in WVP is generally explained by the increase in water vapor sorption due to the hydrophilic character of lignocellulosic fillers compared to PHBV [30,190]. The lower increase of WVP in case of WiPo-based composites may be due to a lower water vapor sorption of WiPo particles, owing to the higher lignin content. Lignin is indeed known to be highly hydrophobic (see Chapter I).

The extraction step resulted in a more pronounced increase of WVP in case of ViSh-based composites, while it did not impact the behavior of WiPo-based composites. This would mean that extraction of polyphenols resulted in an increase of the hydrophilicity and thus water vapor sorption of ViSh-E while it did not impact the water sorption behavior of WiPo-E. This is related to the significant increase of holocellulose content in ViSh-E (as highlighted by TGA measurements) proportionally to the decrease in extractive content, cellulose being the most hydrophilic constituent of lignocellulose (see Chapter I). In case of WiPo-E, the high Klason lignin content was assumed to mask any possible increase of hydrophilicity of WiPo.

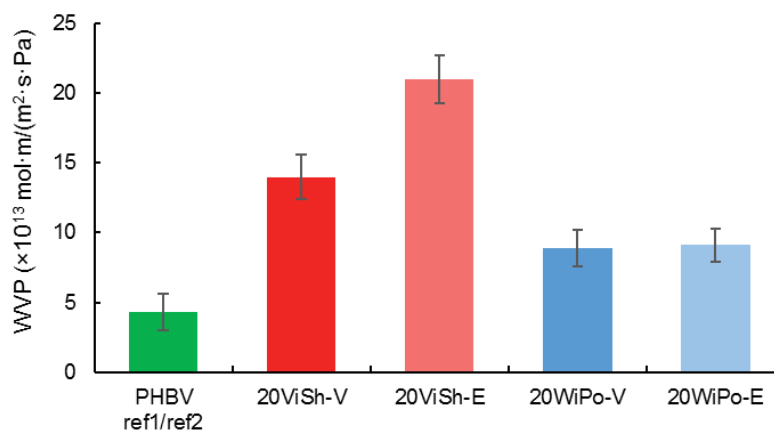


Figure 86. Water vapor permeability of ViSh and WiPo composites filled with 20 wt% of particles.

### III-4 Conclusion

Vine shoots and wine pomaces, two solid lignocellulosic winery residues, were investigated as fillers in composites. It was shown that both residues were thermally stable under 200 °C and can be thus processed to prepare PHBV-composites by melt extrusion. Composites were produced with filler content from 5 to 20 wt%. SEM observations of cryo-fracture of the composites displayed the same filler/matrix interfacial adhesion which was quite good. The addition of fillers decreased the thermal stability especially in case of ViSh. Composites had lower tensile properties compared to neat PHBV. This decrease was moderated especially for PHBV/ViSh composites which displayed higher mechanical performance than PHBV/WiPo composites. As a result, ViSh and WiPo particles can be perfectly used as an alternative fillers composite materials.

In addition, virgin and exhausted ViSh and WiPo were used as fillers to study the effect of polyphenol extraction with an acetone/water mixture. From the present results, it can be considered that a first step of polyphenol extraction before using these agro-residues as filler does not alter significantly the main properties of the composites. Only, WVP of composites with 20 wt% of ViSh-E was increased by 50%. Thus, in a biorefinery approach it would be probably worth extracting polyphenols before using these winery residues as filler for composites, to exploit their full potential.

Funding: This work was carried out in the framework of the NoAW project, which is supported by the European Commission through the Horizon 2020 research and innovation program under the Grant Agreement No. 688338.

## IV. Complementary results

### IV-1 XPS: X-ray Photoelectron Spectroscopy

Similarly, to complementary results from chapter III., the deconvolution of the C1s peak showed the different carbon signal peaks (Figure 87). The four components of the C1s peaks are C1 (C–C/C–H); C2 (C–O); C3 (C=O/O–C–O); and C4 (O=C–O). In case of natural fibers, the C1 can be mostly attributed to the aliphatic carbons and aromatic carbons from extractives and lignin. The C2 carbon arises from the primary and secondary alcohols in lignin, extractives, and carbohydrates (cellulose), whereas C3 and C4 correspond to ethers in lignin, extractives or cellulose, and esters and carboxylic acids in lignin and extractives, respectively.

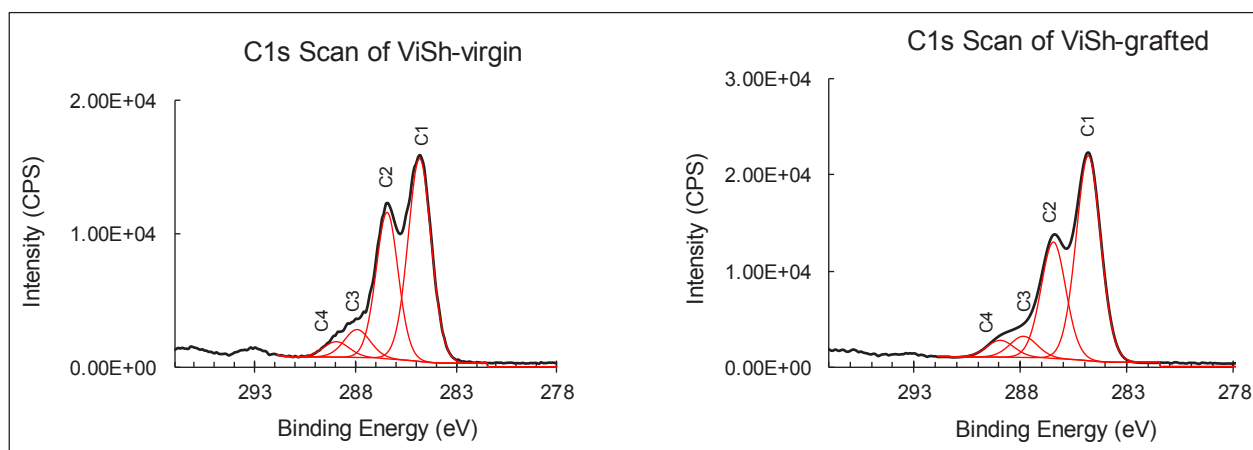


Figure 87. XPS high-resolution spectra for ViSh-virgin and ViSh-grafted

It worth notice that the ratio of C1/C3 increased slightly after grafting. This ratio reflects the number of aliphatic carbons per AGU and shows the presence of palmitate moiety at the cellulose surface. The lower O/C ratio in the grafted ViSh indicated a higher proportion of aliphatic close to the surface. The oxygen–carbon ratios of ViSh fillers were consistent with the oxygen–carbon ratios reported in the literature for lignin indicating a more lignin type surface of these particles.



Table 48. Relative atomic percentages and mass concentration of each element for virgin and grafted ViSh correlated to deconvolution C 1s.

Samples	Experimental values			Deconvolution of C 1s				
	%C	%O	O/C	C1%	C2%	C3%	C4%	C1/C3
ViSh-virgin	70.0	30.0	0.43	51.9	35.6	8.0	4.5	6.4
ViSh-grafted	71.4	28.6	0.40	55.9	32.3	6.6	5.2	8.5
Cellulose <sup>1</sup>	56.4	43.6	0.77	7.7	74.8	17.6	0	0.44
Lignin <sup>2</sup>			0.3-0.4					

<sup>1</sup> from previous results in Annexe 1, <sup>2</sup> O/C value from [351].

Thus, these results explained why virgin ViSh had already a good compatibility with the matrice.

## IV-2 Repeatability of the gas-phase esterification of vine shoots particles

The experimental condition of “C-G2” were chosen to produce ViSh fillers in the Article 3. Same experimental conditions were used for each batch of 100 g: 100 °C, 15 hours, 2 mbars.

<sup>13</sup>C NMR analysis of grafted vine shoots from three different reactions (A, B and C) using the same reaction conditions (C-G2) were performed to assess the repeatability of the esterification of ViSh. As shown in Figure 88, the gas-phase esterification with C-G2 conditions was repeatable with a DS<sub>C-H</sub> variation of 0.002. The difference between DS<sub>C=O</sub> and DS<sub>C-H</sub> values came from the fact that the signal for carboxylic carbon from the esterification was very weak and was overlapped with an existing signal in ViSh-V. Thus, the DS<sub>C-H</sub> value was preferred.

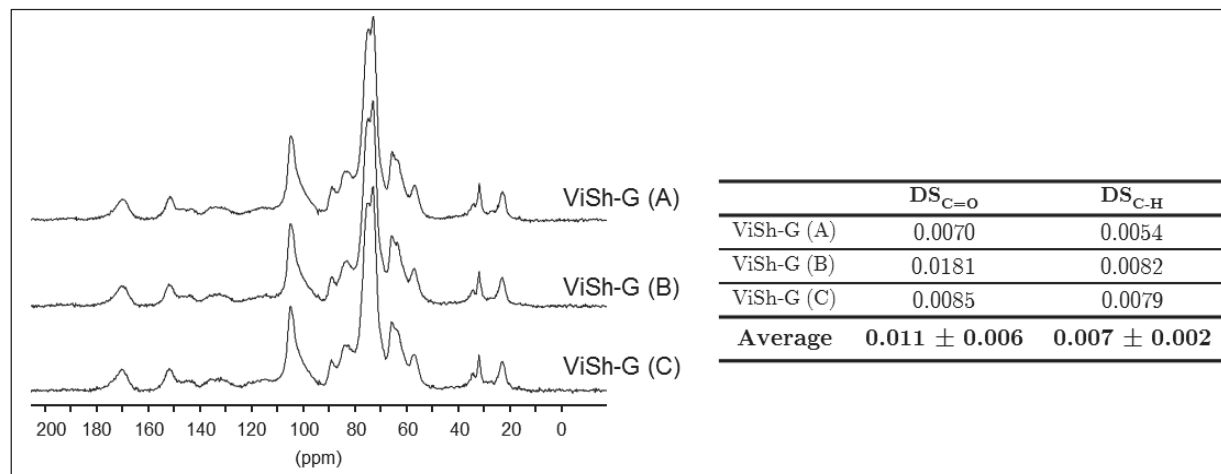


Figure 88. Cellulose <sup>13</sup>C NMR spectra and calculated DS for the three repetition of the gas-phase esterification.

## IV-4 Color of the samples

After the gas-phase esterification the difference of color ( $\Delta E$ ) of the ViSh particles was calculated with color parameters  $L^*$ ,  $a^*$  and  $b^*$  (Table 49). The main difference was concerning the parameter  $a^*$  and  $b^*$  representing respectively the red/green and the yellow/blue opponent and ranging from positive (red or yellow) to negative (green or blue) values trough zero (grey).  $a^*$  and  $b^*$  increased with the grafting. This can be partly explained by the experimental conditions for  $a^*$  as it also increased for ViSh-C. However,  $b^*$  should be attributed only to the grafted molecules.

Similarly, the color parameters of composites materials were measured according to the filler content and the type of fillers (Figure 89). Composites films were darker than neat PHBV. Composites with ViSh-G were slightly darker than composite with ViSh-V at equal filler content. In both case, the lightness and  $a^*$  parameters increased with the filler content.

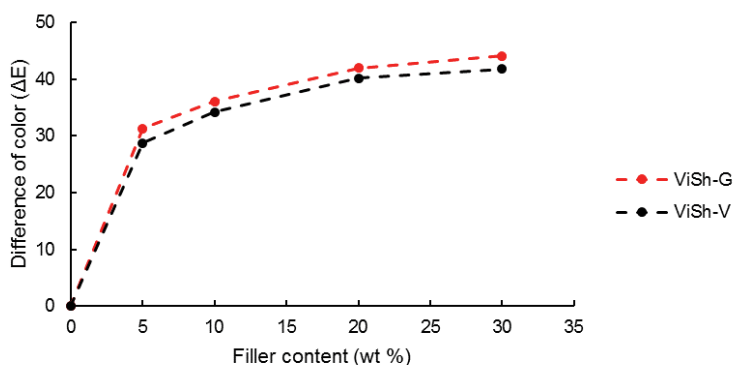


Figure 89. Effect of grafting on the color change ( $\Delta E$ ) of final PHBV-based composites.

Table 49. Color parameters of cellulose and PHBV-based composites

Sample	$L^*$	$a^*$	$b^*$	$\Delta E$
Cellulose	76.78	1.31	5.12	0.00
ViSh-V	66.94	6.59	23.12	21.18
ViSh-C	67.24	7.34	22.19	20.46
ViSh-G	68.28	8.78	25.34	23.17
PHBV	82.062	1.896	10.428	0.00
PHBV-5ViShV	54.34	7.37	15.83	28.77
PHBV-5ViShG	51.79	8.03	15.77	31.35
PHBV-10ViShV	48.74	8.30	14.71	34.20
PHBV-10ViShG	46.85	9.17	13.37	36.08
PHBV-20ViShV	42.54	9.21	11.48	40.21
PHBV-20ViShG	41.00	10.61	10.61	41.98
PHBV-30ViShV	40.74	8.49	10.45	41.85
PHBV-30ViShG	38.585	9.375	9.53	44.12

## IV-5 Pukánszky's model

Similarly to the Article 2 (Chapter III, 0), the Pukánszky's model was used to assess the quality of interfacial adhesion (see Eq. 37). The model provides information about the filler/matrix interface thanks to the parameter B: a low B corresponds to a low adhesion. In the present study, in both cases (composites with ViSh-V and ViSh-G) experimental data were well fitted with  $B = 2$  (Figure 90). It was higher than composites with virgin and grafted cellulose ( $B = -0.8$  and  $0.5$  respectively) confirming the quite good adhesion. This model also confirmed the idea that grafting did not have impact on ViSh incorporation.

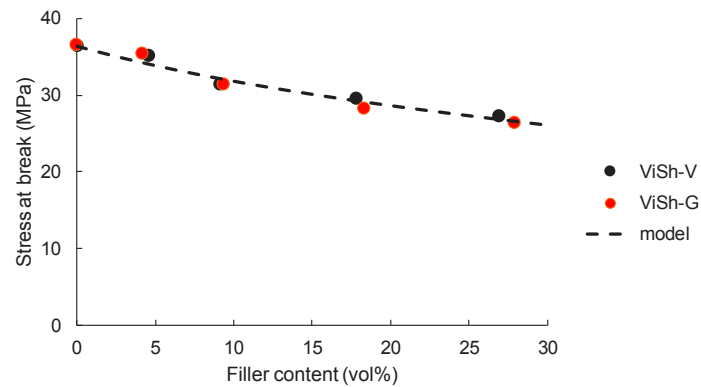


Figure 90. Pukánszky's model applied for virgin ViSh, and grafted ViSh based composites.

## Conclusion

Pour augmenter l'usage des biocomposites dans les applications industrielles, il est nécessaire de réduire le coût des matières premières. Ainsi, les résidus agricoles lignocellulosiques ont été considérés pour être incorporés dans les matrices polymères. L'utilisation de ce type de charge naturelle induit une variabilité inhérente. Concernant les sarments, une variabilité modérée existe à l'échelle de la particule. La différence entre les années, due à la pluviométrie et l'ensoleillement, semble avoir plus d'impact que les cépages concernant la composition chimique et la stabilité thermique. Malgré une différence de couleur avant broyage entre les différents cépages, les particules broyées ont des couleurs quasiment identiques. Les faibles variabilités observées devraient s'effacer lors de la mise en œuvre des composites avec des procédés tels que l'extrusion. Ainsi, l'usage de sarments de différents cépages ou de différentes saisonnalités ne devrait pas affecter la qualité des matériaux composites finaux. Afin de s'en assurer des matériaux composites avec des charges présentant la plus grande variabilité devront être préparés et comparés.

Des particules de sarments de vigne (Syrah 2016) d'environ 50  $\mu\text{m}$  ont été incorporées dans des matériaux à base de PHBV. Il a été démontré que cette addition réduisait les propriétés mécaniques du PHBV. La stabilité thermique et la cristallinité du PHBV diminue également avec un taux de charge croissant. Néanmoins, ces diminutions restent faibles et parfaitement acceptables. Ainsi, ces biocomposites peuvent certainement constituer une alternative durable aux matériaux d'origine fossile et une nouvelle façon de gérer les résidus agricoles. En outre, du point de vue économique, l'utilisation de ViSh réduirait considérablement le coût final des composites à base de PHBV.

De plus, la compatibilisation en surface des particules de ViSh avec des chaînes grasses via la formation d'esters a été obtenue en phase gaz en reprenant le procédé de l'article 1. La RMN du  $^{13}\text{C}$  des particules greffées a montré que la structure de la lignocellulose n'était pas modifiée avec un indice de cristallinité constant. Après le greffage, les valeurs d'angle de contact avec l'eau sont passées de  $59^\circ$  à plus de  $114^\circ$ , ce qui confirme l'hydrophobisation des ViSh. Les propriétés mécaniques des composites PHBV avec 10, 20 et 30% de taux de charge (en masse) ont révélé que le greffage chimique n'améliorait pas l'effet de renforcement de la matrice. Cela s'explique par le fait que le PHBV est moins hydrophobe par rapport aux polyoléfinés. La perméabilité à la vapeur d'eau des films composites contenant 30% en masse de ViSh est réduite de 27% avec des charges greffées. L'estérification en phase gazeuse a montré un effet plus important dans les composites avec des charges de cellulose qu'avec les particules lignocellulosiques.

Les sarments de vigne et le marc de vin ont été étudiés comme charges dans les composites. Il a été démontré que les deux résidus étaient thermiquement stables à  $250^\circ\text{C}$  et pouvaient ainsi être utilisés pour préparer des composites de PHBV par extrusion. Dans cette étude, du ViSh

et du WiPo vierges et épuisés ont été mélangés avec du PHBV à 180°C pour obtenir des composites ayant une teneur en charge de 5 à 20% en masse. Le mélange acétone/eau extrait des molécules dotées de propriétés antioxydantes telles que les polyphénols. D'après les résultats, une première étape d'extraction de polyphénols peut parfaitement être envisagée avant d'utiliser ces résidus d'agro-résidus comme charge de renfort. Les propriétés des composites ne sont que très peu modifiées par rapport à des matériaux avec des charges vierges. Les propriétés mécaniques des composites PHBV/ViSh sont supérieures à celle des composites PHBV/WiPo.

Des matériaux composites à base de PHBV et de sarments de vigne ont été développés. Il s'agit maintenant de quantifier l'impact environnemental et économique de l'usage de ces résidus agricoles dans les composites. La biodégradabilité des biocomposites doit également être vérifiée.

# Chapter V. Sustainability of biocomposites

## Chapter V. Sustainability of biocomposites

La conception de matériaux composites lignocellulosiques compétitifs nécessite la mise en œuvre d'un processus d'éco-conception et d'analyse du rapport bénéfices/risques, dès la phase de recherche, ce qui n'est actuellement pas le cas. Lors du développement d'un projet de recherche, des problèmes sociétaux et environnementaux majeurs aident à identifier les défis et à définir les stratégies de recherche du futur projet. Cependant, ces stratégies ne sont pas toujours pondérées avec un point de vue environnemental global. Les outils d'éco-conception traditionnels (ACV, empreinte carbone, etc.) sont généralement utilisés dans les projets pour évaluer l'impact environnemental d'un processus ou d'un produit après le développement. L'inconvénient majeur de cette approche est qu'elle se produit *a posteriori*, notamment à la fin du projet de recherche lorsque les développements sont au stade préindustriel sans grande possibilité de retour. L'approche actuelle n'est finalement que plus ou moins une simple optimisation entre la faisabilité et le coût environnemental. Elle relève davantage de l'observation écologique que de l'éco-conception. Il existe de nombreuses connaissances scientifiques sur l'impact des procédés ou des matériaux sur l'environnement, mais elles ne sont pas utilisées dans une véritable approche d'éco-conception a priori, notamment à partir de la phase de validation et de validation du concept (TRL 2-3).

L'Article 6 examinera l'intérêt environnemental d'utiliser les sarments dans les composites. L'objectif est de quantifier les impacts environnementaux grâce à l'outil ACV afin de comparer différents matériaux. Une ACV comparative de barquettes rigides réalisées en PHBV, PLA ou PP comme matrice et de sarments comme charge de renfort est menée. La contribution de chaque étape du cycle de vie est identifiée et discutée. De plus, l'impact des sarments sur le coût économique d'une barquette sera étudié.

L'Article 7 évaluera l'impact de l'addition des sarments de vigne sur l'aptitude des composites PHBV/ViSh à se biodégrader dans le sol. Cette biodégradabilité est une caractéristique essentielle pour des emballages à courte durée de vie. L'impact de l'extraction des polyphénols avec un mélange acétone / eau (v:v, 75:25) sur le comportement de biodégradation de ViSh et les biocomposites résultants a été mesuré par des tests respirométriques contrôlés en conditions aérobies.

# I. Life Cycle Assessment of biocomposite packaging materials introducing vine shoots as fillers (Article 6)

*Grégoire David<sup>a</sup>, Giovanna Croxatto<sup>b</sup>, Joshua Sohn<sup>b</sup>, Anna Ekmann Nilsson<sup>c</sup>, Arnaud Hélias<sup>d</sup>, Nathalie Gontard<sup>a</sup>, Hélène Angellier-Coussy<sup>a</sup>.*

<sup>a</sup> *JRU IATE 1208—CIRAD/INRA/Montpellier Supagro/University of Montpellier, 2 Place Pierre Viala, Bat 31, CEDEX 01, F-34060 Montpellier, France*

<sup>b</sup> *Technical University of Denmark, Department of Management Engineering, Lyngby, Denmark*

<sup>c</sup> *RISE Research Institutes of Sweden, Agrifood and Bioscience, Ideon, 223 70 Lund, Sweden*

<sup>d</sup> *LBE, Univ Montpellier, INRA, Montpellier SupAgro, Narbonne, France*

## I-1 Introduction

In viticulture, every winter after pruning, large quantities of vine wood are produced that are currently underutilized. Pruning of vine shoots (ViSh) is necessary in order to improve growing conditions for the plant, as well as to increase the yield and quality of grapes. Vine shoots can be from 1 to 2 meters long, and production amounts to between 1 and 2.5 tons of dry matter per hectare per year [46]. The productivity of the vine plant depends on the region where it grows, the pruning method and the vine species. In Languedoc-Roussillon (LR), a wine region in the south of France, ViSh production amounts to 500 000 tons every year [6]. Currently, management of vine shoots in France is done by either collecting and burning the ViSh or leaving them on the vineyards where they are cut roughly and used as organic fertilizer, as it is usually practiced in the Languedoc Roussillon area [376]. When used as biofertilizers, ViSh should be considered as by-products and not waste. However, their use as soil amendment can be problematic, as decomposing ViSh may serve as vector for diseases for the following vine crop [69]. Furthermore, it is worth noting that ViSh is not the most judicious biofertilizer since its biodegradation, i.e. mineralization in soil, comes in competition with the vine's growth as regards the nitrogen consumption [67]. Less commonly, ViSh are used as fuel wood or compost, which are considered low value uses for this potential resource. Regarding the ambitious goals set by the European community for a bioeconomy, which include the decarbonization of the economy by an 80-95% decrease of CO<sub>2</sub> emissions by 2050 [377], ViSh present a valuable resource for implementing decarbonizing recovery strategies. These strategies can be achieved in a biorefinery context, where cascading treatments of ViSh are investigated to produce added-



value products, including the production of lignocellulosic fillers for biocomposite applications [19,378,379]. Lignocellulosic fillers from agricultural residues present the advantages, in addition to their fully biodegradability in natural conditions, to have a lower density than conventional inorganic fillers and to be highly available at a low price, with no competition with the food sector [141]. ViSh present a great opportunity in the field of biocomposites [362], a potential application being rigid food packaging [362,380].

On the other hand, the global plastic market is continuously growing, with 40% of the production used in the packaging sector [7]. The massive amount of plastics used each year results in a constant accumulation of plastic wastes in our environment [8]. The associated effect of this on ecosystems, wildlife, and humans is worrying even if not yet fully understood. For this reason and the concern about global warming, fully biosourced and biodegradable materials such as biocomposites are emerging as a possible solution to tackle the problem of accumulation of plastic in our environment and to reduce greenhouse gas emissions. Poly(3-hydroxybutyrate-co-3-hydroxyvalerate), called PHBV, is a promising bacterial biopolymer that is biodegradable in soil and ocean, and that can be synthesized from all kinds of carbon residues. PHBV can be combined with natural fillers to give fully biodegradable biocomposites, for example for rigid trays applications [30,33]. Moreover, PHBV displays similar mechanical and barrier properties as polypropylene (PP) and can therefore substitute this fossil and non-biodegradable conventional polymer [381]. A competitor to PHBV is poly(lactic acid) (PLA), which is the most widely commercialized bio-sourced plastic currently in the market. However, it is worth noting that PLA is not fully biodegradable in natural conditions, but only compostable in industrial conditions [286], which requires collection and sorting in order to achieve a valuable end-of-life management and does not avoid concerns related to plastic accumulation from littering or leakage.

The development of biocomposites is largely motivated by either an improvement of the overall technical performance, insisting on mechanical properties, a decrease of the overall cost of materials, and the improvement of the carbon footprint, by replacing a part of non-renewable fossil resources [255]. Biocomposites are thus generally presented as eco-friendly materials. However, most of the time, the environmental benefit is not quantitatively proven [382]. It is thus necessary to ensure they are actually capable of mitigating the abovementioned environmental problems, as the use of bioplastics and natural fillers to produce biocomposites does not automatically make them sustainable. In order to quantitatively verify environmental claims made about biocomposites and other innovative materials, it is possible to carry out environmental assessments. Life cycle assessment (LCA), which is a holistic tool capable of measuring environmental impacts of products and services, can be applied to emerging biomaterials [383]. It investigates the inputs (i.e. resources and energy) and outputs (i.e. waste gases, wastewater and solid waste) across the entire life-cycle stages (cradle-to-grave). LCA allows to locate “hot spots” in the life cycle and avoids the problem shifting from one life cycle stage to another while accounting for all types of emissions and resource consumption [384]. Its main limits are the collection of data that can be difficult and the initial assumptions that need

to be justified. Most of the LCA carried out for biocomposites focused on the comparison of natural fillers with synthetic fibers [382,385,386], especially for applications in the automotive industry [222,224,387]. Generally, natural fillers tend to have a better environmental performance than glass fibers, notably thanks to the weight reduction of the composites and their low energy demand for production [222].

There are fewer papers in the literature regarding the environmental advantage of incorporating natural fillers in polymer matrices. In a previous study considering 1 kg of material as functional unit, the environmental impacts of materials made of virgin polyolefins (PP and HDPE) and biocomposites with natural fillers (derived from rice husks and cotton linters) were compared [388]. LCA showed that composites displayed lower environmental impacts in all impact categories, except eutrophication, due to the use of fertilizers for rice cultivation. Similarly, it was shown that the incorporation of either wood flour or wood fiber allowed for reducing the environmental impacts of HDPE [225] and PP [225], respectively, in proportion to the filler content.

LCAs of vine shoots and their incorporation in composites were not found in the literature. The combustion of ViSh and induced emissions have previously been studied [389,390] without LCA tools. More recently, Gullón et al. performed a LCA of the valorization of vine shoots into antioxidant extracts, and other bioproducts from a biorefinery perspective [391]. They determined that ViSh production related processes should be burden free in the biorefinery system since the environmental impacts were entirely allocated to the grape harvesting, as ViSh were considered agricultural waste [45,61].

Concerning PHBV, no process data is currently available in the Ecoinvent database. However, as shown by Yates et al. [392], several LCAs about bioplastics including PHBV are available in the literature. Inventory data from these papers can be used [392,393].

In this context, the objective of the present study was to better understand the potential environmental benefit of using vine shoots as raw resources for the production of lignocellulosic fillers for biocomposite applications. For this purpose, a comparative life cycle assessment was carried out, first on rigid trays made out of virgin PHBV, polylactic acid (PLA) or polypropylene (PP). Then, the effect of ViSh incorporation in these 3 polymer matrices was studied by considering a cradle-to-grave approach. The contribution of each life cycle step was identified and discussed. Besides, the balance between the environmental and the economic benefits of composite trays was discussed.

## I-2 Methodology

### I-2.1 Goal and scope

The aim of this article was to determine to what extent addition of ViSh fillers in packaging trays was environmentally beneficial compared to trays produced entirely from virgin plastics.

For that purpose, the environmental performance of packaging trays produced in France from either 100% virgin plastics or related ViSh-based biocomposites was assessed. Three polymer matrices, i.e. PHBV, PLA and PP, and different filler contents were considered in the predictions.

## I-2.2 Functional unit and system boundary

The functional unit was a tray of standard model (176 x 162 x 40 mm, GN 1/6 type), 25 cm<sup>3</sup> in volume, for single use packaging, produced by injection molding. It was assumed that all the considered trays had the sufficient properties to provide the same service. The volume of the trays was thereby kept equal throughout the assessment. However, due to the intrinsic densities of the considered materials, the final weight of the trays varied according to the nature and the proportion of each constituent (Table 50).

The scenarios included in this study were trays of virgin PHBV, PLA and PP, and trays of PHBV, PLA and PP filled with milled vine shoots.

The main properties of the raw materials are presented in Table 50. They correspond to commercial grades PHBV (PHI002 from Natureplast), PLA (PLI 003 from Natureplast) and PP (PPH9020 from Total Petrochemical). The density of ViSh was experimentally determined, as explained in Supplementary Data.

Table 50. Different properties for the components of the studied biocomposites.

	Density (g.cm <sup>-3</sup> )	Weight (g) (25 cm <sup>3</sup> tray)	Melting temperature (°C)	Degradation (°C)	Young's modulus* (GPa)	Stress at break* (%)	Strain at break* (%)
PHBV	1.23	30.75	170	200	4.2	40	3.2
PLA	1.24	31	150	250	3.5	45	3
PP	0.91	22.75	165	320	1.7	37	8
ViSh	1.36	-	-	230	na	na	na

\* according to the standard ISO 527

It was previously shown that increasing the content of ViSh in PP [18], PE [18] or PHBV [362,379] resulted in a slight decrease of the mechanical properties of the materials. Ahankari et al. studied the reinforcement of PHBV and PP with agro-residues and recommended to incorporate filler contents lower than 40 wt% to avoid a decrease in mechanical properties, due to an increased filler agglomeration in the polymer matrix [193]. Confirming this, Berthet et al. observed that the processability of PHBV/wheat straw biocomposites became difficult when the filler content was above 40 wt% [190]. Authors usually considered weight filler contents. However, considering that the volume of the injected molding tray remains constant whatever the matter, it was considered that the use of volume filler contents was more pertinent to compare the different formulations. Given that, it was assumed that the maximum ViSh filler

content to get the enough properties for the tray application was 30 vol% for all the composites. This was also in accordance with the filler content currently used in commercialized composites (*Vitis valorem*, Meursault, France, PLA or PP- Sarminé® products). This set limit of 30 vol% corresponded to weight contents of 32 wt% for PHBV and PLA, and 39 wt% for PP (for given a filler volume content and a tray volume, the filler weight content depends on the density of each constituent).

Figure 91 displays the system boundary considered in the present study, with the different life cycle steps that were included. It was assumed that the collection of vine shoots and the production of the trays were done in the Languedoc-Roussillon region of France. It was also assumed that the use of the biocomposite trays by the consumer was the same for all assessed materials and thus, the use phase was left out of the assessment. In case of 100% virgin plastic trays, the steps encased by dashed lines in Figure 91 were irrelevant because they concerned the ViSh treatment and compounding steps.

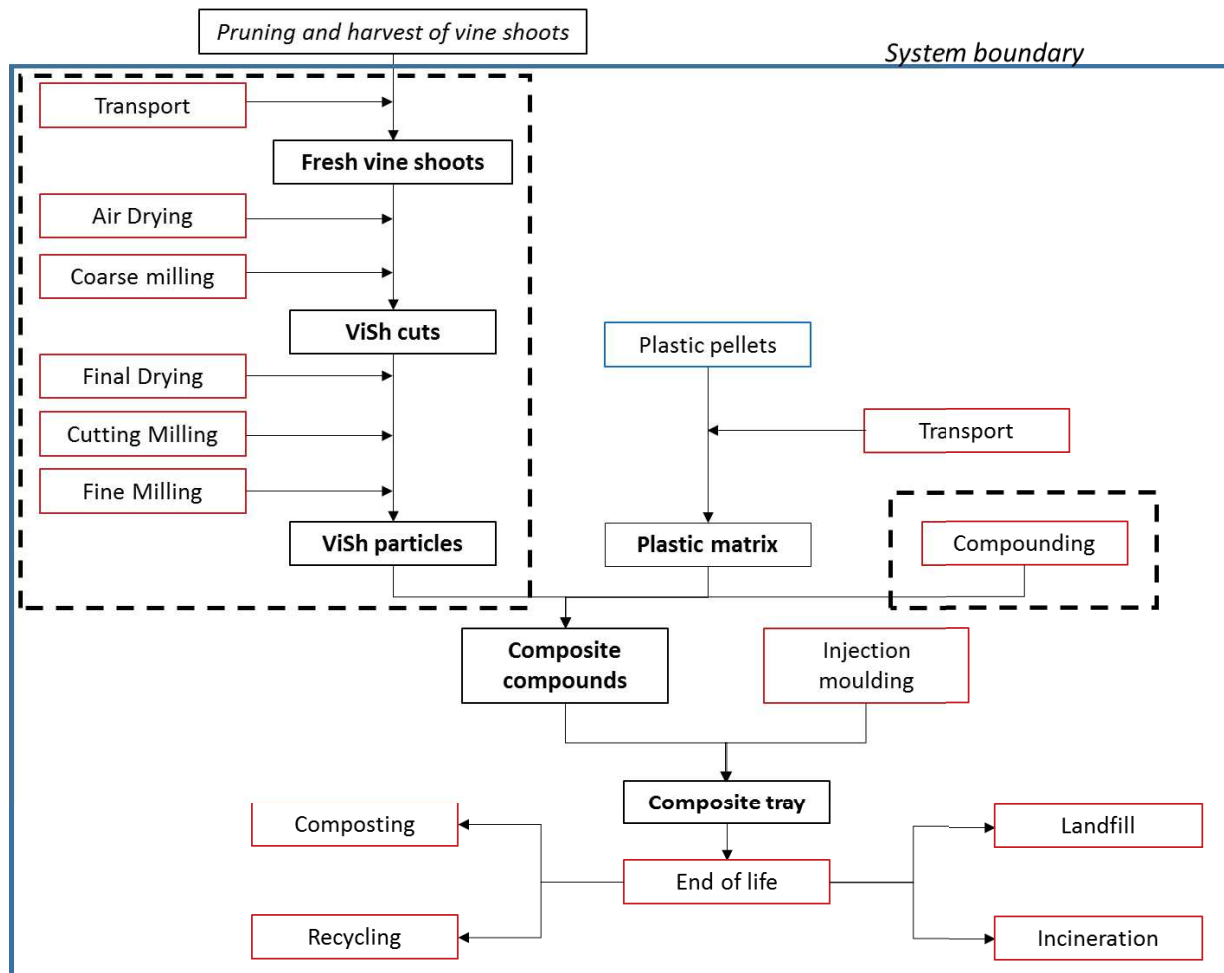


Figure 91. Boundary of the studied system.

### I-2.3 System description and inventory

All background data used in the assessment were obtained from the Ecoinvent v.3.4 database with the Cut-off system model and processed using the LCA software Simapro v.8.5. The ReCiPe 2016 Midpoint Hierarchist (H) methodology was used in the interpretation phase of the assessment. In accordance with the geographical boundary, all the electricity used in the system was assumed to conform to the French energy mix.

### I-2.4 Raw materials

Polymer matrices were PHBV, PLA and PP. Ecoinvent processes data recorded for fossil-based PP and PLA from maize grain were used in the LCA. Inventory for PHBV made from sugar cane was obtained from the work of Harding et al [393]. Transport of plastic matter to the production facility was taken into account using the "Background data for transport" sheet from Ecoinvent as the specific transport mode was unknown [394].

For all tested scenarios, lignocellulosic fillers were obtained from the dry milling of ViSh collected in the Languedoc-Roussillon region. It was assumed that ViSh came from the same varieties. In keeping with status quo practices, ViSh were collected during the winter after pruning and initially had a moisture content of 40 %wt.

Vine shoots are viticultural residues that can be seen as by-products if they are used as soil amendment, wood fuel or compost, or as a waste if they are simply burnt without energy recovery. The pruning is a necessary process that is independent from the fate of the ViSh. It is difficult to estimate the exact proportion of burnt ViSh because this practice, which is a common fate for ViSh, is in theory forbidden, but derogations and tolerances still exist [395]. According to FranceAgriMer, burning of ViSh accounts for between 25 and 50% in France [376,396]. In the present study, ViSh burnt on site or without valorization were considered. In that case, the collection of the ViSh happens anyway in order to remove ViSh from the vineyards and it was therefore considered a part of the grape cultivation production system. Besides, vine shoots have no market value and thereby, zero environmental impact would be allocated to them. ViSh were thus, considered burden free in the present system. Additionally, ViSh being produced in a wine-grape production system, all the environmental impacts of production were ascribed to the production of wine-grapes. Finally, transport of ViSh from the field to the filler producing site was assumed to be done by a 3.5-7 t lorry with an average distance of 10 km according to *Vitis Valorem* (France) information.

### I-2.5 Production of biocomposite trays

Practical information about the handling of ViSh as raw material for the production of biocomposites was provided by *Vitis Valorem* (France). Commonly, ViSh are first air-dried outdoors for seven months, between January and August. The corresponding land use was determined considering that the ViSh are arranged on the ground reaching an average height

of 2 meters, with an apparent density of  $30 \text{ kg}\cdot\text{m}^{-3}$ . Only manual labor was used during this step. At the end of this period, the moisture content of ViSh was 20 wt% (w.b.).

Coarse milling with a common wood chipper (Greentec 952, Ufkes Greentec BV, Netherlands) was utilized to mill the ViSh. Based on data provided by *Vitis Valorem (France)*, the throughput was set at  $2000 \text{ kg}\cdot\text{h}^{-1}$ , and 10% of the initial ViSh mass were lost during the milling process. Output chips sizes ranged between 3 and 6 cm in their largest dimension.

An additional drying step was required to reduce the moisture content of the ViSh to 5 wt% after air drying. An existing drying process from the Ecoinvent database was used (see Supplementary data), modified to utilize the French electricity grid.

After coarse milling, a finer milling process in two steps is needed in order to obtain particles of between 0.3 and 0.05 mm in size. First, ViSh were milled using a cutting mill type SM 300 (Retsch, Germany) with a 2.0 mm sieve and secondly they were milled with a fine impact mill (CUM 150, Netzsch Condux, Germany). The final output is hereafter called “ViSh particles”. Data for milling were provided by *SD-Tech Group* (Alès, France).

Flexible Intermediate Bulk Containers (FIBC, commonly known as “Big Bags”) were used to store the ViSh chips after coarse milling, ViSh particles after fine milling and composite granules after compounding. It was assumed that each FIBC was used 3 times per year during a period of 5 years before being discarded. Each FIBC had a mass of 2.5 kg with a capacity of  $1 \text{ m}^3$  and it is made from PP. ViSh chips after coarse milling, fine milled ViSh particles and composite granules had a bulk apparent density of  $200 \text{ kg}\cdot\text{m}^{-3}$ ,  $420 \text{ g}\cdot\text{m}^{-3}$  and  $700 \text{ g}\cdot\text{m}^{-3}$  respectively.

During the compounding step, the plastic was mixed with ViSh fillers in an extruder. Data for compounding were obtained from *Vitis Valorem*, which uses a compounder, model ZSE 160 HP (Leistritz, Nuremberg, Germany). Electricity consumption of the compounding step was  $300 \text{ kWh}\cdot\text{t}^{-1}$  and the yield is 97.6%. In the assessment, the same yield and energy data is used for all compounding regardless of composite granule type. No plasticizer nor additive was used.

Trays were assumed to be produced by injection molding of compounds. The injection molding process in Ecoinvent was modified to provision electricity from the French electricity mix. The yield was assumed to be 99.4% because scrap and waste could be recycled in a nearly closed loop.

All the previously described steps (from air-drying to injection molding) were assumed to occur at the same location.

## I-2.6 End of life

The end of life (EoL) of each tray was defined according to French practices for municipal waste [230] and considering the characteristics of the materials and existing facilities (Table 51). With regard to transport in the end of life, it was estimated that the trays travelled on

average 100 km from household to a waste treatment center [397]. Transport was assumed to happen by a 16-32 t lorry, EURO5 from Ecoinvent.

Table 51. Current possible end of life of the different trays (% in weight, from [230])

Tray material	Landfill	Incineration	Recycling	Composting
PP	34.6%	36.5%	28.9%	0.0%
PP-ViSh composite	48.7%	51.3%	0.0%	0.0%
PHBV	38.0%	40.0%	0.0%	22.0%
PHBV-ViSh composite	38.0%	40.0%	0.0%	22.0%
PLA	38.0%	40.0%	0.0%	22.0%
PLA-ViSh composite	38.0%	40.0%	0.0%	22.0%

Concerning composting, only industrial composting was included due to the lack of data for home composting. The incineration process of Ecoinvent was adapted to account for CO<sub>2</sub> emissions and the nature of carbon (biogenic or fossil). Anaerobic digestion could be an end-of-life option for bioplastics and biocomposite trays, but was not included in the possibilities because it is not widely used in France, and it is more dedicated to agricultural wastes than composite materials.

A more detailed inventory for the production of biocomposites is given in the supplementary inventory of this paper.

## I-3 Results and discussion

### I-3.1 Environmental impact of 100% virgin plastic trays: Comparison of PHBV, PLA and PP

First, the environmental performances of 100% plastic trays without ViSh fillers were compared (Figure 92). Trays made of PP displayed lower impacts than PLA or PHBV trays in all the categories except for *fossil resource scarcity*. This could be explained by the fact that the density of PP (0.91 g.cm<sup>-3</sup>) was lower than those of PHBV or PLA (1.23 and 1.24 g.cm<sup>-3</sup>, respectively). Thus, in order to get the same tray, i.e. with the same volume, a smaller amount of PP (in mass terms) was needed, i.e. 22.75 g instead of 30.75 g for PHBV (Table 1). Similar results were found showing that when compared by volume rather than weight, PHBV had higher environmental impacts than PP or PE [398]. Moreover, the production of 1 kg of either PHBV or PLA had higher impacts than PP. Impacts for *stratospheric ozone depletion*, *freshwater and marine eutrophication*, *land use*, and *water consumption* were very low for PP, in comparison to the bioplastics because the life cycle of PP did not have agriculture activities which heavily impacted the above named impact categories. On the other hand, the *fossil resource scarcity* impact for PP was the highest because it PP is entirely made from fossil

resources. In regards to PHBV, results showed that PLA had the highest impact for 13 out of the 18 categories.

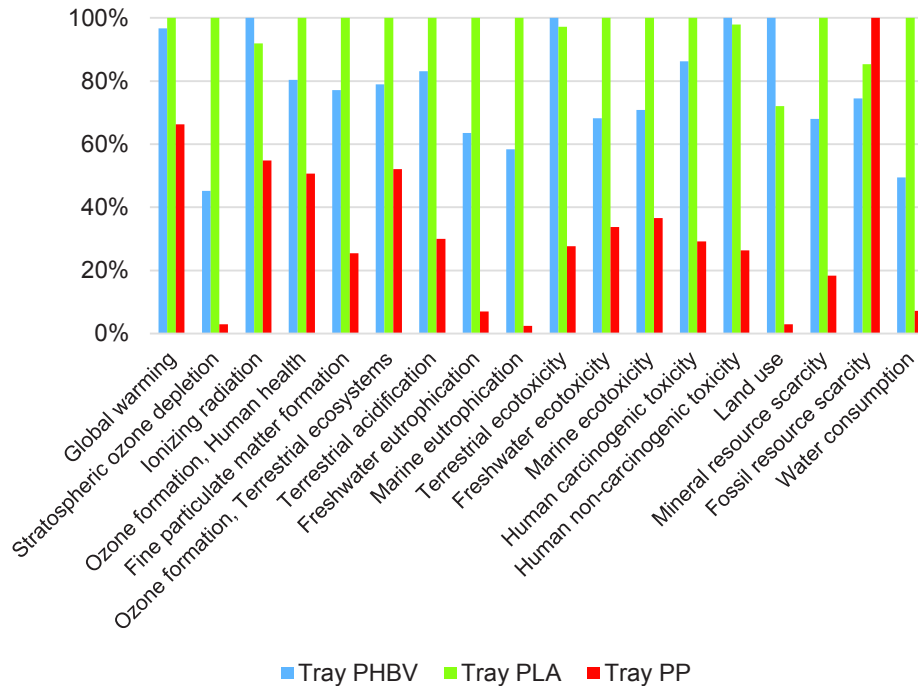


Figure 92. Environmental impact for all impact categories of the ReCiPe 2016 (H) method, for 100% virgin plastic trays.

The impact of each production step on *global warming* is presented in Figure 93. The production of polymer pellets appeared as the most impacting step of the process accounting for more than half of the burden for PP and more than 80% for PLA and PHBV. The PP tray impacts were 30% lower compared to bioplastic trays. This suggests that the substitution of traditional plastic trays with bio-based materials does not always result in a lower environmental impact. Nevertheless, conventional plastic industries have a high degree of optimization which is not the case of bioplastics that are produced in low tonnage. This is exemplified by PP, a petrochemical matrix polymer, which the production has been highly improved, whereas the development of biopolymers is recent and they have not yet reached the same level of technological maturity. Further research on the optimization of the bioplastics processing toward their environmental improvement should be conducted [388]. In the future, their environmental impact is expected to reach lower levels than those reflected in the present study.

Transport of the polymers had low impact in the overall life cycle, representing less than 3% of the *global warming* for each tray. It is interesting to note that the end of life was more important for PP, accounting for 27% of the total burden, than for bioplastics (2%). This was mainly attributed to the incineration process. Incineration was more favorable to bioplastics



and biocomposites because the carbon released was biogenic, unlike that from fossil-based plastics. The landfilling contribution to *global warming* was low, representing less than 5% of the PP end of life impacts, because PP was not assumed to be decomposed in the landfill. It must be noted that recycling of PP is an empty process because of the cut-off at recycling. The recycling benefit and costs are allocated to the production of new PP material.

In the present study, it was considered that all the plastic wastes were managed without littering, but in reality a non-negligible proportion of plastic waste ends in nature. In the world since 1950, 79% of plastic waste was accumulated in landfills or natural environment [8]. Long-term impacts such as the accumulation of micro-plastics in the environment are currently not taken into account in LCA. The advantage and benefits of using bioplastics that fully biodegrade in natural conditions are thus not quantified nor included in the analysis. This is particularly relevant for PHBV, which is fully biodegradable in soil and does not require industrial composting, contrary to PLA [399]. Furthermore, gas emissions from petrochemical polymer degradation, which have recently been demonstrated to produce methane and ethylene emissions under sunlight conditions in both water and air, are also not accounted for in LCA [400].

The nutrient contents of bioplastics (e.g., nitrogen, phosphorus, etc.) are so small that the benefit for reducing fertilizer use can be ignored. However, the sequestration of carbon in soil and the soil improvement properties are potential benefits of organic compost [385]. Nevertheless, these are difficult to quantify and are considered outside of the scope of the present work.

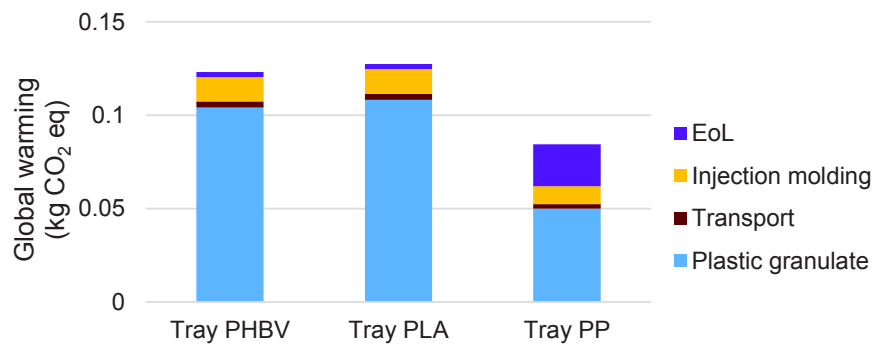


Figure 93. Global warming impact of one 100% plastic tray (without fillers)

### I-3.2 Effect of the incorporation of ViSh fillers on the environmental performance of trays

A composite is the combination of two components: a matrix that constitutes the continuous phase, i.e. either PHBV, PLA or PP in the present study, and fillers that corresponds to the dispersed phase, i.e. ViSh particles in the present study. The *global warming* impact for 1 kg of material is displayed in Figure 94 for the 4 possible constituents of composite materials. It clearly appeared that ViSh fillers had a lower impact (0.26 kg CO<sub>2</sub>eq/kg) than the polymer matrices (respectively 3.47, 3.58 and 2.29 kg CO<sub>2</sub>eq/kg for PHBV, PLA and PP). The ViSh impact was almost 9 times lower than those of PP matrix. This was due to the advantage of using agricultural residues that only required transport, drying and milling.

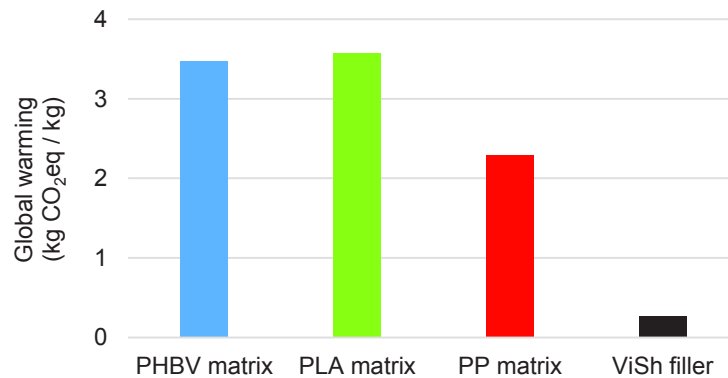


Figure 94. Global warming impact (kg CO<sub>2</sub>eq/kg) of 1 kg of each composite component

Figure 95 shows how the *global warming* impact was affected by an increasing filler content in biocomposites. Similar figures for the other impact categories are available in SI. A decreasing burden of the composite with increasing filler content was observed. The incorporation of ViSh appeared to be beneficial concerning *global warming*. It is worth noting that the production of composites required an additional compounding step and that the density of ViSh was 50% greater than that of PP, i.e. 1.36 g·cm<sup>-3</sup> for ViSh against 0.91 g·cm<sup>-3</sup> for PP. The burden incurred by the compounding step was visible for composites with very low filler contents. As the production of biocomposites induced an additional use of energy, in all cases, composite with 1 vol% of ViSh had a higher *global warming* impact than respective virgin polymer matrices. The negative impact of both the additional compounding step should be thus compensated by the incorporation of increasing contents of ViSh particles in the polymer matrix. The magnitude of the decrease in impacts varied depending on the matrix type. For PHBV, PLA and PP, the slope was respectively 1.00, 1.05 and 0.69 mg CO<sub>2</sub>eq/%ViSh. Then, the use of ViSh was beneficial from 5.5 vol% for PHBV and PLA, whereas the ViSh benefit in PP was first observed for a volume filler content of 20 vol%. PHBV-based composites had a lower contribution to *global warming* than 100% virgin PP tray, starting from a PHBV matrix with ViSh content of 44 vol%. However, this filler content is too high to be considered realistic, when taking into account the processability of the materials and their resulting mechanical properties. *Global warming* of PP-based composites was higher than PHBV-ViSh composites,

only when reaching a ViSh content of 98.5 vol% and higher, which was of course a non-realistic formulation.

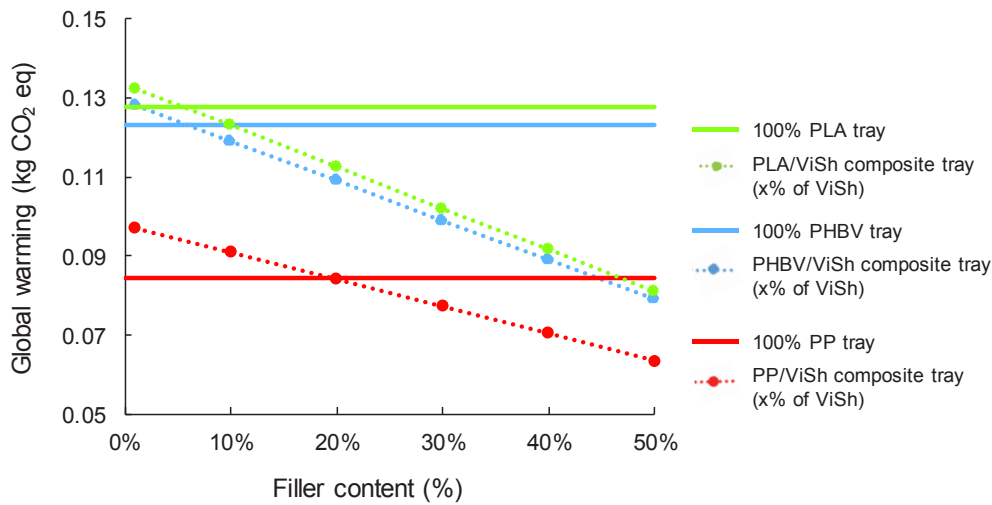


Figure 95. Global warming impact (kgCO<sub>2</sub> eq) as influenced by the filler content (vol%) for composite trays.

The filler content from which the addition of ViSh in the composite resulted in a benefit for all impact categories is displayed in Figure 96. PHBV and PLA displayed similar results; the incorporation of ViSh improved the environmental impacts for all the categories except for *ionizing radiation*. If *ionizing radiation* was to be used as a single score indicator, then biocomposites would never exhibit lower impact than 100% virgin plastic trays because of the electricity needed for the milling, drying and compounding steps of ViSh. The high *ionizing radiation* impact is mainly due to the French electricity mix, which is largely produced from nuclear power. In case of PP, PP-based composite trays can be better than 100% PP trays in 10 categories over 18. The ViSh burden was higher than PP matrix in 4 categories which explains the higher impact of composite in *stratospheric ozone depletion*, *ionizing radiation*, *land use* and *mineral resource scarcity*. Similarly, the compounding step was responsible for the higher impact in *water consumption* and *terrestrial ecotoxicity*. Finally, *freshwater and marine eutrophication* burden was due to the end of life of the composite. The black dash line in Figure 96 represents the limit of acceptable filler content of 30 vol% in the composite to ensure the functional unit. Thus, *freshwater* and *marine ecotoxicity* and *human non-carcinogenic toxicity* were other impacts that PP-based composite could not improve.

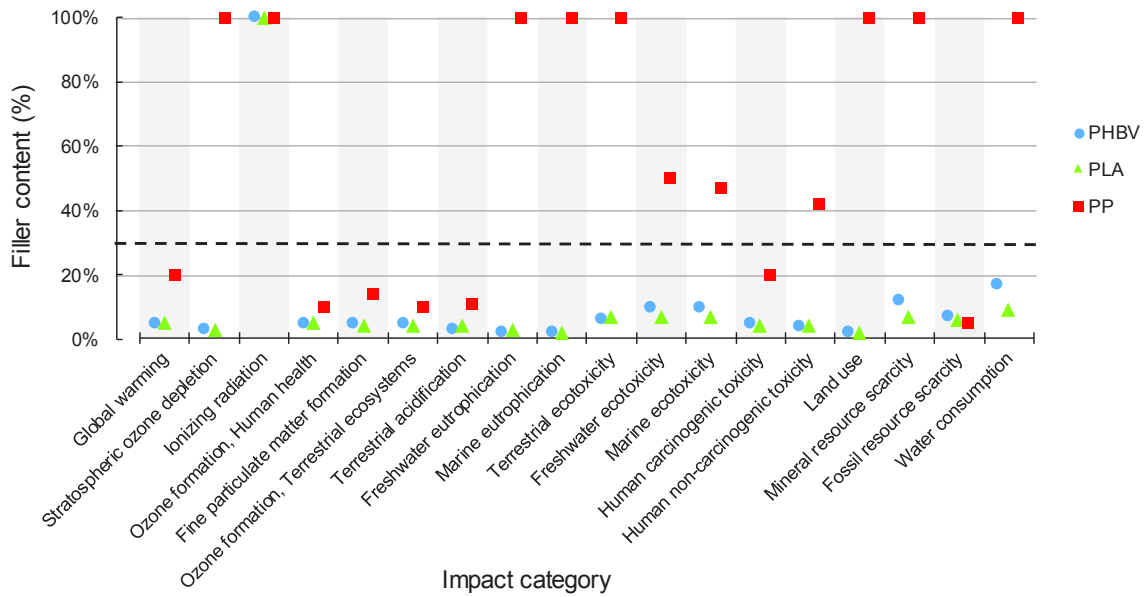


Figure 96. Filler content (vol%) from which a composite tray results in lower impacts than a 100% plastic tray for each assessed impact categories. The black dashed line represents the physical limitation of filler content (30 vol%) in the composite to ensure the functional unit. For dots shown at 100% filler content, no benefit can be realized by the addition of filler.

According to results presented in Figure 95 and Figure 96, it could be concluded that increasing the ViSh filler content as much as possible in the composites, while respecting the restrictions set by material properties, was globally the best for the environment.

The environmental performance of composite trays filled with 30 vol% of ViSh particles was assessed in detail (Figure 97). The 100% virgin PP tray was also added as reference. As previously described in part I-3.1, results were largely influenced by the nature of the matrix, mainly due to differences in density. PLA composites exhibited the highest environmental impact except for *ionizing radiation*, *terrestrial ecotoxicity*, *human non-carcinogenic toxicity* and *land use* where PHBV exhibited the worst impacts. As expected, PP-based materials exhibited the highest impacts concerning *fossil resource scarcity*.

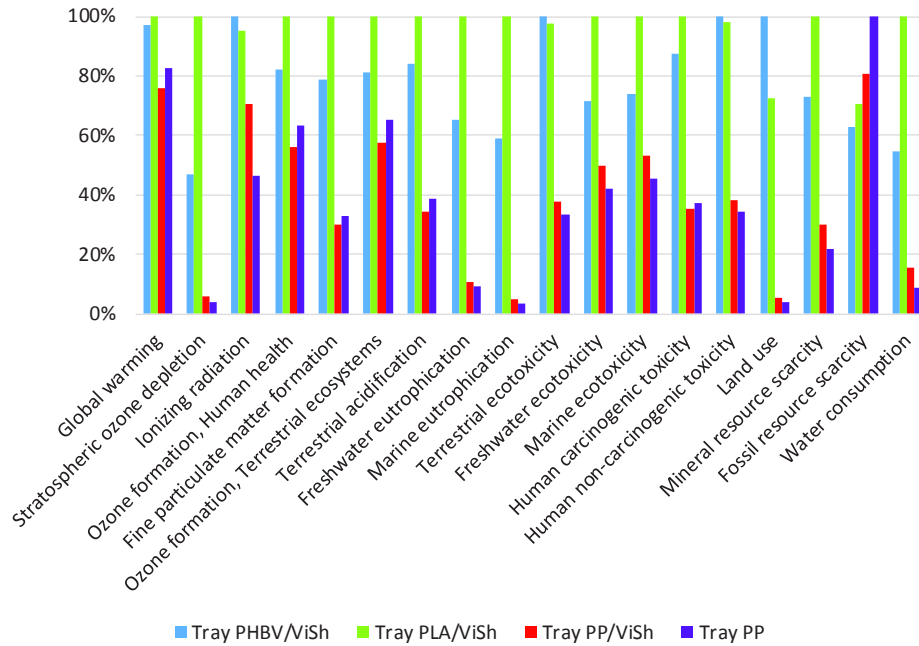


Figure 97. Environmental impact of composite trays filled with 30 vol% of ViSh fillers (all impact categories)

As shown on Figure 98, *global warming* impacts of trays with 30 vol% ViSh fillers were significantly lower than those of trays made from 100% virgin plastics. This was in line with a previous study on the production of biocomposites with wheat straw [401]. The contributions were divided in three categories: (i) raw materials for matrix and ViSh fillers, (ii) processing for compounding and injection steps, and (iii) the end of life. The incorporation of 30 vol% of fillers reduced the *global warming* burden of the raw materials by 25% compared to 100% plastic tray. Moreover, the end of life impacts was also reduced for bioplastics. In case of PP-based composite, PP could not be considered recyclable anymore, due to the presence of ViSh filler, inducing a slight increase of the EoL impact. On the other hand, the higher density of the composite materials relative to the pure plastics resulted in higher impacts from the injection molding step. The addition of ViSh came with an additional step of compounding, which had a relatively low impact compared to the injection molding process, as it represented 20% of the burden of the processing. The incorporation of 30 vol% of ViSh in trays reduced their *global warming* effects by 19.7%, 20.0% and 9.1% for PHBV, PLA and PP based trays, respectively.

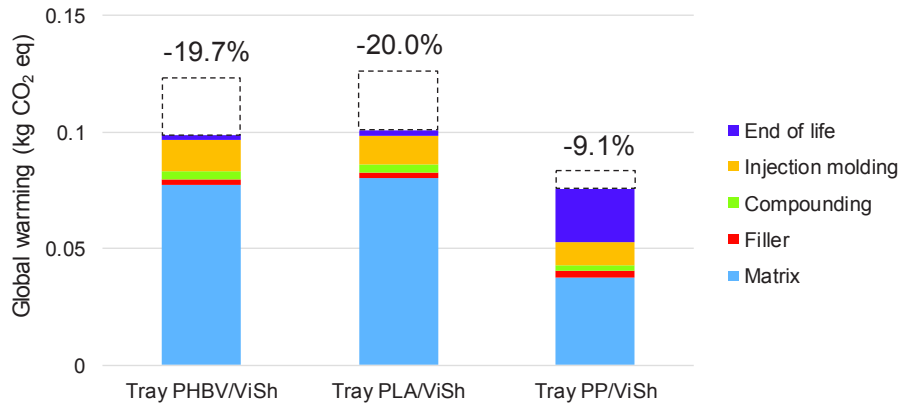


Figure 98. Global warming impact of trays with 30 vol% filler. The percentages above the bars indicate the reduction of the impact compared to trays without ViSh filler.

### I-3.3 Identification of the hot spots

#### I-3.3.1 ViSh filler production: contribution of each step on the environmental impact

The main contributor to the environmental impacts of ViSh particles was the milling steps (Figure 99). Milling represented 72% of the *global warming* impact, followed by the drying steps, with a contribution of 22%. The most burdensome type of milling was coarse milling, though there was no impact for *ionizing radiation* because the energy came from diesel fuel. This was contrary to electricity powered cutting and fine millings. The final drying step also consumed energy, but in the form of heat from steam in chemical industry, which explained the low impact value in the *ionizing radiation* category.

The impact of ViSh transport was low in all the categories because it was considered that the production of trays took place in the same region (Languedoc-Roussillon) as the generation of ViSh, allowing for short transportation distances.

Air drying showed burdens in only one impact category, since it only required space to spread the vine shoots on the floor without the help of machinery. Thus, this step only appeared in the category land use and represented 56% of it.

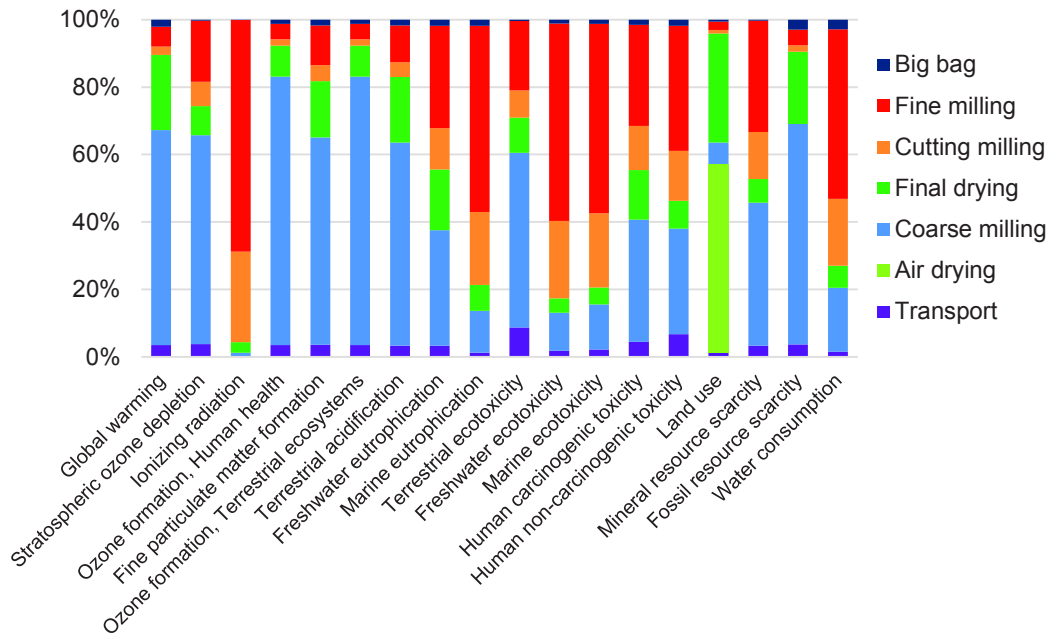


Figure 99. Contribution for ViSh filler production

### I-3.3.2 Polymer/ViSh (30 vol%) composite trays production: contribution of each step on the environmental impact

The analysis of the biocomposites burden clearly showed the strong contribution of the components of the composite and especially the matrix (Figure 100). The contributions of PLA are not shown in Figure 100 to increase clarity and because the results were very close to those of PHBV composites.

For PHBV-based composites, the production of the polymer matrix was the most impacting element for 15 categories, ahead of the end of life (*freshwater and marine ecotoxicity*) and the injection molding (*ionizing radiation*). In case of PP-based composites, results were more balanced with 9 categories dominated by the matrix, 4 by the injection molding or end of life and 1 by the compounding (*water consumption*). When comparing *global warming* potential, the polymer matrix caused the largest contribution to environmental impact for the composite trays. The *global warming* impacts associated with polymer production outweighed those from the filler, manufacturing or end of life.

As expected, *ionizing radiation* impacts were mainly due the manufacturing steps: injection molding and compounding. These processes required electricity. In case of PLA and PHBV composite, land use impact was principally on account of their production requiring respectively corn and sugar cane as carbon source.

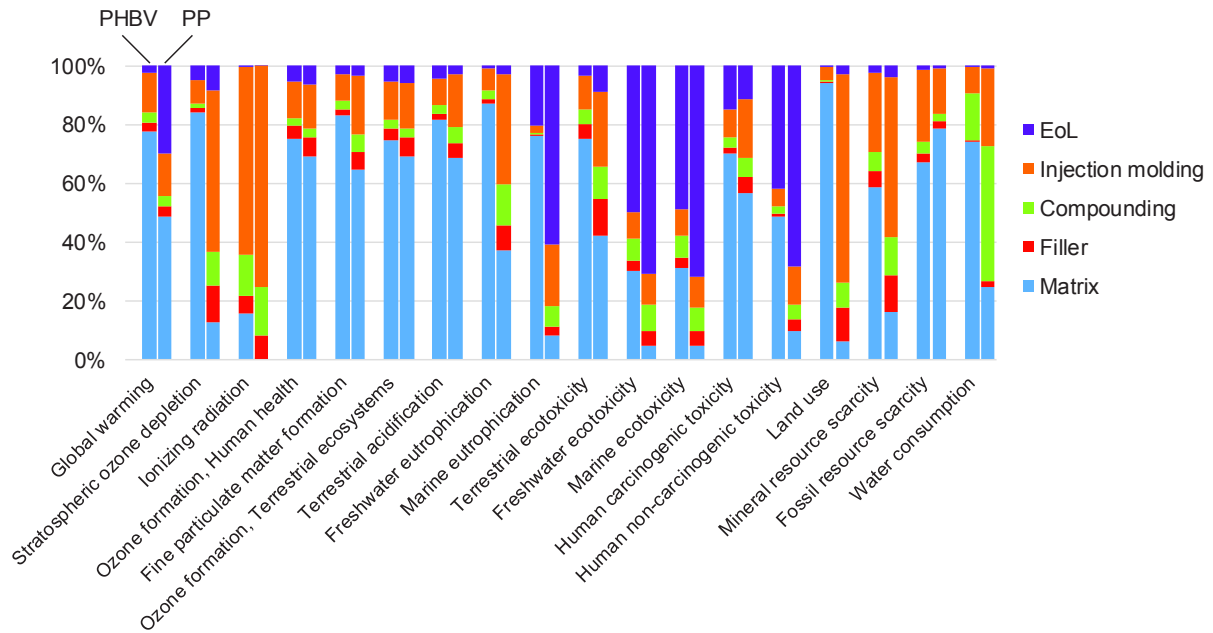


Figure 100. Contribution for PHBV and PP-ViSh (30 vol%) composites

### I-3.4 Economic vs environmental balance analysis

The price of the different trays was estimated from data given by industrials (Table 52). From an economical point of view, the incorporation of 30 vol% of fillers reduced the price of a PHBV tray by 25.4%, and to a lesser extent in case of PP (12.0%) because the price of raw PP is much lower than PHBV (Table 52). It is interesting to note that the injection molding accounted for a large share of the price, ranging from 12% for 100% PHBV trays to 50% for PP-based composite trays. On the contrary, in case of composite materials, the additional price of compounding was almost negligible. The factory price of final trays was not only a rule of mixtures with the price of raw materials. Thus, the addition of ViSh in trays reduced the final price but not as much as expected according to the price of raw materials. There are two reasons for this: the price of injection molding, which was constant, and the density of ViSh was higher from the one of plastics.

Table 52. Price of the studied composite trays. ViSh is 0.30 €/kg (*Vitis valorem*, ADEME), the compounding is 0.04 €/kg (ICP) and the injection molding is 0.03 €/p (Fürstplast).

	Price (€/ton)	Price 100% plastic tray (€/100p)	Price 30 vol% ViSh filler tray (€/100p)	Reduction of the price due to 30 vol% of ViSh filler
PHBV	7 750 <sup>a</sup>	26.95	20.11	-25.4 %
PLA	2 800 <sup>b</sup>	11.73	9.46	-19.4 %
PP	1 240 <sup>c</sup>	6.94	6.10	-12.0 %

<sup>a</sup> NaturePlast, grade PHI 002, 2019

<sup>b</sup> NaturePlast, grade PLI 003, 2019

<sup>c</sup> French customs department, 2017



## I-4 Conclusion

It is important to quantify the environmental impact of a product before claiming environmental benefits. This study dealt with environmental impacts of a tray used for packaging, which contained ViSh particles.

Bioplastics matrices that are supposed to be eco-friendly displayed higher environmental impacts than petrochemical polypropylene. This result should be tempered by the fact that long-term impacts such as plastic accumulation are not considered and that the production of bioplastics is still at a much lower level of technological development. The processes are being optimized and the available data will evolve accordingly. A general conclusion about the environmental efficiency of bioplastics compared to conventional plastics is therefore difficult to be drawn because of the evolution of the database. For example, database for the production of PLA has been recently changed in the new version of Ecoinvent V3.5. As described by Yates et Barlow in a critical review on biopolymers [392], it is difficult to compare their environmental impacts with other studies for different reasons: updated eco-profiles, feedstocks used, sources of energy...

PHBV is the only truly biodegradable bioplastic among the three studied. Current LCA tools can not anticipate the long-term effects of plastic accumulation in the environment. There is currently no factor that quantifies the effect of plastic debris on biodiversity [402]. The biodegradability of PHBV can thus not be assessed in the LCA framework. However, there is ongoing research on this issue (for example, the Marilca initiative supported by the Life Cycle Initiative of the UN Environment [403]). One has to wonder how the conclusions of this work will change when such data will become available. The interest of a biodegradable material, compared to a non-biodegradable material but recycled, may seem low from a short-term life cycle analysis point of view. It is neglected the fate of the recycled material which, after a few cycles, will eventually be released into the environment (the recycling of plastic, whether closed short loop or long loop, is limited in time).

The incorporation of ViSh in plastic trays, an agricultural residue, despite additional processing steps, achieved reductions in environmental impacts. The density of ViSh is higher than the one of plastics. Trays with a higher filler content are therefore heavier inducing more matter to be processed. Despite that fact, this study proved the interest of using agro-residues in composites. The maximum filler content of 30 vol% should be increased to reduce the environmental impacts even further.

Thus, it can be concluded that most of the research efforts should be devoted to the optimization and scale up of the bioplastics production, PP production being already optimized. The use of cleaner energy should help to achieve this goal but also reduce the impact of injection molding step. Finally, the end of life should be also improved by increasing recycling for PP, ensuring separate collection for composting of PLA, and home composting for PHBV.

**Funding:** This work was carried out in the framework of the NoAW project, which is supported by the European Commission through the Horizon 2020 research and innovation program under the Grant Agreement No. 688338.

**Acknowledgments:** The authors would like to acknowledge the research group ELSA in Montpellier for providing SimaPro software.

## II. How vine shoots as fillers impact the biodegradation of PHBV-based composites (Article 7)

*Grégoire David<sup>a</sup>, Julie Michel<sup>a</sup>, Emmanuelle Gastaldi<sup>a</sup>, Nathalie Gontard<sup>a</sup>, H el ene Angellier-Coussy<sup>a</sup>*

*<sup>a</sup> JRU IATE 1208—CIRAD/INRA/Montpellier Supagro/University of Montpellier, 2 Place Pierre Viala, Bat 31, CEDEX 01, F-34060 Montpellier, France*

### II-1 Introduction

The demand in plastic materials is continually increasing, reaching 350 million tons in 2018 while it was 250 million tons in 2010 [7]. The packaging sector stands for the plastics' largest market with 40% of the overall plastic demand in Europe. A global shifting from reusable to single-use containers has accelerated the growth of plastic consumption. Most of them are materials designed for immediate disposal. Geyer et al. [8] estimated that 60% of all plastics ever produced has been discarded and are accumulating in landfills or in the natural environment. Today, 32% of plastic packaging leaks out of collection systems worldwide, of which at least, 8 million tons end into the ocean [404,405]. To address the overwhelming negative environmental issues of plastic packaging and to enter the virtuous loop of circular economy, it is urgent and crucial to mitigate the negative burden of packaging resources (renewable without competition with food resources vs. oil-based) and waste management (fully biodegradable in natural conditions vs. accumulation). The main driver of biodegradable plastics is that biodegradability offers a closed loop value chain.

Biodegradable plastics have raised great interest especially for packaging and agriculture sectors, which have usually short-term and single use applications. Polyhydroxyalkanoates (PHA) are a class of polyesters that are synthesized by bacteria grown on carbon sources stemming from renewable resources and even organic residues. Up to now, the global production of PHAs represents 3.2% of all the biopolymers after starch blends, PLA and PBAT [183]. They are attracting attention from academia and industry due to their fully biodegradability in natural conditions, even in marine conditions, and the possibility to synthesize a large range of copolymers with different properties. Among PHAs, PHBV is a short-chain length copolymer, which is deeply studied and already available on the market. Depending on its hydroxyvalerate (HV) content, mechanical properties are close to those of common polyolefins, with interesting oxygen and water vapor transfer properties, which makes it a good candidate for packaging applications [406]. The biodegradation behavior of PHBV at laboratory scale has been well investigated [203,407]. Poly(3-hydroxybutyrate) (PHB) is even considered as a

suitable alternative for cellulose as a reference material in the standards of biodegradation for soil and water environments, respectively NF EN 17033 and ISO DIS 14852. Increasing the HV content is one of the strategies to improve the biodegradability [202] in addition to get better functional properties: lower melting temperature and higher elongation at break [408].

Vine crop is a very important economic activity that generates vast amounts of agricultural residues, particularly vine shoots (ViSh). In average, 2 tons of dry shoots are obtained per hectare every year [46]. Vine shoots correspond to the woody part obtained after pruning and are one of the most important primary solid lignocellulosic residues in agriculture. Depending on the region, ViSh are either collected and burnt or let on the vineyards where they could be roughly grounded and used as soil amendment. Their current economic value is therefore very small and better options for management are awaited. Several studies reported that ViSh could be an interesting source of high value added molecules such as polyphenols that are used in pharmaceutical and cosmetic sectors due to their antioxidant properties [49,51,52]. Hence, in a biorefinery context, polyphenols could be first extracted from vine shoots, and the exhausted lignocellulosic residues could be further used as fillers in biocomposites [379]. A recent study has shown the potential of using ViSh as fillers in a PHBV matrix [362,379]. It was concluded that such biocomposites can surely provide a sustainable alternative to fossil-based materials and a new way to manage agro-residues.

Generally, composite materials displayed a higher biodegradation rate than the virgin polymer matrix due to the higher water sorption of lignocellulosic fillers. It was the case with PHA-based composites filled with wood flour or olive pomace [409,410]. In another study dealing with PHBV/wheat straw composites, it has been reported that the presence of straw did not affect the biodegradation rate when it was evaluated in liquid environment and in long term soil burial tests [179]. However, in composting conditions, the rate of biodegradation was reduced for composites filled with more than 10 wt% of wheat straw. This negative effect was attributed to the fact that fungi that degrade lignin were not favored by the neutral pH encountered in compost medium. Several studies have shown that after removal of extractives, wood was more susceptible to degrade [411,412]. Nascimiento et al. [413] demonstrated the role of phenolic compounds in natural resistance of wood biodegradation. Wood extractives such as flavonoids or stilbenes are even considered as natural preservatives against wood decay organisms.

In this context, the aim of the present study was to examine for the first time the impact of vine shoots on the aptitude of PHBV/ViSh composites to biodegrade in soil. This is a main feature for such materials that are destined to short-term applications like packaging with trays or agriculture with pots. For that purpose, ViSh fillers were produced by dry milling. The impact of polyphenols extraction with a mixture acetone/water (v:v, 75:25) on the biodegradation behavior of ViSh and resulting biocomposites was investigated. PHBV/ViSh composites were prepared by microcompounding with a filler content of 20 wt%. The biodegradation behavior of both virgin and exhausted ViSh fillers and resulting composites was

assessed through respirometric tests monitored in aerobic conditions. Results were discussed in relation to the composition and the structure of materials.

## II-1.1 Materials and Methods

### II-1.2 Materials

Vine shoots of the Syrah species was kindly provided by Jean-Michel Salmon (UEPR, INRA). They were from Gruissan, in the Languedoc-Roussillon region in the South of France. These residues displayed an initial moisture content of around 40 wt% when they were pruned in the field. Cellulose was supplied by Arbocel J. Rettenmaier & Söhne (France) under the reference Arbocel<sup>®</sup> (grade BE 600-10 TG) in the form of a fine powder obtained after milling and sorting from pine cellulose. Particles were characterized by a cellulose content of 99.5%, a bulk density of 0.23 – 0.30 g.cm<sup>-3</sup> (in accordance with DIN EN ISO 60), a skeletal density of 1.56 g.cm<sup>-3</sup>, an average thickness of 15 µm and an average length of 18 µm (data given by the supplier).

Acetone from (99.8% of purity) and ethanol (99.9% of purity) were respectively purchased from Biosolve Chimie and Meridis.

#### II-1.2.1 Preparation of vine shoot fillers

Before dry fractionation, the fresh vine shoots were air dried during 2 months, then they were dried in an oven at 60°C for 24 h. They were then milled using a cutting mill type SM 300 (Retsch, Germany) with a 4.0 mm sieve and then 2.0 mm sieve. The resulting ViSh particles size was around between 1 and 0.5 mm, and were noted ViSh-V.

ViSh were extracted following the same protocol as David *et al.* [379]. Batches of 10 g of substrates were introduced in Pyrex glass reagent bottles with 50 mL of 75% v/v acetone that were incubated at 50°C in a shaking bath. The bottles were closed to avoid solvent evaporation. At the end of the incubation, liquid extract was separated from solid residue by centrifugation (5 min, 5000 rpm). The solid residue, noted ViSh-E, was dried under the hood overnight then dried at 60°C during 24 h.

Finally, ViSh-V and ViSh-E, after being dried overnight at 60°C, were then milled with centrifugal mill ZM 200 (Retsch, Germany) at 14000 rpm with 0.5 mm sieve.

The lignin content was determined by the Klason method [414]. The first hydrolysis was done using 72 % H<sub>2</sub>SO<sub>4</sub> solution at 30°C for 1 h and the second one was carried out using 4 % H<sub>2</sub>SO<sub>4</sub> solution at 121°C for 1 h. Ash content was determined in triplicate from the residue after thermogravimetric analysis (Mettler TGA2, Schwerzebach, Switzerland) at 800°C under air. The protein content was determined from elemental analysis. Nitrogen content was multiplied by a factor of 6.25 to obtain the protein content [415]. Analytical mercaptolyses developed by

Roumeas *et al.* [245] were conducted to determine the phenolic composition of milled vine shoots. The samples were then analyzed by an UPLC-DAD-MS system [245]. The quantification was done by UV absorbance monitoring at 280 nm.

#### II-1.2.2 Wide angle X-ray diffraction (XRD)

Wide angle X-ray diffraction analysis was carried with an “in house” setup from L2C lab (Montpellier) to characterize the crystallinity of the fillers. A high brightness low power X-ray tube, coupled with aspheric multilayer optic (GeniX<sup>3D</sup> from Xenocs with Cu K $\alpha$  radiation  $\lambda=1.54$  Å) was used delivering an ultralow divergent beam (0.5 mrad). The experiments were done in the transmission configuration and the scattered intensity was measured by a Schneider 2D image plate detector prototype, at a distance of 1.9 m. Capillary was used as support to load ViSh powder. All intensities were corrected by transmission and the empty cell contribution was subtracted.

#### II-1.2.3 Preparation of PHBV/ViSh biocomposites

Biocomposites were prepared by melt mixing PHBV with virgin and exhausted vine shoots (20 wt%). A Brabender Plasticoder 2000 equipped with an electrically heated mixer was used. The internal temperature of the mixer was maintained at 180°C and the mixing speed was 60 rpm. The total mixing time was 6 min, whereas the mixing time after the residue addition was 3 min.

#### II-1.2.4 Scanning electron microscopy (SEM)

The ViSh fillers and the cross-section of PHBV-based composites were observed by scanning electron microscopy (SEM). In case of composites, the cross-sections were obtained after cryo-fracturing in liquid nitrogen. A SEM S4800 microscope (Hitachi, Japan) was used with an acceleration voltage of 2 kV. The samples were previously coated with Pt by cathode pulverization.

### II-1.3 Biodegradation tests

Respirometric tests were conducted in soil at 28°C under aerobic conditions to evaluate the biodegradability of composite materials. The method was adapted from the US standard ASTM D5988-96, which describes the method for determining aerobic biodegradation in soil of plastic materials, the released CO<sub>2</sub> being proportional to the amount of biodegraded substrate. The measure of CO<sub>2</sub> gives information about the ultimate degradation step, namely the mineralization, during which the substrate is broken down into final products.

First, the composite samples were milled with a coffee grinder (Moulinex type DPA1, France), then sieved at 0.5 mm to get the same size of particles between the different samples. The carbon contents were measured by elemental analysis (ThermoQuest NA 2500) for each sample. Thus, exactly 50 mg of equivalent carbon were introduced into 25 g of soil. The soil used in this study was a top soil (Verve, pH = 7.5, C/N = 39). The soil was air dried during one week then it was sieved through a sieve of 2 mm. The dry matter content was 97%. It was determined by drying the soil at 105°C until constant weight.

The biodegradation tests were carried out as described by Chevillard *et al.* [416], in hermetic glass jars (1 L, Le Parfait, France) which contained three open polypropylene vials (60 mL). One vial contained 25 g of dry soil mixed with 50 mg equivalent carbon of samples. The water content of soil was adjusted to reach 80% of the water holding capacity of the soil. The water holding capacity of soil was determined based on the weight of the soil saturated by water and the dry weight of the soil. A second vial of 15 mL of NaOH (0.2 M) trapped the CO<sub>2</sub> released by the microorganisms. The relative humidity was maintained at 100% inside the jar thanks to the third vial filled with distilled water. The jars were hermetically closed and incubated in the dark at 28 ± 1°C. At selected time, the glass jars were opened to determine the amount of CO<sub>2</sub> trapped by the NaOH solution by back titration with a HCl solution (0.1 M) in the presence of thymophthaleine (0.10% in ethanol), 5 mL of barium chloride solution (20% in water) was added in each flask to precipitate carbonate ions. The vials containing soil were weighted and if necessary appropriate amount of water was added to stay at 80 % of the soil water retention capacity. A new vial containing a NaOH solution (0.2 M) replaced the one which was just titrated. The glass jars were left open during 2 min in order to be aerated. Then each glass jar was closed and put again in the dark at 28°C until next measurements.

The biodegradation tests included a control and a blank. A powder of pure cellulose (BE 600-10 TG grade) was used as control because of its well-known degradation. For the blank, the experiment was conducted without addition of carbon source in the soil to be able to measure the CO<sub>2</sub> naturally produced by the soil and the CO<sub>2</sub> present in the air of the glass jar. The tests were measured in triplicate. Results were calculated by subtracting the CO<sub>2</sub> production of the blank. The percentage of biodegradation D is calculated using Eq. 48:

$$D = \frac{\text{CO}_2 \text{ material} - \text{CO}_2 \text{ blank}}{\text{CO}_2 \text{ theoretical}} \times 100 \quad \text{Eq. 48}$$

where “CO<sub>2</sub> materials” and “CO<sub>2</sub> blank” are the amount of carbon dioxide (mg) released in the test jar and in the blank control jar. “CO<sub>2</sub> theoretical” is the theoretical amount of carbon dioxide (mg) produced by total oxidation of the tested material. In the same way the percentage of biodegradation of the reference material is calculated to check in the soil activity. As required by the ASTM D5988-96 standard, to check the activity of the soil and to ensure the validity of the test, cellulose (used as a positive control) should reach a biodegradation percentage higher than 70% in less than 6 months. The biodegradation curves of all the tested materials

were finally normalized according to the biodegradation percentage of cellulose reached at the plateau.

The experimental degradation data were modeled with the Hill equation (Eq. 49):

$$\text{Deg} = \frac{\text{Deg}_{\max} \times t^n}{k^n + t^n} \quad \text{Eq. 49}$$

where Deg is the percentage of degradation at time  $t$  (day),  $\text{Deg}_{\max}$  the percentage of degradation at infinite time,  $k$  (days) the time for which  $\text{Deg} = \frac{1}{2} \text{Deg}_{\max}$  and  $n$  the curve radius of the sigmoid function.

## II-2 Results and Discussion

### II-2.1 Biodegradability of ViSh fillers

Both fillers, ViSh-V and ViSh-E, were subjected to the same milling route in order to get particles with the same size. It was verified by SEM observations that both fillers did not display notable difference in terms of morphology and surface aspect (Figure 101). Laser diffraction analysis (Malvern Mastersizer 2000) allowed measuring their median apparent diameter, that was  $143 \pm 10 \mu\text{m}$  for the two fractions. Fillers were introduced in the soil medium without additional milling.

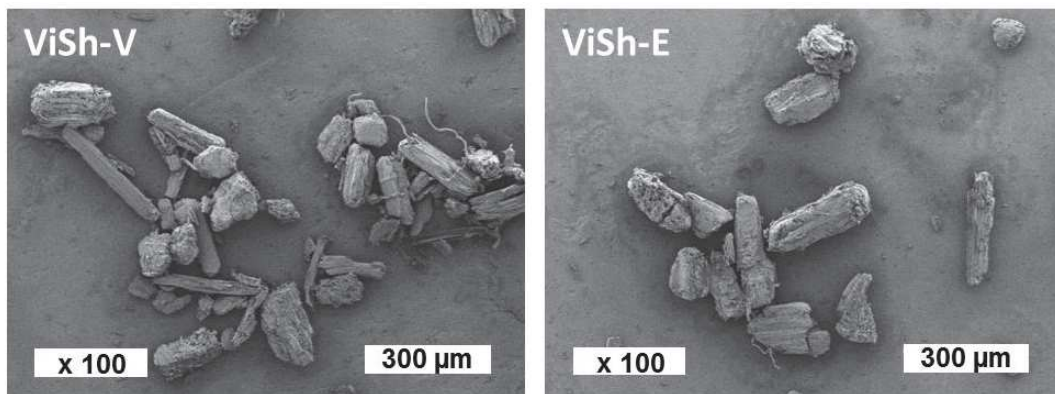


Figure 101. SEM pictures of vine shoots fillers

Table 53 presents the biochemical composition of the two ViSh fillers. It can be noticed that the Klason lignin was slightly lower for ViSh-E. This was probably due to the removal of condensed tannins during extraction that were first included in the Klason lignin in the case of ViSh-V. The ash content was slightly higher in the case of ViSh-E due to the removal of 10



wt% of the total mass during the extraction. As expected, the tannin content was reduced by 67 % and resveratrol, a stilbenoid compound, was almost absent in Vish-E (Table 53).

The protein content of ViSh-V fillers was slightly lower than values reported in the literature, with 3.3 % instead of 5 % [46]. After extraction the protein content was reduced by half. The N content of ViSh particles was low, inducing C/N ratio as high as 87 and 170 respectively for ViSh-V and ViSh-E. A high C/N ratio was expected to induce a decrease of the biodegradability due to a surplus of degradable substrate [417].

Table 53. Biochemical composition (% dry basis) of ViSh fillers.

Sample	Klason lignin	Ashes	Tannins	Resveratrol	Proteins	C	N
ViSh-V	19.4 ± 0.5	3.9 ± 0.2	1.25 ± 0.07	0.07 ± 0.01	3.3	46.05	0.53
ViSh-E	17.7 ± 0.5	4.7 ± 0.5	0.41 ± 0.07	0.01 ± 0.00	1.7	45.96	0.27

In order to analyze the crystallinity of the ViSh particles, XRD patterns were used (Figure 102). The crystallinity index (CrI) can be determined by using the following equation (Eq. 50) [250]:

$$\text{Crystallinity index (CI)} = \frac{I_{002} - I_{\text{am}}}{I_{002}} \quad \text{Eq. 50}$$

where  $I_{002}$  is the peak intensity at  $22^\circ$  representing the crystalline cellulose regions and  $I_{\text{am}}$  was the intensity at  $18^\circ$  representing the amorphous part.

The deduced crystallinity from the X-ray diffractograms were 30 % and 32 % respectively for ViSh-V and ViSh-E. It could be concluded that the acetone/water based extraction treatment did not significantly impact the crystallinity of ViSh.

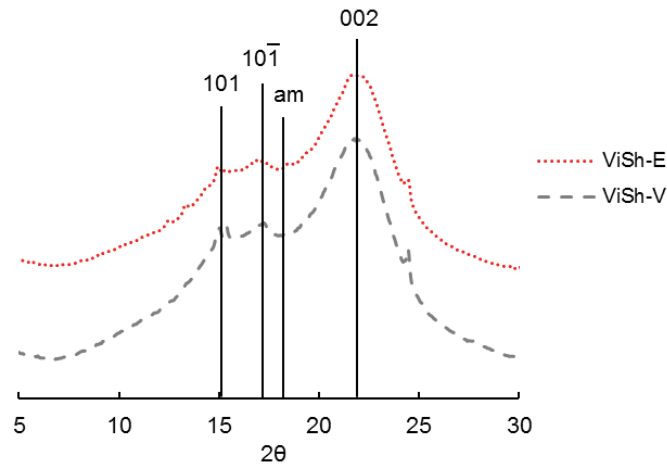


Figure 102. X-ray diffractograms of ViSh-V and ViSh-E

The biodegradation rate of ViSh-V and ViSh-E fillers was assessed by monitoring the released carbon dioxide. The CO<sub>2</sub> evolution is an indicator of the ultimate biodegradability resulting from mineralization of the organic carbon of the tested materials. The biodegradation curves of ViSh-V and ViSh-E presented in Figure 103 displayed a characteristic Hill sigmoidal shape with a low radius, close to 1 (Table 55). Generally, when microorganisms are involved, two phases are ascribed to the polymer degradation process. First, extracellular enzymes cleave the polymers chains into small fragments. Then, these fragments are mineralized into the cell and transformed into CO<sub>2</sub>, water minerals and biomass [418]. Here the two steps seemed to occur simultaneously.

Leaving aside standard requirements, the ViSh fillers biodegraded rather well compared to cellulose. The inherent structure and crystallinity of lignocellulose can be altered by milling. Mais *et al.* suggested that reducing the size of the sample by milling would make it more available for enzymatic degradation [419]. However, in the present case the particle sizes were the same and the crystallinity indexes were very close, which would be expected not to induce a significant effect on the biodegradability.

Interestingly, the biodegradation curves showed that ViSh-V particles were not fully biodegradable because the entire material was not fully mineralized into CO<sub>2</sub>. The final biodegradation rate reached only 83.1 % which was below the standard of 90 % (in absolute or relative to cellulose) to be considered as fully biodegradable as claimed by the NF EN 17033 standard. These results were not surprising since lignocellulosic materials are complex materials in terms of structure and chemistry, resulting usually in a quite low biodegradation. Lignin is particularly recalcitrant to microbial degradation [420], fungi being the main lignin destroyers. It had been proved that biodegradation level of biomass is higher for hemicellulose and cellulose than lignin [421]. Besides, lignin is more hydrophobic than cellulose as already shown using water contact angle measurements [362].

Moreover, as shown in Table 53, ViSh contained polyphenols notably tannins that are known to be recalcitrant to microbial attack [422,423]. They can even be toxic to some microorganisms even if reports related to the ability of bacteria to degrade tannins are scarce. However, works had shown that fungi can degrade tannins, which can be useful to treat tannery effluents [423].

It can be noticed that ViSh-E degraded better than ViSh-V. The exhausted ViSh had a final biodegradation level of 97%, allowing to conclude that ViSh-E were biodegradable according to the NF EN 17033 standard. Such a behavior was mainly explained by the polyphenol removal.

It is worth noting that ViSh-V and ViSh-E started to degrade at the same rate and differentiated only after the 20<sup>th</sup> day. In addition, although ViSh-E reached a plateau at almost 100% of mineralization, its initial biodegradation rate was much lower than these of cellulose (Figure 103). This pointed out the fact that it is delicate to forecast the final biodegradation

levels from the initial biodegradation rate. It is also the reason why the biodegradation curves obtained from the evolution of carbon dioxide release should reach a plateau phase similar to the positive control (cellulose), which reflected that no further biodegradation was expected. This is a proof that the entire material was fully mineralized into carbon dioxide attesting its final assimilation by microorganisms as requested in the majority of the standards dealing with the biodegradation assessment and notably NF EN 17033.

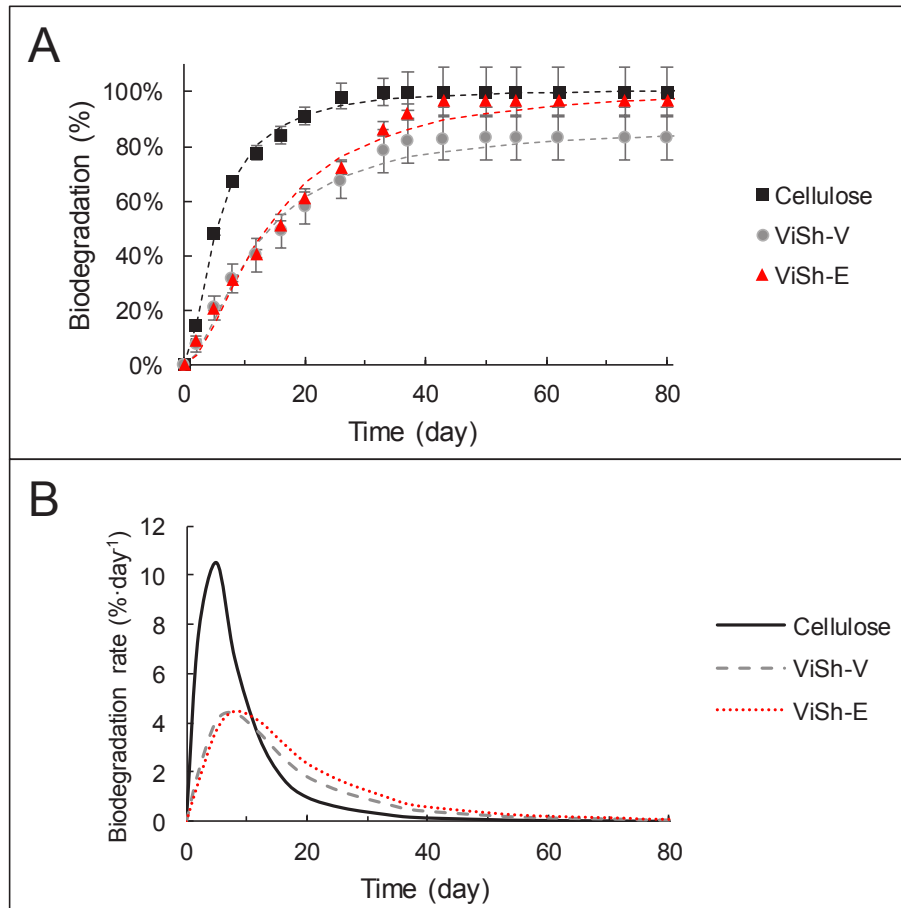


Figure 103. Kinetic of biodegradation (A) and biodegradation rate (B) of ViSh-fillers in soil.

## II-2.2 Biodegradability of PHBV-based composites

Composite materials were introduced in the soil after a milling and sieving step. Their median size determined by a laser diffraction particle size analyzer (Malvern Mastersizer 2000) was  $350 \pm 20 \mu\text{m}$ .

SEM image of the surface of PHBV film (Figure 104) displayed a smooth and homogeneous surface as previously shown by AFM 3D pictures of films made of the same PHBV grade [203]. As already reported in literature a smooth surface can favor the microorganisms adhesion at the material surface thus promoting its subsequent biodegradation [424]. On SEM image of the

fracture of PHBV film (Figure 104), small elements were visible. They were boron nitride that were added in the commercial grade of PHBV as nucleating agents at the rate of 1 wt%. Composite materials displayed a rougher fractured surface due to the presence ViSh fillers. No significant difference was observable between composite materials when comparing ViSh previously exhausted or not. In both cases, interfacial gaps between the matrix and the fillers were visible at high magnification attesting that the filler/matrix adhesion was not perfect. Such defects would allow water to better diffuse in the bulk and improve accessibility to microorganisms as compared to neat PHBV.

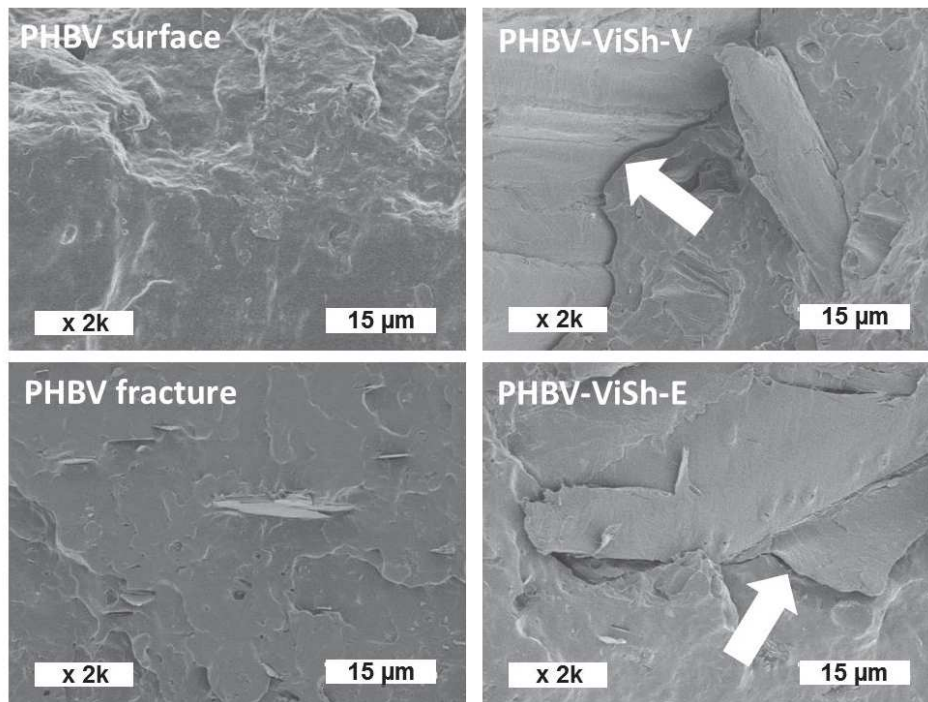


Figure 104. SEM pictures of PHBV surface and fracture (on the left) and SEM picture of the PHBV-based composites fractures (filler content of 20 wt%) (on the right).

The neat PHBV and PHBV/ViSh composites were subjected to respirometric tests undertaken in soil in the same aerobic conditions than those used for ViSh fillers. The resulting biodegradation curves of the composites materials are shown in Figure 105.

No significant difference between the samples was revealed in this experiment with respect to their degradation rate. Although bacterial PHBV is known as easy biodegradable polymer, it can be noticed that its biodegradation proceeds more slowly than cellulose reference material. However, the biodegradation curves confirmed that PHBV was fully biodegradable with evolution of CO<sub>2</sub> reaching a plateau phase of  $96 \pm 5\%$  after 55 days in soil. Even if reached later, the plateau phase of PHBV curves was similar to these of cellulose (positive control), which reflected that no additional biodegradation was expected. The rate of biodegradation of a given material being strongly dependent of soil composition, it should be always compared

to these of a positive control like cellulose. In the present study, it is worth noting that PHBV exhibited a rather high rate of biodegradation. This could be explained by the milling treatment applied on composite samples that is expected to cause an easy accessibility to enzymes and microorganisms thus increasing the available surface for degradation [15].

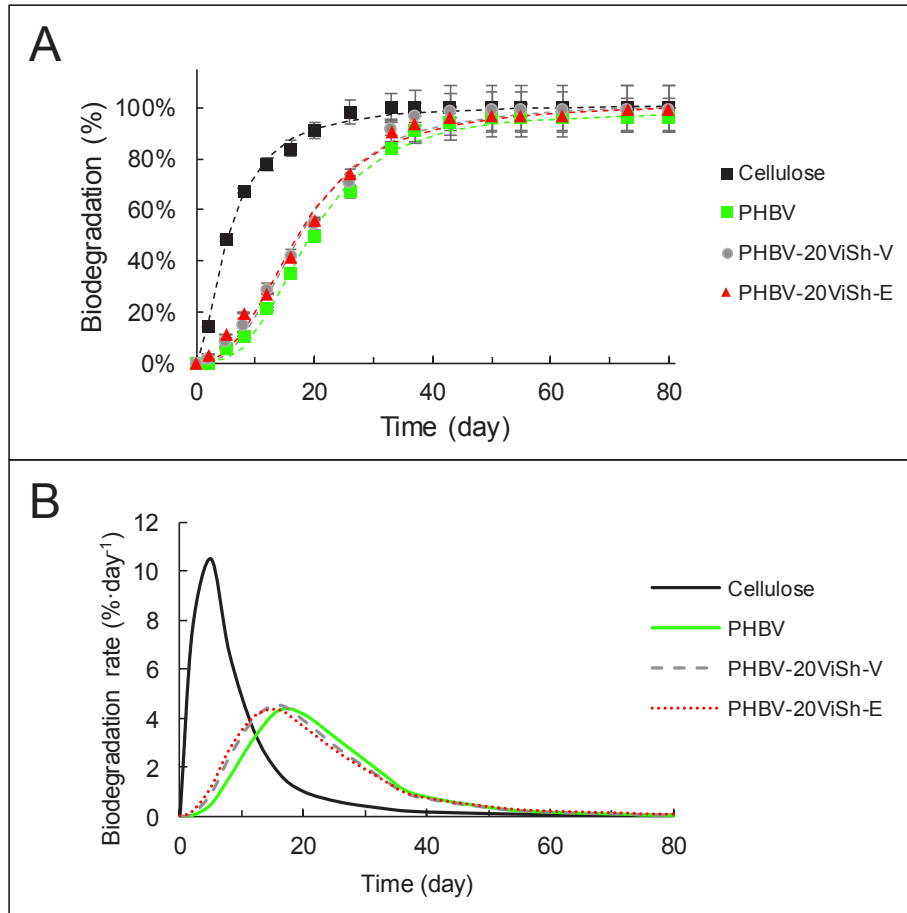


Figure 105. Kinetic of biodegradation (A) and biodegradation rate (B) of PHBV-based composites in soil.

Even if the differences were weak, both composite materials degraded slightly better than neat PHBV, as evidenced in Figure 105B. There are different possible reasons to explain it. Firstly, it has been shown that the permeability to water vapor increased with the incorporation of natural fillers (Table 54). Hydrolytic chain scission mechanism being expected to increase with the water permeability of the materials, this could contribute to improve the biodegradation of composites material as compared to the neat matrix. Secondly, the stiffness values of composites were higher than neat PHBV with higher Young's modulus determined in a previous paper [379]. Material stiffness being also a factor able to promote the colonization of its surface by microorganisms [425], this could also be a reason why composites degraded faster than neat matrix. Lastly, difference in polymer crystallinity might also lead to changes in their biodegradation patterns. However, no significant differences of crystallinity were measured between the tested materials. Generally, the amorphous phase of a polymer is more susceptible

to be degraded than the crystalline phase. On another note, in the case of PHBV this argue could not be evoked since both amorphous and crystalline phase have been shown to degrade at the same rate by Salomez et al. [203].

Another point that could be noted is that the difference of biodegradation observed between ViSh-V and ViSh-E was no longer visible in the PHBV-based composites. Indeed, PHBV-20ViSh-V and PHBV-20ViSh-E exhibited the same kinetics and the same final biodegradation levels (100 %). This underlined that the biodegradation rate of PHBV-based composites was driven by the behavior of the PHBV matrix.

Table 54. Properties of PHBV-based composites with ViSh fillers (from [379])

	WVP ( $\times 10^{13}$ mol·m/(m <sup>2</sup> ·s·Pa))	Young's modulus (GPa)	PHBV crystallinity (%)
PHBV	4.3 ± 1.3	2.16 ± 0.02	55.9
PHBV-20ViSh-V	14.0 ± 1.6	2.50 ± 0.03	52.0
PHBV-20ViSh-E	21.1 ± 2.0	2.43 ± 0.04	55.4

The biodegradation curves were modeled using Hill equation and corresponding parameters are presented in Table 55. Deg<sub>max</sub> that represents the percentage of degradation at infinite time according to Hill equation was close to the plateau phase observed in Figure 103 and Figure 105. Cellulose exhibited the highest maximum of biodegradation with ViSh-E and PHBV composites. It took less than 20 days for all the samples to reach 50% of Deg<sub>max</sub> as indicated by k values. The constant n, representing the curve radius of the sigmoid function, was higher for PHBV-based materials especially for neat PHBV than for the fillers alone. This illustrated that the biodegradation started a little later for PHBV than for lignocellulosic materials with probably a better availability and access for microorganism's enzymes in the latter case. As a result, the time needed to reach the maximum of biodegradation rate (Time<sub>rate max</sub>) was lower for the fillers (8 days) than for the composites materials (16 days). On the contrary, all the samples tested had similar maximum degradation rate (Deg<sub>rate max</sub>) with value around 4.5 %·day<sup>-1</sup> suggesting a predominance of the PHBV on the overall mechanism of biodegradation of the composite materials.

Table 55: Hill parameters and related biodegradation indicators of fillers

	Hill parameters				Time <sub>rate max</sub> (day)	Deg <sub>rate max</sub> (%·day <sup>-1</sup> )
	Deg <sub>max</sub> (%)	k (day)	n	R <sup>2</sup>		
Cellulose	101 (±1)	5.5 (±0.1)	1.7 (±0.1)	0.99	5	10.5
ViSh-V	87 (±2)	11.8 (±0.6)	1.7 (±0.1)	0.98	8	4.5
ViSh-E	102 (±2)	13.9 (±0.8)	1.8 (±0.2)	0.98	8	4.3
PHBV	98 (±1)	19.1 (±0.4)	3.1 (±0.2)	0.99	16	4.3
PHBV-20ViSh-V	102 (±1)	17.6 (±0.5)	2.8 (±0.1)	0.99	16	4.4
PHBV-20ViSh-E	102 (±1)	17.3 (±0.5)	2.6 (±0.2)	0.99	16	4.5

## II-3 Conclusion

Vine shoots were milled using dry fractionation to be used as fillers in PHBV-based composites. The impact of ViSh fillers on the biodegradability in soil of the resulting composite materials was investigated in relation to their polyphenols content. It was found that the incorporation of ViSh fillers in PHBV (filler content of 20 wt%) slightly accelerated the biodegradation kinetic of the composites. All the PHBV-based composites were considered as fully biodegradable in soil medium whereas ViSh-V fillers degraded only until 80% compared to the cellulose reference. ViSh-E was fully biodegraded, confirming the negative impact of polyphenols in the biodegradation mechanism. These assumptions were supported by measurements of crystallinity and SEM observations, which showed the absence of difference in structure nor morphology between particles.

The present work displays a promising valorization pathway for vine shoots considered as an agro-residue. Their incorporation into a PHBV matrix allows to design biodegradable materials. Moreover, in a biorefinery context, the extraction of polyphenols extraction has the advantage to improve the biodegradability of vine shoots.

## Acknowledgments

The authors gratefully acknowledge Didier Cot (IEM, Montpellier) for SEM observations.

This work was carried out in the framework of the NoAW project, which is supported by the European Commission through the Horizon 2020 research and innovation program under the Grant Agreement No. 688338.

### III. Complementary results

#### III-1.1 Supplementary results

III-1.1.1 “In situ” density of ViSh particles: density of ViSh fillers inside the composite materials.

The density of the ViSh particles once embedded in the composite materials is between the apparent density and the true density. It could be called “in situ density”.

The “in situ” density of ViSh particles inside the composite was deduced from the density of PHBV-ViSh composite films (measured with a pycnometer for different filler contents) and the true density of ViSh particles, also measured by pycnometry (Table 56).

Table 56. Density of composite films and ViSh particles measured by pycnometry

Filler content (wt%)	Density (g.cm <sup>-3</sup> )	Standard deviation
0	1.246	0.003
5	1.253	0.004
10	1.259	0.005
20	1.268	0.005
30	1.281	0.005
ViSh particles	1.468	0.002
ViSh particles in composite	1.364	-

The evolution of the density of composite films as a function of the weight filler content is displayed on Figure 106. The results showed that there was linear relation ( $R^2 = 0.9993$ ) between the composite density and the weight filler content (Figure 106). However, it can be noticed that the density measured for only ViSh particles did not follow this linearity. The ViSh density that is needed for the LCA of composites should be in conformity with the density measured for composite using a mixing rule. The “in situ” density of ViSh particles was deduced from the linear relationship. The deduced density was 1.364 g.cm<sup>-3</sup>. This value was lower than the density of ViSh particles due to the micro-porosity in the fibers (that are not filled by the polymer matrix) and the possible micro-voids at the filler/matrix interface in the composites (Figure 107).



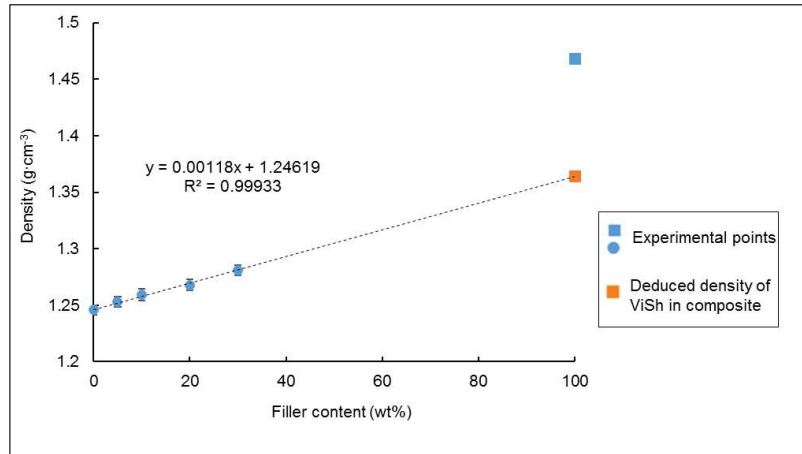


Figure 106. Determination of the density of ViSh fillers in composite.

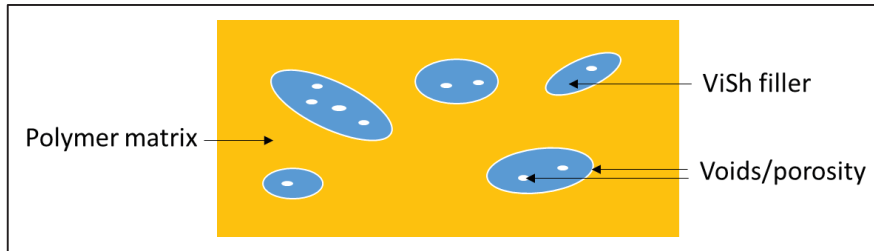


Figure 107. Scheme of composites filled with ViSh particles.

## III-1.1.3 Environmental impacts

Table 57. Environmental impact of 100% plastic trays

100% plastic tray				
Impact category	Unit	Tray PHBV	Tray PLA	Tray PP
Global warming	kg CO2 eq	0.12324266	0.127545345	0.08452881
Stratospheric ozone depletion	kg CFC11 eq	1.47311E-07	3.25562E-07	9.74326E-09
Ionizing radiation	kBq Co-60 eq	0.038296604	0.035202319	0.021013941
Ozone formation, Human health	kg NOx eq	0.000210588	0.000262092	0.000132674
Fine particulate matter formation	kg PM2.5 eq	0.000163097	0.000211406	5.38288E-05
Ozone formation, Terrestrial ecosystems	kg NOx eq	0.000218428	0.00027672	0.000144078
Terrestrial acidification	kg SO2 eq	0.000432729	0.000520676	0.000156031
Freshwater eutrophication	kg P eq	2.98875E-05	4.70116E-05	3.282E-06
Marine eutrophication	kg N eq	3.79059E-05	6.48952E-05	1.61378E-06
Terrestrial ecotoxicity	kg 1,4-DCB	0.242687886	0.235790306	0.067083659
Freshwater ecotoxicity	kg 1,4-DCB	0.00432803	0.00634943	0.002143046
Marine ecotoxicity	kg 1,4-DCB	0.005845332	0.00825518	0.003019349
Human carcinogenic toxicity	kg 1,4-DCB	0.003788349	0.004395154	0.001283093
Human non-carcinogenic toxicity	kg 1,4-DCB	0.111555561	0.109191198	0.029448098
Land use	m2a crop eq	0.052363716	0.037707128	0.001524081
Mineral resource scarcity	kg Cu eq	0.000184609	0.00027153	4.97332E-05
Fossil resource scarcity	kg oil eq	0.030884171	0.03535764	0.041443222
Water consumption	m3	0.004312782	0.008718666	0.000624627

Table 58. Environmental impact of 100% plastic trays

30 vol% filler content				
Impact category	Unit	Tray PHBV/ViSh	Tray PLA/ViSh	Tray PP/ViSh
Global warming	kg CO <sub>2</sub> eq	0.098988531	0.102090259	0.077278008
Stratospheric ozone depletion	kg CFC11 eq	1.12915E-07	2.40768E-07	1.36235E-08
Ionizing radiation	kBq Co-60 eq	0.045314633	0.043126618	0.031918198
Ozone formation, Human health	kg NO <sub>x</sub> eq	0.000171755	0.000208716	0.00011712
Fine particulate matter formation	kg PM <sub>2.5</sub> eq	0.000127777	0.000162443	4.88344E-05
Ozone formation, Terrestrial ecosystems	kg NO <sub>x</sub> eq	0.000178419	0.000220249	0.000126375
Terrestrial acidification	kg SO <sub>2</sub> eq	0.000340357	0.000403482	0.000138195
Freshwater eutrophication	kg P eq	2.29674E-05	3.52523E-05	3.79801E-06
Marine eutrophication	kg N eq	2.80615E-05	4.74196E-05	2.37578E-06
Terrestrial ecotoxicity	kg 1,4-DCB	0.2013237	0.196429401	0.07584904
Freshwater ecotoxicity	kg 1,4-DCB	0.003632278	0.005083563	0.002533892
Marine ecotoxicity	kg 1,4-DCB	0.004873149	0.006603417	0.003512749
Human carcinogenic toxicity	kg 1,4-DCB	0.002990004	0.003425714	0.001209998
Human non-carcinogenic toxicity	kg 1,4-DCB	0.085465075	0.08377988	0.032649187
Land use	m <sup>2</sup> a crop eq	0.038576965	0.028065979	0.002094647
Mineral resource scarcity	kg Cu eq	0.000166815	0.00022921	6.89058E-05
Fossil resource scarcity	kg oil eq	0.026013689	0.029226589	0.033509612
Water consumption	m <sup>3</sup>	0.003818456	0.006981661	0.001072443

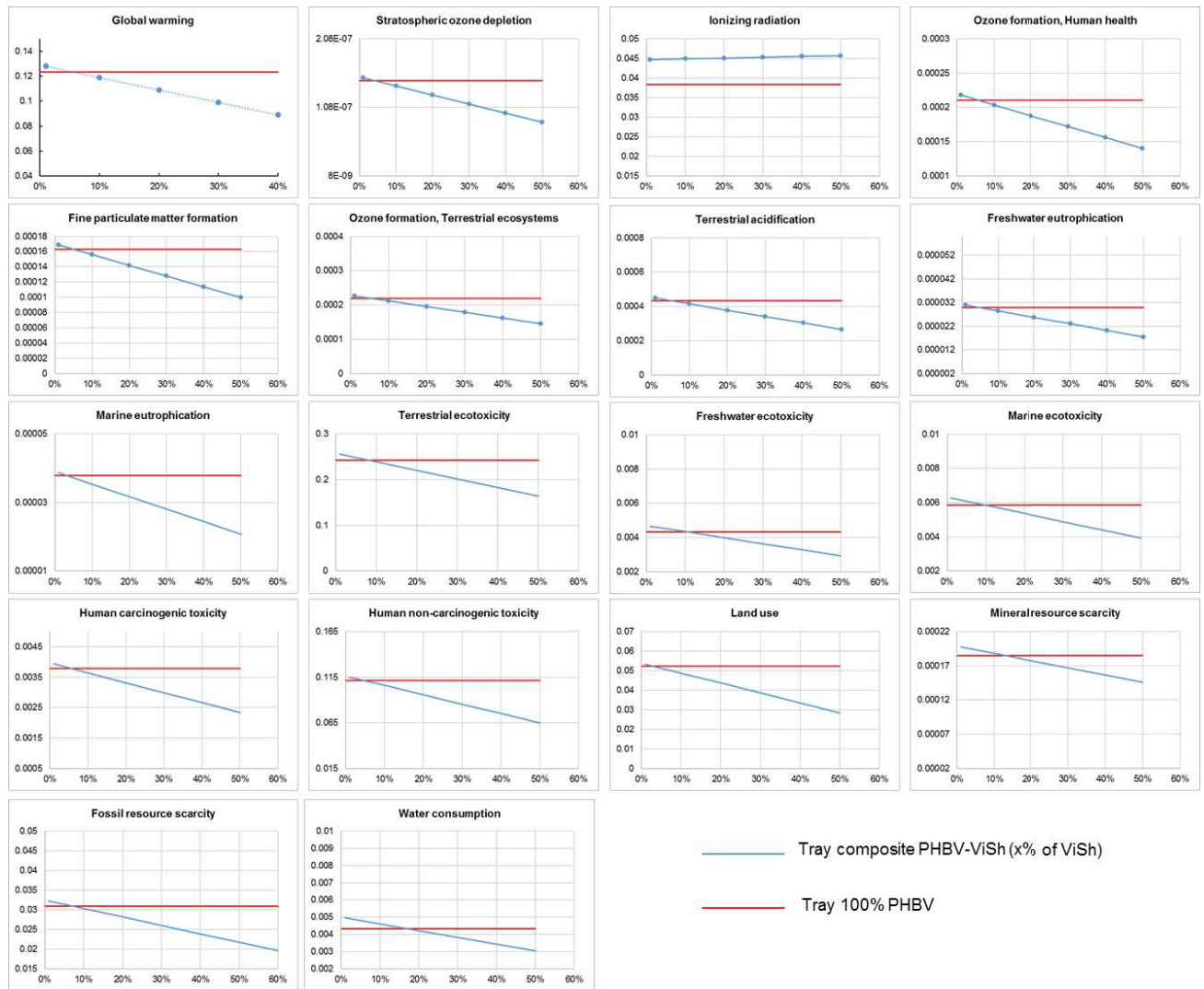


Figure 108. Environmental impact of PHBV-based composite tray according to the ViSh content

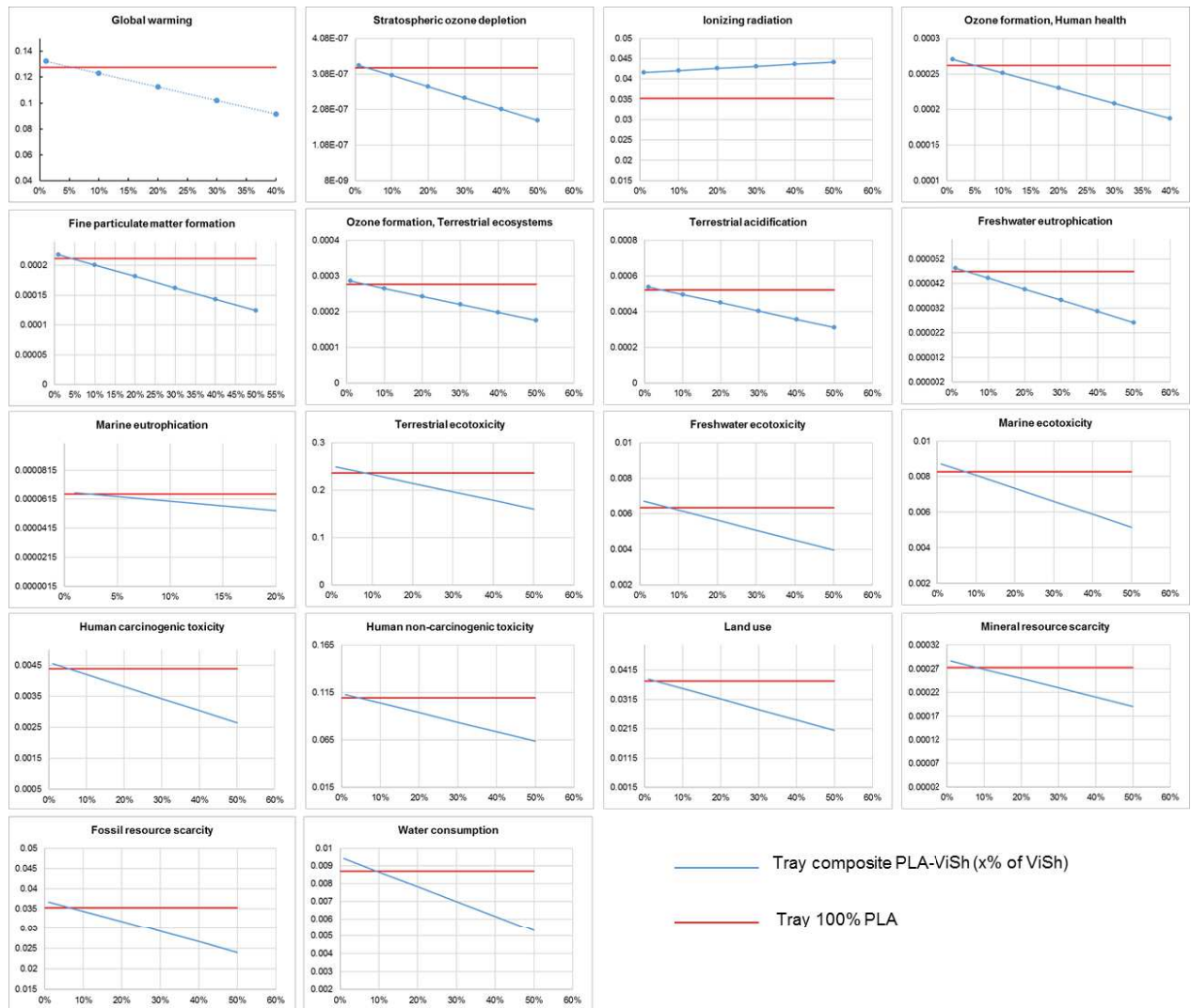


Figure 109. Environmental impact of PLA-based composite tray according to the ViSh content

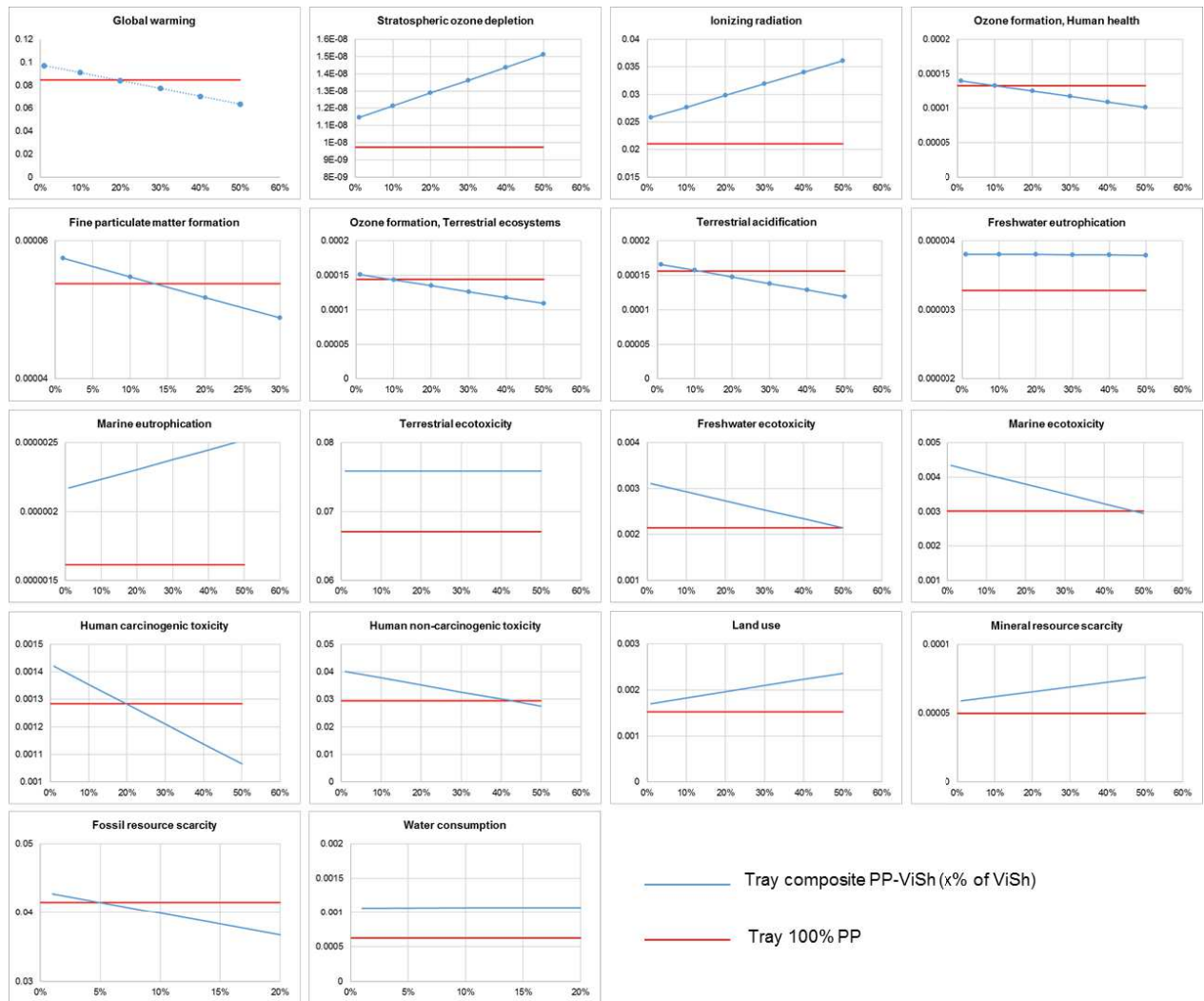


Figure 110. Environmental impact of PP-based composite tray according to the ViSh content

III-1.2 Supplementary inventory

<b>X</b>	filler content, in volume
<b>1-X</b>	matrix content, in volume
<b>d(filler)</b>	density of the filler
<b>d(matrix)</b>	density of the matrix
<b>f</b>	filler content, in weight ( $f = d(\text{filler}) \cdot X / (d(\text{filler}) \cdot X + d(\text{matrix}) \cdot (1-X))$ )
<b>m</b>	matrix content, in weight ( $m = 1 - f$ )
<b>d(composite)</b>	density of the composite = $d(\text{matrix}) \cdot (1-X) + d(\text{filler}) \cdot X$

Fresh vine shoots	Transport, freight, lorry 3.5-7.5 metric ton, EUROS (RER)   transport, freight, lorry 3.5-7.5 metric ton, EUROS   Cut-off, S	0.0100	tkm	10 km for 1 kg	1 kg
Air drying	Occupation, industrial area, built up (Inputs from nature)	0.0130	m3	2 meter high, density of 30kg/m3, 7 months in a year	1 kg
Big bag	Fresh vine shoots	1.3333	kg	1/0.75=1.33 (1kg at 40% gives 0.75kg at 20%, 0.6/0.8=0.75)	15 m3 1 bag is used 3 times during 5 years
	Polypropylene, granulate (GLO)   production for   Cut-off, S	2.5000	kg	1 big bag is 2.5 kg	
	Extrusion, plastic film (GLO)   market for   Cut-off, S	2.5615	kg	1 kg gives 0.976kg of matter (2.5/0.976=2.561)	
	Transport plastics	2.5615	tkm	1 kg gives 0.976kg of matter (2.5/0.976=2.561)	
	PP (waste treatment) (GLO)   recycling of PP   Cut-off, S	0.7225	kg	28.9% recycling	
	Waste polypropylene (CH)   treatment of, municipal incineration   Cut-off, S	0.9125	kg	36.5% incineration	
VISH cuts	Waste polypropylene (CH)   treatment of, sanitary landfill   Cut-off, S	0.8650	kg	34.6% landfilling	1 kg
	Wood chipping, chipper, mobile, diesel, at forest road (GLO)   market for   Cut-off, S	0.0005	hr	Throughput: 2000 kg/h (output)	
	Air drying	1.1111	kg	1/0.9=1.11, yield of 90%	
Final drying	Big bag	0.0050	m3	bulk density of wood chips: 200kg/m3	1 kg
	GD-Drying of maize straw and whole-plant (CH)   processing   Cut-off, S	0.1875	l	1.1875kg at 20% gives 1kg at 5% in water mass of water to evaporated: 1.1875-1=0.1875kg and 1kg=1l	
	Electricity, low voltage (FR)   market for   Cut-off, S			instead of (CH), adapted for French electricity mix	
	Heat, from steam, in chemical industry (RER)   steam production, as energy carrier, in chemical industry   Cut-off, S			heat, direct or indirect, other than natural gas (RER)   market for   Cut-off, S instead of (CH), adapted for French electricity mix	
VISH particles 1mm	VISH cuts	1.1875	kg	1.1875kg at 20% gives 1kg at 5% in water	1 kg
	GD1-Wood chipping, industrial residual wood, stationary electric chipper (RER)   processing   Cut-off, S	1.0101	kg	yield of 99%	
	Electricity, low voltage (FR)   market for   Cut-off, S	0.1	kWh	instead of medium voltage 0.02 kWh SM 300 Retsch: 30 kg/h, 3kW and 3/30=0.1 no big bag needed direct, two the next milling	
VISH fillers	Final drying	1.01	kg	yield of 99%	1 kg
	GD2-Wood chipping, industrial residual wood, stationary electric chipper (RER)   processing   Cut-off, S	1.0101	kg	yield of 99%	
	Electricity, low voltage (FR)   market for   Cut-off, S	0.25862069	kWh	instead of medium voltage 0.02 kWh CUM 150 Netzsch Condux: 29 kg/h, 7.5kW and 7.5/29=0.258	
	VISH particles 1mm	1.01	kg	yield of 99%	
Transport plastics	Big bag	2.381E-03	m3	density of milled VISH in bag 420 kg/m3	1 kg
	Transport, freight, lorry 16-32 metric ton, EUROS (GLO)   market for   Cut-off, S	4.500E-01	tkm	450 kg.km average shipping distance of plastics by truck	
	Transport, freight train (GLO)   market group for   Cut-off, S	2.890E-01	tkm	289 kg.km by train	
	Transport, freight, sea, transoceanic ship (GLO)   market for   Cut-off, S	5.250E-01	tkm	525 kg.km by boat	
PP matrix	Transport, freight, aircraft (GLO)   market for   Cut-off, S	8.000E-03	tkm	8 kg.km average shipping distance of plastics by plane	1 kg
	Polypropylene, granulate (GLO)   production for   Cut-off, S	1	kg		
PLA matrix	Transport plastics	1	kg		1 kg
	Poly(lactide, granulate (GLO)   production   Cut-off, S	1	kg		
PHBV matrix	PHBV (ecobiocap)	1	kg		1 kg
	Transport plastics	1	kg		

Name	inputs/outputs	amount	unit	Comments	Amount final
Compounding (matrix:VISH, 1-X:X) pellets	GD-Extrusion, plastic film (RER)   production   Cut-off, S	1.024590	kg	1 kg of this process equals 0.976 kg of extruded plastic film.	1.0 kg (yield of 97.6% already included)
	Electricity, low voltage (FR)   market for   Cut-off, S	0.300	kWh	300 kWh/t so 0.3 kWh <del>instead of medium voltage 0.55 kWh</del>	
	EoL matrix	$((1/0.976)-1)*m$	kg	m% plastic, loss of the yield 97.6%	
	EoL VISH	$((1/0.976)-1)*f$	kg	f% VS, loss of the yield 97.6%	
	Matrix	$1/0.976*m$	kg	f% filler, yield 97.6%	
	VISH fillers	$1/0.976*f$	kg	m% plastic, yield 97.6%	
100% plastic tray	Big bag	0.001429	m3	density of granules in big bag: 700 kg/m3	1p a 100% matrix tray is $d(matrix)*0.025$ kg
	GD-Injection moulding (RER)   processing   Cut-off, S	0.030935614	kg	adapted for French electricity mix, 1kg of this process is for 0.994kg of injection moulded plastic	
	Electricity, medium voltage (FR)   market for   Cut-off, S			<del>instead of 1.015</del> , adapted for French electricity mix	
	Matrix	$(1/0.994)*d(matrix)*0.025$	kg	yield of injection is 99.4%	
	EoL matrix	$1*d(matrix)*0.025$	kg	EoL of tray	
Composite tray matrix:VISH (1-X):X	EoL matrix	$((1/0.994)-1)*d(matrix)*0.025$	kg	EoL of loss during injection (99.4%)	1p a composite tray matrix:VISH (1-x):x is $d(composite)*0.025$ kg
	GD-Injection moulding (RER)   processing   Cut-off, S	$1/0.994*d(composite)*0.025$	kg	1kg of this process is for 0.994kg of injection moulded plastic	
	Electricity, medium voltage (FR)   market for   Cut-off, S			<del>instead of 1.015</del> , adapted for French electricity mix	
	Compounding (matrix:VISH, 1-X:X) pellets	$1/0.994*d(composite)*0.025$	kg	yield of injection is 99.4%	
	EoL matrix	$m*d(composite)*0.025$	kg	EoL of tray, m% matrix	
	EoL VISH	$f*d(composite)*0.025$	kg	EoL of tray, f% VISH	
PHBV (Harding)	EoL matrix	$((1/0.994)-1)*m*d(composite)*0.025$	kg	EoL of PHB loss during injection (99.4%)	1000 kg
	EoL VISH	$((1/0.994)-1)*f*d(composite)*0.025$	kg	EoL of VS loss during injection (99.4%)	
	Wastewater, unpolluted (RoW)   treatment of, capacity 5E9l/year   Cut-off, S	65.2	m3		
	Tap water (RER)   market group for   Cut-off, S	78.3	kg		
	Hydrogen peroxide, without water, in 50% solution state (GLO)   market for   Cut-off, S	52.9	kg		
	Sulfuric acid (GLO)   market for   Cut-off, S	3.0	kg		
	Phosphoric acid, industrial grade, without water, in 85% solution state (GLO)   market for   Cut-off, S	8.1	kg		
	Sugar, from sugarcane (GLO)   market for   Cut-off, S	1010.0	MJ		
	Heat, district or industrial, natural gas (RER)   market group for   Cut-off, S	2123.0	MJ	Spraydrying	
	Electricity, medium voltage (UCTE)   market group for   Cut-off, S	1360.0	MJ	Microbial growth reactor	
	Electricity, medium voltage (UCTE)   market group for   Cut-off, S	18.1	MJ	Enzyme washing reactor	
	Electricity, medium voltage (UCTE)   market group for   Cut-off, S	18.1	MJ	Detergent washing	
	Electricity, medium voltage (UCTE)   market group for   Cut-off, S	1770.0	MJ	High pressure homogeniser	
	Electricity, medium voltage (UCTE)   market group for   Cut-off, S	263.5	MJ	Centrifugation	
	Electricity, medium voltage (UCTE)   market group for   Cut-off, S	512.0	MJ	Aeration	
	Steam, in chemical industry (RER)   production   Cut-off, S	1065.0	kg	Medium sterilisation	
	Steam, in chemical industry (RER)   production   Cut-off, S	9.6	kg	Steam out vessel	
Steam, in chemical industry (RER)   production   Cut-off, S	3819.0	kg	Backing steam		
PLA	Poly lactide, granulate (GLO)   production   Cut-off, S	1	kg		1 kg
PP	Polypropylene, granulate (GLO)   production for   Cut-off, S	1	kg		1 kg



Name	inputs/outputs	amount	unit	Comments	Amount final
EoL PP	Transport, freight, lorry 16-32 metric ton, EUROS (RER)   transport, freight, lorry 16-32 metric ton, EUROS   Cut-off, S	0.1	tkm	100km of transport before EoL	1 kg
	Waste polypropylene (CH)   treatment of, sanitary landfill   Cut-off, S	0.289	kg	34.6% landfilling	
	Waste polypropylene (CH)   treatment of, municipal incineration   Cut-off, S	0.365	kg	36.5% incineration	
	PP (waste treatment) (GLO)   recycling of PP   Cut-off, S	0.346	kg	28.9% recycling	
EoL PHBV	Transport, freight, lorry 16-32 metric ton, EUROS (RER)   transport, freight, lorry 16-32 metric ton, EUROS   Cut-off, S	0.1	tkm	100km of transport before EoL	1 kg
	Waste plastic, mixture (CH)   treatment of, sanitary landfill   Cut-off, S	0.38	kg	38.0% landfilling	
	GD-EoL PHB-Waste plastic, mixture (CH)   treatment of, municipal incineration   Cut-off, U	0.4	kg	40.0% incineration	
	Carbon dioxide, biogenic	1.94	kg	Instead of Carbon dioxide, fossil 2.3kg PHBV has 55.8%carbon, $0.558 \cdot 44 / 12 \cdot 0.95 = 1.94$ kg CO <sub>2</sub> (95% of the carbon become CO <sub>2</sub> )	
EoL PLA	Biowaste (CH)   treatment of biowaste, industrial composting   Cut-off, S	0.22	kg	22.0% composting	1 kg
	Transport, freight, lorry 16-32 metric ton, EUROS (RER)   transport, freight, lorry 16-32 metric ton, EUROS   Cut-off, S	0.1	tkm	100km of transport before EoL	
	Waste plastic, mixture (CH)   treatment of, sanitary landfill   Cut-off, S	0.38	kg	38.0% landfilling	
	GD-EoL PLA-Waste plastic, mixture (CH)   treatment of, municipal incineration   Cut-off, U	0.4	kg	40.0% incineration	
EoL VS	Biowaste (CH)   treatment of biowaste, industrial composting   Cut-off, S	0.22	kg	22.0% composting	1 kg
	Transport, freight, lorry 16-32 metric ton, EUROS (RER)   transport, freight, lorry 16-32 metric ton, EUROS   Cut-off, S	0.10	tkm	100km of transport before EoL	
	Waste wood, untreated (CH)   treatment of, sanitary landfill   Cut-off, S	0.38	kg	38.0% landfilling	
	Waste wood, untreated (CH)   treatment of, municipal incineration   Cut-off, S	0.40	kg	40.0% incineration	
EoL PP for PP/VS	Biowaste (RoW)   treatment of biowaste, industrial composting   Cut-off, S	0.22	kg	22.0% composting	1 kg
	Transport, freight, lorry 16-32 metric ton, EUROS (RER)   transport, freight, lorry 16-32 metric ton, EUROS   Cut-off, S	0.10	tkm	100km of transport before EoL	
	Waste polypropylene (CH)   treatment of, sanitary landfill   Cut-off, S	0.38	kg	48.7% landfilling	
	Waste polypropylene (CH)   treatment of, municipal incineration   Cut-off, S	0.40	kg	51.3% incineration	
EoL VS for PP/VS	Transport, freight, lorry 16-32 metric ton, EUROS (RER)   transport, freight, lorry 16-32 metric ton, EUROS   Cut-off, S	0.10	tkm	100km of transport before EoL	1 kg
	Waste wood, untreated (CH)   treatment of, sanitary landfill   Cut-off, S	0.38	kg	48.7% landfilling	
	Waste wood, untreated (CH)   treatment of, municipal incineration   Cut-off, S	0.40	kg	51.3% incineration	

## Conclusion

Avant de pouvoir revendiquer de potentiels avantages environnementaux, l'impact environnemental de différentes barquettes biocomposites incluant des sarments de vigne a été quantifié. Les bioplastiques (PHBV et PLA) sont actuellement moins favorables à l'environnement que le polypropylène selon nos travaux. Ces résultats sont à nuancer par l'actuelle impossibilité de prendre en compte les effets de l'accumulation de plastiques dans la nature et par le fait que les bioplastiques encore en développement avec de plus faibles tonnages de production. Le PHBV est le seul bioplastique véritablement biodégradable parmi les trois plastiques étudiés.

L'incorporation des sarments, un résidu agricole, dans des barquettes plastiques, en dépit d'étapes supplémentaires, a permis de réduire les impacts sur l'environnement du produit. L'impact sur le réchauffement climatique est diminué de 20% pour les barquettes en bioplastique et de 10% pour les barquettes en polypropylène. L'étude a donc prouvé l'intérêt de l'utilisation des agro-résidus dans les composites. D'après l'analyse des contributions des étapes de cycle de vie, le taux de charge maximal de 30% en volume devrait être augmenté et la production de bioplastiques optimisée afin de réduire encore les impacts environnementaux. L'utilisation d'une énergie plus propre devrait aider à atteindre cet objectif mais également à réduire l'impact de l'étape de moulage par injection. Enfin, la fin de vie devrait également être améliorée en augmentant le recyclage du PP, en assurant une collecte séparée pour le compostage du PLA et un compostage à domicile pour le PHBV. La recherche en ACV et l'optimisation de la production de bioplastiques changeront probablement les conclusions de ce travail dans le sens des composites PHBV/sarments. D'autre part, ajouter des sarments de vigne dans barquettes permet de diminuer leur prix : -25%, -20% et -12% respectivement pour le PHBV, le PLA et le PP. Ainsi, il y a un double intérêt (environnementale et économique) à utiliser les sarments de vigne dans les composites.

Les sarments de vigne broyés par fractionnement à sec ont été incorporés comme charge dans des composites à base de PHBV. L'impact de ces charges sur la biodégradabilité dans le sol des matériaux composites résultants a été étudié en relation avec leur teneur en polyphénols. On constate que ces charges (taux de charge de 20% en masse) accélèrent légèrement la cinétique de biodégradation des composites. Tous les composites à base de PHBV sont considérés comme entièrement biodégradables dans le sol, tandis que les sarments vierges ne se dégradent que jusqu'à 80% par rapport à la référence (cellulose). Les sarments épuisés, eux, se biodégradent entièrement, confirmant ainsi l'impact négatif des polyphénols sur le mécanisme de biodégradation. Ces hypothèses ont été étayées par des mesures de la cristallinité et des observations au SEM, qui ont montré l'absence de différence de structure ni de morphologie entre les particules.

Ce travail présente une voie de valorisation prometteuse pour les sarments de vigne considérés comme des résidus agricoles. Leur incorporation dans une matrice PHBV permettrait de concevoir industriellement des matériaux biodégradables. De plus, dans un contexte de bioraffinage, l'extraction de polyphénols des sarments présente l'avantage d'améliorer leur biodégradabilité.

# General conclusion

# Conclusion générale

## Rappel des objectifs

L'agriculture génère chaque année de très grandes quantités de résidus dont la gestion n'est actuellement pas bien contrôlée. La valorisation de ces résidus concerne de nombreux domaines (énergie, matériaux, pharmacie, etc...) du fait de leur grande diversité (pailles, sarments, fumiers, etc...). Le projet NoAW, financé par la Commission Européenne, vise à étudier le potentiel des résidus agricoles, les transformer en nouveaux produits et ainsi mettre en place une « économie circulaire sans déchets ». Dans ce cadre, les sarments de vigne ont été identifiés comme une ressource locale abondante et peu valorisée en région Languedoc-Roussillon. Par ailleurs, la consommation des matériaux plastiques augmente fortement, provoquant une accumulation de déchets plastiques non biodégradables dans l'environnement. La production de matériaux durables, notamment pour des applications dans le domaine de l'emballage (courte durée de vie), est ainsi devenu une nécessité. Le développement de matériaux biocomposites biodégradables en conditions naturelles avec incorporation de résidus agricoles a donc été étudié dans cette thèse. L'incorporation de résidus agricoles dans des matériaux composites présente deux avantages : elle évite la consommation de nouvelles ressources naturelles et offre un nouveau moyen de gestion des déchets.

La conception de tels matériaux composites fait face aujourd'hui à plusieurs verrous. Le principal verrou des charges naturelles est leur caractère polaire et hydrophile qui les rendent sensibles à l'eau et peu compatibles avec la plupart des matrices polymères (apolaires). Une plus grande affinité charge/matrice est donc recherchée afin d'obtenir une meilleure dispersion de la charge dans la matrice et une meilleure adhésion interfaciale charge/matrice. De nombreux traitements ont été développés pour modifier les propriétés de surface des fibres naturelles. Dans notre étude, un maintien des propriétés intrinsèques de la charge est recherché, nécessitant le choix d'un traitement de surface. Un deuxième verrou concerne la variabilité des charges naturelles et notamment des sarments de vigne. Les propriétés des fibres naturelles varient entre autres selon les espèces, les conditions climatiques et les conditions de cultures. Ce manque d'uniformité de la ressource peut être un obstacle pour leur usage par les industriels. L'enjeu est donc de produire des charges lignocellulosiques à partir de sarments de vigne et les biocomposites associés avec des propriétés contrôlées et constantes.

L'objectif appliqué de cette thèse était de mettre au point des matériaux composites, biodégradables et biosourcés, à partir de résidus agricoles ; les sarments de vigne en tant que charge de renfort et le PHBV (produit à partir de résidus agricoles) comme matrice. L'objectif scientifique était la compréhension de ces systèmes et de la relation structure-propriétés fonctionnelles (mécaniques et de transfert) ainsi que l'évaluation environnementale des composites produits.

Cette thèse s'est ainsi focalisée sur deux questions scientifiques majeures :

- L'étude de l'impact de l'interface charge/matrice sur les propriétés fonctionnelles des matériaux biocomposites via un traitement de surface des particules lignocellulosiques
- L'analyse de la durabilité de tels matériaux par évaluation dès la conception des impacts environnementaux, de leur biodégradabilité et de l'impact de la variabilité de la biomasse.

### Principaux résultats

Le premier travail a consisté en la modulation de l'interface charge/matrice par une estérification en phase gazeuse. L'objectif était d'améliorer l'adhésion interfaciale entre les charges végétales cellulosesiques et les matrices dans les biocomposites. Pour bien comprendre l'effet de ce traitement sur les propriétés de renfort des sarments de vigne, une première étude a déjà été menée sur des particules de cellulose pure. L'estérification en phase gazeuse appliquée aux particules de cellulose a permis de greffer des chaînes d'acide palmitique (acide gras saturé en C16 d'origine végétale et animale) à leur surface afin de les rendre plus hydrophobes et davantage compatibles avec les thermoplastiques non polaires pour les applications composites (Article 1). Ce traitement de surface a été choisi notamment pour conserver la biodégradabilité du composite et ne pas altérer les propriétés massives des charges. L'efficacité du traitement a été mise en évidence par une analyse FT-IR et le degré de substitution (DS) a été quantifié par spectroscopie RMN du  $^{13}\text{C}$  à l'état solide. De toutes les caractéristiques intrinsèques des particules de cellulose, seule l'énergie libre de surface a été modifiée, la cristallinité, la stabilité thermique, la morphologie étant restées stables. Il a été démontré qu'un DS aussi faible que 0,01 était suffisant pour augmenter considérablement l'hydrophobicité de surface des particules de cellulose sans affecter les propriétés massives de la cellulose. Des analyses XPS sur la cellulose greffée ont permis de mettre en évidence le greffage quasi-total des groupes hydroxyles de surface. Il a été montré également que ce traitement de surface était reproductible.

La réaction a été transposée sur 100 g de particules micrométriques de cellulose à 100°C pendant 15 heures. Les films composites ont été préparés en utilisant une extrudeuse bi-vis et du PHBV comme matrice (Article 2). Les observations en microscopie électronique à balayage (MEB) des surfaces de fracture ont mis en évidence un bon mouillage des charges estérifiées par la matrice polymère contrairement aux composites obtenus avec de la cellulose vierge. Cela suggère que l'estérification en phase gazeuse est une méthode prometteuse pour améliorer l'affinité charge/matrice. Nous avons montré que l'incorporation de particules de cellulose greffées dans les composites conduit à une augmentation de la contrainte et de la déformation à la rupture des composites PHBV/cellulose. Le gain est par exemple de 33% pour la déformation des composites chargés à 33% (m/m). Concernant la perméabilité à la vapeur d'eau (WVP), une diminution de 58% a été obtenue pour les composites chargés avec 33%

(m/m) de charges greffées, comparativement à ceux contenant des charges vierges, ce qui est principalement attribué à une diminution de la sorption.

Cette estérification avec un chlorure d'acide gras a été par la suite appliquée dans les mêmes conditions sur des particules de sarments de vigne obtenues après fractionnement par voie sèche (Article 4). Ces particules avaient un diamètre médian proche de celui de la cellulose précédemment étudiée ce qui autorise la comparaison avec l'étude sur la cellulose pure. Les propriétés intrinsèques n'ont pas été altérées après greffage. L'hydrophobicité de surface des particules de sarments de vigne a augmenté significativement, avec un angle de contact à l'eau passant de 59° à 114°. Néanmoins, le greffage n'a pas permis d'améliorer la mouillabilité de la charge par le PHBV qui était déjà bonne avec des sarments vierges. Nous avons montré que les propriétés mécaniques des composites n'ont pas été significativement impactées par le traitement. Seule la perméabilité à l'eau des composites a été réduite de 27% pour des taux de charges de 30% (m/m).

Les résultats présentés dans le Tableau 59 permettent de se rendre compte de l'effet du greffage sur les principales propriétés des composites suivant la nature de la charge (cellulose ou sarments de vigne) et le taux de charge (20% ou 30%). On remarque ainsi que l'effet de l'estérification est plus important sur les composites contenant de la cellulose, qui est plus hydrophile que la lignocellulose. L'effet limité du greffage des sarments provient du fait que les particules de sarments se dispersent bien d'elles-mêmes dans le PHBV grâce à leur faible polarité et aux forces de cisaillement de l'extrusion. De plus, les charges greffées ne présentant pas de liaisons covalentes avec la matrice PHBV, les effets sur les propriétés mécaniques restent donc limités. L'estérification en phase gaz avec des molécules difonctionnelles introduisant un groupe réactif avec la matrice polymère pourrait être envisagée.

Tableau 59. Effet du greffage des charges sur les propriétés des composites de PHBV (évolution des propriétés par rapport aux composites avec charges vierges)

	Module d'Young	Contrainte à la rupture	Déformation	Température de dégradation	Perméabilité à la vapeur d'eau
20% cellulose	-13%	+7%	+28%	+1%	-11%
33% cellulose	NS	+20%	+33%	+2%	-58%
20% ViSh	NS	-4%	-7%	+2%	-15%
30% ViSh	NS	-4%	NS	+2%	-27%

Par ailleurs, la variabilité des sarments de vigne sur quatre cépages et quatre années a été mesurée (Article 3). Il a été montré que cette variabilité restait faible et dépendait principalement des conditions environnementales (précipitations et ensoleillement). Concernant la composition biochimique, des tendances ont été observées. La teneur en lignine semble augmenter en cas de manque d'eau tandis que la teneur en cendre augmente avec l'ensoleillement. De même la teneur en tanins dépend de facteurs environnementaux car la synthèse de ces molécules représente un mécanisme de défense de la vigne. Les stabilités

thermiques des échantillons testés sont proches. Il a également été constaté que la couleur des charges obtenues après broyage était quasiment identique malgré des différences de couleur visibles entre cépages lors de la taille. Ces interprétations restent des suppositions dues à la faible taille de l'échantillon et mériteraient une analyse statistique. De plus, les effets de ces variations à l'échelle des matériaux composites qui en résultent devraient être étudiés. Ainsi, l'impact de la variabilité des charges naturelles pourra être prise en compte si elle subsiste dans les matériaux. En effet, les différentes étapes du procédé, notamment le broyage et l'extrusion, sont susceptibles d'atténuer encore cette variabilité.

Il est à noter que la variabilité est également présente pour la matrice elle-même, le PHBV, qui malgré sa production industrielle peut présenter des différences selon les lots. Ainsi plusieurs matrices témoins provenant de la même référence commerciale ont dû être utilisées au cours de cette thèse. Les propriétés finales sont donc dépendantes du système étudié.

Les sarments de vigne du cépage Syrah ont été choisis pour la fabrication de charges de renfort car ce cépage est le plus répandu en Occitanie et en France. Pour la première fois, des composites PHBV/sarment de vigne ont été produits (Article 4). Afin de s'adapter aux contraintes de l'emballage alimentaire (épaisseur des emballages au maximum de 0.5 mm dans le cas de barquettes injectées), les ViSh ont subi un processus de broyage successif jusqu'à atteindre une taille moyenne (diamètre apparent) de 50  $\mu\text{m}$ . Cette taille relativement faible augmente la ductilité des matériaux, qui a été identifiée comme un verrou pour les composites à base de PHBV, et permet d'augmenter le taux de charge. A taux de charge égal, les composites PHBV/sarments ont présenté de meilleures propriétés mécaniques que les composites PHBV/cellulose.

Dans une logique de valorisation en cascade, des sarments épuisés (extraction de polyphénols) ont été étudiés en tant que charges de renfort (Article 5). L'idée est d'extraire des molécules d'intérêt pour la cosmétique ou la pharmacie avant d'utiliser la biomasse restante épuisée (le résidu) dans les matériaux. Nous avons montré que l'épuisement de ces agro-résidus pour extraire des biomolécules de haute valeur représentait une stratégie intéressante, car elle ne modifie pas les propriétés mécaniques des composites obtenus. Ainsi, un schéma de bioraffinerie pourrait être mis en place afin d'exploiter au maximum le potentiel de cette biomasse. En parallèle, les propriétés de renfort des sarments de vigne ont été comparées à celles de marc de raisin, un autre résidu solide de la filière vigne et vin. Nous avons montré que l'addition de sarments limitait davantage la dégradation des propriétés mécaniques des matériaux.

Le PHBV ayant quelques propriétés limitées par rapport aux plastiques conventionnels, il est nécessaire de pouvoir moduler ses propriétés pour ouvrir de nouveaux champs d'application. Par exemple, l'incorporation de charges lignocellulosiques dans la matrice polymère (PHBV) permet d'obtenir des perméabilités plus élevées à la vapeur d'eau. Cela peut être utile pour l'emballage de produits respirants tels que les fruits et les légumes. Cela évite la condensation de l'eau dans l'emballage et le produit peut être mieux conservé. En ce qui concerne les propriétés mécaniques, la contrainte et l'allongement à la rupture diminuent avec le taux de



charge. Néanmoins, il est nécessaire de se référer au cahier de charges de l'application envisagée pour déterminer les propriétés « juste nécessaires ». En effet, les produits en PP ou PE possèdent souvent de meilleures propriétés que celles nécessaires. Les biocomposites pourraient présenter des propriétés mécaniques largement suffisantes pour assurer les fonctions requises.

Finalement, l'impact environnemental des biocomposites pour une application de barquette a été évalué par analyse de cycle de vie (ACV) (Article 6). L'objectif était de mieux comprendre le potentiel bénéfique environnemental d'utiliser les sarments de vigne dans les matériaux biocomposites. Les effets de l'incorporation de particules de sarments dans trois matrices (PP, PLA et PHBV) a été étudié dans une analyse de type « du berceau à la tombe ». Afin de pouvoir comparer les différents matériaux, il a été considéré que le volume de matière nécessaire à la fabrication de la barquette était constant (formation de la barquette par injection moulage). Nous montrons ainsi l'importance de la densité des différents matériaux. Pour comparer les formulations, un taux de charge maximal de 30% en volume dans les composites a été fixé. Il a été montré que l'ajout des sarments présente un intérêt environnemental à partir de différents taux de charges suivant les matrices et la catégorie d'impact concerné. Concernant le réchauffement climatique, les barquettes composites deviennent moins impactantes que les barquettes en plastiques vierges à partir de 5 vol% de ViSh pour le PHBV et le PLA, et à partir de 20 vol% de ViSh pour le PP. Ces résultats sont à nuancer, du fait de la différence d'optimisation des procédés de production des plastiques fossiles et des bioplastiques. De plus, le coût économique des barquettes a été évalué. La Figure 111 montre l'intérêt double (économique et environnemental) d'incorporer des sarments de vigne dans les matrices polymères. Ce gain est d'autant plus important lorsque la matrice est du PHBV avec une réduction du prix et de l'impact sur le réchauffement climatique respectivement de 25% et 20% lorsque 30 vol% de sarments sont ajoutés.

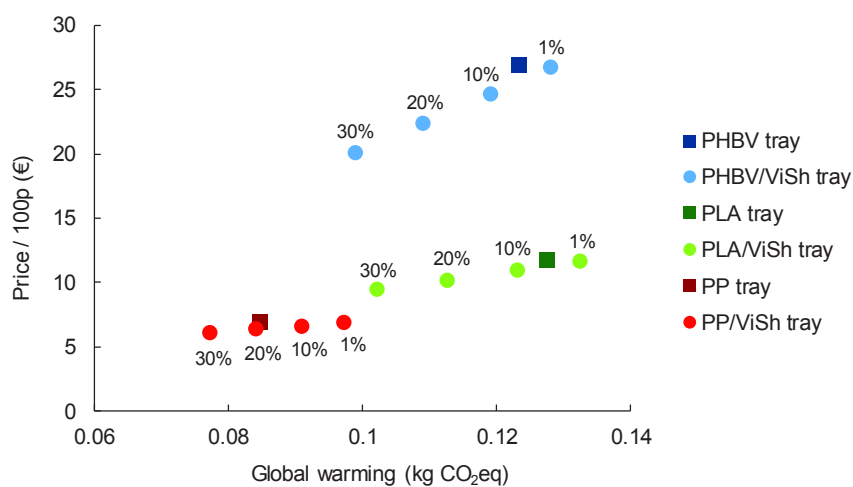


Figure 111. L'impact sur le réchauffement climatique et le prix des différentes barquettes en fonction de la fraction volumique de sarments de vigne

Finalement, l'impact des charges de sarments de vigne (épuisés ou vierges) sur l'aptitude des composites PHBV/ViSh à se biodégrader dans un sol a été évalué (Article 7). Du fait de leur courte durée de vie et du risque de relargage dans notre environnement, la biodégradabilité est une caractéristique essentielle pour les emballages. Nous avons montré que la biodégradation a été légèrement accélérée dans le cas des composites, comparativement au PHBV pur. La biodégradabilité en sol de tous les composites a été validée. Les sarments épuisés se sont mieux biodégradés que les sarments vierges, démontrant l'effet négatif des polyphénols sur les mécanismes de biodégradations. Cette idée renforce l'intérêt de l'extraction des polyphénols avant la fabrication des composites.

Ainsi, cette thèse a permis d'apporter des éléments de réponse à deux enjeux sociétaux majeurs : la valorisation des résidus agricoles et la substitution des plastiques non biodégradables d'origine fossile.

### Perspectives

Montée en échelle. La production de biocomposites à partir de sarments de vigne a été choisie dans le cadre du projet NoAW pour un up-scaling. Trois technologies ont été sélectionnées : la production de PHA, l'extraction de polyphénols et la production de composites. Cette perspective « pratique » va soulever des problématiques de transposition d'échelle.

Etude de la stabilité en conditions d'usage. Quelle que soit l'application visée, la stabilité en conditions d'usage devra être étudiée (impact des conditions de stockage, par exemple : humidité, température et lumière, et des conditions d'utilisation des matériaux). Les critères de stabilité sont d'autant plus contraignants si l'on considère l'application emballage et le contact alimentaire. Les matériaux devront alors satisfaire au Règlement Européen No 10/2011 qui correspond au Règlement No 1935/2004 pour les matériaux plastiques, qui établit une liste positive d'additifs et de monomères autorisés au contact alimentaire, et inclut des spécifications et des restrictions telles que les limites de migration spécifique. Dans le cas des sarments de vigne, on peut craindre la présence de contaminants tels que métaux lourds (traitement des vignes au sulfate de cuivre) et des pesticides. Concernant la présence de pesticides, les traitements contre le mildiou dans les vignes ont lieu au printemps et au début de l'été, ce qui devrait limiter leur présence dans les sarments coupés en fin d'année. Néanmoins, une approche de « challenge test » avec des substituts modèles, représentatives des additifs utilisés ou pesticides devrait nous donner des informations précieuses sur ce potentiel danger. L'idée est d'enrichir volontairement les matériaux avec ces molécules et de regarder comment elles perdurent au cours du procédé.

La comparaison entre des sarments issus de l'agriculture biologique et des sarments classiques concernant la migration des substances toxiques pourrait être envisagé.

Si les migrations dans le cadre d'une application d'emballages alimentaires sont trop élevées, une étude sur la mise en place d'une couche barrière fonctionnelle 100% en polymère pourra être réalisée. Si cette dernière solution n'est ni viable, ni faisable, il faudra alors renoncer à l'application emballage alimentaire, ou se limiter à l'emballage des produits secs.

Prise en compte de la variabilité. Un plus large échantillonnage de sarments de vigne issus de la région Occitanie et des composites résultants devrait être étudié et comparé. De même, il faut s'assurer que les propriétés de la matrice PHBV soient constantes. C'est une condition nécessaire afin de pouvoir fournir des matériaux de qualité constante.

Amélioration de la performance des composites et éco-conception a priori. A l'avenir de nouveaux traitements et des formulations innovantes seront sans doute développés avec une approche éco-conception qui intégrera davantage le rapport performance /coût économique-coût environnemental

Prise en compte des effets environnementaux à long terme. Une connaissance plus fine des effets de l'accumulation des plastiques sur les écosystèmes est nécessaire afin de pouvoir les quantifier et les prendre en compte dans les analyses ACV.

Pour conclure, cette thèse a permis de démontrer l'intérêt d'utiliser les sarments de vigne, et potentiellement d'autres agro-résidus, dans les matériaux biocomposites. Ces matériaux biodégradables apportent une solution intéressante pour la substitution des ressources fossiles. Néanmoins, les propriétés fonctionnelles sont encore trop éloignées des plastiques conventionnels pour espérer une substitution rapide. De plus, ces matériaux devront être certifiés conformes pour chacune des applications visées. Le recyclage pour lutter contre l'accumulation de plastiques dans la nature est actuellement favorisé par la Commission Européenne mais il ne sera efficace qu'en boucle fermée. C'est potentiellement le cas pour les bouteilles en PET ou en utilisant le recyclage chimique/enzymatique. Le développement de substituts universels biodégradables, notamment les biocomposites, apportera également une solution. Néanmoins pour le moment ces solutions ne sont pas suffisamment développées pour être appliquées et répondre à l'ampleur du phénomène. Une solution immédiate consisterait donc dans un premier temps à réduire fortement notre consommation de plastiques et à ne continuer la production que des plastiques strictement indispensables.

# References

---

## References

1. Santana-Méridas, O.; Gonzalez-Coloma, A.; Sanchez-Vioque, R. Agricultural residues as a source of bioactive natural products. *Phytochem. Rev.* 2012, *11*, 447–466, doi:10.1007/s11101-012-9266-0.
2. Biomass Futures Project *Biomass Futures project: Final report*; 2011;
3. Bayard, R.; Gourdon, R. Traitement Biologique des Déchets. *Tech. l'Ingénieur, Génie des Procédés* 2010, *g2060*.
4. Berthet, M.-A.; Angellier-Coussy, H.; Guillard, V.; Gontard, N. Vegetal fiber-based biocomposites: Which stakes for food packaging applications? *J. Appl. Polym. Sci.* 2016, *133*, doi:10.1002/app.42971.
5. John, M. J.; Thomas, S. Biofibres and biocomposites. *Carbohydr. Polym.* 2008, *71*, 343–364, doi:10.1016/j.carbpol.2007.05.040.
6. IFN; FCBA; Solagro *Biomasse forestière, populicole et bocagère disponible pour l'énergie à l'horizon 2020*; 2009;
7. PlasticsEurope *Plastics – the Facts 2018*; 2018;
8. Geyer, R.; Jambeck, J. R.; Law, K. L. Production, use, and fate of all plastics ever made. *Sci. Adv.* 2017, *3*, 25–29, doi:DOI: 10.1126/sciadv.1700782.
9. Zalasiewicz, J.; Waters, C. N.; Ivar, J. A.; Corcoran, P. L.; Barnosky, A. D.; Cearreta, A.; Edgeworth, M.; Ga, A.; Jeandel, C.; Leinfelder, R.; McNeill, J. R.; Steffen, W.; Summerhayes, C.; Wagnreich, M.; Williams, M.; Wolfe, A. P.; Yonah, Y. Anthropocene The geological cycle of plastics and their use as a stratigraphic indicator of the Anthropocene. *Anthropocene* 2016, *13*, 4–17, doi:10.1016/j.ancene.2016.01.002.
10. ADEME *Evaluation de la disponibilité et de l'accessibilité de fibres végétales à usages matériaux en France*; 2011;
11. FAO *Global food losses and food waste – Extent, causes and prevention*; Rome, 2011;
12. Berthet, M.-A. Biocomposites durables pour l'emballage alimentaire, à partir de sous-produits de l'industrie alimentaire: Relations procédé-structure-propriétés, Centre international d'études supérieures en sciences agronomiques, 2013.
13. Berthet, M. A.; Commandré, J. M.; Rouau, X.; Gontard, N.; Angellier-Coussy, H. Torrefaction treatment of lignocellulosic fibres for improving fibre/matrix adhesion in a biocomposite. *Mater. Des.* 2016, *92*, 223–232, doi:10.1016/j.matdes.2015.12.034.
14. Pickering, K. L.; Efendy, M. G. A.; Le, T. M. A review of recent developments in natural fibre composites and their mechanical performance. *Compos. Part A Appl. Sci. Manuf.* 2016, *83*, 98–112, doi:10.1016/j.compositesa.2015.08.038.
15. CVI; FranceAgriMer *La filière viti-vinicole en Languedoc Roussillon: chiffres-clés et représentations*; 2015;
16. Berthet, M. A.; Mayer-Laigle, C.; Rouau, X.; Gontard, N.; Angellier-Coussy, H. Sorting natural fibres: A way to better understand the role of fibre size polydispersity on the

- mechanical properties of biocomposites. *Compos. Part A Appl. Sci. Manuf.* 2017, *95*, 12–21, doi:10.1016/j.compositesa.2017.01.011.
17. Lammi, S.; Barakat, A.; Mayer-Laigle, C.; Djenane, D.; Gontard, N.; Angellier-Coussy, H. Dry fractionation of olive pomace as a sustainable process to produce fillers for biocomposites. *Powder Technol.* 2018, *326*, 44–53, doi:10.1016/j.powtec.2017.11.060.
  18. Girones, J.; Vo, L. T. T.; Di Giuseppe, E.; Navard, P. Natural filler-reinforced composites: comparison of reinforcing potential among technical fibers, stem fragments and industrial by-products. *Cellul. Chem. Technol.* 2017, *51*, 839–855.
  19. Kilinc, A. C.; Atagur, M.; Ozdemir, O.; Sen, I.; Kucukdogan, N.; Sever, K.; Seydibeyoglu, O.; Sarikanat, M.; Seki, Y. Manufacturing and characterization of vine stem reinforced high density polyethylene composites. *Compos. Part B Eng.* 2016, *91*, 267–274, doi:10.1016/j.compositesb.2016.01.033.
  20. Satyanarayana, K. G.; Arizaga, G. G. C.; Wypych, F. Biodegradable composites based on lignocellulosic fibers-An overview. *Prog. Polym. Sci.* 2009, *34*, 982–1021, doi:10.1016/j.progpolymsci.2008.12.002.
  21. Mohanty, A. K.; Misra, M.; Hinrichsen, G. Biofibres, biodegradable polymers and biocomposites: An overview. *Macromol. Mater. Eng.* 2000, *276–277*, 1–24, doi:10.1002/(SICI)1439-2054(20000301)276:1<1::AID-MAME1>3.0.CO;2-W.
  22. Faruk, O.; Bledzki, A. K.; Fink, H. P.; Sain, M. Biocomposites reinforced with natural fibers: 2000-2010. *Prog. Polym. Sci.* 2012, *37*, 1552–1596, doi:10.1016/j.progpolymsci.2012.04.003.
  23. Väisänen, T.; Haapala, A.; Lappalainen, R.; Tomppo, L. Utilization of agricultural and forest industry waste and residues in natural fiber-polymer composites: A review. *Waste Manag.* 2016, *54*, 62–73, doi:10.1016/j.wasman.2016.04.037.
  24. Moriana, R.; Vilaplana, F.; Ek, M. Forest residues as renewable resources for bio-based polymeric materials and bioenergy: chemical composition, structure and thermal properties. *Cellulose* 2015, *22*, 3409–3423, doi:10.1007/s10570-015-0738-4.
  25. Rowell, R. M.; Neill, E. O.; Krzysik, A.; Bossmasn, D.; Hemenover, M. Incorporation of Animal Manures as Reinforcing Fillers in High-Density Polyethylene and High-Density Polypropylene Composites. *9th Int. Conf. Wood Biofiber Plast. Compos.* 2007, 371–374.
  26. Habibi, Y.; El-Zawawy, W. K.; Ibrahim, M. M.; Dufresne, A. Processing and characterization of reinforced polyethylene composites made with lignocellulosic fibers from Egyptian agro-industrial residues. *Compos. Sci. Technol.* 2008, *68*, 1877–1885, doi:10.1016/j.compscitech.2008.01.008.
  27. Ashori, A.; Nourbakhsh, A. Bio-based composites from waste agricultural residues. *Waste Manag.* 2010, *30*, 680–684, doi:10.1016/j.wasman.2009.08.003.
  28. Nourbakhsh, A.; Ashori, A. Wood plastic composites from agro-waste materials: Analysis of mechanical properties. *Bioresour. Technol.* 2010, *101*, 2525–2528, doi:10.1016/j.biortech.2009.11.040.
  29. Gowman, A.; Wang, T.; Rodriguez-Uribe, A.; Mohanty, A. K.; Misra, M. Bio-poly(butylene succinate) and Its Composites with Grape Pomace: Mechanical Performance and Thermal Properties. *ACS Omega* 2018, *3*, 15205–15216,

- doi:10.1021/acsomega.8b01675.
30. Lammi, S.; Le Moigne, N.; Djenane, D.; Gontard, N.; Angellier-Coussy, H. Dry fractionation of olive pomace for the development of food packaging biocomposites. *Ind. Crops Prod.* 2018, *120*, 250–261, doi:10.1016/j.indcrop.2018.04.052.
  31. Le Digabel, F.; Boquillon, N.; Dole, P.; Monties, B.; Averous, L. Properties of thermoplastic composites based on wheat-straw lignocellulosic fillers. *J. Appl. Polym. Sci.* 2004, *93*, 428–436, doi:10.1002/app.20426.
  32. Ashori, A.; Nourbakhsh, A. Mechanical Behavior of Agro-Residue-Reinforced Polypropylene Composites. *J. Appl. Polym. Sci.* 2009, *111*, 2616–2620, doi:10.1002/app.
  33. Berthet, M. A.; Angellier-Coussy, H.; Chea, V.; Guillard, V.; Gastaldi, E.; Gontard, N. Sustainable food packaging: Valorising wheat straw fibres for tuning PHBV-based composites properties. *Compos. Part A Appl. Sci. Manuf.* 2015, *72*, 139–147, doi:10.1016/j.compositesa.2015.02.006.
  34. Bengtsson, M.; Gatenholm, P.; Oksman, K. The effect of crosslinking on the properties of polyethylene/wood flour composites. *Compos. Sci. Technol.* 2005, *65*, 1468–1479, doi:10.1016/j.compscitech.2004.12.050.
  35. Dányádi, L.; Janecska, T.; Szabó, Z.; Nagy, G.; Móczó, J.; Pukánszky, B. Wood flour filled PP composites: Compatibilization and adhesion. *Compos. Sci. Technol.* 2007, *67*, 2838–2846, doi:10.1016/j.compscitech.2007.01.024.
  36. Isikgor, F. H.; Becer, C. R. Lignocellulosic biomass: a sustainable platform for the production of bio-based chemicals and polymers. *Polym. Chem.* 2015, *6*, 4497–4559, doi:10.1039/c5py00263j.
  37. Le Moigne, N.; Otazaghine, B.; Corn, S.; Angellier-Coussy, H.; Bergeret, A. *Surfaces and Interfaces in Natural Fibre reinforced Composites – Fundamentals, modifications and characterization*; Navard, P., Ed.; Springer briefs in molecular science: Cham, 2018; ISBN 978-3-319-71409-7.
  38. Hon, D. N. S. Cellulose: a random walk along its historical path. *Cellulose* 1994, *1*, 1–25, doi:10.1007/BF00818796.
  39. Klemm, D.; Philipp, B.; Heinze, U.; Wagenknecht, W. *Comprehensive Cellulose Chemistry, Fundamentals and Analytical Methods*; Wiley-VCH, Ed.; Wiley-VCH, 1998; Vol. 1; ISBN 3527294139.
  40. Akin, D. E. *Industrial applications of natural fibres: structure, properties and technical applications*; Mussig, J., Ed.; Wiley: West Sussex, 2010; ISBN 9780470695081.
  41. Gould, K. S.; Lister, C. Flavonoid Functions in Plants. In *Flavonoids Chemistry, Biochemistry, and Applications*; Taylor & Francis, Ed.; CRC Press: Boca Raton, 2006; pp. 397–442 ISBN 9780849320217.
  42. Van Soest, P. J.; Wine, R. H. Use of Detergents in the Analysis of Fibrous Feeds . IV . Determination of Plant Cell-Wall Constituents. *J. Assoc. Off. Anal. Chem.* 1967, *58*, 50–55.
  43. Barakat, A.; Chuetor, S.; Monlau, F.; Solhy, A.; Rouau, X. Eco-friendly dry chemo-mechanical pretreatments of lignocellulosic biomass: Impact on energy and yield of the enzymatic hydrolysis. *Appl. Energy* 2014, *113*, 97–105,

- doi:10.1016/j.apenergy.2013.07.015.
44. Lin, L.; Yan, R.; Liu, Y.; Jiang, W. In-depth investigation of enzymatic hydrolysis of biomass wastes based on three major components: Cellulose, hemicellulose and lignin. *Bioresour. Technol.* 2010, *101*, 8217–8223, doi:10.1016/j.biortech.2010.05.084.
  45. Sanchez, A.; Ysunza, F.; Neltran-Garcia, M.; Esqueda, M. Biodegradation of Viticulture Wastes by *Pleurotus*: A Source of Microbial and Human Food and Its Potential Use in Animal Feeding. *J. Agric. Food Chem.* 2002, *50*, 2537–2542, doi:10.1021/jf011308s.
  46. Galanakis, C. M. *Handbook of grape processing by-products*; Galanakis, C., Ed.; Elsevier.; 2017; ISBN 9780128098707.
  47. Dávila, I.; Gordobil, O.; Labidi, J.; Gullón, P. Assessment of suitability of vine shoots for hemicellulosic oligosaccharides production through aqueous processing. *Bioresour. Technol.* 2016, *211*, 636–644, doi:10.1016/j.biortech.2016.03.153.
  48. Jiménez, L.; Angulo, V.; Ramos, E.; De la Torre, M. J.; Ferrer, J. L. Comparison of various pulping processes for producing pulp from vine shoots. *Ind. Crops Prod.* 2006, *23*, 122–130, doi:10.1016/j.indcrop.2005.05.001.
  49. Sánchez-Gómez, R.; Zalacain, A.; Alonso, G. L.; Salinas, M. R. Vine-shoot waste aqueous extracts for re-use in agriculture obtained by different extraction techniques: Phenolic, volatile, and mineral compounds. *J. Agric. Food Chem.* 2014, *62*, 10861–10872, doi:10.1021/jf503929v.
  50. Delgado-Torre, M. P.; Ferreiro-Vera, C.; Priego-Capote, F.; Perez-Juan, P.; Luque de Castro, M. Comparison of Accelerated Methods for the Extraction of Phenolic Compounds from Different Vine-Shoot Cultivars. *J. Agric. Food Chem.* 2012, *60*, 3051–3060, doi:10.1021/jf205078k.
  51. Rayne, S.; Karacabey, E.; Mazza, G. Grape cane waste as a source of trans-resveratrol and trans-viniferin: High-value phytochemicals with medicinal and anti-phytopathogenic applications. *Ind. Crops Prod.* 2008, *27*, 335–340, doi:10.1016/j.indcrop.2007.11.009.
  52. Karacabey, E.; Mazza, G.; Bayindirli, L.; Artik, N. Extraction of Bioactive Compounds from Milled Grape Canes (*Vitis vinifera*) Using a Pressurized Low-Polarity Water Extractor. *Food Bioprocess Technol* 2012, *5*, 359–371, doi:10.1007/s11947-009-0286-8.
  53. Lambert, C.; Richard, T.; Renouf, E.; Bisson, J.; Wa, P.; Bordenave, L.; Ollat, N.; Me, J. Comparative Analyses of Stilbenoids in Canes of Major *Vitis vinifera* L. Cultivars. *J. Agric. Food Chem.* 2013, *61*, 11392–11399, doi:10.1021/jf403716y.
  54. Rodríguez-Cabo, T.; Rodríguez, I.; Ramil, M.; Cela, R. Industrial Crops & Products Assessment of alcoholic distillates for the extraction of bioactive polyphenols from grapevine canes. *Ind. Crop. Prod.* 2018, *111*, 99–106, doi:10.1016/j.indcrop.2017.10.011.
  55. Mendivil, M. A.; Muñoz, P.; Morales, M. P.; Juárez, M. C.; García-Escudero, E. Chemical characterization of pruned vine shoots from La Rioja (Spain) for obtaining solid bio-fuels. *J. Renew. Sustain. Energy* 2013, *5*, 033113, doi:10.1063/1.4808043.
  56. Moldes, A. B.; Bustos, G.; Torrado, A.; Domínguez, J. M. Comparison between Different Hydrolysis Processes of Vine-Trimming Waste to Obtain Hemicellulosic Sugars for Further Lactic Acid Conversion. *Appl Biochem Biotechnol* 2007, *143*, 244–256, doi:10.1007/s12010-007-8021-2.



57. Mansouri, S.; Khiari, R.; Bendouissa, N.; Saadallah, S.; Mhenni, F. Chemical composition and pulp characterization of Tunisian vine stems. *Ind. Crop. Prod.* 2012, *36*, 22–27, doi:10.1016/j.indcrop.2011.07.036.
58. Nabais, J. M. V.; Laginhas, C.; Carrott, P. J. M.; Carrott, M. M. L. R. Thermal conversion of a novel biomass agricultural residue (vine shoots) into activated carbon using activation with CO<sub>2</sub>. *J. Anal. Appl. Pyrolysis* 2010, *87*, 8–13, doi:10.1016/j.jaap.2009.09.004.
59. Pérez-Rodríguez, N.; Outeiriño, D.; Torrado Agrasar, A.; M., D. J. Vine Trimming Shoots as Substrate for Ferulic Acid Esterases Production. *Appl. Biochem. Biotechnol.* 2017, *181*, 813–826, doi:10.1007/s12010-016-2251-0.
60. Jiménez, L.; Rodríguez, A.; Antonio, P.; Moral, A.; Serrano, L. Alternative raw materials and pulping process using clean technologies. *Ind. Crops Prod.* 2008, *8*, 11–16, doi:10.1016/j.indcrop.2007.12.005.
61. Max, B.; Salgado, J. M.; Cortes, S.; Dominguez, J. M. Extraction of phenolic acids by alkaline hydrolysis from the solid residue obtained after prehydrolysis of trimming vine shoots. *J. Agric. Food Chem.* 2010, *58*, 1909–1917, doi:10.1021/jf903441d.
62. Downey, M. O.; Hanlin, R. L. Comparison of ethanol and acetone mixtures for extraction of condensed tannin from grape skin. *South African J. Enol. Vitic.* 2010, *31*, 154–159.
63. Pedroza, M. A.; Amendola, D.; Maggi, L.; Zalacain, A.; De Faveri, D.; Spigno, G. Microwave-Assisted Extraction of Phenolic Compounds from Dried Waste Grape Skins. *Int. J. Food Eng.* 2015, *11*, doi:doi.org/10.1515/ijfe-2015-0009.
64. Rodríguez-Rojo, S.; Visentin, A.; Maestri, D.; Cocero, M. J. Assisted extraction of rosemary antioxidants with green solvents. *J. Food Eng.* 2012, *109*, 98–103, doi:10.1016/j.jfoodeng.2011.09.029.
65. Corcho-Corral, B.; Olivares-Marin, M.; Fernandez-Gonzalez, C.; Gomez-Serrano, V.; Macias-Garcia, A. Preparation and textural characterisation of activated carbon from vine shoots (*Vitis vinifera*) by H<sub>3</sub>PO<sub>4</sub>— Chemical activation. *Appl. Surf. Sci.* 2006, *252*, 5961–5966, doi:10.1016/j.apsusc.2005.11.007.
66. Gañán, J.; Abdulla, A. A.; Correa, E. M. C.; Macías-garcía, A. Energetic exploitation of vine shoot by gasification processes A preliminary study. *Fuel Process. Technol.* 2010, *87*, 891–897, doi:10.1016/j.fuproc.2006.06.004.
67. Keller, M. Water Relations and Nutrient Uptake. In *The Science of Grapevines*; Keller, M., Ed.; Academic Press: San Diego, 2015; pp. 101–124 ISBN 978-0-12-419987-3.
68. Institut Technique de la Vigne et du vin. Les maladies du bois en viticulture. 2002, 1–4.
69. Chambre régionale d’agriculture Nouvelle Aquitaine; DRAAF/SRAL Nouvelle-Aquitaine *Guide de l’observateur : La vigne*; 2017;
70. Pardo, A.; Perona, M. A.; Pardo, J. Indoor composting of vine by-products to produce substrates for mushroom cultivation. *Spanish J. Agric. Res.* 2007, *5*, 417–424.
71. Devesa-Rey, R.; Vecino, X.; Varela-Alende, J. L.; Barral, M. T.; Cruz, J. M.; Moldes, A. B. Valorization of winery waste vs . the costs of not recycling. *Waste Manag.* 2011, *31*, 2327–2335, doi:10.1016/j.wasman.2011.06.001.

72. Rivas, B.; Torrado, A.; Rivas, S.; Bel, A.; Dom, M. Simultaneous lactic acid and xylitol production from vine trimming wastes. *J. Sci. Food Agric.* 2007, *87*, 1603–1612, doi:10.1002/jsfa.
73. Jiménez, L.; Perez, A.; Moral, A.; Serrano, L.; Angulo, V. Acid Hydrolysis of Lignocellulosic Residues from Pulping Processes as a Method of Obtaining Sugar for the Production of Ethanol. *Afinidad* 2007, 574–580.
74. Pezzuto, J. M. Grapes and Human Health : A Perspective. *J. Agric. Food Chem.* 2008, *56*, 6777–6784.
75. Corcho-Corral, B.; Olivares-Marín, M.; Valdes-Sánchez, E.; Fernández-González, C.; Macías-García, A.; Gómez-Serrano, V. Development of activated carbon using vine shoots (*Vitis Vinifera*) and its use for wine treatment. *J. Agric. Food Chem.* 2005, *53*, 644–650, doi:10.1021/jf048824d.
76. Ruiz-Fernández, M.; Alexandre-Franco, M.; Fernández-González, C.; Gómez-Serrano, V. Adsorption Isotherms of Methylene Blue in Aqueous Solution onto Activated Carbons Developed from Vine Shoots (*Vitis Vinifera*) by Physical and Chemical Methods. *Adsorpt. Sci. Technol.* 2010, *28*, 751–759.
77. Moldes, A.; Torrado, A.; Barral, M.; Dominguez, J. Evaluation of Biosurfactant Production from Various Agricultural Residues by *Lactobacillus pentosus*. *J. Agric. Food Chem.* 2007, *55*, 4481–4486, doi:10.1021/jf063075g.
78. Romain, C.; Gaillet, S.; Carillon, J.; Vidé, J.; Ramos, J.; Izard, J.-C.; Cristol, J.; Rouanet, J. Vineatrol and Cardiovascular Disease: Beneficial Effects of a Vine-Shoot Phenolic Extract in a Hamster Atherosclerosis Model. *J. Agric. Food Chem.* 2012, *60*, 11029–11036, doi:10.1021/jf303549t.
79. Raposo, R.; Chinnici, F.; Ruiz-Moreno, M. J.; Puertas, B.; Cuevas, F. J.; Carbú, M.; Guerrero, R. F.; Ortiz-Somovilla, V.; Moreno-Rojas, J. M.; Cantos-Villar, E. Sulfur free red wines through the use of grapevine shoots : Impact on the wine quality. *Food Chem.* 2018, *243*, 453–460, doi:10.1016/j.foodchem.2017.09.111.
80. Richard, T.; Abdelli-belhadj, A.; Vitrac, X.; Teguo, P. W.; Mérillon, J. *Vitis vinifera* canes, a source of stilbenoids against downy mildew. *OENO One* 2016, *50*, 137–143.
81. Portilla, O. M.; Rivas, B.; Torrado, A.; Moldes, A. B.; Dominguez, J. M. Revalorisation of vine trimming wastes using *Lactobacillus acidophilus* and *Debaryomyces hansenii*. *J. Sci. of Food Agric.* 2008, *88*, 2298–2308, doi:10.1002/jsfa.
82. Sanchez-Gomez, R.; Zalacain, A.; Alonso, G. L.; Salinas, M. R. Effect of toasting on non-volatile and volatile vine-shoots low molecular weight phenolic compounds. *Food Chem.* 2016, *204*, 499–505, doi:10.1016/j.foodchem.2016.02.137.
83. Ntalos, G. A.; Grigoriou, A. H. Characterization and utilisation of vine prunings as a wood substitute for particleboard production. *Ind. Crops Prod.* 2002, *16*, 59–68, doi:10.1016/S0926-6690(02)00008-0.
84. Yeniocak, M.; Göktaş, O.; Erdil, Y. Z.; Özen, E. Investigating the use of vine pruning stalks (*Vitis Vinifera* L. CV. Sultani) as raw material for particleboard manufacturing. *Wood Res.* 2014, *59*, 167–176.
85. Faruk, O.; Bledzki, A. K.; Fink, H.-P.; Sain, M. Progress Report on Natural Fiber

- Reinforced Composites. *Macromol. Mater. Eng.* 2014, *299*, 9–26, doi:10.1002/mame.201300008.
86. Choi, H. Y.; Han, S. O.; Lee, J. S. The Effects of Morphological Properties of Henequen Fiber Irradiated by EB on the Mechanical and Thermal Properties of Henequen Fiber / PP Composites. *Compos. Interfaces* 2009, *16*, 751–768, doi:10.1163/092764409X12477436469871.
87. Cassie, A. B. D.; Baxter, S. Wettability of porous surfaces. *Trans. Faraday Soc.* 1944, *40*, 546, doi:10.1039/tf9444000546.
88. Le Duigou, A.; Bourmaud, A.; Balnois, E.; Davies, P.; Baley, C. Improving the interfacial properties between flax fibres and PLLA by a water fibre treatment and drying cycle. *Ind. Crop. Prod.* 2012, *39*, 31–39, doi:10.1016/j.indcrop.2012.02.001.
89. Park, S.; Venditti, R. A.; Jameel, H.; Pawlak, J. J. Changes in pore size distribution during the drying of cellulose fibers as measured by differential scanning calorimetry. *Carbohydr. Polym.* 2006, *66*, 97–103, doi:10.1016/j.carbpol.2006.02.026.
90. Faruk, O.; Sain, M. *Biofiber reinforcement in composite materials*; Faruk, O., Sain, M., Eds.; Woodhead Publishing: Cambridge, 2015; ISBN 9780857092700.
91. Belgacem, M. N.; Gandini, A. The surface modification of cellulose fibres for use as reinforcing elements in composite materials. *Compos. Interfaces* 2005, *12*, 41–75, doi:10.1163/1568554053542188.
92. Marques, G.; Río, J. C.; Gutiérrez, A. Lipophilic extractives from several nonwoody lignocellulosic crops (flax, hemp, sisal, abaca) and their fate during alkaline pulping and TCF/ECF bleaching. *Bioresour. Technol.* 2010, *101*, 260–267, doi:10.1016/j.biortech.2009.08.036.
93. Bismarck, A.; Aranberri-Askargorta, I.; Springer, J.; Lampke, T.; Wielage, B.; Stamboulis, A.; Shenderovich, I.; Limbach, H.-H. Surface characterization of flax, hemp and cellulose fibers; Surface properties and the water uptake behavior. *Polym. Compos.* 2002, *2*, 872–894.
94. Fernández, J. A.; Moigne, N. Le; Caro-bretelle, A. S.; Hage, R. El; Duc, A. Le; Lozachmeur, M.; Bono, P.; Bergeret, A. Role of flax cell wall components on the microstructure and transverse mechanical behaviour of flax fabrics reinforced epoxy biocomposites. *Ind. Crop. Prod.* 2016, *85*, 93–108, doi:10.1016/j.indcrop.2016.02.047.
95. Cech, V.; Palesch, E.; Lukes, J. The glass fiber-polymer matrix interface/interphase characterized by nanoscale imaging techniques. *Compos. Sci. Technol.* 2013, *83*, 22–26, doi:10.1016/j.compscitech.2013.04.014.
96. Le Moigne, N.; Longerey, M.; Taulemesse, J.; Bénézet, J.; Bergeret, A. Study of the interface in natural fibres reinforced poly(lactic acid) biocomposites modified by optimized organosilane treatments. *Ind. Crop. Prod.* 2014, *52*, 481–494, doi:10.1016/j.indcrop.2013.11.022.
97. Regazzi, A.; Corn, S.; Ienny, P.; Bénézet, J.-C.; Bergeret, A. Reversible and irreversible changes in physical and mechanical properties of biocomposites during hydrothermal aging. *Ind. Crops Prod.* 2016, *84*, 358–365, doi:10.1016/j.indcrop.2016.01.052.
98. Bledzki, A. K.; Gassan, J. Composites reinforced with cellulose based fibers. *Prog.*

- Polym. Sci.* 1999, *24*, 221–274, doi:10.1016/S0079-6700(98)00018-5.
99. George, J.; Sreekala, M. S.; Thomas, S. A review on interface modification and characterization of natural fiber reinforced plastic composites. *Polym. Eng. Sci.* 2001, *41*, 1471–1485, doi:10.1002/pen.10846.
  100. Kim, J.-K.; Mai, Y.-W. *Engineered interfaces in fiber reinforced composites*; 1998; Vol. 2; ISBN 9780080426952.
  101. Enciso, B.; Abenojar, J.; Martínez, M. A. Influence of plasma treatment on the adhesion between a polymeric matrix and natural fibres. *Cellulose* 2017, doi:10.1007/s10570-017-1209-x.
  102. Tendero, C.; Tixier, C.; Tristant, P.; Desmaison, J.; Leprince, P. Atmospheric pressure plasmas: A review. *Spectrochim. Acta - Part B At. Spectrosc.* 2006, *61*, 2–30, doi:10.1016/j.sab.2005.10.003.
  103. Popescu, M.; Totolin, M.; Mihaela, C.; Sdrobis, A.; Stevanovic, T.; Vasile, C. Grafting of softwood kraft pulps fibers with fatty acids under cold plasma conditions. *Int. J. Biol. Macromol.* 2011, *48*, 326–335, doi:10.1016/j.ijbiomac.2010.12.011.
  104. Pizzi, A.; Kueny, R.; Lecoanet, F.; Massetau, B.; Carpentier, D.; Krebs, A.; Loiseau, F.; Molina, S.; Ragoubi, M. High resin content natural matrix–natural fibre biocomposites. *Ind. Crops Prod.* 2009, *30*, 235–240, doi:10.1016/j.indcrop.2009.03.013.
  105. Ragoubi, M.; George, B.; Molina, S.; Bienaimé, D.; Merlin, A.; Hiver, J.; Dahoun, A. Effect of corona discharge treatment on mechanical and thermal properties of composites based on miscanthus fibres and polylactic acid or polypropylene matrix. *Compos. Part A* 2012, *43*, 675–685, doi:10.1016/j.compositesa.2011.12.025.
  106. Driscoll, M.; Stipanovic, A.; Winter, W.; Cheng, K.; Manning, M.; Spiese, J.; Galloway, R. A.; Cleland, M. R. Electron beam irradiation of cellulose. *Radiat. Phys. Chem.* 2009, *78*, 539–542, doi:10.1016/j.radphyschem.2009.03.080.
  107. Taylor, P.; Han, S. O.; Cho, D.; Park, W. H.; Lawrence, T. Henequen/poly(butylene succinate ) biocomposites: electron beam irradiation effects on henequen fiber and the interfacial properties of biocomposites. *Compos. Interfaces* 2012, *13*, 231–247, doi:10.1163/156855406775997123.
  108. Le Moigne, N.; Sonnier, R.; El Hage, R.; Rouif, S. Radiation-induced modifications in natural fibres and their biocomposites: Opportunities for controlled physico-chemical modification pathways? *Ind. Crop. Prod.* 2017, *109*, 199–213, doi:10.1016/j.indcrop.2017.08.027.
  109. Khan, F. Characterization of Methyl Methacrylate Grafting onto Preirradiated Biodegradable Lignocellulose Fiber by gamma-Radiation. *Macromol. Biosci.* 2005, 78–89, doi:10.1002/mabi.200400137.
  110. Ly, B.; Thielemans, W.; Dufresne, A.; Chaussy, D.; Belgacem, M. N. Surface functionalization of cellulose fibres and their incorporation in renewable polymeric matrices. *Compos. Sci. Technol.* 2008, *68*, 3193–3201, doi:10.1016/j.compscitech.2008.07.018.
  111. Lee, S.; Wang, S. Biodegradable polymers / bamboo fiber biocomposite with bio-based coupling agent. *Compos. Part A* 2006, *37*, 80–91, doi:10.1016/j.compositesa.2005.04.015.

112. Xie, Y.; Hill, C. A. S.; Xiao, Z.; Militz, H.; Mai, C. Silane coupling agents used for natural fiber/polymer composites: A review. *Compos. Part A Appl. Sci. Manuf.* 2010, *41*, 806–819, doi:10.1016/j.compositesa.2010.03.005.
113. Reulier, M.; Perrin, R.; Avérous, L. Biocomposites based on chemically modified cellulose fibers with renewable fatty-acid-based thermoplastic systems: Effect of different fiber treatments. *J. Appl. Polym. Sci.* 2016, *133*, 1–13, doi:10.1002/app.43878.
114. Yu, T.; Ren, J.; Li, S.; Yuan, H.; Li, Y. Effect of fiber surface-treatments on the properties of poly (lactic acid)/ramie composites. *Compos. Part A* 2010, *41*, 499–505, doi:10.1016/j.compositesa.2009.12.006.
115. Li, Y.; Hu, C.; Yu, Y. Interfacial studies of sisal fiber reinforced high density polyethylene (HDPE) composites. *Compos. Part A* 2008, *39*, 570–578, doi:10.1016/j.compositesa.2007.07.005.
116. Srubar, W. V.; Pilla, S.; Wright, Z. C.; Ryan, C. A.; Greene, J. P.; Frank, C. W.; Billington, S. L. Mechanisms and impact of fiber – matrix compatibilization techniques on the material characterization of PHBV/oak wood flour engineered biobased composites. *Compos. Sci. Technol.* 2012, *72*, 708–715, doi:10.1016/j.compscitech.2012.01.021.
117. Wang, P.; Tao, B. Y. Synthesis and characterization of long-chain fatty acid cellulose ester (FACE). *J. Appl. Polym. Sci.* 1994, *52*, 755–761, doi:10.1002/app.1994.070520605.
118. Edgar, K. J.; Buchanan, C. M.; Debenham, J. S.; Rundquist, P. A.; Seiler, B. D.; Shelton, M. C.; Tindall, D. Advances in cellulose ester performance and application. *Prog. Polym. Sci.* 2001, *26*, 1605–1688.
119. Jandura, P.; Kokta, B. V.; Riedl, B. Cellulose fibers/polyethylene hybrid composites: Effect of long chain organic acid cellulose esters and organic peroxide on rheology and tensile properties. *J. Reinf. Plast. Compos.* 2001, *20*, 697–717, doi:10.1106/Y1CM-4XV7-UAKV-VCH3.
120. Pasquini, D.; Teixeira, E. de M.; Curvelo, A. A. da S.; Belgacem, M. N.; Dufresne, A. Surface esterification of cellulose fibres: Processing and characterisation of low-density polyethylene/cellulose fibres composites. *Compos. Sci. Technol.* 2008, *68*, 193–201, doi:10.1016/j.compscitech.2007.05.009.
121. Freire, C. S. R.; Silvestre, A. J. D.; Neto, C. P.; Gandini, A.; Martin, L.; Mondragon, I. Composites based on acylated cellulose fibers and low-density polyethylene: Effect of the fiber content, degree of substitution and fatty acid chain length on final properties. *Compos. Sci. Technol.* 2008, *68*, 3358–3364, doi:10.1016/j.compscitech.2008.09.008.
122. Klemm, D.; Heublein, B.; Fink, H.; Bohn, A. Polymer Science Cellulose: Fascinating Biopolymer and Sustainable Raw Material. *Polym. Sci.* 2005, *44*, 3358–3393, doi:10.1002/anie.200460587.
123. Glegg, R. E.; Ingerick, D.; Parmerter, R. R.; Salzer, J. S. T.; Warburton, R. S. Acetylation of cellulose I and II studied by limiting viscosity and X-ray diffraction. *J. Polym. Sci. Part A-2 Polym. Phys.* 1968, *6*, 745–773, doi:10.1002/pol.1968.160060410.
124. Jandura, P.; Kokta, B. V.; Riedl, B. Fibrous long-chain organic acid cellulose esters and their characterization by diffuse reflectance FTIR spectroscopy, solid-state CP/MAS <sup>13</sup>C-NMR, and X-ray diffraction. *J. Appl. Polym. Sci.* 2000, *78*, 1354–1365,

- doi:10.1002/1097-4628(20001114)78:7<1354::AID-APP60>3.0.CO;2-V.
125. Braun, B.; Dorgan, J. R. Single-Step Method for the Isolation and Surface Functionalization of Cellulosic Nanowhiskers. *Biomacromolecules* 2009, *10*, 334–341.
  126. Peydecastaing, J.; Girardeau, S.; Vaca-Garcia, C.; Borredon, M. E. Long chain cellulose esters with very low DS obtained with non-acidic catalyts. *Cellulose* 2005, *13*, 95–103, doi:10.1007/s10570-005-9012-5.
  127. McCormick, C. L.; Lichatowich, D. K.; Pelezo, J. A.; Anderson, K. W. Homogeneous solution reactions of cellulose, chitin, and other polysaccharides. *J. Polym. Sci. Part C Polym. Lett.* 1979, *17*, 479–484, doi:10.1021/bk-1980-0121.ch024.
  128. Samaranayake, G.; Glasser, W. G. Cellulose derivatives with low DS . I . A novel acylation system. *Carbohydr. Polym.* 1993, *22*, 1–7.
  129. Sealey, J. E.; Samaranayake, G.; Todd, J. G.; Glasser, W. G. Novel cellulose derivatives .4. Preparation and thermal analysis of waxy esters of cellulose. *J. Polym. Sci. Part B-Polymer Phys.* 1996, *34*, 1613–1620, doi:10.1002/(sici)1099-0488(19960715)34:9<1613::aid-polb10>3.0.co;2-a.
  130. Shimizu, Y.; Hayashi, J. A new method for cellulose acetylation with acetic acid. *Sen-I Gakkaishi* 1988, *44*, 451–456.
  131. Vaca-Garcia, C.; Borredon, M. E. Solvent-free fatty acylation of cellulose and lignocellulosic wastes . Part 2 : reactions with fatty acids. *Bioresour. Technol.* 1999, *70*, 135–142.
  132. Zini, E.; Letizia, M.; Noda, I.; Scandola, M. Bio-composite of bacterial poly(3-hydroxybutyrate-co-3-hydroxyhexanoate) reinforced with vegetable fibers. *Compos. Sci. Technol.* 2007, *67*, 2085–2094, doi:10.1016/j.compscitech.2006.11.015.
  133. Zini, E.; Baiardo, M.; Armelao, L.; Scandola, M. Biodegradable Polyesters Reinforced with Surface-Modified Vegetable Fibers. *Macromol. Biosci.* 2004, *4*, 286–295, doi:10.1002/mabi.200300120.
  134. Baiardo, M.; Zini, E.; Scandola, M. Flax fibre – polyester composites. *Compos. Part A* 2004, *35*, 703–710, doi:10.1016/j.compositesa.2004.02.004.
  135. Yuan, H.; Nishiyama, Y.; Kuga, S. Surface esterification of cellulose by vapor-phase treatment with trifluoroacetic anhydride. *Cellulose* 2005, *12*, 543–549, doi:10.1007/s10570-005-7136-2.
  136. Tosh, B.; Saikia, C. N.; Dass, N. N. Homogeneous esterification of cellulose in the lithium chloride – N,N-dimethylacetamide solvent system: effect of temperature and catalyst. *Carbohydr. Res.* 2000, *327*, 345–352.
  137. Satgé, C.; Verneuil, B.; Branland, P.; Granet, R.; Krausz, P.; Rozier, J.; Petit, C. Rapid homogeneous esterification of cellulose induced by microwave irradiation. *Carbohydr. Polym.* 2002, *49*, 3–6.
  138. Missoum, K.; Belgacem, N.; Barnes, J.; Brochier-salon, M. Nanofibrillated cellulose surface grafting in ionic liquid. *Soft Matter* 2012, *8*, 8338–8349, doi:10.1039/c2sm25691f.
  139. Sehaqui, H.; Zimmermann, T.; Tingaut, P. Hydrophobic cellulose nanopaper through a mild esterification procedure. *Cellulose* 2014, *21*, 367–382, doi:10.1007/s10570-013-0110-5.

140. Possidonio, S.; Fidale, L. C.; El Seoud, O. A. Microwave-assisted derivatization of cellulose in an ionic liquid: An efficient, expedient synthesis of simple and mixed carboxylic esters. *J. Polym. Sci. Part A Polym. Chem.* 2010, *48*, 134–143, doi:10.1002/pola.23770.
141. Mohanty, A. K.; Misra, M.; Drzal, L. T. Surface modifications of natural fibers and performance of the resulting biocomposites: An overview. *Compos. Interfaces* 2001, *8*, 313–343, doi:10.1163/156855401753255422.
142. La Mantia, F. P.; Morreale, M. Green composites: A brief review. *Compos. Part A Appl. Sci. Manuf.* 2011, *42*, 579–588, doi:10.1016/j.compositesa.2011.01.017.
143. Yuan, H.; Nishiyama, Y.; Wada, M.; Kuga, S. Surface Acylation of Cellulose Whiskers by Drying Aqueous Emulsion. *Biomacromolecules* 2006, *50*, 696–700, doi:10.1021/bm050828j.
144. Borysiak, S. Fundamental studies on lignocellulose/polypropylene composites: Effects of wood treatment on the transcrystalline morphology and mechanical properties. *J. Appl. Polym. Sci.* 2013, *127*, 1309–1322, doi:10.1002/app.37651.
145. Cunha, A. G.; Gandini, A. Turning polysaccharides into hydrophobic materials: A critical review. Part 1. Cellulose. *Cellulose* 2010, *17*, 875–889, doi:10.1007/s10570-010-9434-6.
146. Freire, C. S. R.; Silvestre, A. J. D.; Neto, C. P.; Belgacem, M. N.; Gandini, A. Controlled heterogeneous modification of cellulose fibers with fatty acids: Effect of reaction conditions on the extent of esterification and fiber properties. *J. Appl. Polym. Sci.* 2006, *100*, 1093–1102, doi:10.1002/app.23454.
147. Nair, K. C. M.; Diwan, S. M.; Thomas, S. Tensile Properties of Short Sisal Fiber Reinforced Polystyrene Composites. *J. Appl. Polym. Sci.* 1996, *60*, 1483–1497.
148. Kwatra, H. S.; Caruthers, J. M.; Tao, B. Y. Synthesis of long chain fatty acids esterified onto cellulose via the vacuum-acid chloride process. *Ind. Eng. Chem. Res.* 1992, *31*, 2647–2651, doi:10.1021/ie00012a004.
149. Thiebaud, S.; Borredon, M. E. Solvent-free wood esterification with fatty acid chlorides. *Bioresour. Technol.* 1995, *52*, 169–173, doi:10.1016/0960-8524(95)00018-A.
150. Berlioz, S.; Molina-Boisseau, S.; Nishiyama, Y.; Heux, L. Gas-phase surface esterification of cellulose microfibrils and whiskers. *Biomacromolecules* 2009, *10*, 2144–2151, doi:10.1021/bm900319k.
151. Fumagalli, M.; Sanchez, F.; Molina-Boisseau, S.; Heux, L. Surface-restricted modification of nanocellulose aerogels in gas-phase esterification by di-functional fatty acid reagents. *Cellulose* 2015, *22*, 1451–1457, doi:10.1007/s10570-015-0585-3.
152. Dankovich, T. A.; Hsieh, Y. Surface modification of cellulose with plant triglycerides for hydrophobicity. *Cellulose* 2007, *14*, 469–480, doi:10.1007/s10570-007-9132-1.
153. Malm, C. J.; Mench, J. W.; Kendall, D. L.; Hiatt, G. D. Aliphatic Acid Esters of Cellulose. Preparation by Acid-Chloride-Pyridine Procedure. *Ind. Eng. Chem.* 1951, *43*, 684–688, doi:10.1021/ie50495a033.
154. Glasser, W. G.; McCartney, B. K.; Samaranyake, G. Cellulose Derivatives with Low Degree of Substitution. 3. The Biodegradability of Cellulose Esters Using a Simple

- Enzyme Assay. *Biotechnol. Prog.* 1994, *10*, 214–219, doi:10.1021/bp00026a011.
155. Gourson, C.; Benhaddou, R.; Granet, R.; Krausz, P.; Saulnier, L.; Thibault, J. F. Preparation of biodegradable plastic in microwave oven and solvent-free conditions. *Comptes Rendus L Acad. Des Sci. Ser. Ii Fasc. C-Chimie* 1999, *2*, 75–78, doi:10.1016/S1387-1609(99)80004-8.
156. Uschanov, P.; Johansson, L.-S.; Maunu, S. L.; Laine, J. Heterogeneous modification of various celluloses with fatty acids. *Cellulose* 2011, *18*, 393–404, doi:10.1007/s10570-010-9478-7.
157. Fumagalli, M.; Ouhab, D.; Boisseau, S. M.; Heux, L. Versatile gas-phase reactions for surface to bulk esterification of cellulose microfibrils aerogels. *Biomacromolecules* 2013, *14*, 3246–3255, doi:10.1021/bm400864z.
158. Cunha, A. G.; Freire, C.; Silvestre, A.; Neto, C. P.; Gandini, A.; Belgacem, M. N.; Chaussy, D.; Beneventi, D. Preparation of highly hydrophobic and lipophobic cellulose fibers by a straightforward gas-solid reaction. *J. Colloid Interface Sci.* 2010, *344*, 588–595, doi:10.1016/j.jcis.2009.12.057.
159. Stinga, N. C. Utilisation de la chimie chromatogénique pour la conception et la réalisation de matériaux cellulosiques barrières à l'eau, aux graisses et aux gaz, Université Joseph Fourier - Grenoble 1, 2008.
160. Berlioz, S. Etude de l'estérification de la cellulose par une synthèse sans solvant. Application aux matériaux nanocomposites, Université Joseph Fourier, 2007.
161. Samain, D. Procédé de traitement d'un matériau solide pour le rendre hydrophobe, matériau obtenu et applications. 1998, Patent PCT 98.94 2743.0 (WO9908784).
162. Scandola, M.; Sandri, S.; Baiardo, M.; Frisoni, G. Chemical modification of the surface of natural fibers 2004, *1*.
163. Heinrich, J.; Mischnick, P. Determination of the Substitution Pattern in the Polymer Chain of Cellulose Acetates. *J. Polym. Sci. Part A Polym. Chem.* 1999, *37*, 3011–3016.
164. Freire, C. S. R.; Silvestre, A. J. D.; Neto, C. P.; Rocha, R. M. A. An efficient method for determination of the degree of substitution of cellulose esters of long chain aliphatic acids. *Cellulose* 2005, *12*, 449–458, doi:10.1007/s10570-005-2203-2.
165. Tindall, G. W.; Perry, R. L. Determination of ester substituents in cellulose esters. *J. Chromatogr.* 1993, *633*, 227–233.
166. Tindall, G. W.; Boyd, B. W.; Perry, R. L. Determination of acid substituents and unesterified hydroxyl groups in cellulose esters. *J. Chromatogr. A* 2002, *977*, 247–250.
167. Samaranayake, G.; Glasser, W. G. Cellulose derivatives with low DS. II. Analysis of alkanoates. *Carbohydr. Polym.* 1993, *22*, 79–86, doi:10.1016/0144-8617(93)90069-G.
168. Vaca-Garcia, C.; Borredon, M. E. Determination of the degree of substitution (DS) of mixed cellulose esters by elemental analysis. *Cellulose* 2001, *8*, 225–231, doi:10.1023/A:1013133921626.
169. Matsumura, H.; Sugiyama, J.; Glasser, W. G. Cellulosic nanocomposites. I. Thermally deformable cellulose hexanoates from heterogeneous reaction. *J. Appl. Polym. Sci.* 2000, *78*, 2242–2253, doi:10.1002/1097-4628(20001220)78:13<2242::AID-APP20>3.0.CO;2-5.



170. Peydecastaing, J.; Bras, J.; Borredon, E.; Iftimie, N.; Giurginca, M.; Meghea, A. Molecular Crystals and Liquid Crystals NIR Study of Chemically Modified Cellulosic Biopolymers. *Mol. Cryst. Liq. Cryst.* 2006, *448*, 115–122, doi:10.1080/15421400500385027.
171. Heinze, T.; Liebert, T. Unconventional methods in cellulose functionalization. *Prog. Polym. Sci.* 2001, *26*, 1689–1762, doi:10.1016/S0079-6700(01)00022-3.
172. Baiardo, M.; Frisoni, G.; Scandola, M.; Licciardello, A. Surface chemical modification of natural cellulose fibers. *J. Appl. Polym. Sci.* 2002, *83*, 38–45, doi:10.1002/app.2229.
173. Ratanakamnuan, U.; Atong, D.; Aht-Ong, D. Cellulose esters from waste cotton fabric via conventional and microwave heating. *Carbohydr. Polym.* 2011, *87*, 84–94, doi:10.1016/j.carbpol.2011.07.016.
174. Prakash, G. K.; Mahadevan, K. M. Enhancing the properties of wood through chemical modification with palmitoyl chloride. *Appl. Surf. Sci.* 2008, *254*, 1751–1756, doi:10.1016/j.apsusc.2007.07.137.
175. El Seoud, O. A.; Heinze, T. Organic esters of cellulose: New perspectives for old polymers. *Adv. Polym. Sci.* 2005, *186*, 103–149, doi:10.1007/b136818.
176. Samios, E.; Dart, R. K.; Dawkins, J. V. Preparation, characterization and biodegradation studies on cellulose acetates with varying degrees of substitution. *Polymer (Guildf)*. 1997, *38*, 3045–3054, doi:10.1016/S0032-3861(96)00868-3.
177. Buchanan, C. M.; Gardner, R. M.; Komarek, R. Aerobic Biodegradation of Cellulose Acetate. *J. Appl. Polym. Sci.* 1993, *47*, 1709–1719, doi:10.1002/app.1993.070471001.
178. Fan, M.; Naughton, A. Mechanisms of thermal decomposition of natural fibre composites. *Compos. Part B Eng.* 2016, *88*, 1–10, doi:10.1016/j.compositesb.2015.10.038.
179. Avella, M.; La Rota, G.; Martuscelli, E.; Raimo, M.; Sadocco, P.; Elegir, G.; Riva, R. Poly(3-hydroxybutyrate-co-3-hydroxyvalerate) and wheat straw fibre composites: Thermal, mechanical properties and biodegradation behaviour. *J. Mater. Sci.* 2000, *35*, 829–836, doi:10.1023/A:1004773603516.
180. Ludueña, L.; Vázquez, A.; Alvarez, V. Effect of lignocellulosic filler type and content on the behavior of polycaprolactone based eco-composites for packaging applications. *Carbohydr. Polym.* 2012, *87*, 411–421, doi:10.1016/j.carbpol.2011.07.064.
181. Petinakis, E.; Yu, L.; Edward, G.; Dean, K.; Liu, H.; Scully, A. D. Effect of Matrix-Particle Interfacial Adhesion on the Mechanical Properties of Poly(lactic acid)/Wood-Flour Micro-Composites. *J. Polym. Environ.* 2009, *17*, 83–94, doi:10.1007/s10924-009-0124-0.
182. Brundtland, G. H. *Our Common Future: Report of the World Commission on Environment and Development*; 1987; Vol. 4;.
183. European Bioplastics; Nova-Institute Global production of bioplastics 2018 Available online: <https://www.european-bioplastics.org/market/>.
184. European bioplastics *Life Cycle Assessment of Bioplastics*; Berlin, 2008;
185. McCarthy, S.; Andrady, A. “Biodegradable polymers” in *Plastics and the Environment*; Wiley: Hoboken, 2003; ISBN 3175723993.

186. Villano, M.; Valentino, F.; Barbetta, A.; Martino, L.; Scandola, M.; Majone, M. Polyhydroxyalkanoates production with mixed microbial cultures: From culture selection to polymer recovery in a high-rate continuous process. *N. Biotechnol.* 2014, *31*, 289–296, doi:10.1016/j.nbt.2013.08.001.
187. Grousseau, E.; Blanchet, E.; Déléris, S.; Albuquerque, M. G. E.; Paul, E.; Uribelarrea, J. L. Phosphorus limitation strategy to increase propionic acid flux towards 3-hydroxyvaleric acid monomers in *Cupriavidus necator*. *Bioresour. Technol.* 2014, *153*, 206–215, doi:10.1016/j.biortech.2013.11.072.
188. Kourmentza, C.; Plácido, J.; Venetsaneas, N.; Burniol-Figols, A.; Varrone, C.; Gavala, H. N.; Reis, M. A. M. Recent Advances and Challenges towards Sustainable Polyhydroxyalkanoate (PHA) Production. *Bioengineering* 2017, *4*, 55, doi:10.3390/bioengineering4020055.
189. Guillard, V.; Angellier-Coussy, H. Emballages issus d'agro-ressources. *Tech. l'Ingénieur* 2018, *288*, 1–44.
190. Berthet, M. A.; Angellier-Coussy, H.; Machado, D.; Hilliou, L.; Staebler, A.; Vicente, A.; Gontard, N. Exploring the potentialities of using lignocellulosic fibres derived from three food by-products as constituents of biocomposites for food packaging. *Ind. Crops Prod.* 2015, *69*, 110–122, doi:10.1016/j.indcrop.2015.01.028.
191. Singh, S.; Mohanty, A. K.; Sugie, T.; Takai, Y. Renewable resource based biocomposites from natural fiber and polyhydroxybutyrate-co-valerate (PHBV) bioplastic. *Compos. Part A* 2008, *39*, 875–886, doi:10.1016/j.compositesa.2008.01.004.
192. Macedo, J. D. S.; Costa, M. F.; Tavares, M. I. B.; Thire, R. M. S. M. Preparation and Characterization of Composites Based on Polyhydroxybutyrate and Waste Powder From Coconut Fibers Processing. *Polym. Eng. Sci.* 2010, doi:10.1002/pen.
193. Ahankari, S. S.; Mohanty, A. K.; Misra, M. Mechanical behaviour of agro-residue reinforced poly(3-hydroxybutyrate-co-3-hydroxyvalerate), (PHBV) green composites: A comparison with traditional polypropylene composites. *Compos. Sci. Technol.* 2011, *71*, 653–657, doi:10.1016/j.compscitech.2011.01.007.
194. Barkoula, N. M.; Garkhail, S. K.; Peijs, T. Biodegradable composites based on flax/polyhydroxybutyrate and its copolymer with hydroxyvalerate. *Ind. Crop. Prod. J.* 2010, *31*, 34–42, doi:10.1016/j.indcrop.2009.08.005.
195. Keller, A. Compounding and mechanical properties of biodegradable hemp fibre composites. *Compos. Sci. Technol.* 2003, *63*, 1307–1316, doi:10.1016/S0266-3538(03)00102-7.
196. Bledzki, A. K.; Jaszkiwicz, A. Mechanical performance of biocomposites based on PLA and PHBV reinforced with natural fibres - A comparative study to PP. *Compos. Sci. Technol.* 2010, *70*, 1687–1696, doi:10.1016/j.compscitech.2010.06.005.
197. Dufresne, A.; Dupeyre, D.; Paillet, M. Lignocellulosic Flour-Reinforced Poly(hydroxybutyrate-co-valerate) Composites. *J. Appl. Polym. Sci.* 2003, *87*, 1302–1315, doi:https://doi.org/10.1002/app.11546.
198. Kunioka, M.; Doi, Y. Biodegradation of Microbial Copolyesters: Poly(3-hydroxybutyrate-co-3-hydroxyvalerate) and Poly(3-hydroxybutyrate-co-4-hydroxybutyrate). *Macromolecules* 1990, *23*, 1933–1936, doi:10.1021/ma00203a006.

- 
199. Berthet, M. A.; Gontard, N.; Angellier-Coussy, H. Impact of fibre moisture content on the structure/mechanical properties relationships of PHBV/wheat straw fibres biocomposites. *Compos. Sci. Technol.* 2015, *117*, 386–391, doi:10.1016/j.compscitech.2015.07.015.
200. Biodegradability, Compostability & Ecotoxicity (BCE) | OWS Available online: [http://www.ows.be/lc\\_divisions/biodegradability-compostability-ecotoxicity-bce/](http://www.ows.be/lc_divisions/biodegradability-compostability-ecotoxicity-bce/) (accessed on Feb 26, 2017).
201. Chinaglia, S.; Tosin, M.; Degli-Innocenti, F. Biodegradation rate of biodegradable plastics at molecular level. *Polym. Degrad. Stab.* 2018, *147*, 237–244, doi:10.1016/j.polymdegradstab.2017.12.011.
202. Mergaert, J.; Anderson, C.; Wouters, A.; Swings, J.; Kersters, K. Biodegradation of polyhydroxyalkanoates. *FEMS Microbiol. Lett.* 1992, *103*, 317–321, doi:https://doi.org/10.1016/0378-1097(92)90325-I.
203. Salomez, M.; George, M.; Fabre, P.; Touchaleaume, F.; Cesar, G.; Lajarrige, A.; Gastaldi, E. A comparative study of degradation mechanisms of PHBV and PBSA under laboratory-scale composting conditions. *Polym. Degrad. Stab.* 2019, *167*, 102–113, doi:10.1016/j.polymdegradstab.2019.06.025.
204. Muniyasamy, S.; Anstey, A.; Reddy, M. M.; Misra, M.; Mohanty, A. Biodegradability and Compostability of Lignocellulosic Based Composite Materials. 2013, *1*, 253–272, doi:10.7569/JRM.2013.634117.
205. Iovino, R.; Zullo, R.; Rao, M. A.; Cassar, L.; Gianfreda, L. Biodegradation of poly(lactic acid)/starch/coir biocomposites under controlled composting conditions. *Polym. Degrad. Stab.* 2008, *93*, 147–157, doi:10.1016/j.polymdegradstab.2007.10.011.
206. Scaffaro, R.; Morreale, M.; Re, G. Lo; Mantia, F. P. La Degradation of Mater-Bi/wood flour biocomposites in active sewage sludge. *Polym. Degrad. Stab.* 2009, *94*, 1220–1229, doi:10.1016/j.polymdegradstab.2009.04.028.
207. Deng, Y. Life Cycle Assessment of biobased fibre-reinforced polymer composites, KU Leuven, 2008.
208. ISO 14040 ISO 14040:2006 - Environmental management - Life cycle assessment - Principles and framework 2006.
209. ISO 14044 ISO 14044:2006 - Environmental management - Life cycle assessment - Requirements and guidelines 2006.
210. Burgess, A. A.; Brennan, D. J. Application of life cycle assessment to chemical processes. *Chem. Eng. Sci.* 2001, *56*, 2589–2604.
211. Suh, S.; Huppes, G. Methods for Life Cycle Inventory of a product. *J. Clean. Prod.* 2005, *13*, 687–697, doi:10.1016/j.jclepro.2003.04.001.
212. Weidema, B. P.; Bauer, C.; Hischier, R.; Mutel, C.; Nemecek, T.; Reinhard, J.; Vadenbo, C. O.; Wernet, G. *Overview and methodology Data quality guideline for the ecoinvent database version 3*; St. Gallen, 2013; Vol. 3;.
213. Dreyer, L. C.; Niemann, A. L.; Hauschild, M. Z. Comparison of Three LCIA Methods Comparison of Three Different LCIA Methods: *Int. J. Life Cycle Assess.* 2003, *2001*, 191–200.

- 
214. Jolliet, O.; Margni, M.; Charles, R.; Humbert, S.; Payet, J.; Rebitzer, G. Presenting a New Method IMPACT 2002 + : A New Life Cycle Impact Assessment Methodology. *Int. J. Life Cycle Assess.* 2003, 8, 324–330.
215. European Commission - JRC *Recommendations for Life Cycle Impact Assessment in the European context - based on existing environmental impact assessment models and factors*; 2011; ISBN 9789279174513.
216. Wolf, M.; Pant, R.; Chomkham Sri, K.; Sala, S.; Pennington, D. *The International Reference Life Cycle Data System (ILCD) Handbook. Towards more sustainable production and consumption for a resource-efficient Europe.*; 2012;
217. Dutch National Institute for Public Health and the Environment LCIA: the ReCiPe model Available online: <https://www.rivm.nl/en/life-cycle-assessment-lca/recipe>.
218. European Commission -JRC *Framework and requirements for LCIA models and indicators*; 2010;
219. Jacquemin, L.; Pontalier, P.; Sablayrolles, C. Life cycle assessment ( LCA ) applied to the process industry : a review. 2012, 1028–1041, doi:10.1007/s11367-012-0432-9.
220. Kikuchi, Y.; Mayumi, K.; Hirao, M. *Integration of CAPE and LCA Tools in Environmentally-Conscious Process Design : A Case Study on Biomass-Derived Resin*; Elsevier B.V., 2010; Vol. 28;.
221. Le Duigou, A.; Davies, P.; Baley, C. Environmental impact analysis of the production of flax fibres to be used as composite material reinforcement. *J. Biobased Mater. Bioenergy* 2011, 5, 153–165, doi:10.1166/jbmb.2011.1116.
222. Joshi, S. V.; Drzal, L. T.; Mohanty, A. K.; Arora, S. Are natural fiber composites environmentally superior to glass fiber reinforced composites? *Compos. Part A* 2004, 35, 371–376, doi:10.1016/j.compositesa.2003.09.016.
223. Simões, C. L.; Costa Pinto, L. M.; Bernardo, C. A. Modelling the environmental performance of composite products : Benchmark with traditional materials. *Mater. Des.* 2012, 39, 121–130, doi:10.1016/j.matdes.2012.02.027.
224. Boland, C. *Life Cycle Energy and Greenhouse Gas Emissions of Natural Fiber Composites for Automotive Applications : Impacts of Renewable Material Content and Lightweighting by*; Ford Motor Company, Ed.; 2014;
225. Xu, X.; Jayaraman, K.; Morin, C.; Pecqueux, N. Life cycle assessment of wood-fibre-reinforced polypropylene composites. *J. Mater. Process. Technol.* 2008, 8, 168–177, doi:10.1016/j.jmatprotec.2007.06.087.
226. Bernstad, A.; Pacheco, E. B. A. V; Gomes, G. M.; Visconte, L. L. Y.; Soares, A. G.; Bernardo, C. A.; Sim, C. L. Comparative lifecycle assessment of mango packaging made from a polyethylene/natural fiber-composite and from cardboard material. *J. Clean. Prod.* 2016, 139, 1168–1180, doi:10.1016/j.jclepro.2016.08.135.
227. Wikström, F.; Williams, H.; Venkatesh, G. The influence of packaging attributes on recycling and food waste behaviour e An environmental comparison of two packaging alternatives. 2016, 137, 895–902, doi:10.1016/j.jclepro.2016.07.097.
228. Vidal, R.; Martinez, P.; Mulet, E.; Gonzalez, R.; Lopez-Mesa, B.; Fowler, P.; Fang, J. M. Environmental assessment of biodegradable multilayer film derived from

- carbohydrate polymers. *J. Polym. Environ.* 2007, *15*, 159–168, doi:10.1007/s10924-007-0056-5.
229. Robertson, K.; Garnham, M. Life cycle carbon footprint of the packaging and transport of New Zealand kiwifruit. *Int. J. Life Cycle Assess.* 2014, *19*, 1693–1704, doi:10.1007/s11367-014-0775-5.
230. ADEME *Déchets chiffres-clés - L'essentiel 2018*; 2018;
231. Duflou, J. R.; Yelin, D.; Acker, K. Van; Dewulf, W. Comparative impact assessment for flax fibre versus conventional glass fibre reinforced composites: Are bio-based reinforcement materials the way to go? *CIRP Ann. - Manuf. Technol.* 2014, *63*, 45–48, doi:10.1016/j.cirp.2014.03.061.
232. Pervaiz, M.; Sain, M. M. Carbon storage potential in natural fiber composites. *Resour. Conserv. Recycl.* 2003, *39*, 325–340, doi:10.1016/S0921-3449(02)00173-8.
233. Hou, P.; Xu, Y.; Taiebat, M.; Lastoskie, C.; Miller, S. A. Life cycle assessment of end-of-life treatments for plastic film waste. *J. Clean. Prod.* 2018, *201*, 1052–1060, doi:10.1016/j.jclepro.2018.07.278.
234. Bras, B. J.; Mendez, J. A.; Krouit, M.; Lopez, J. P.; Pelach, M.; Belgacem, N. Process and Recyclability Analyses of Innovative Bio-Composite for Tray. *Packag. Technol. Sci.* 2010, *23*, 177–188, doi:10.1002/pts.
235. Beg, M. D. H.; Pickering, K. L. Reprocessing of wood fibre reinforced polypropylene composites . Part I: Effects on physical and mechanical properties. *Compos. Part A* 2015, *39*, 1091–1100, doi:10.1016/j.compositesa.2008.04.013.
236. Soccalingame, L.; Bourmaud, A.; Perrin, D.; Bénézet, J.-C.; Bergeret, A. Reprocessing of wood flour reinforced polypropylene composites: Impact of particle size and coupling agent on composite and particle properties. *Polym. Degrad. Stab. J.* 2015, *113*, 72–85, doi:10.1016/j.polymdegradstab.2015.01.020.
237. Le Duigou, A.; Pillin, I.; Bourmaud, A.; Davies, P.; Baley, C. Effect of recycling on mechanical behaviour of biocompostable flax/poly( L-lactide) composites. *Compos. Part A* 2008, *39*, 1471–1478, doi:10.1016/j.compositesa.2008.05.008.
238. Deloitte Sustainability *Blueprint for plastics packaging waste: Quality sorting & recycling Final report*; 2017;
239. Knight, P.; Jenkins, J. O. Adopting and applying eco-design techniques: a practitioners perspective. *J. Clean. Prod.* 2009, *17*, 549–558, doi:10.1016/j.jclepro.2008.10.002.
240. Luttrupp, C.; Lagerstedt, J. EcoDesign and The Ten Golden Rules: generic advice for merging environmental aspects into product development. *J. Clean. Prod.* 2006, *14*, 1396–1408, doi:10.1016/j.jclepro.2005.11.022.
241. Charter, M.; Chick, A. Editorial of The Journal of Sustainable Product Design. *J. Sustain. Prod. Des.* 1997, *1*, 5–6.
242. Deniaud, I.; Lerch, C.; Caillaud, E. Strategies d'éco-conception: du produit au service. In *9th International Conference on Modeling, Optimization*; Bordeaux, 2012.
243. Fumagalli, M. Elaboration et caractérisation de nanocomposites à base de renforts biosourcés. 2013.

- 
244. NoAW project *Deliverable n°: D 4.1 Biotechnological and physical-chemical optimized strategies to extract and convert biomolecules from agro-wastes*; 2018;
245. Roumeas, L.; Aouf, C.; Dubreucq, E.; Fulcrand, H. Depolymerisation of condensed tannins in ethanol as a gateway to biosourced phenolic synthons. *Green Chem.* 2013, *15*, 3268, doi:10.1039/c3gc41281d.
246. Yahia, L.; Mireles, L. K. *X-ray photoelectron spectroscopy (XPS) and time-of-flight secondary ion mass spectrometry (ToF SIMS)*; Elsevier Ltd., 2017; ISBN 9780081007372.
247. Owens, D.; Wendt, R. Estimation of the surface free energy of polymers. *J. Appl. Polym. Sci.* 1969, *13*, 899–928, doi:10.1002/app.1969.070130815.
248. Blancher, G.; Morel, M. H.; Gastaldi, E.; Cuq, B. Determination of surface tension properties of wheat endosperms, wheat flours, and wheat gluteins. *Cereal Chem.* 2005, *82*, 158–165, doi:10.1094/CC-82-0158.
249. Theodoratou, A.; Bonnet, L.; Dieudonné, P.; Massiera, G.; Robin, J.; Lapinte, V.; Chopineau, J.; Oberdisse, J. Vegetable oil hybrid films cross-linked at the air-water interface: Formation kinetics and physical characterization. *Soft Matter* 2017, *13*, 1–26, doi:10.1039/c7sm00596b.
250. Segal, L.; Creely, J. J.; Martin, A. E.; Conrad, C. M. Empirical method for estimating the degree of crystallinity of native cellulose using the X-ray diffractometer. *Text. Res. J.* 1959, *29*, 786–794, doi:10.1177/004051755902901003.
251. Dyamenahalli, K.; Famili, A.; Shandas, R. Characterization of shape-memory polymers for biomedical applications. In *Shape Memory Polymers for Biomedical Applications*; Elsevier Ltd., 2015; pp. 35–63 ISBN 9780857096982.
252. Barham, P. J.; Keller, A.; Otun, E. L.; Holmes, P. A. Crystallization and morphology of a bacterial thermoplastic: poly-3-hydroxybutyrate. *J. Mater. Sci.* 1984, *19*, 2781–2794, doi:10.1007/BF01026954.
253. Thoury-Monbrun, V. Formalisation des relations structure/propriétés de transfert de matière dans un biocomposite modèle, Université de Montpellier, 2018.
254. Crank, J. *The mathematics of diffusion*; Second edi.; Oxford University press: London, 1975; ISBN 0198533446.
255. Mohanty, A. K.; Misra, M.; Drzal, L. T. *Natural Fibers, Biopolymers, and Biocomposites*; Taylor & Francis, 2005; ISBN 9780849317415.
256. Raj, R. G.; Kokta, B. V.; Dembele, F.; Sanschagrain, B. Compounding of cellulose fibers with polypropylene: Effect of fiber treatment on dispersion in the polymer matrix. *J. Appl. Polym. Sci.* 1989, *38*, 1987–1996, doi:10.1002/app.1989.070381103.
257. Fonseca-Valero, C.; Ochoa-Mendoza, A.; Arranz-Andrés, J.; González-Sánchez, C. Mechanical recycling and composition effects on the properties and structure of hardwood cellulose-reinforced high density polyethylene eco-composites. *Compos. Part A Appl. Sci. Manuf.* 2015, *69*, 94–104, doi:10.1016/j.compositesa.2014.11.009.
258. Hubbe, M. A.; Rojas, O. J.; Lucia, L. A. Green modification of surface characteristics of cellulosic materials at the molecular or nano scale: a review. *BioResources* 2015, *10*, 6095–6206.

- 
259. Hiatt, G. D.; Crane, C. L. Method of preparing higher fatty acid esters of cellulose 1941.
260. Vaca-Garcia, C.; Thiebaud, S.; Borredon, M. E.; Gozzelino, G. Cellulose esterification with fatty acids and acetic anhydride in lithium chloride/N,N-dimethylacetamide medium. *J. Am. Oil Chem. Soc.* 1998, *75*, 315–319, doi:10.1007/s11746-998-0047-2.
261. Jandura, P.; Riedl, B.; Kokta, B. V. Thermal degradation behavior of cellulose fibers partially esterified with some long chain organic acids. *Polym. Degrad. Stab.* 2000, *70*, 387–394, doi:10.1016/S0141-3910(00)00132-4.
262. Stinga, C.; Guerin, D.; Samain, D. Development of biocompatible flexible films with high barriers properties against water, grease and gases using smart reacto-chromatogenic nanoparticles. In *Advanced Coating Fundamentals Symposium*; 2012.
263. Fumagalli, M.; Sanchez, F.; Boisseau, S. M.; Heux, L. Gas-phase esterification of cellulose nanocrystal aerogels for colloidal dispersion in apolar solvents. *Soft Matter* 2013, *9*, 11309–11317, doi:10.1039/c3sm52062e.
264. David, G.; Gontard, N.; Angellier-Coussy, H. Mitigating the Impact of Cellulose Particles on the Performance of Biopolyester-Based Composites by Gas-Phase Esterification. *Polymers (Basel)*. 2019, *11*, doi:10.3390/polym11020200.
265. Marechal, Y.; Chanzy, H. The hydrogen bond network in I $\beta$  cellulose as observed by infrared spectrometry. *J. Mol. Struct.* 2000, *523*, 183–196, doi:10.1016/S0022-2860(99)00389-0.
266. Wada, M.; Okano, T.; Sugiyama, J. Synchrotron-radiated X-ray and neutron diffraction study of native cellulose. *Cellulose* 1997, *4*, 221–232, doi:10.1023/A:1018435806488.
267. Park, S.; Baker, J. O.; Himmel, M. E.; Parilla, P. A.; Johnson, D. K. Cellulose crystallinity index: measurement techniques and their impact on interpreting cellulase performance. *Biotechnol. Biofuels* 2010, *3*, 1–10, doi:10.1186/1754-6834-3-10.
268. Hu, Z.; Berry, R. M.; Pelton, R.; Cranston, E. D. One-pot water-based hydrophobic surface modification of cellulose nanocrystals using plant polyphenols. *ACS Sustain. Chem. Eng.* 2017, *5*, 5018–5026, doi:10.1021/acssuschemeng.7b00415.
269. Stubicar, B. N.; Smit, I.; Stubicar, M.; Tonejc, A.; Janosi, A.; Schurz, J.; Zipper, P. An X-Ray Diffraction Study of the Crystalline to Amorphous Phase Change in Cellulose During High-Energy Dry Ball Milling. *Holzforschung* 1998, *52*, 455–458, doi:10.1515/hfsg.1998.52.5.455.
270. Atalla, R. H.; Vanderhart, D. L. The role of solid state C-13 NMR spectroscopy in studies of the nature of native celluloses. *Solid State Nucl. Magn. Reson.* 1999, *15*, 1–19, doi:10.1016/s0926-2040(99)00042-9.
271. Junior De Menezes, A.; Siqueira, G.; Curvelo, A. A. S.; Dufresne, A. Extrusion and characterization of functionalized cellulose whiskers reinforced polyethylene nanocomposites. *Polymer (Guildf)*. 2009, *50*, 4552–4563, doi:10.1016/j.polymer.2009.07.038.
272. Tomé, L. C.; Freire, M. G.; Rebelo, L. P. N.; Silvestre, A. J. D.; Neto, C. P.; Marrucho, I. M.; Freire, C. S. R. Surface hydrophobization of bacterial and vegetable cellulose fibers using ionic liquids as solvent media and catalysts. *Green Chem.* 2011, *13*, 2464, doi:10.1039/c1gc15432j.

- 
273. Soares, S.; Camino, G.; Levchik, S. Comparative study of the thermal decomposition of pure cellulose and pulp paper. *Polym. Degrad. Stab.* 1995, *49*, 275–283, doi:10.1016/0141-3910(95)87009-1.
274. Feng, L.; Li, S.; Li, Y.; Li, H.; Zhang, L.; Zhai, J.; Song, Y.; Liu, B.; Jiang, L.; Zhu, D. Super-hydrophobic surfaces: From natural to artificial. *Adv. Mater.* 2002, *14*, 1857–1860, doi:DOI 10.1002/adma.200290020.
275. Cunha, A. G.; Freire, C. S. R.; Silvestre, A. J. D.; Neto, C. P.; Gandini, A. Reversible hydrophobization and lipophobization of cellulose fibers via trifluoroacetylation. *J. Colloid Interface Sci.* 2006, *301*, 333–336, doi:10.1016/j.jcis.2006.04.078.
276. Tze, W.; Walinder, M. E. P.; Gardner, D. J. Inverse gas chromatography for studying interactions of materials used for cellulose fiber/polymer composites. *J. Adhes. Sci. Technol.* 2006, *20*, 743–759, doi:10.1163/156856106777638644.
277. Gaiolas, C.; Belgacem, M. N.; Silva, L.; Thielemans, W.; Costa, A. P.; Nunes, M.; Santos Silva, M. J. Green chemicals and process to graft cellulose fibers. *J. Colloid Interface Sci.* 2009, *330*, 298–302, doi:10.1016/j.jcis.2008.10.059.
278. Pasquini, D.; Naceur, M.; Gandini, A. Surface esterification of cellulose fibers: Characterization by DRIFT and contact angle measurements. *J. Colloid Interface Sci.* 2006, *295*, 79–83, doi:10.1016/j.jcis.2005.07.074.
279. Peydecastaing, J.; Vaca-Garcia, C.; Borredon, E. Interactions with water of mixed acetic-fatty cellulose esters. *Cellulose* 2011, *18*, 1023–1031, doi:10.1007/s10570-011-9530-2.
280. Brunauer, S.; Deming, L. S.; Deming, W. E.; Teller, E. On a Theory of the van der Waals Adsorption of Gases. *J. Am. Chem. Soc.* 1940, *62*, 1723–1732, doi:10.1021/ja01864a025.
281. Thoury-Monbrun, V.; Gaucel, S.; Rouessac, V.; Guillard, V.; Angellier-Coussy, H. Assessing the potential of quartz crystal microbalance to estimate water vapor transfer in micrometric size cellulose particles. *Carbohydr. Polym.* 2018, *190*, 307–314, doi:10.1016/j.carbpol.2018.02.068.
282. Banik, G.; Brückle, I. Principles of Water Absorption and Desorption in Cellulosic Materials. *Restaur. Int. J. Preserv. Libr. Arch. Mater.* 2010, *31*, 164–177, doi:10.1515/rest.2010.012.
283. Céline, A.; Gonçalves, O.; Jacquemin, F.; Fréour, S. Qualitative and quantitative assessment of water sorption in natural fibres using ATR-FTIR spectroscopy. *Carbohydr. Polym.* 2014, *101*, 163–170, doi:10.1016/j.carbpol.2013.09.023.
284. Bessadok, A.; Langevin, D.; Gouanvé, F.; Chappey, C.; Roudesli, S.; Marais, S. Study of water sorption on modified Agave fibres. *Carbohydr. Polym.* 2009, *76*, 74–85, doi:10.1016/j.carbpol.2008.09.033.
285. Eichhorn, S. J.; Baillie, C. A.; Zafeiropoulos, N.; Mwaikambo, L. Y.; Ansell, M. P.; Dufresne, A.; Entwistle, K. M.; Herrera-Franco, P. J.; Escamilla, G. C.; Groom, L.; Hughes, M.; Hill, C.; Rials, T. G.; Wild, P. M. Current international research into cellulosic fibres and composites. *J. Mater. Sci.* 2001, *36*, 2107–2131, doi:10.1023/A:1017512029696.



286. Gurunathan, T.; Mohanty, S.; Nayak, S. K. A review of the recent developments in biocomposites based on natural fibres and their application perspectives. *Compos. Part A Appl. Sci. Manuf.* 2015, *77*, 1–25, doi:10.1016/j.compositesa.2015.06.007.
287. Henrique, P.; Pereira, F.; Rosa, M. D. F.; Odila, M.; Cioffi, H.; Cristina, K.; Carvalho, C. De; Milanese, A. C.; Jacobus, H.; Voorwald, C.; Mulinari, D. R. Vegetal fibers in polymeric composites: a review. *Polimeros* 2015, *25*, 9–22, doi:10.1590/0104-1428.1722.
288. Pöllänen, M.; Suvanto, M.; Pakkanen, T. T. Cellulose reinforced high density polyethylene composites - Morphology, Mechanical and thermal expansion properties. *Compos. Sci. Technol.* 2013, *76*, 21–28, doi:10.1016/j.compscitech.2012.12.013.
289. Trejo-O'Reilly, J.-A.; Cavaille, J.-Y.; Gandini, A. The surface chemical modification of cellulosic fibres in view of their use in composite materials. *Cellulose* 1997, *4*, 305–320, doi:10.1023/A:1018452310122.
290. Gauthier, R.; Joly, C.; Coupas, A. C.; Gauthier, H.; Escoubes, M. Interfaces in polyolefin/cellulosic fiber composites: Chemical coupling, morphology, correlation with adhesion and aging in moisture. *Polym. Compos.* 1998, *19*, 287–300, doi:10.1002/pc.10102.
291. Li, X.; Tabil, L. G.; Panigrahi, S. Chemical treatments of natural fiber for use in natural fiber-reinforced composites: A review. *J. Polym. Environ.* 2007, *15*, 25–33, doi:10.1007/s10924-006-0042-3.
292. Wei, L.; McDonald, A. G. A review on grafting of biofibers for biocomposites. *Materials (Basel)*. 2016, *9*, doi:10.3390/ma9040303.
293. Jandura, P.; Riedl, B.; Kokta, B. V. Inverse gas chromatography study on partially esterified paper fiber. *J. Chromatogr. A* 2002, *969*, 301–311, doi:10.1016/S0021-9673(02)00892-0.
294. Yano, H.; Omura, H.; Honma, Y.; Okumura, H.; Sano, H.; Nakatsubo, F. Designing cellulose nanofiber surface for high density polyethylene reinforcement. *Cellulose* 2018, *25*, 3351–3362, doi:10.1007/s10570-018-1787-2.
295. David, G.; Gontard, N.; Guerin, D.; Heux, L.; Lecomte, J.; Angellier-Coussy, H. Gas-phase esterification of cellulose particles for the production of PHBV based biocomposites. In *3rd International EPNOE Junior Scientists Meeting*; Maribor, 2018.
296. Ku, H.; Wang, H.; Pattarachaiyakoo, N.; Trada, M. A review on the tensile properties of natural fiber reinforced polymer composites. *Compos. Part B Eng.* 2011, *42*, 856–873, doi:10.1016/j.compositesb.2011.01.010.
297. Espert, A.; Vilaplana, F.; Karlsson, S. Comparison of water absorption in natural cellulosic fibres from wood and one-year crops in polypropylene composites and its influence on their mechanical properties. *Compos. Part A Appl. Sci. Manuf.* 2004, *35*, 1267–1276, doi:10.1016/j.compositesa.2004.04.004.
298. Tănase, E. E.; Popa, M. E.; Râpă, M.; Popa, O. PHB/Cellulose Fibers Based Materials: Physical, Mechanical and Barrier Properties. *Agric. Agric. Sci. Procedia* 2015, *6*, 608–615, doi:10.1016/j.aaspro.2015.08.099.
299. Martinez-Sanz, M.; Vicente, A.; Gontard, N.; Lopez-Rubio, A.; Lagaron, J. M. On the extraction of cellulose nanowhiskers from food by-products and their comparative

- reinforcing effect on a polyhydroxybutyrate-co-valerate polymer. *Cellulose* 2015, *22*, 535–551, doi:10.1007/s10570-014-0509-7.
300. Ambrosio-Martin, J.; Fabra, M. J.; Lopez-Rubio, A.; Gorrasi, G.; Sorrentino, A.; Lagaron, J. M. Assessment of Ball Milling as a Compounding Technique to Develop Nanocomposites of Poly ( 3-Hydroxybutyrate-co-3- Hydroxyvalerate ) and Bacterial Cellulose Nanowhiskers. *J. Polym. Environ.* 2016, *24*, 241–254, doi:10.1007/s10924-016-0767-6.
301. Wolf, C.; Guillard, V.; Angellier-Coussy, H.; Silva, G. G. D.; Gontard, N. Water vapor sorption and diffusion in wheat straw particles and their impact on the mass transfer properties of biocomposites. *J. Appl. Polym. Sci.* 2016, *133*, 1–10, doi:10.1002/app.43329.
302. Bhardwaj, R.; Mohanty, A. K.; Drzal, L. T.; Pourboghraat, F.; Misra, M. Renewable Resource-Based Green Composites from Recycled Cellulose Fiber and Poly (3-hydroxybutyrate-co-3-hydroxyvalerate) Bioplastic. *Biomacromolecules* 2006, 2044–2051, doi:10.1021/bm050897y.
303. Jiang, L.; Huang, J.; Qian, J.; Chen, F.; Zhang, J.; Wolcott, M. P.; Zhu, Y. Study of poly(3-hydroxybutyrate-co-3-hydroxyvalerate) (PHBV)/bamboo pulp fiber composites: Effects of nucleation agent and compatibilizer. *J. Polym. Environ.* 2008, *16*, 83–93, doi:10.1007/s10924-008-0086-7.
304. Yu, H.; Qin, Z. Effect of Cellulose nanocrystal on Crystallization Behavior of Poly ( 3-hydroxybutyrate-co-3-hydroxyvalerate ). *Adv. Mater. Res.* 2012, *432*, 20–23, doi:10.4028/www.scientific.net/AMR.430-432.20.
305. Ten, E.; Jiang, L.; Wolcott, M. P. Crystallization kinetics of poly ( 3-hydroxybutyrate-co -3-hydroxyvalerate )/ cellulose nanowhiskers composites. *Carbohydr. Polym.* 2012, *90*, 541–550, doi:10.1016/j.carbpol.2012.05.076.
306. Srithep, Y.; Ellingham, T.; Peng, J.; Sabo, R.; Clemons, C.; Turng, L.; Pilla, S. Melt compounding of poly (3-hydroxybutyrate-co-3-hydroxyvalerate)/nanofibrillated cellulose nanocomposites. *Polym. Degrad. Stab.* 2013, *98*, 1439–1449, doi:10.1016/j.polymdegradstab.2013.05.006.
307. Yu, H.; Yan, C.; Yao, J. Fully biodegradable food packaging materials based on functionalized cellulose nanocrystals/poly(3-hydroxybutyrate-co-3-hydroxyvalerate) nanocomposites. *RSC Adv.* 2014, doi:10.1039/C4RA12691B.
308. Sánchez-Safont, E. L.; González-Ausejo, J.; Gámez-Pérez, J.; Lagarón, J. M.; Cabedo, L. Poly(3-Hydroxybutyrate-co-3-Hydroxyvalerate)/Purified Cellulose Fiber Composites by Melt Blending: Characterization and Degradation in Composting Conditions. *J. Renew. Mater.* 2016, *4*, 123–132, doi:10.7569/JRM.2015.634127.
309. Malmir, S.; Montero, B.; Rico, M.; Barral, L.; Bouza, R. Morphology , thermal and barrier properties of biodegradable films of poly ( 3-hydroxybutyrate-co-3-hydroxyvalerate ) containing cellulose nanocrystals. *Compos. Part A* 2017, *93*, 41–48, doi:10.1016/j.compositesa.2016.11.011.
310. Thoury-Monbrun, V.; Angellier-Coussy, H.; Guillard, V.; Legland, D.; Gaucel, S. Impact of two-dimensional particle size distribution on estimation of water vapor diffusivity in micrometric size cellulose particles. *Materials (Basel)*. 2018, *11*,

- doi:10.1017/9781108332859.
311. Thoury-Monbrun, V.; Gaucel, S.; Gontard, N.; Guillard, V.; Angellier-Coussy, H. Adapting gravimetric sorption analyzer to estimate water vapor diffusivity in micrometric size cellulose particles. Forthcoming.
  312. Spitalsky, Z.; Lacik, I.; Lathova, E.; Janigova, I.; Chodak, I. Controlled degradation of polyhydroxybutyrate via alcoholysis with ethylene glycol or glycerol. *Polym. Degrad. Stab.* 2006, *91*, 856–861, doi:10.1016/j.polymdegradstab.2005.06.019.
  313. Bugnicourt, E.; Cinelli, P.; Lazzeri, A.; Alvarez, V. Polyhydroxyalkanoate (PHA): Review of synthesis, characteristics, processing and potential applications in packaging. *Express Polym. Lett.* 2014, *8*, 791–808, doi:10.3144/expresspolymlett.2014.82.
  314. Marais, S.; Nguyen, Q. T.; Devallencourt, C.; Metayer, M.; Nguyen, T. U.; Schaezel, P. Permeation of water through polar and nonpolar polymers and copolymers: determination of the concentration-dependent diffusion coefficient. *J. Polym. Sci. Part B Polym. Phys.* 2000, *38*, 1998–2008, doi:10.1002/1099-0488(20000801)38:15<1998::AID-POLB50>3.0.CO;2-A.
  315. Shogren, R. Water vapor permeability of biodegradable polymers. *J. Environ. Polym. Degrad.* 1997, *5*, 91–95, doi:10.1007/bf02763592.
  316. Tomé, L. C.; Pinto, R. J. B.; Trovatti, E.; Freire, C. S. R.; Silvestre, A. J. D.; Neto, C. P.; Gandini, A. Transparent bionanocomposites with improved properties prepared from acetylated bacterial cellulose and poly(lactic acid) through a simple approach. *Green Chem.* 2011, *13*, 419–427, doi:10.1039/c0gc00545b.
  317. Singh, S.; Mohanty, A. K. Wood fiber reinforced bacterial bioplastic composites: Fabrication and performance evaluation. *Compos. Sci. Technol.* 2007, *67*, 1753–1763, doi:10.1016/j.compscitech.2006.11.009.
  318. Pukánszky, B. Influence of interface interaction on the ultimate tensile properties of polymer composites. *Composites* 1990, *21*, 255–262, doi:10.1016/0010-4361(90)90240-W.
  319. Andresen, M.; Johansson, L.; Tanem, B. S.; Stenius, P. Properties and characterization of hydrophobized microfibrillated cellulose. *Cellulose* 2006, *13*, 665–677, doi:10.1007/s10570-006-9072-1.
  320. Carus, M.; Eder, A.; Dammer, L.; Korte, H.; Scholz, L.; Essel, R.; Breitmayer, E.; Barth, M. *Wood-Plastic Composites (WPC) and Natural Fibre Composites (NFC): European and Global Markets 2012 and Future Trends in Automotive and Construction*; 2015;
  321. Williams, C. L.; Westover, T. L.; Emerson, R. L.; Tumuluru, J. S.; Li, C. Sources of Biomass Feedstock Variability and the Potential Impact on Biofuels Production. *BioEnergy Res.* 2016, *9*, 1–14, doi:10.1007/s12155-015-9694-y.
  322. Silva, G. G. D.; Rouau, S. G. X. Successive centrifugal grinding and sieving of wheat straw. *Powder Technol.* 2011, *208*, 266–270, doi:10.1016/j.powtec.2010.08.015.
  323. Beaugrand, J.; Nottez, M.; Konnerth, J.; Bourmaud, A. Multi-scale analysis of the structure and mechanical performance of woody hemp core and the dependence on the sampling location. *Ind. Crops Prod.* 2014, *60*, 193–204, doi:10.1016/j.indcrop.2014.06.019.
  324. Yan, L.; Chouw, N.; Jayaraman, K. Flax fibre and its composites - A review. *Compos.*

- Part B Eng.* 2014, *56*, 296–317, doi:10.1016/j.compositesb.2013.08.014.
325. Keller, M. *The science of grapevines: anatomy and physiology*; 2013; Vol. 48; ISBN 9780124199873.
326. ASTM D2244 *Standard Practice for Calculation of Color Tolerances and Color Differences from Instrumentally Measured Color Coordinates*; West Conshohocken, 2005;
327. Moura, J. C. M. S.; Bonine, C. A. V.; de Oliveira Fernandes Viana, J.; Dornelas, M. C.; Mazzafera, P. Abiotic and biotic stresses and changes in the lignin content and composition in plants. *J. Integr. Plant Biol.* 2010, *52*, 360–376, doi:10.1111/j.1744-7909.2010.00892.x.
328. Boudet, A. M. Lignins and lignification: Selected issues. *Plant Physiol. Biochem.* 2000, *38*, 81–96, doi:10.1016/S0981-9428(00)00166-2.
329. Liu, Q.; Luo, L.; Zheng, L. Lignins: Biosynthesis and biological functions in plants. *Int. J. Mol. Sci.* 2018, *19*, doi:10.3390/ijms19020335.
330. Cetin, E. S.; Altinoz, D.; Tarcan, E.; Baydar, N. Chemical composition of grape canes. *Ind. Crops Prod.* 2011, *34*, 994–998, doi:10.1016/j.indcrop.2011.03.004.
331. Kenney, K. L.; Smith, W. A.; Gresham, G. L.; Westover, T. L. Understanding biomass feedstock variability. *Biofuels* 2013, *4*, 111–127, doi:10.4155/bfs.12.83.
332. Mossi, A.; Mazutti, M.; Paroul, N.; Corazza, M.; Dariva, C.; Cansian, R.; Oliveira, J. Chemical variation of tannins and triterpenes in Brazilian populations of *Maytenus ilicifolia* Mart. Ex Reiss. *Brazilian J. Biol.* 2009, *69*, 339–345, doi:10.1590/s1519-69842009000200015.
333. Houillé, B.; Besseau, S.; Courdavault, V.; Oudin, A.; Glévarec, G.; Delanoue, G.; Guérin, L.; Simkin, A. J.; Papon, N.; Clastre, M.; Giglioli-Guivarch, N.; Lanoue, A. Biosynthetic origin of e-resveratrol accumulation in grape canes during postharvest storage. *J. Agric. Food Chem.* 2015, *63*, 1631–1638, doi:10.1021/jf505316a.
334. Van der Weijde, T.; Huxley, L. M.; Hawkins, S.; Sembiring, E. H.; Farrar, K.; Dolstra, O.; Visser, R. G. F.; Trindade, L. M. Impact of drought stress on growth and quality of miscanthus for biofuel production. *GCB Bioenergy* 2017, *9*, 770–782, doi:10.1111/gcbb.12382.
335. View, S.; R-genes, S. R.; Scab, I.; Mir, M. A. Structural and Functional Changes in *Arabidopsis thaliana* Cell Wall under Drought Stress. 2019.
336. Emery, I. R.; Mosier, N. S. The impact of dry matter loss during herbaceous biomass storage on net greenhouse gas emissions from biofuels production. *Biomass and Bioenergy* 2012, *39*, 237–246, doi:10.1016/j.biombioe.2012.01.004.
337. Montano-Leyva, B.; Silva, G. G.; Gastaldi, E.; Torres-Chávez, P.; Gontard, N.; Angellier-Coussy, H. Biocomposites from wheat proteins and fibers: Structure/Mechanical properties relationships. *Ind. Crops Prod.* 2013, *43*, 545–555, doi:10.1016/j.indcrop.2012.07.065.
338. Panthapulakkal, S.; Sain, M. Injection Molded Wheat Straw and Corn Stem Filled Polypropylene Composites. *J. Polym. Environ.* 2006, *14*, 265–272, doi:10.1007/s10924-006-0021-8.

- 
339. Zhang, L.; Zhong, J.; Ren, X. Natural fiber-based biocomposites. In *Green Biocomposites. Green Energy and Technology*; Jawaid, M., Sapuan, S., Allothman, O., Eds.; Springer, Cham, 2017; pp. 31–70 ISBN 9783319466101.
340. David, G.; Gontard, N.; Guerin, D.; Heux, L.; Lecomte, J. Exploring the potential of gas-phase esterification to hydrophobize the surface of micrometric cellulose particles. *Eur. Polym. J.* 2019, *115*, 138–146, doi:10.1016/j.eurpolymj.2019.03.002.
341. Gardea-Hernández, G.; Ibarra-Gómez, R.; Flores-Gallardo, S. G.; Hernández-Escobar, C. A.; Pérez-Romo, P.; Zaragoza-Contreras, E. A. Fast wood fiber esterification. I. Reaction with oxalic acid and cetyl alcohol. *Carbohydr. Polym.* 2008, *71*, 1–8, doi:10.1016/j.carbpol.2007.05.014.
342. Wei, L.; McDonald, A. G.; Freitag, C.; Morrell, J. J. Effects of wood fiber esterification on properties, weatherability and biodurability of wood plastic composites. *Polym. Degrad. Stab.* 2013, *98*, 1348–1361, doi:10.1016/j.polymdegradstab.2013.03.027.
343. Newman, R. H. Homogeneity in cellulose crystallinity between samples of *Pinus radiata* wood. *Holzforschung* 2004, *58*, 91–96, doi:10.1515/HF.2004.012.
344. Heux, L.; Dinand, E.; Vignon, M. R. Structural aspects in ultrathin cellulose microfibrils followed by <sup>13</sup>C CP-MAS NMR. *Carbohydr. Polym.* 1999, *40*, 115–124, doi:10.1016/S0144-8617(99)00051-X.
345. Sun, X.-F.; Sun, R. C.; Sun, J.-X. Acetylation of Rice Straw with or without Catalysts and Its Characterization as a Natural Sorbent in Oil Spill Cleanup. *J. Agric. Food Chem.* 2002, *50*, 6428–6433, doi:10.1021/jf020392o.
346. Meijer, M. De; Haemers, S.; Cobben, W.; Militz, H. Surface Energy Determinations of Wood: Comparison of Methods and Wood Species. *Langmuir* 2000, *44*, 9352–9359, doi:10.1021/la001080n.
347. Van Hazendonk, J. M.; Van der Putten, J. C.; Keurentjes, J. T. F.; Prins, A. A simple experimental method for the measurement of the surface tension of cellulosic fibres and its relation with chemical composition. *Colloids Surfaces A Physicochem. Eng. Asp.* 1993, *81*, 251–261, doi:10.1016/0927-7757(93)80252-A.
348. Yu, H.; Qin, Z.; Wang, L.; Zhou, Z. Crystallization behavior and hydrophobic properties of biodegradable ethyl cellulose-g-poly ( 3-hydroxybutyrate-co-3-hydroxyvalerate ): The influence of the side-chain length and grafting density. *Carbohydr. Polym.* 2012, *87*, 2447–2454, doi:10.1016/j.carbpol.2011.11.022.
349. Luo, S.; Cao, J.; McDonald, A. G. Interfacial Improvements in a Green Biopolymer Alloy of Poly(3-hydroxybutyrate-co-3-hydroxyvalerate) and Lignin via in Situ Reactive Extrusion. *ACS Sustain. Chem. Eng.* 2016, *4*, 3465–3476, doi:10.1021/acssuschemeng.6b00495.
350. Hornsby, P. R.; Hinrichsen, E.; Tarverdi, K. Preparation and properties of polypropylene composites reinforced with wheat and flax straw fibres Part I Fibre characterization. *J. Mater. Sci.* 1997, *32*, 443–449.
351. Panthapulakkal, S.; Sain, M. Agro-residue reinforced high-density polyethylene composites: Fiber characterization and analysis of composite properties. *Compos. Part A* 2007, *38*, 1445–1454, doi:10.1016/j.compositesa.2007.01.015.

352. Meric, M.; Christen, M. *Etude sur les gisements valorisables par la filière pyrogazéification. Fiche gisement n°05 – Sarments et pieds de vigne*; 2015;
353. Gullón, B.; Eibes, G.; Moreira, M. T.; Dávila, I.; Labidi, J.; Gullón, P. Antioxidant and antimicrobial activities of extracts obtained from the refining of autohydrolysis liquors of vine shoots. *Ind. Crops Prod.* 2017, *107*, 105–113, doi:10.1016/j.indcrop.2017.05.034.
354. European Commission Council Regulation (EC) No 479/2008 of 29 April 2008 on the common organisation of the market in wine, amending Regulations (EC). *Off. J. Eur. Union* 2008, 9–40.
355. Beres, C.; Costa, G. N. S.; Cabezudo, I.; da Silva-James, N. K.; Teles, A. S. C.; Cruz, A. P. G.; Mellinger-Silva, C.; Tonon, R. V.; Cabral, L. M. C.; Freitas, S. P. Towards integral utilization of grape pomace from winemaking process: A review. *Waste Manag.* 2017, *68*, 581–594, doi:10.1016/j.wasman.2017.07.017.
356. Antonioli, A.; Fontana, A. R.; Piccoli, P.; Bottini, R. Characterization of polyphenols and evaluation of antioxidant capacity in grape pomace of the cv. Malbec. *Food Chem.* 2015, *178*, 172–178, doi:10.1016/j.foodchem.2015.01.082.
357. Muhlack, R. A.; Potumarthi, R.; Jeffery, D. W. Sustainable wineries through waste valorisation: A review of grape marc utilisation for value-added products. *Waste Manag.* 2018, *72*, 99–118, doi:10.1016/j.wasman.2017.11.011.
358. Georgiev, V.; Ananga, A.; Tsoleva, V. Recent advances and uses of grape flavonoids as nutraceuticals. *Nutrients* 2014, *6*, 391–415, doi:10.3390/nu6010391.
359. Brenes, A.; Viveros, A.; Chamorro, S.; Arija, I. Use of polyphenol-rich grape by-products in monogastric nutrition. A review. *Anim. Feed Sci. Technol.* 2016, *211*, 1–17, doi:10.1016/j.anifeedsci.2015.09.016.
360. Borsoi, C.; Menin, C.; Lavoratti, A.; Zattera, A. J. Grape stalk fibers as reinforcing filler for polymer composites with a polystyrene matrix. *J. Appl. Polym. Sci.* 2019, *136*, 1–10, doi:10.1002/app.47427.
361. Jiang, Y.; Simonsen, J.; Zhao, Y. Compression-Molded Biocomposite Boards from Red and White Wine Grape Pomaces. *J. Appl. Polym. Sci.* 2010, *119*, 2834–2846, doi:10.1002/app.32961.
362. David, G.; Heux, L.; Pradeau, S.; Gontard, N.; Angellier-Coussy, H. Upcycling vine shoots for biocomposites applications: About the interest of filler surface esterification to improve their performance. *Forthcoming*.
363. Nanni, A.; Messori, M. A comparative study of different winemaking by-products derived additives on oxidation stability, mechanical and thermal proprieties of polypropylene. *Polym. Degrad. Stab.* 2018, *149*, 9–18, doi:10.1016/j.polymdegradstab.2018.01.012.
364. Krouit, M.; Belgacem, M. N.; Bras, J. Chemical versus solvent extraction treatment: Comparison and influence on polyester based bio-composite mechanical properties. *Compos. Part A* 2010, *41*, 703–708, doi:10.1016/j.compositesa.2010.01.014.
365. Singleton, V. L.; Rossi, J. R. Colorimetry of total phenolics with phosphomolybdic-phosphotungstic acid. *Am. J. Enol. Vitic.* 1965, *16*, 144–158.
366. Torres-Giner, S.; Hilliou, L.; Melendez-Rodriguez, B.; Figueroa-Lopez, K. J.; Madalena, D.; Cabedo, L.; Covas, J. A.; Vicente, A. A.; Lagaron, J. M. Melt processability,

- characterization, and antibacterial activity of compression-molded green composite sheets made of poly(3-hydroxybutyrate-co-3-hydroxyvalerate) reinforced with coconut fibers impregnated with oregano essential oil. *Food Packag. Shelf Life* 2018, *17*, 39–49, doi:10.1016/j.fpsl.2018.05.002.
367. Angellier-Coussy, H.; Gastaldi, E.; Gontard, N.; Guillard, V. Influence of processing temperature on the water vapour transport properties of wheat gluten based agromaterials. *Ind. Crop. Prod.* 2011, *33*, 457–461, doi:10.1016/j.indcrop.2010.10.028.
368. Saura-Calixto, F.; Goñi, I.; Mañas, E.; Abia, R. Klason lignin, condensed tannins and resistant protein as dietary fibre constituents: Determination in grape pomaces. *Food Chem.* 1991, *39*, 299–309, doi:10.1016/0308-8146(91)90147-G.
369. Arnous, A.; Meyer, A. S. Comparison of methods for compositional characterization of grape (*Vitis vinifera* L.) and apple (*Malus domestica*) skins. *Food Bioprod. Process.* 2008, *86*, 79–86, doi:10.1016/j.fbp.2008.03.004.
370. Mendes, J. A. S.; Prozil, S. O.; Evtuguin, D. V.; Lopes, L. P. C. Towards comprehensive utilization of winemaking residues: Characterization of grape skins from red grape pomaces of variety Touriga Nacional. *Ind. Crops Prod.* 2013, *43*, 25–32, doi:10.1016/j.indcrop.2012.06.047.
371. García-Lomillo, J.; González-SanJosé, M. L.; Del Pino-García, R.; Rivero-Pérez, M. D.; Muñoz-Rodríguez, P. Antioxidant and antimicrobial properties of wine byproducts and their potential uses in the food industry. *J. Agric. Food Chem.* 2014, *62*, 12595–12602, doi:10.1021/jf5042678.
372. Khiari, B.; Jeguirim, M. Pyrolysis of grape marc from Tunisian wine industry: Feedstock characterization, thermal degradation and kinetic analysis. *Energies* 2018, *11*, doi:10.3390/en11040730.
373. Totaro, G.; Sisti, L.; Vannini, M.; Marchese, P.; Tassoni, A.; Lenucci, M. S.; Lamborghini, M.; Kalia, S.; Celli, A. A new route of valorization of rice endosperm by-product: Production of polymeric biocomposites. *Compos. Part B Eng.* 2018, *139*, 195–202, doi:10.1016/j.compositesb.2017.11.055.
374. Persico, P.; Ambrogio, V.; Baroni, A.; Santagata, G.; Carfagna, C.; Malinconico, M.; Cerruti, P. Enhancement of poly(3-hydroxybutyrate) thermal and processing stability using a bio-waste derived additive. *Int. J. Biol. Macromol.* 2012, *51*, 1151–1158, doi:10.1016/j.ijbiomac.2012.08.036.
375. Hassaini, L.; Kaci, M.; Touati, N.; Pillin, I.; Kervoelen, A.; Bruzard, S. Valorization of olive husk flour as a filler for biocomposites based on poly(3-hydroxybutyrate-co-3-hydroxyvalerate): Effects of silane treatment. *Polym. Test.* 2017, *59*, 430–440, doi:10.1016/j.polymertesting.2017.03.004.
376. FranceAgriMer *L'observatoire national des ressources en biomasse: Évaluation des ressources disponibles en France*; 2016;
377. Scarlat, N.; Dallemand, J.-F.; Monforti-Ferrario, F.; Nita, V. The role of biomass and bioenergy in a future bioeconomy: Policies and facts. *Environ. Dev.* 2015, *15*, 3–34, doi:10.1016/J.ENVDEV.2015.03.006.
378. David, G.; Gontard, N.; Angellier-Coussy, H. Assessing the potential of vine shoots particles as fillers in biopolyester based biocomposites. In *Polymer Blends Conference*

- 2019; Palermo, 2019.
379. David, G.; Vannini, M.; Sisti, L.; Celli, A.; Gontard, N.; Angellier-Coussy, H. Eco-conversion of two winery lignocellulosic wastes into fillers for biocomposites: Vine Shoots and Wine Pomace. *Forthcoming*.
380. Guillard, V.; Gaucel, S.; Fornaciari, C.; Angellier-Coussy, H.; Buche, P.; Gontard, N. The Next Generation of Sustainable Food Packaging to Preserve Our Environment in a Circular Economy Context. *Front. Nutr.* 2018, *5*, 1–13, doi:10.3389/fnut.2018.00121.
381. Chodak, I. Polyhydroxyalkanoates: Origin, properties and applications. In *Monomers, Polymers and Composites from Renewable Resources*; 2008; pp. 451–477 ISBN 9780080453163.
382. Civancik-Uslu, D.; Ferrer, L.; Puig, R.; Fullana-i-Palmer, P. Are functional fillers improving environmental behavior of plastics? A review on LCA studies. *Sci. Total Environ.* 2018, *626*, 927–940, doi:10.1016/j.scitotenv.2018.01.149.
383. Hauschild, M.; Rosenbaum, R. K.; Olsen, S. *Life Cycle Assessment: Theory and Practice*; 1st ed.; Springer International Publishing, 2018; ISBN 978-3-319-56474-6.
384. Qiang, T.; Yu, D.; Zhang, A.; Gao, H.; Li, Z.; Liu, Z. Life cycle assessment on polylactide-based wood plastic composites toughened with polyhydroxyalkanoates. *J. Clean. Prod.* 2014, *66*, 139–145, doi:10.1016/j.jclepro.2013.11.074.
385. Kim, S.; Dale, B. E.; Drzal, L. T.; Misra, M. Life cycle assessment of kenaf fiber reinforced biocomposite. *J. Biobased Mater. Bioenergy* 2008, *2*, 85–93, doi:10.1166/jbmb.2008.207.
386. Le Duigou, A.; Davies, P.; Baley, C. Replacement of Glass/Unsaturated Polyester Composites by Flax/PLLA Biocomposites: Is It Justified? *J. Biobased Mater. Bioenergy* 2011, *5*, 466–482, doi:10.1166/jbmb.2011.1178.
387. Dufloy, J. R.; Deng, Y.; Acker, K. Van; Dewulf, W. Do fiber-reinforced polymer composites provide environmentally benign alternatives? A life-cycle-assessment-based study. 2012, doi:10.1557/mrs.2012.33.
388. Vidal, R.; Martínez, P.; Garraín, D. Life cycle assessment of composite materials made of recycled thermoplastics combined with rice husks and cotton linters. *Int. J. Life Cycle Assess.* 2009, *14*, 73–82, doi:10.1007/s11367-008-0043-7.
389. Spinelli, R.; Nati, C.; Pari, L.; Mescalchin, E.; Magagnotti, N. Production and quality of biomass fuels from mechanized collection and processing of vineyard pruning residues. *Appl. Energy* 2012, *89*, 374–379, doi:10.1016/j.apenergy.2011.07.049.
390. Picchi, G.; Silvestri, S.; Cristoforetti, A. Vineyard residues as a fuel for domestic boilers in Trento Province (Italy): Comparison to wood chips and means of polluting emissions control. *Fuel* 2013, *113*, 43–49, doi:10.1016/j.fuel.2013.05.058.
391. Gullón, P.; Gullón, B.; Dávila, I.; Labidi, J.; Gonzalez-Garcia, S. Comparative environmental Life Cycle Assessment of integral revalorization of vine shoots from a biorefinery perspective. *Sci. Total Environ.* 2018, *624*, 225–240, doi:10.1016/j.scitotenv.2017.12.036.
392. Yates, M. R.; Barlow, C. Y. Life cycle assessments of biodegradable, commercial biopolymers — A critical review. *Resour. Conserv. Recycl.* 2013, *78*, 54–66,



- doi:10.1016/j.resconrec.2013.06.010.
393. Harding, K. G.; Dennis, J. S.; Blottnitz, H. Von; Harrison, S. T. L. Environmental analysis of plastic production processes: Comparing petroleum-based polypropylene and polyethylene with biologically-based poly- $\beta$ -hydroxybutyric acid using life cycle analysis. *J. Biotechnol.* 2007, *130*, 57–66, doi:10.1016/j.jbiotec.2007.02.012.
  394. Borken-Kleefeld, J. Weidema, B. P. Background data for transport Available online: [https://www.ecoinvent.org/files/transport\\_default\\_20130722.xlsx](https://www.ecoinvent.org/files/transport_default_20130722.xlsx).
  395. Ministère de l'écologie et du développement durable *Circulaire du 18 novembre 2011 relative à l'interdiction du brûlage à l'air libre des déchets verts*; 2011; pp. 1–9;.
  396. Gazeau, G.; Sibe, V.; Mouton, R.; Remy, J. *Etude sur les options de valorisation matière (valorisation sous forme d'éco-matériaux) ou énergie des résidus de culture.*; 2018; Vol. 1;.
  397. Beigbeder, J.; Soccalingame, L.; Perrin, D.; Bénézet, J.; Bergeret, A. How to manage biocomposites wastes end of life? A life cycle assessment approach ( LCA ) focused on polypropylene ( PP )/ wood flour and polylactic acid ( PLA )/ flax fibres biocomposites. *Waste Manag.* 2019, *83*, 184–193, doi:10.1016/j.wasman.2018.11.012.
  398. Tabone, M.; Cregg, J.; Beckman, E.; Landis, A. Sustainability Metrics: Life Cycle Assessment and Green Design in Polymers. *Environ. Sci. Technol.* 2010, *44*, 8264–8269.
  399. Hermann, B. G.; Debeer, L.; De Wilde, B.; Blok, K.; Patel, M. K. To compost or not to compost: Carbon and energy footprints of biodegradable materials' waste treatment. *Polym. Degrad. Stab.* 2011, *96*, 1159–1171, doi:10.1016/j.polymdegradstab.2010.12.026.
  400. Royer, S. J.; Ferrón, S.; Wilson, S. T.; Karl, D. M. Production of methane and ethylene from plastic in the environment. *PLoS One* 2018, *13*, 1–13, doi:10.1371/journal.pone.0200574.
  401. EcoBioCAP 265669 *Deliverable D5.1 Environmental assessment of different packaging materials*; 2013;
  402. Woods, J. S.; Veltman, K.; Huijbregts, M. A. J.; Verones, F.; Hertwich, E. G. Towards a meaningful assessment of marine ecological impacts in life cycle assessment ( LCA ). *Environ. Int.* 2016, *89–90*, 48–61, doi:10.1016/j.envint.2015.12.033.
  403. Boulay, A.-M.; Vazquez, I.; Verones, F.; Woods, J. Marine impacts in LCA Available online: [www.marilca.org](http://www.marilca.org).
  404. European Commission's Directorate-General for Research and Innovation *A Circular Economy for Plastics, Insights from Research and Innovation to Inform Policy and Funding Decisions*; 2019;
  405. Ellen MacArthur Foundation *The New Plastics Economy: Rethinking the future of plastics*; 2016;
  406. Jost, V. Packaging related properties of commercially available biopolymers - An overview of the status quo. *Express Polym. Lett.* 2018, *12*, 429–435, doi:10.3144/expresspolymlett.2018.36.
  407. Weng, Y. X.; Wang, Y.; Wang, X. L.; Wang, Y. Z. Biodegradation behavior of PHBV films in a pilot-scale composting condition. *Polym. Test.* 2010, *29*, 579–587, doi:10.1016/j.polymertesting.2010.04.002.

408. Avella, M.; Martuscelli, E.; Raimo, M. Review Properties of blends and composites based on poly(3-hydroxy)butyrate (PHB) and poly(3-hydroxybutyrate-hydroxyvalerate) (PHBV) copolymers. *J. Mater. Sci.* 2000, *35*, 523–545, doi:<https://doi.org/10.1023/A:1004740522751>.
409. Casarin, S. A.; Rodrigues, C. P.; Souza Júnior, O. F. de; Rosário, F.; Agnelli, J. A. M. Biodegradation in Soil of the PHB/Wood Flour (80/20) and PHB/Sisal Fiber (80/20) Tubes. *Mater. Res.* 2017, *20*, 47–50, doi:10.1590/1980-5373-mr-2016-0904.
410. Lammi, S.; Gastaldi, E.; Gaubiac, F.; Angellier-Coussy, H. How olive pomace can be valorized as fillers to tune the biodegradation of PHBV based composites. *Polym. Degrad. Stab.* 2019, *166*, 325–333, doi:10.1016/j.polymdegradstab.2019.06.010.
411. Taylor, A. M.; Gartner, B. L.; Morrell, J. J.; Tsunoda, K. Effects of heartwood extractive fractions of *Thuja plicata* and *Chamaecyparis nootkatensis* on wood degradation by termites or fungi. *J. Wood Sci.* 2006, *52*, 147–153, doi:10.1007/s10086-005-0743-6.
412. Oliveira, L. S.; Santana, A. L. B. D.; Maranhão, C. A.; de Miranda, R. D. C. M.; Galvão de Lima, V. L. A.; da Silva, S. I.; Nascimento, M. S.; Bieber, L. Natural resistance of five woods to *Phanerochaete chrysosporium* degradation. *Int. Biodeterior. Biodegrad.* 2010, *64*, 711–715, doi:10.1016/j.ibiod.2010.08.001.
413. Nascimento, M. S.; Santana, A. L. B. D.; Maranhão, A. C.; Oliveira, L. S.; Bieber, L. Phenolic Extractives and Natural Resistance of Wood. In *Biodegradation - Life of Science*; Intech, 2013; pp. 349–370.
414. Nicholson, D. J.; Leavitt, A. T.; Francis, R. C. A Three-Stage Klason Method for More Accurate Determinations of Hardwood Lignin Content. *Cellul. Chem. Technol* 2014, *48*, 53–59.
415. Mariotti, F.; Tomé, D.; Mirand, P. P. Converting nitrogen into protein - Beyond 6.25 and Jones' factors. *Crit. Rev. Food Sci. Nutr.* 2008, *48*, 177–184, doi:10.1080/10408390701279749.
416. Chevillard, A.; Angellier-Coussy, H.; Guillard, V.; Gontard, N.; Gastaldi, E. Investigating the biodegradation pattern of an ecofriendly pesticide delivery system based on wheat gluten and organically modified montmorillonites. *Polym. Degrad. Stab.* 2012, *97*, 2060–2068, doi:10.1016/j.polymdegradstab.2012.02.017.
417. de Bertoldi, D.; Vallini, G.; Pera, A. The Biology of Composting: a Review. *Waste Manag. Res.* 1983, *1*, 157–176, doi:10.1177/0734242X8300100118.
418. Bastioli, C. *Handbook of Biodegradable Polymers*; Smithers Rapra Technology, 2005;
419. Mais, U.; Esteghlalian, A. R.; Saddler, J. N.; Mansfield, S. D. Enhancing the Enzymatic Hydrolysis of Cellulosic Materials Using Simultaneous Ball Milling. In *Biotechnology for Fuels and Chemicals*; Humana Press: Totowa, 2002; pp. 815–832.
420. Dashtban, M.; Schraft, H.; Syed, T. A.; Qin, W. Fungal biodegradation and enzymatic modification of lignin. *Int. J. Biochem. Mol. Biol.* 2010, *1*, 36–50.
421. Cooperband, L. *The Art and Science of Composting: A Resource for Farmers and Compost Producers*; University of Wisconsin: Madison, 2002;
422. Scalbert, A. Tannins in Woods and Their Contribution to Microbial Decay Prevention. In *Plant Polyphenols*; Springer: Boston, 1992; pp. 935–952.

- 
423. Saxena, R. K.; Sharmila, P.; Singh, V. P. Microbial degradation of tannins. *Biotransformations Microb. Degrad. Heal. Risk Compd.* 1995, *32*, 259–270, doi:10.1016/S0079-6352(06)80038-X.
424. Riedewald, F. Bacterial adhesion to surfaces: The influence of surfaces roughness. *PDA J. Pharm. Sci. Technol.* 2006, *60*, 164–171.
425. Song, F.; Koo, H.; Ren, D. Effects of material properties on bacterial adhesion and biofilm formation. *J. Dent. Res.* 2015, *94*, 1027–1034, doi:10.1177/0022034515587690.



## Eco-conversion de résidus lignocellulosiques de l'agriculture en matériaux composites durables à matrice biopolyester.

Cette thèse consiste à développer et étudier de nouveaux matériaux composites biosourcés et biodégradables à partir de constituants dérivés des déchets de l'agriculture dans le cadre du projet européen NoAW (<https://noaw2020.eu>). Tous les composants sont dérivés de sous-produits agricoles : des polyhydroxyalcanoates (PHA, biopolyester bactérien et biodégradable en conditions naturelles) produits par digestion anaérobie d'effluents agricoles sont utilisés comme matrices et des fibres de sarments de vigne comme charges de renfort. Les composites sont préparés par extrusion. L'objectif de cette thèse est d'apporter de nouvelles connaissances sur les relations entre le procédé de mise en œuvre des biocomposites, leur structure et leurs propriétés fonctionnelles. Les biocomposites sont développés en considérant une balance performance-coût environnemental. Pour cela, la thèse se focalise sur 2 questions scientifiques majeures : (i) étude de l'impact de l'interface charge/matrice sur les propriétés fonctionnelles des matériaux biocomposites via pré-traitements de surface des particules lignocellulosiques ; (ii) étude de la durabilité de tels matériaux par évaluation dès la conception des impacts environnementaux. Ainsi, une attention particulière est accordée à l'interface charge/matrice, identifiée comme un facteur clé influençant les propriétés finales du composite. Un prétraitement de surface des fibres sans solvant (chromatogénie) est adapté afin de moduler l'interface charge/matrice. Cette nouvelle méthode d'estérification en voie gazeuse est tout d'abord étudiée sur des particules micrométriques de cellulose. Une fois la preuve de concept établie, elle est appliquée aux fibres lignocellulosiques, plus complexes. Les sarments de vigne, déchets agricoles abondant en région Occitanie, sont étudiés comme ressource potentielle pour la production de charges de renfort. Une fois collectés et séchés, ils sont broyés en voie sèche afin d'obtenir des particules micrométriques. La variabilité de la matière première étant un des verrous concernant l'utilisation de la biomasse par les industriels, différents cépages sur plusieurs années ont été étudiés. Dans une logique de bioraffinerie, l'extraction préalable de molécules d'intérêt tels que les polyphénols est envisagée avant d'utiliser le résidu, à savoir les sarments épuisés, comme charge de renfort. L'impact environnemental des matériaux développés est évalué afin de guider les choix stratégiques et obtenir le matériau alliant à la fois performance et faible empreinte écologique. Une analyse de cycle de vie dans le cadre d'une application de barquette rigide alimentaire est réalisée en réunissant des données des acteurs de la filière. De plus, une étude de la biodégradabilité des matériaux finaux est menée. Cette thèse englobe plusieurs composantes pluridisciplinaires afin d'avoir une vision d'ensemble et décloisonnée des matériaux composites mis au point.

## Eco-conversion of agricultural lignocellulosic residues into biopolyester-based composite materials.

This thesis aims at developing new fully biosourced and biodegradable composite materials from agricultural residues in the frame of the European project NoAW (<https://noaw2020.eu>). All the components are derived from agrowastes: polyhydroxyalkanoates (PHA, bacterial biopolyester and biodegradable in natural conditions) produced by anaerobic digestion of agricultural effluents are used as matrix and vine shoot fibers as fillers. Biocomposites are prepared by melt extrusion. The objective of this thesis is to bring new knowledge on the relationships between the processes used to produce the fillers and the biocomposites, the resulting structure of biocomposites and their functional properties. Biocomposites are developed considering a balance between performance and environmental cost. For this purpose, the thesis focuses on 2 major scientific questions: (i) study of the impact of the filler/matrix interface on the functional properties of biocomposite materials via surface pre-treatments of lignocellulosic particles; (ii) study of the durability of such materials by assessment from the design of the environmental impacts. Thus, special attention is given to the filler/matrix interface, identified as a key factor for the final properties of the composite. A solvent-free surface pretreatment of fibers (chromatogeny) is adapted to modulate the filler/matrix interface. This new method of gas-phase esterification is first studied on micrometric particles of cellulose. Once the proof of concept is established, it is applied to lignocellulosic fibers that are more complex. The vine shoots, agricultural waste abundant in Occitania region, are studied as a potential resource for the production of fillers for composites. Once collected and dried, they are milled using dry fractionation to obtain micrometric sized particles. The variability of the raw material being one of the bottlenecks concerning the use of lignocellulosic biomass by manufacturers, different grape species over several years are studied. In a biorefinery approach, the extraction of molecules of interest, e.g. polyphenols, is considered before using the residue, namely exhausted shoots, as a reinforcing fillers. The environmental impact of the produced biocomposites is evaluated to guide strategic choices and obtain materials displaying a good balance between performance and environmental footprint. A life cycle assessment in the context of a food rigid tray application is carried out, collecting data from sector's players. In addition, a study of the biodegradability of the final materials is conducted. This thesis encompasses multidisciplinary fields in order to have a decompartmentalized overview of the developed composite materials.